From the: *Institute of immunology, Ludwig-Maximilians-Universität München*

Dissertation

zum Erwerb des Doctor of Philosophy (Ph.D.) an der

Medizinischen Fakultät der

Ludwig-Maximilians-Universität zu München

Modulation of human dendritic cell phenotype and function in response to yellow fever vaccination and SARS-CoV-2 infection

vorgelegt von:

Elena Patricia Winheim

aus:

Frankfurt am Main, Germany

Jahr:

2022

Mit Genehmigung der Medizinischen Fakultät der

Ludwig-Maximilians-Universität zu München

First supervisor: *Prof. Dr. Anne Krug*

Second supervisor*:* *Prof. Dr. Simon Rothenfusser*

Third supervisor: Prof. Dr. *Barbara Schraml-Schotta*

Dean: **Prof. Dr. med. Thomas Gudermann**

Datum der Verteidigung:

04.06.2022

I. Table of content

V

II. Abstract:

Acute viral infections caused by RNA viruses such as flaviviruses (Yellow Fever, Dengue, West Nile) or SARS coronaviruses (SARS-CoV, SARS-CoV-2) represent a major global health threat. The recent worldwide pandemic of SARS-CoV-2 has shown the importance of researching viral infections to identify immune defense mechanisms against these pathogens and understand immune-mediated pathology.

In this study, live-attenuated yellow fever 17D (YF17D) vaccination was used as a model of an acute self-limited RNA virus infection in humans, and the role of dendritic cells (DCs) and monocyte subsets in the innate immune response was elucidated using multi-parametric flow cytometry, RNA sequencing, and in vitro experiments. Blood was sampled from vaccinees at time points before (day 0) and after (days 3, 7, 14, 28) YF17D vaccination to analyze the kinetics of the innate immune response.

After vaccination with YF17D, DCs and monocytes in the peripheral blood showed concerted activation indicated by the upregulation of CD86 and PD-L1 on the cell surface on day 7 in all DC and monocyte populations (cDC1, cDC2, DC3, tDC, pDC, and classical, intermediate, and non-classical monocytes). At the same time, a robust interferon-induced response was detected in these cells marked by upregulation of Siglec 1 mRNA and surface expression in most cell types - except tDCs and pDCs - and increased expression of a multitude of interferon-induced genes (ISG). A common set of ISGs, consisting of *OAS1*, *OASL*, *OAS3*, *RSAD2*, *IFIT3*, *IFIT1*, and *EIF2AK2*, was concertedly upregulated in all antigen-presenting subsets analyzed, with peak expression on day 7 after vaccination. Besides this common gene signature induced by vaccination, cell-type-specific effects were also seen, indicating that each DC subset plays a unique role in the innate immune response to YF17D vaccination. Interestingly, DC3, a population with high similarities to both classical monocytes and cDC2, and marked by a CD1c^{+} CD5^{-} CD14$^{+/-}$ phenotype, showed higher similarity to cDC2 in their transcriptomic response to YF17D vaccination than to classical monocytes, with common gene sets of ISGs and genes relevant for MHC I presentation significantly upregulated on day 7 after vaccination in both cell populations.

In vitro experiments using a reporter YF17D virus and flow cytometric detection of YF17D-RNA showed that all DCs and monocytes from the peripheral blood can be infected by YF17D. Infected cells exhibited upregulation of activation markers and secretion of cytokines and chemokines such as type I IFN and CXCL10. Since the viral infection rate was not very high,

this direct infection of antigen-presenting cells (APCs) could be used as a mechanism to induce cell activation and allow for antigen presentation. After blocking the IFN-α/β receptor in vitro, higher YF17D infection rates were found in DCs and monocytes, indicating that the type I interferon response is essential in controlling viral replication of YF17D in APCs. Therefore, the strong ISG response found in the transcriptome of peripheral DC and monocyte subsets indicates the induction of an antiviral state in the peripheral blood and suggests highly efficient viral control after vaccination.

This posed the question, how viral antigens can be delivered to and efficiently presented by DCs if infection of DCs by YF17D is highly restricted by type I IFNs. It was therefore investigated whether the infection of DCs is more efficient when they are in contact with other infected cells. Indeed, a higher infection rate of DCs and monocytes was achieved after coculture with YF17D-infected cell lines, and this effect depended on cell-to-cell contact. Thus, contact of DCs with YF17D-susceptible cells at the injection site could promote infection and activation of DCs, leading to the presentation of viral antigens to T cells in the draining lymph node.

To put the efficient innate immune response to YF17D vaccination into context with another acute RNA virus infection, the innate immune responses to YF17D and SARS-CoV-2 infection were compared. The SARS-CoV-2 viral infection leads to the disease called COVID-19 with different degrees of disease severities and, in some patients, even death. In the early phase after infection, a slow and inefficient control of the virus by the innate immune system may lead to a delayed response which is characterized by hyperinflammation and causes severe immune pathology systemically and in the lung.

Compared to the YF17D vaccination, patients with more severe COVID-19 showed low expression of costimulatory molecule CD86 in the cDC2, DC3, and monocytes in the peripheral blood. In contrast, non-hospitalized patients with a mild COVID-19 disease progression showed an upregulation of CD86 similar to what was observed in YF17D vaccinees. The downregulation of CD86 in severe COVID-19 was accompanied by upregulation of PD-L1, which is known to interact with PD-1 on T cells, thereby regulating their inhibiting activation. This altered phenotype of peripheral APCs coincided with a reduced capability of DC3 and monocytes isolated from the blood of COVID-19 patients to stimulate autologous T cell activation and proliferation in vitro, thereby revealing functional impairment of circulating DCs and monocytes in this disease. An increase of Ki67$^+$ cells in both YF17D vaccinees and COVID-19 patients, together with temporary reductions in cDC1 and cDC2 frequencies in the peripheral blood, indicated an increased turnover of the blood DC compartment in acute viral infection.

VIII

While in YF17D vaccinees only a temporary relative reduction of cDC1 and cDC2 was observed, absolute DC numbers and also pDCs were reduced in the peripheral blood of COVID-19 patients. The depletion was transient in patients with a mild disease progression and long-lasting in patients with severe COVID-19.

Additionally, a cell population lacking markers of lymphocytes, granulocytes, DCs, and monocytes but expressing HLA-DR and Ki67 was also found to be increased in the peripheral blood of COVID-19 patients, but not YF17D vaccinees, as a sign of dysregulated myelopoiesis. Furthermore, in COVID-19 patients – but not in YF17D vaccinees – a subset of $CD14^+$ DC3 expanded within the DC3 population and correlated with inflammatory markers and the accumulation of activated T_{fh} and B cells. Therefore, the innate immune response in COVID-19 patients seems to be a critical factor influencing inflammatory and adaptive immune responses. Dysregulation of innate immune cells as seen by the altered phenotype, impaired function and long-lasting reduction found in DCs and monocytes could lead to an increased susceptibility to secondary infections as a consequence of severe COVID-19. While YF17D vaccination induces a transient coordinated response of blood APC subsets with a peak on day 7 after vaccination, the responses in COVID-19 are long-lasting and show unusual phenotypes of monocytes and DCs accompanied by functional impairment.

III.   List of figures

XI

IV.　List of tables

V. List of abbreviations

Abbreviation	Name
AIM2	absent in melanoma-2
ALR	AIM2-like receptors
APCs	antigen-presenting cells
BCR	B cell receptor
BTM	Blood transcriptional module
BX	BX795
cDCs	conventional DC
CDP	common DC precursor
CLR	C-type lectins receptors
COVID-19	coronavirus disease 2019
d	day
DAMP	damage-associated molecular pattern
DAPI	4′,6-diamidino-2-phenylindole
DCs	dendritic cells
DEG	differentially expressed genes
DMSO	Dimethyl sulfoxide
dsRNA	double-stranded RNA
FOXP3	forkhead box P3
GMP	granulocyte-macrophage progenitor
H	Healthy patient
HPC	hematopoietic stem cell
HUVEC	human umbilical vein endothelial cells
IFN	interferon
IFNAR	interferon-α/β receptor
IRF	interferon regulatory factor
ISG	interferon-stimulated gene
LPS	Lipopolysaccharide
M	Mild/moderate patient with COVID-19
MACS	magnetic activated cell sorting
MFI	Mean fluorescence intensity
min	minute
mo-DCs	monocyte-derived DC
MOI	multiplicity of infection
NETS	neutrophil extracellular traps
NF-κB	nuclear factor κ B

NK	natural killer
NLR	NOD-like receptor
NRG-HIS	Non-obese diabetic (NOD) mice
pAb	polyclonal antibody
PAMP	pathogen-associated molecular pattern
PBMCs	peripheral blood mononuclear cells
PCA	principal component analysis
PCR	polymerase chain reaction
pDCs	plasmacytoid DC
PRR	pattern recognition receptor
pt	patient
RLR	retinoic acid-inducible gene I like receptor
RT	room temperature
Ruxo	Ruxolitinib
S	severe patient with COVID-19
SARS-CoV-2	SARS-CoV-2
SLE	Systemic lupus erythematosus
ssRNA	single-stranded RNA
TCR	T cell receptor
tDC	transitional DC
T_{fh}	follicular helper cell
T_h	T helper cell
TLR	toll like receptor
T_{regs}	regulatory T cell
VST	variance stabilizing transformation
WHO	World health organisation
WHOMax	maximal WHO score a COVID-19 patient reached
YF17D	yellow fever vaccine strain 17D-204

1. Introduction

1.1 The innate and the adaptive immune response and their role in the defense against viral infections

Vertebrates have developed an immune system consisting of adaptive (acquired) and innate immunity as an intrinsic defense against pathogens. A well-founded understanding of how these systems work is essential for the development of suitable treatment and vaccinations against viral infections and other pathogens. The innate immune response is the first line of defense against pathogens. It is responsible for recognizing microbial and viral components, generating activation signals, and subsequently initiating the adaptive immune response. Innate immunity comprises mechanical and chemical barriers as well as complement proteins and innate immune cells. The mechanical barriers such as skin and the respiratory and intestinal mucosa are constantly exposed to microorganisms and viruses but prevent their entry. If this barrier is breached, the complement system and antimicrobial peptides immediately come into play and lyse pathogens and virus-infected cells. Phagocytes, such as macrophages/monocytes, neutrophils, and dendritic cells (DCs), consistently patrol the bloodstream and monitor peripheral tissues. They detect components of invading microorganisms and viruses in addition to inflammatory mediators released by infected cells. Activated phagocytes subsequently attempt to directly eliminate the pathogen by mechanisms such as phagocytosis and recruit and activate other innate and adaptive immune cells by releasing cytokines and chemokines. DCs and macrophages take up, process and present microbial antigens to T lymphocytes, thereby initiating the adaptive immune response. The process of innate immunity is rapid and occurs within hours after infection, while adaptive immunity usually takes several days or weeks to develop.

Each innate cell type has a unique function in this complex process: Macrophages are highly competent phagocytes and have a limited capability to present antigen. Neutrophils can also phagocytize and can physically trap pathogens through the secretion of neutrophil extracellular traps (NETs). The primary cells responsible for antigen presentation are DCs, which are also called professional antigen-presenting cells (APCs) [1, 2]. Adaptive

1

immunity follows the innate immune response and involves the clonal expansion of antigen-specific B and T lymphocytes.

Upon infection with a novel pathogen, DCs take up antigens from the pathogen, migrate to the lymph nodes and present the antigen as peptides on MHC class I and class II molecules to naïve CD8$^+$ and CD4$^+$ T cells. T cells that recognize the peptide-MHC complexes via their T cell receptor (TCR) then get activated, proliferate, and differentiate into effector T cells. While CD8$^+$ cytotoxic T cells can directly lyse and kill infected cells, CD4$^+$ helper T cells can differentiate into distinct types of T helper cells (T$_h$), e.g. T$_{h1}$, T$_{h2}$, T$_{h17}$, follicular helper T cells (T$_{fh}$) or regulatory T cells (T$_{regs}$), and start producing cytokines and growth factors modulating the immune response. Depending on the costimulatory molecules expressed on APCs and the cytokines secreted, different T$_h$ polarizations are induced. Naïve B cells take up antigens that bind to surface immunoglobin and present them to specific CD4$^+$ T cells in the lymph follicle, namely the T$_{fh}$ cells. Subsequently, T$_{fh}$ cells further stimulate the B cells, which then expand and differentiate into memory B cells or antibody-secreting plasma cells. Some T cells can also differentiate into memory cells and, together with memory B cells, generate a long-lasting immunological memory.

1.2 Innate immune cells

1.2.1 Conventional DCs

DCs were first discovered in murine spleen in 1973 by Ralph Steinman and were defined by their distinct morphology consisting of protruding cytoplasmic dendrites as well as their migratory behavior and strong antigen-presenting capacity [3]. It is now known that multiple DC subsets with specific functions exist. Human DCs express high levels of HLA-DR and lack the typical markers of T cells (CD3), B cells (CD19, CD20), and natural killer cells (NK cells, CD56), defined as lineage markers. A distinction is made between conventional DCs (cDCs), also known as classical or myeloid DCs, and plasmacytoid DCs (pDCs).

cDCs are highly efficient APCs and adept in stimulating naïve T cells to expand and differentiate. They can be further classified into different subsets defined by distinct functions and the expression of surface molecules. Two main cDC populations can currently be distinguished in the human peripheral blood: cDC1 that express CD141/BDCA-3 and cDC2 that express CD1c/BDCA-1 [4, 5].

cDC1 can be found in human lymph nodes, tonsils, bone marrow, and blood as well as in the skin, lung, and liver [6]. They are efficient cross-presenters of antigen from extracellular sources on MHC I molecules to $CD8^+$ T cells. Additionally, upon stimulation they secrete large amounts of IL-12p70 and CXCL10 and highly express Toll-like receptor 3 (TLR3) [7] and XCR1 [8]. Most cDCs in the peripheral blood express CD1c [4, 9] which contain cDC2 and DC3. cDC2 are $CD1c^+$ $CD14^-$ $CD5^+$ $BTLA^+$ and are responsible for inducing $CD4^+$ T_h responses by presenting endocytic antigens via MHC II molecules. cDC2 can be found in the blood, lymph nodes, spleen, skin, liver, gut, and lungs [10-12]. Upon stimulation they secrete IL-1, IL-8, IL-10, IL-12, IL-23 and TNF-α [13]. $CD1c^+$ $CD5^-$ $BTLA^-$ cells are the DC3 and they express multiple genes associated with monocytes [14]. Recent multi-dimensional flow cytometry and single-cell RNA sequencing studies have confirmed these subsets: the $CD5^+$ $CD1c^+$ cells which express HLA-DQ, IRF4, and BTLA are cDC2 and $CD5^-$ $CD1c^+$ that express varying levels of CD14 and CD163 are defined as DC3. Even though DC3 express typical monocyte-associated markers such as CD14 and CD163, their gene expression profile clusters them separately from monocytes and they have a separate ancestry than monocytes and cDC2 [15-18]. However, to date little is known about their function in viral infections. In systemic lupus erythematosus (SLE) patients, DC3 are described as an inflammatory subset that increases in frequency and has a high capacity to prime $CD4^+$ T cells toward T_{h2} and T_{h17} [15] and an ability to induce tissue-resident memory cells in $CD8^+$ T cells [18].

1.2.2 Plasmacytoid DCs

pDCs are entirely distinct from cDCs in terms of their morphology and function. They are lineage negative, lack expression of monocyte markers CD14 and CD16, and are defined by the expression of CD123 and CD303. pDCs were first discovered in 1953 when the pathologists Lennert and Remmele described a plasmacytoid cell located in the T cell

zone of human lymph nodes [19]. Since then, many different functions have been at-tributed to pDCs but some of their previously attributed functions are at the moment being questioned. The nature of pDCs as a DC is currently debated, and the existence of a com-mon DC ancestor is still under dispute [20]. pDCs participate in the antiviral defense, and their hallmark is the rapid and massive production of type I IFNs (IFN-α and IFN-β) in response to viruses and TLR7/9 agonists [21-23]. During viral infections, type I IFNs act on host cells via the IFN-α/β receptor (IFNAR), prompting the expression of interferon-stimulated genes (ISGs), which induce an antiviral state. Type I IFNs also affect the mat-uration and activation of several cell populations, such as cDCs and NK cells [24, 25].

pDCs recognize viral RNA through TLR7 and TLR9 [26, 27], can also present antigens to T cells - albeit less efficiently than cDCs - and induce T cell polarization [28, 29]. However, these DC-like functions attributed to pDCs could be caused by the inclusion of functionally distinct transitional DC (tDC) within the pDC population due to their over-lapping phenotype. This concept is discussed in more detail in Chapter 1.2.3. More recent studies showed that when separating tDCs from pDCs, freshly isolated pDCs were poor inducers of T cell proliferation [30] whereas bona fide pDCs cultured with CD40L and IL-3, after delineation of tDCs, induced T cell proliferation [31]. Another function of pDCs currently under dispute is their putative ability to differentiate into cDCs when stimulated [32] which may have been due to tDCs contaminating the pDC population in earlier studies. See et al. (2017) found no differentiation of pure, tDC-free pDCs into cDCs [30]. However, contrary to this finding, after removing tDC contamination and upon stimulation with the influenza virus, (A/PR/8/34, H1N1) pDCs were shown to di-versify into 3 separate populations based on the surface expression of markers PD-L1 and CD80 with a CD80^{+} PD-L1^{-} expressing population adopting a cDC-like morphology and able to induce CD4^{+} T cell differentiation [33]. This finding indicated that pDCs either need to be defined more clearly to exclude any cDC progenitors or that pDCs retain the ability to differentiate into cDCs under certain conditions such as in response to viral infections or other types of stimulation. Leylek et al. (2019) also suggest, that tDCs may arise from pDCs [34], which is discussed in more detail in Chapter 1.2.5. Studies in mice were able to show that the pDCs both function as type I interferon producers and can later converge transcriptionally towards a cDC/tDC phenotype and stimulate CD4^{+} T cell ex-pansion, thereby suggesting pDC plasticity [35].

Besides type I interferons, pDCs can also secrete other pro-inflammatory cytokines and chemokines such as IL-6, IL-12, CCL3, CCL4, CXCL8 and CXCL10. Due to their ability to rapidly produce type I interferon and several inflammatory cytokines, they are highly significant for antiviral immunity.

1.2.3 Transitional DCs

DCs with a transitional phenotype and gene expression profile were first identified as Axl^+ DCs [16, 31]. This population overlaps with $CD123^+$ $CD33^+$ $CD45RA^+$ DCs, pre-DCs [30], and is found in the spleen and blood [16, 31]. In mice, a similar population expressing Siglec H, CX3CR1, and Zbtb46 was also recently identified in the spleen and lymph nodes but not in the bone marrow [34, 36, 37]. The common factor among these populations is a phenotype and gene expression profile that lies in between that of pDCs and cDCs and their distinct immune functions. Due to their transitional phenotype, this cell population is termed tDCs in most publications, whereas others utilize the terms Axl^+ DCs, AS-DCs and pre-DCs. Due to their pDC-like surface marker expression, e.g., CD123 and CD303, tDCs were probably included in the pDC population in previous studies. In fact, a small subpopulation of $CD5^+$ pDCs that overlaps with the tDC subset has been described previously [38]. Therefore, the delineation of tDCs from pDCs is necessary to determine their specific functions and their role in the innate immune response.

In both humans and in mice, tDCs induce the proliferation of allogeneic naïve $CD4^+$ and $CD8^+$ T cells and T_h cell polarization comparable to cDCs [16, 34]. Delineation of tDCs from pDCs showed that pDCs do not share this ability when freshly isolated from peripheral blood [16, 30, 34, 39, 40]. tDCs were shown to be better at polarizing the T_{h2} phenotype than cDC1 and cDC2, while polarization towards T_{h1} and T_{h17} was lower than in cDCs, which can be explained by the fact that tDCs are able to secrete IL-12p40 but only show a limited capability to secrete IL-12p70 wherefore they are not able to form productive IL-12 [16, 34]. It is controversial whether tDCs are finally differentiated non-canonical DCs with specific functional properties [34] or if these cells are circulating precursors of cDCs. See et al. (2017) demonstrated the differentiation of these cells, here being characterized as $CD123^+$ $CD33^+$ $CD45RA^+$ pre-DCs, which were shown to overlap with tDCs [15], into both cDC1 and cDC2 [30], indicating a precursor function of tDCs. However, as described previously, tDCs could also be differentiated from pDCs [34] and

distinct ontogeny from pre-cDCs has been described. This is covered in more detail in chapter 1.2.5.

As tDCs were shown to both be able to secrete cytokines associated with viral infections and activate the adaptive immune response by inducing T cell proliferation, they may play a role the antiviral host defense. Additionally, tDCs express several receptors that can be used for viral entry, such as Siglec 1 [41] and Axl [42] and might thus be susceptible to viral infections. For example, human immunodeficiency virus (HIV) was able to infect tDCs in a Siglec 1 dependent manner and was then shown to replicate productively in internal compartments within tDCs [43].

	cDC1	cDC2	DC3	tDC	pDC
surface markers	CD141+ CLEC9a+ XCR1+	CD1c+ CD5+ BTLA+	CD1c+ CD5- CD14+/- CD163+/- BTLA-	BDCA-2+ CD123+ Axl+ CD5+ Siglec-6/-1+	BDCA-2+ CD123+
functions	TLR3 Crosspresentation Th1 responses IL12-production Response to intracellular pathogens	Th2 and Th17 responses IL-23 production Response to extracellular pathogens	subset of cDC2 Th1/17 and TRM induction pro-inflammatory	Immediate precursor of cDC2 found in blood and secondary lymphoid organs Induce CD4/CD8 T cell proliferation	TLR7/TLR9 Type I IFN Response to viruses

Figure 1: DC subsets in the peripheral blood.
Expression of characteristic surface markers and function of cDC1, cDC2, DC3, tDC, and pDCs in the innate immune response.

1.2.4 Monocytes

Monocytes express HLA-DR and CD33 and can be separated into three subtypes by the differential expression of surface markers CD14 and CD16: the classical CD14$^+$ CD16$^-$ monocytes (mo1, around 85%), intermediate CD14$^+$ CD16$^+$ monocytes (mo int, 5–10%), and non-classical CD14$^-$ CD16$^+$ monocytes (mo2, 5–10%). CCR2 is highly expressed on mo1 in the human blood and was shown to be essential for the emigration of monocytes from the bone marrow and migration to inflamed tissue in mice [44-46]. Upon migration into the tissue, monocytes can differentiate into macrophages or DCs when conditioned with growth factors and cytokines [47, 48].

Mo1 are known for their production of IL-10, and multiple other cytokines such as IL-6, IL-8, CCL2, CCL5, and G-CSF in response to a broad range of stimuli [49-51]. They specialize in phagocytosis and the production of reactive oxygen species [52, 53].

Mo int express higher HLA-DR levels than mo1 and produce large amounts of TNF- α [54]. In addition, these cells were shown to accumulate in severe inflammatory conditions, such as viral infections and sepsis [55, 56].

Mo2 are known for patrolling as they migrate along the endothelium and survey for potential damage [57]. In addition, they express high amounts of CX3CR1 [58] and have been shown to secrete TNF- α and multiple other cytokines [49, 59]. Deuterium labeling in humans has shown sequential differentiation trajectories from classical monocytes towards intermediate and non-classical monocytes [60]. Microarray data support this transitional relation, showing gene expression patterns of intermediate monocytes lying between the classical and non-classical [49].

	Classical monocytes - mo 1	**intermediate monocytes - mo int**	**non-classical monocytes - mo 2**
surface markers	CD14+ CD16−	CD14+ CD16+	CD14lo CD16+
functions	Extravasation phagocytic production of cytokines (IL-10) and ROS	phagocytic pro-inflammatory cytokines TNFalpha secretion	patrolling vascular endothelium pro-inflammatory cytokines TNFalpha secretion

Figure 2: Monocyte subsets in the peripheral blood.
Surface markers and functions of classical monocytes (mo1, CD14^{+}CD16^{-}), intermediate monocytes (mo int, CD14^{+}CD16^{+}), and non-classical monocytes (mo2, CD14^{low}CD16^{+}).

1.2.5 DC and monocyte development

DCs and monocytes are closely related and develop from adult hematopoietic stem cell progenitors in the bone marrow. In humans, DC and monocyte commitment sequentially increases from hematopoietic stem cells (HPCs) to granulocyte-macrophage progenitors (GMPs). These GMPs can still give rise to either monocytes or common DC progenitors (CDPs) [61, 62]. Similar to what can be seen in mice [63, 64], CDPs give rise to a committed pre-cDC population in humans [61]. Short-lived pre-cDC can be found in the human blood and can replenish cDC1 and cDC2 in blood and tissue [65]. Pre-cDCs in the peripheral blood are already pre-committed, showing either cDC1 or cDC2 potential and expressing HLA-DR, CD117, and CD45RA [16, 30, 66]. This phenotype of pre-cDCs at least partly overlaps with that of the previously described tDCs.

In vitro culture of CD34^{+} GMP showed that pDCs, tDCs, cDC1, and cDC2 developed from IRF8^{high} CD33^{-} GMPs while DC3 and monocytes differentiated from IRF8^{low}

7

CD33^{+} GMPs. However, DC3 differentiate separately from monocytes [17, 18] indicating that they are distinct in their ontogeny. The development of cDC1 is dependent on transcription factors BATF and IRF8, while cDC2 development is IRF4 dependent [17, 67, 68]. pDC differentiation is regulated by E2-2 in humans and mice, and blocking E2-2 arrests pDC development and impairs IFN responses. In Pitts-Hopkins syndrome, caused by a loss-of-function mutation in *TCF4* encoding transcription factor E2-2, patients showed impaired pDC responses [69]. tDCs seem to be closely related to pDCs in their development and also require E2-2/*TCF4* [30, 34, 69] which indicates that tDCs do not seem to follow the developmental program of pre-cDCs. Whether tDCs and pre-cDCs are populations with similar functions and surface markers but distinct ontogeny or are overlapping populations with the same ontogeny is still debated [16, 34, 70]. Recent studies employing single-cell transcriptomics and cellular barcoding show that DC commitment is already present in early multipotent lymphoid progenitors and not only in CDP, thereby allowing for more plasticity in DC development. Both early DC commitment in hematopoiesis at the level of multipotent lymphoid progenitors and late commitment, downstream of the CMPs contribute to the generation of DC subpopulations [71, 72] (see DC and monocyte development in Figure 3).

FLT3L and GMCSF are growth factors that drive human DC development. Administration of FLT3L leads to expansion of cDCs in humans, and the combination of FLT3L and GMCSF causes cDC expansion in humanized mice [73, 74]. While FLT3L is essential for the generation of all DC subsets, GMCSF is required for survival and maintenance of non-lymphoid tissue-resident CD103^{+} CD116^{+} DC as shown in the murine system [75]. Most tissue-resident macrophages in steady-state develop from precursors from the yolk sac and fetal liver and are not monocyte-derived [76, 77], and only in the heart, dermis, and gut do the circulating monocytes contribute to the macrophage populations [78].

1.2.6   Monocyte derived DCs

mo-DCs can be generated in vitro from monocytes using a culture system that involves stimulating monocytes with IL-4 and GMCSF. These mo-DCs have morphological, phenotypical, and functional similarities to DC subsets identified in vivo. They express HLA-DR, CD11c, CD11b, CD1c, and downregulate CD14, and can present antigen and stimulate T cells [79]. In vitro generated mo-DCs have been shown to secrete IL-18, IL-12p40,

IL-6, TNF-α, IL-8, IL-1β, and IP-10 [80, 81]. While primary DCs only account for 1-2 % of all PBMCs, monocytes make up about 10 %. Therefore, differentiating mo-DCs from monocytes in vitro enables the generation of a large number of DC-like cells and has been an important in vitro APC model leading to multiple key discoveries of DC function and biology [82]. In vitro generated mo-DCs do however differ from ex vivo DC populations. Multiple publications showed in vitro generated mo-DCs transcriptome [83, 84] as well as surface marker expression [31] separates them from ex vivo DC subtypes.

DCs derived from monocytes have been observed in both steady-state and inflammation in vivo. Fate mapping in mice has demonstrated the differentiation of monocytes into DC-like cells under inflammatory conditions in tissues [85, 86]. Similarly, during chemotherapy in mice, the development of Ly6C$^+$ CD103$^+$ mo-DCs that can activate CD8$^+$ T cells in vitro and transport antigen to draining lymph nodes, has been identified, thereby showing phenotypic and functional similarities to CD103$^+$ cDC1 [87]. Mo-DCs have also been identified in humans and can be found in the peritoneum [88], intestine [48, 89], and lung [90] as well as in steady-state [91] and inflamed skin [84]. Recently, mo-DCs and DC3 have been proposed to comprise the same cell subset [15]. However, mo-DCs and DC3 were shown to have distinct ontogeny, with DC3 not being directly generated from monocytes [17, 18, 92], as well as distinct gene expression patterns with, for example, *DAB2* being expressed on mo-DCs but not DC3 [16, 93]. Further analysis and direct comparisons of ex vivo DC subsets and in vitro generated mo-DCs are required to better define their similarities and differences.

Functionally, ex vivo mo-DCs secrete IL-23, IL-1β, IL-6, TNF-α, and IL-12p70 [94]. Although, they are also efficient cross-presenters, they use a non-conventional intracellular pathway dependent on lysosomal proteases [93]. Mo-DCs can induce CD8$^+$ T cell differentiation and stimulate CD4$^+$ T cell proliferation [93, 94]. Therefore, mo-DCs are not only an in vitro APC model that mimics DC functions but also exist in the human body and have relevant functions during inflammatory responses in vivo. Due to their functional capabilities that emulate bona fide DCs and their involvement in inflammation and disease, in vitro generated mo-DCs are a highly relevant and convenient in vitro model to study DC biology and function.
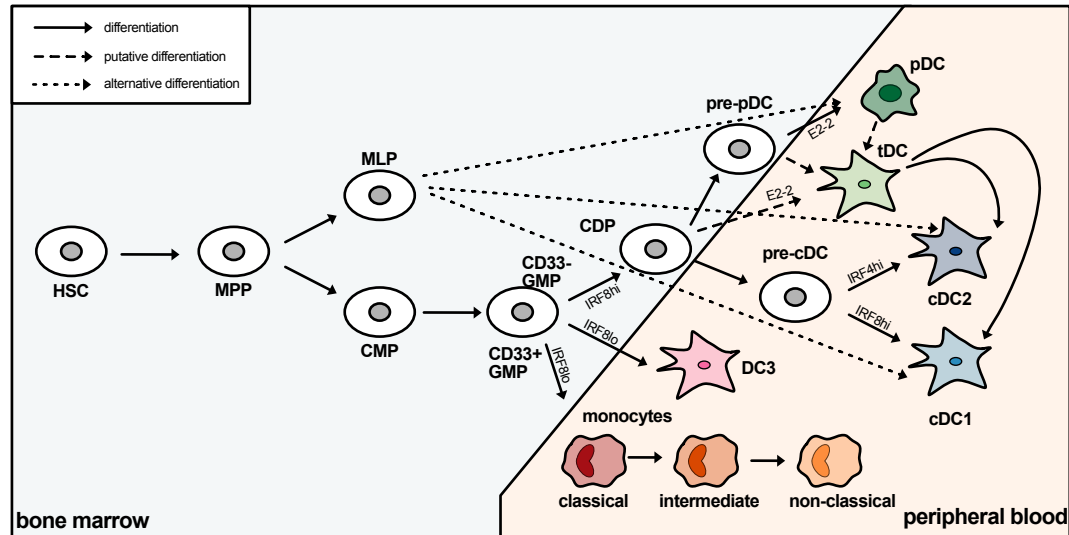
Figure 3: Stages of DC and monocyte development.
pDCs, cDC1, cDC2, DC3, and monocytes are distinct cell subsets that can be identified in the human blood. CD14$^+$ monocytes and DC3 are derived from bone marrow IRF8^{low} GMPs. The developmental pathway of tDCs remains to be confirmed. They may derive from CDPs, pre-cDCs, pre-pDCs, or pDCs. Differentiation of tDCs and pDCs is dependent on E2-2, while cDC1 and cDC2 development depend on IRF8 and IRF4, respectively. Classical monocytes develop from IRF8^{low} GMPs and can further differentiate into intermediate and non-classical monocytes.

1.3 Pattern recognition receptors and pathways

Innate immune cells such as DCs and other APCs utilize specialized pattern recognition receptors (PRR) to identify different pathogen- and damage-associated molecular patterns (PAMPS, DAMPS) to react to invading microorganisms or endogenous danger signals. The first PRR Toll was discovered in 1996 as an essential surface receptor in the innate immunity against bacteria and fungi in Drosophila [95]. Soon after, a homolog was found in humans and shown to regulate the adaptive immune response by inducing the expression of costimulatory molecules and secretion of cytokines [96].

In contrast to the considerable specificity generated by gene rearrangement leading to a vast repertoire of specific TCRs and BCRs, PRRs are germ-line encoded and limited in number. They consist of only five receptor families: membrane-bound C-type lectins receptors (CLR), Toll-like receptors (TLRs) and cytoplasmic NOD-like receptors (NLR), retinoic acid-inducible gene I like receptors (RLR) and absent in melanoma-2 (AIM2)-like receptors (ALRs) [97].

Each PRR recognizes a fixed set of PAMPs and several signaling pathways can be activated, thereby allowing a for some specificity in the innate immune response. On sensing of PAMPs or DAMPs, PRRs trigger signaling cascades leading to an antiviral state and inflammatory responses. Different pathways can be induced, leading, for example, to nuclear factor κ B dependent (NF-κB) cytokine responses or interferon regulatory factor (IRF) dependent IFN-α/β responses. On the cell surface, TLR1, 2, 4, 5, 6, and 10 are expressed and generally known for recognizing bacterial, fungal, and parasitic PAMPs. However, it has been shown that some surface TLRs such as TLR2, TLR4 also sense viral proteins [98, 99].

Endosomal TLRs (TLR3, TLR7/8, TLR9) can recognize viral dsRNA, ssRNA, and DNA and are only expressed in certain DC cell types [100]. The adaptor molecules MyD88 and TRIF are responsible for activating downstream signaling leading to the production of proinflammatory cytokines and type I interferons. Except for TLR3, all endosomal TLRs use MyD88 as the adaptor molecule [101].

TLR3 signaling and NF-κB activation leads to IRF3 phosphorylation and are mediated by TRIF while TLR7/8/9 signaling leads to IRF7 phosphorylation and also to activation of the NF-κB and MAPK pathway. dsRNA, which is produced by several viruses during their replication cycles, can activate cytosolic RIG-I and MDA5, which associate with adaptor molecule MAVS, and activate TBK1/IKKε thereby also inducing the phosphorylation of IRF3 and IRF7 [102, 103]. IRF3 and IRF7 phosphorylation leads to homo- or heterodimerization. After dimerization, IRF3 and IRF7 can translocate into the nucleus and induce type I IFN transcriptions [104, 105]. NF-κB can also translocate into the nucleus and induce the secretion of pro-inflammatory cytokines such as TNF-α, IL-12 and IL-6 and the expression of costimulatory molecules [106]. In a positive feedback loop, secreted IFN-α/β can bind the IFNAR receptor. This signal is transduced via the Janus kinases (Jak1) and signal transducers of transcription (STAT1/STAT2) and induces the expression of assorted ISGs, thereby establishing an antiviral state in the cells [107].

1.4 Viral infections and the human immune response

1.4.1 Yellow fever vaccination

Yellow fever virus (YFV) is a mosquito-borne pathogen belonging to the family of flaviviruses, which includes the West Nile virus (WNV), Dengue virus (DENV), and Japanese Encephalitis virus (JEV). According to the global World Health Organization's (WHO) statistics, approximately 200 000 cases of yellow fever occur annually, leading to 30 000 deaths worldwide, mainly in Africa and Central and South America.

In contrast to other flaviviruses, a successful vaccine against yellow fever was already developed in 1937 [108, 109]. The yellow fever vaccine strain 17D-204 (YF17D) is an attenuated virus that was generated by multiple passages through mouse and chicken tissue. The YF17D vaccine is one of the most successful live-attenuated vaccines available and provides life-long immunity against infection with the yellow fever virus after only one vaccination dose. Therefore, this vaccine is an excellent model to study RNA virus infections in humans and the immune response against flaviviruses and other RNA virus infections. Despite its success, the vaccine's effect on the immune system has not been completely elucidated yet.

1.4.1.1 Adaptive immune response to YF17D

One hallmark of the YF17D vaccination is the induction of a strong neutralizing antibody response. IgM antibodies can already be detected between 3 to 7 days after vaccination and then decline over several months. B cells are activated at 15 days post-vaccination, with the early B cell response being dominated with IgM$^+$ and class-switched memory B cells. Atypical IgM$^+$ IgD$^+$ and switched memory B cells then mediated the late B cell response, and affinity maturation was shown to continue for up to 9 months after vaccination [110, 111]. Neutralizing IgG antibodies are detected within 14 days after vaccination, can persist for 45 years, and are protective against challenges with virulent strains of YF17D [109, 112]. Plasmablasts showed increased frequencies 2 weeks after vaccination [113, 114] and correlated with the subsequent magnitude of the neutralizing antibody response at day 90 after vaccination [115].

Although the antibody response plays a central role, the cellular immune response is also thought to be important for the vaccine's effectiveness. $CD4^+$ T cells are activated early and $CD8^+$ T cells at later time points after vaccination [116]. YF17D-specific $CD4^+$ T cells produce T_{h1} and T_{h2} cytokines such as IL-2, IFN-γ, TNF-α, IL-4, and IL-10 [117, 118]. IFN-γ from T_{h1} and NK cells further promote $CD8^+$ responses, whereas IL-4 and IL-10 promote B-cell and antibody responses. Circulating T_{fh} cells were expanded after vaccination with YF17D with a peak 2 weeks after vaccination and dominated by T_{fh1} expansion which correlated with the strength of the neutralizing antibody response [113, 115]. Additionally, T_{regs}, which are characterized by their expression of forkhead box P3 (FOXP3) and their immunosuppressive function, were shown to be transiently activated in response to YF17D vaccination [119].

After the induction of $CD4^+$ T cells, vaccinees show an expansion of specific $CD8^+$ T cells that gradually differentiate into long-lived memory $CD8^+$ T cells [120-122], while memory $CD4^+$ T cells are also expanded after vaccination [123]. Furthermore, the magnitude of the T cell response correlates with the extent of viral load in the blood, thereby indicating that $CD8^+$ T cell proliferation is dependent on the antigen dose [124].

1.4.1.2 Innate immune response to YF17D

Most yellow fever vaccination studies focused on the adaptive immunity and T cell responses, and little is known about the role of the innate response in the efficacy of the vaccination. However, the innate immune system is crucial for initiating the adaptive response through antigen presentation and cytokine production. Optimal activation of APCs such as DCs and monocytes for the presentation of viral antigens leading to efficient T cell priming and induction of adaptive immune responses could explain the high level of success of the YF17D vaccine.

After YF17D vaccination, the frequency of pDCs in the peripheral blood was increased on day 7 post-vaccination, while no significant changes were observed in cDCs [114]. Mo int frequencies were also shown to be increased on day 7 after vaccination, marking the peak of the innate immune response [125] as well as peak viremia.

Transcriptome microarray studies using whole PBMCs from YF17D vaccinated donors in combination with comprehensive flow cytometric analysis revealed the coordinated

expression of master transcription factors such as *STAT1*, *IRF7*, and *ETS2* and the induction of major pathways of the innate immune response, including type I interferon, and inflammasome activation on day 7 after vaccination [118, 126]. An examination of patients with adverse life-threatening YF17D vaccine-associated diseases showed that *IFNAR1* and *IFNAR2* deficiency and neutralizing auto-antibodies against type I IFNs accounted for more than half of the cases, showing the importance of IFNAR signaling in controlling the YF17D infection and possibly also in regulating the antigen dose [127, 128].

1.4.1.3 Yellow fever vaccination as a model of live virus infection in humans

The yellow fever vaccination can be used as a unique model of an acute self-limiting RNA virus infection in the human system to explain how an effective antiviral immune response is formed. Systems vaccinology approaches have been used to study the immune response to YF17D vaccination [129, 130]. Using peripheral blood as well as plasma before and after vaccination, innate immune responses have been analyzed and correlated with the subsequent adaptive response by Querec et al. (2009) [130]. This study analyzed the transcriptome of whole PBMCs and found upregulation of viral sensing and antiviral immune responses (*TLR7*, *OAS1*, *OAS2*, *OAS3* and *OASL*, *DDX58*/RIG-I, and *IFIH1*/MDA-5, *IRF7*, *STAT1*). Surprisingly, this antiviral signature did not correlate with the magnitude of the subsequent T cell or B cell response. However, when looking at total PBMCs, individual gene signatures of rare cell populations such as DCs could be overlooked and a more focused examination of the transcriptome of the innate system in YF17D vaccinees is still missing. Querec et al. (2009) did find some early predictors of immunogenicity such as *SLC2A6* (GLUT1) and *EIF2AK4* upregulation which are important for glucose transport and stress responses, respectively, proving the concept that early innate responses after vaccination can predict critical parameters of the adaptive immune response, such as antibody titers and CD8$^+$ T cell expansion.

Additionally, the initial viral load was shown to determine the magnitude of the subsequent CD8$^+$ T cell response [124], thereby proving the importance of having sufficient antigen to induce the adaptive immunity. Another study then showed a positive correlation of expression levels of antiviral *AIM2*, *IFNGR1*, and *IFNG* with antibody levels on day 7 after vaccination [131]. In addition, *CLEC5A* was found to be highly expressed on

activated monocytes and correlated with antibodies 60 days after vaccination and with activated CD4$^+$ and CD8$^+$ T cells [131].

Examining the peripheral blood cells and plasma cytokine concentration in humans after vaccination can help to explain the intricate interplay of the immune response to viral infections in humans.

1.4.1.4 YF17D replication and cell tropism

Flaviviruses are single-stranded positive-sense RNA viruses that are approximately 50 nm in size and consist of three structural proteins, namely C (capsid), E (envelope) and M (membrane) [132]. Passaging of the wildtype Asibi strain led to the attenuated YF17D virus strain and mutations in 32 amino acids. While the capsid protein remains unchanged between the two strains, 12 amino acids differ in the region coding for the E protein and viral proteins NS1, NS3, and NS5, ns4a and ns4b contain the remaining substitutions [133]. The E glycoprotein is most relevant for the biological activity of the virus and highly significant for binding to receptors on the cell surface. After binding, flaviviruses are eternalized via clathrin-coated pits and traffic through pre-lysosomal endocytic compartments [134, 135]. A low pH induces fusion between the viral and host membranes, thereby releasing the virus nucleocapsid. Following the uncoating [136], viral RNA is then released into the cytoplasm and at 3 hours after infection negative-strand RNA can already be detected while after 12 hours viral progeny is released [137].

The attenuated YF17D vaccination leads to productive but limited infection in humans and causes vaccinees to develop transient viremia which peaks on day 7 after vaccination [138, 139]. In this context, the question concerning which cells are responsible for viral propagation in humans is still being debated [140]. It is likely that in a primary wave of viral replication, cells at the injection site of the vaccinee are first targeted by the virus. Replication in Langerhans cells in the skin was observed for flaviviruses such as DENV and WNV, and this could thus also be possible for YF17D [141]. Additionally, in vitro studies using YF17D showed that human umbilical vein endothelial cells (HUVEC) [142] and hepatocytes [143] can be infected.

Comparing wildtype Asibi and attenuated YF17D virus strain showed that YF17D infected HUVEC and hepatocytes showed stronger antiviral responses as measured by secretion of cytokines such as IL-6 and induction of interferon regulated genes. Interestingly, YF17D can also infect innate immune cells. Several studies show a direct infection of monocyte-derived DCs (mo-DCs) with YF17D inducing cell activation and expression of costimulatory molecules and activation markers in vitro [144-146].

In mo-DCs, YF17D virus already co-localized with Lamp2 in lysosomal compartments 90 minutes after infection. Restricted viral replication in DCs with almost no apoptosis could be found after 48 hours, thereby suggesting rapid containment of the virus in DCs [146]. pDCs were shown to produce IFN-α upon viral infection with YF17D involving viral sensor RIG-I and upon cell-cell contact to YF17D virus-infected cells [147].

Many immunological studies use mice as a model organism to study the interplay of different immune compartments and host-pathogen interactions. However, wild-type mice cannot be productively infected with YF17D due to their strong type I IFN response to YF17D. YFV NS5 protein antagonizes type I IFN signaling by binding STAT2 but mouse STAT2 is resistant to this immune evasion mechanism [148]. Additionally, most laboratory mice express an Oas1b giving them resistance to flavivirus infections [149]. Although mice deficient in key antiviral pathways are susceptible to infection with YF17D, the clinical manifestation of YF17D infection often differs from that seen in humans [150]. Splenic DCs from TLR-deficient mice strains could not be productively infected with YF17D but showed involvement of TLR2, 7, and 9 in the viral recognition and antiviral response to YF17D as seen by changes in the cytokine response [151].

A129 mice that are deficient in type I IFN receptor, showed only localized viral replication and no clinical manifestation after footpad injection. Furthermore, intraperitoneal injection of YF17D led to no viral signal in adult mice and also no clinical manifestation. However, intracranial injection of YF17D induced viral replication in multiple organs, including the brain, lung, heart, spleen, liver, kidney, intestine, and testicle, in addition to invasion of the neuronal system [152]. Infection of A129 mice with YF17D also led to limited replication in the draining lymph nodes after subcutaneous injection in the foot pad [150].

However, in these knockout mice strains the attenuation of adaptive and innate immunity limits the information gained on the interaction of the pathogen with the immune system. A study on humanized mice (NRG-HIS: Non-obese diabetic mice showing deficiencies for Rag1 and IL-2 receptor γ) showed viremia after intravenous infection with YF17D that could not be cleared by the mice [153]. Viral replication was found in peripheral pDCs, B cells, and macrophages and prevailed mainly in B cells and macrophages as well as in spleen resident human cells [153].

The infection and activation of primary human DC subpopulations and other APCs such as B cells and monocyte subpopulations by YF17D vaccination could therefore be one mechanism of viral replication and might lead to a controlled amplification of antigens enabling optimal antigen presentation. However, due to the imperfect representation of the human hematopoietic system in these mice, as well as dissimilarities between the human and murine immune systems, especially in regard to flavivirus infections, immune responses to YF17D in humans need to be further analyzed. Ongoing research is actively investigating which cells from the human peripheral blood are preferably infected by YF17D and which nucleic acid-sensing mechanisms control viral replication and lead to cell activation.

1.4.2 SARS-CoV-2 viral infection and innate immune response

SARS-CoV-2 emerged as a novel virus strain in December 2019 [154], and according to WHO statistics has caused a total of over 265 million infections and over 5 million deaths to date (December 2021). A better understanding of the progression of its associated disease (COVID-19) is crucial to determine patient-specific medical treatment and to develop suitable antiviral agents and vaccines. COVID-19 is characterized by heterogeneous clinical manifestations extending from an asymptomatic, mild, or moderate progression to severe disease, and can lead to acute respiratory distress syndrome and multiorgan failure in some infected persons [155].

Prolonged activation of innate and adaptive immune cells, severe inflammation, and lung immunopathology were observed in patients with severe COVID-19 pneumonia [155]. Furthermore, lymphopenia and T cell dysfunctionality were detected in severe cases [156-158], indicating impaired adaptive immunity. Inflammatory cytokines, e.g., IL-6, TNF-

α, IL-1β, and chemokine (e.g., CXCL10 and CCL2), correlated with disease severity [155, 159, 160].

COVID-19 patients also have decreased numbers of cDCs in their blood, and the frequencies of activated cDC2 were shown to increase in the lungs of COVID-19 patients with a severe form of the disease. Their pDCs were also found to be reduced and functionally impaired [161-164]. In COVID-19, monocytes have been shown to accumulate in the inflamed tissue where they can produce pro-inflammatory cytokines that are thought to promote disease progression and tissue damage [165] and an increase of immature granulocytes and monocytes has been described in the peripheral blood [166].The pathogenesis of this disease seems to be strongly impacted by the host immune response, with dynamic interactions of the virus influencing the disease progression and outcome.

Therefore, a dysregulated innate immune response may lead to an alteration of monocyte and DC activation and function, causing an altered and less efficient T and B cell response. Comparing the highly controlled and effective immune response after YF17D vaccination with a dysregulated immune response as observed in patients with COVID-19 could help identify important regulators of the innate immune response.

2. Aims of the study

The YF17D vaccine is one of the most successful vaccines available, inducing life-long protective immunity without requiring a booster vaccination. The innate immune system is thought to play an important role in inducing this effective immune response, with APCs playing a crucial role in initiating host defense mechanisms through antigen presentation and cytokine production.

Advancing our understanding of how the YF17D vaccine virus triggers the innate immune response, which APC subpopulations participate, and how these signals regulate the adaptive immune response is essential for understanding immune reactions to viral infections, for improving antiviral therapies, and for developing new vaccines.

Aim 1: Characterization of YF17D infected cells and their response to infection

One could hypothesize that the reason for the efficacy of YF17D is the concerted activation of multiple virus nucleic acid sensing pathways, such as TLRs or RIG-I, in specific APC subpopulations. Previous studies showed that the YF17D virus can infect isolated pDCs and mo-DCs in vitro [144, 167]. A direct and controlled viral infection of APCs could be a mechanism leading to a finely adjusted innate immune response with optimal APC activation and presentation of viral antigens. APCs could be infected by the vaccine virus at the injection site and in the draining lymph node, but could also be exposed to the virus when circulating in the blood due to the transient viremia that is detected in YF17D vaccinees. Understanding which cells can be infected in the peripheral blood, how APCs get activated by YF17D infection, and which cells permit viral replication could help elucidate the mechanism whereby the YF17D vaccination leads to such an efficient immune response.
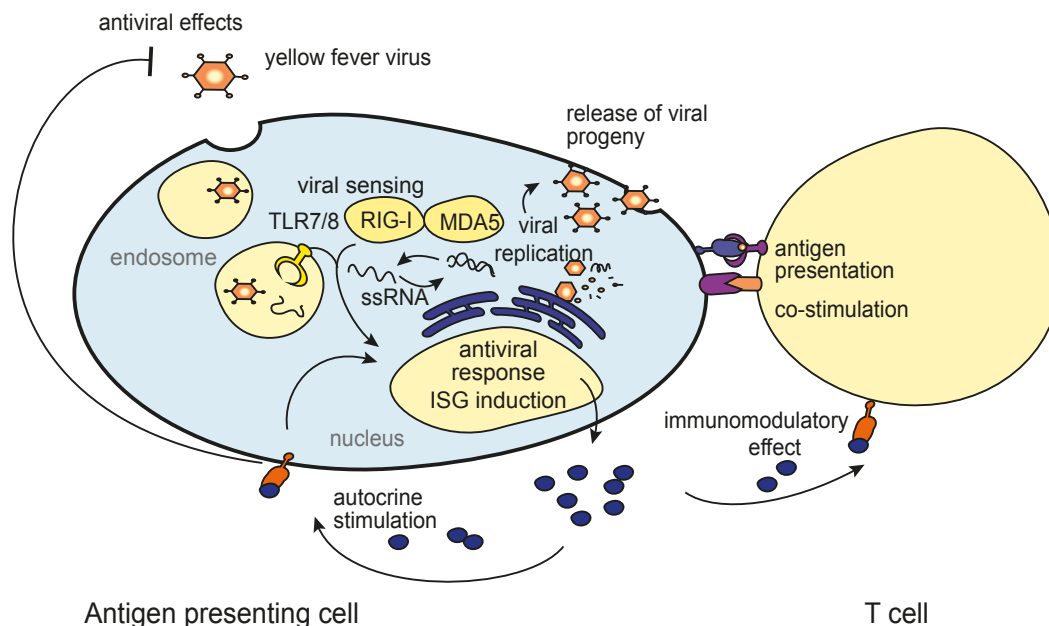
Figure 4: Hypothesis: YF17D infects APCs and replicates.
Viral RNA is potentially detected in APCs by TLR7/8 and RIG-I/MDA5, which activate pathways inducing the transcription of antiviral genes in the cell nucleus. Secretion of inflammatory cytokines and especially type 1 IFN is induced. These soluble molecules have an autocrine effect with the induction of antiviral responses and activation of APCs. At the same time, they can stimulate and recruit immune cells to the site of infection. A controlled viral replication leads to an optimal presentation of viral antigens on MHC class I and II, and together with the costimulatory and cytokine signals specific T cells are activated, expanded, and differentiated.

Aim 2: Determination of the response to YF17D vaccination in human primary antigen-presenting cell subpopulations

Describing the response of APCs to yellow fever vaccination ex vivo could help to identify what an optimally coordinated activation of DC and monocyte subpopulations looks like in the human immune system. These features could then be imitated for the development of effective vaccines against other infectious agents. To explain which cell populations play a role in the well-regulated innate immune response to YF17D, the aim was to analyze the frequency of APC subsets and the expression of functionally relevant cell surface molecules including costimulatory molecules, type I IFN induced molecules, and chemokine receptors before vaccination and at different time points after vaccination by multidimensional flow cytometry. This analysis included all circulating DC and monocyte subsets, also tDCs and DC3, whose response to viral infection and vaccination had not previously been characterized.

Aim 3: Elucidation of the cell-type-specific and time-dependent transcriptome response to YF17D vaccination as an in vivo model of acute RNA virus infection in humans

The next aim was to perform a transcriptome analysis of all human APC subpopulations in healthy donors before and at different time points after YF17D vaccination. The purpose of this high-resolution analysis was to identify time-dependent gene expression programs induced by this acute RNA virus infection that are either common to several APC subsets or cell type-specific and to identify master regulators such as transcription factors and signaling hubs of the innate immune response from these results.

Aim 4: Comparing the well-regulated innate immune response to YF17D vaccination to that of SARS-CoV-2 infection

As highlighted in the section 1.4.2, immune dysregulation is one of the main factors determining disease severity in COVID-19 patients. It was thus hypothesized that in patients that develop severe COVID-19 pneumonia, an imbalanced innate immune response might lead to an alteration of monocyte and DC activation that has direct consequences for the T and B cell response. Therefore, the aim was to compare the highly controlled innate immune response to YF17D vaccination to the response to SARS-CoV-2 infection in non-hospitalized patients with a mild course of COVID-19 and in hospitalized patients with a more severe disease progression.

Aim 5: Understanding the interplay of dysregulated DCs and the adaptive immune response in hospitalized COVID-19 patients

To better understand the immunopathology found in COVID-19 patients with a severe disease progression and its consequence for adaptive immunity, the aim was to correlate parameters of the innate immune response, including the frequency and phenotype of circulating APC subsets and systemic cytokine responses, to clinical and laboratory markers of disease severity and parameters of the adaptive immune response.

3. Materials and Methods

3.1 Materials

3.1.1 Cell lines, virus strains, and primary cells

3.1.1.1 Cell lines

The VeroB4 and BHK21 cell lines were obtained as frozen cultures from DSMZ (ACC33, ACC 61, Braunschweig, Germany).

3.1.1.2 Virus strains

YF17D virus was amplified in-house from the vaccine YF17D-204 Stamaril (Sanofi, Berlin, Germany). The Venus-YF17D virus, in which the Venus fluorescence protein is inserted into the open reading frame of YF17D behind the first 25 amino acids of the capsid, after which the complete YFV polyprotein follows [168], was kindly provided by Dr. Simon Rothenfusser (Department of Internal Medicine, LMU, Munich, Germany).

3.1.2 Cytokines cell stimuli and inhibitors

Table 1: Cytokines, cell stimuli, and inhibitors.

Reagent	Catalog number	Company
GMCSF	300-03	Peprotech
IL-2	202-IL-010	R&D Systems
IL-4	rcyec-hil4	Invivogen
LPS	L4391-1MG	Sigma Aldrich
R848	tlrl-r848	Invivogen
Cpg B 2006	tlrl-2006	Invivogen
Ruxolitinib (solved in DMSO)	tlrl-rux	Invivogen
BX795 (solved in DMSO)	tlrl-bx7	Invivogen
IFNAR blocking antibody IFN α blocking IFN β blocking	PBL31410-1 PBL31101-1 PBL21385-1	Acris

3.1.3 ELISA and Legendplex

Table 2: Cytokine detection kits.

Reagent	Catalog number	Company
LEGENDplex™ human inflammation assay	740809	BioLegend
LEGENDplex™ T helper assay	741028	BioLegend
CXCL10/IP-10 ELISA	550926	BD Biosciences
FLT3L ELISA	DY308	R&D Systems
GMCSF ELISA	555126	BD Biosciences
IFN- β DuoSet ELISA	DY814-05	R&D Systems
Custom human 10-plex Legendplex	IL-10 IL-6 IL-27 IL-12p40 IL-12p70 IFN α IP-10 TNF α IL-23p19 IL-1 β	BioLegend

3.1.4 Cell isolation kits

Table 3: Cell isolation kits.

Kit	Catalog number	Company
CD14 MicroBeads	130-050-201	Miltenyi Biotec
Pan Monocyte Isolation Kit	130-096-537	Miltenyi Biotec
Classical Monocyte Isolation Kit	130-117-337	Miltenyi Biotec
CD3 MicroBeads	130-050-101	Miltenyi Biotec
CD19 MicroBeads	130-050-301	Miltenyi Biotec
Dynabeads™ Human DC Enrichment Kit	11308D	ThermoFisher Scientific

3.1.5   Antibodies

Table 4: Antibody panel used for cell sorting for RNA sequencing.

	Company	Catalog Number	Fluorophore	Dilution
CD3	BioLegend	981002	FITC	1:100
CD123	Invitrogen	45-1239-42	PerCPCy5.5	1:100
CD20	BioLegend	302304	FITC	1:100
CD19	BioLegend	302237	BV650	1:100
CD56	BioLegend	304604	FITC	1:40
CD14	BioLegend	301814	PE Cy7	1:200
CD16	BioLegend	302018	APC Cy7	1:100
HLA-DR	BioLegend	307640	BV605	1:40
CD33	BioLegend	366621	BV421	1:200
CD1c	BioLegend	331534	BV510	1:50
CD141	BioLegend	344116	BV785	1:50
Axl	R&D Systems	FAB154P	PE	1:100
Live	BioLegend	423110	ECD	1:1000
CD88	BioLegend	344310	APC	1:100
CD89	BioLegend	354106	APC	1:50
CD5	BioLegend	364026	AF700	1:50

Table 5: Antibody panel used for in vitro culture of monocytes and mo-DCs.
For monocytes CD88 was measured, for mo-DCs instead CD11c was measured.

	Company	Catalog Number	Fluorophore	Dilution
CD1a	eBioscience	48-0019-42	eF450	1:200
HLA-DR	BioLegend	307646	BV510	1:50
CD86	BioLegend	105036	BV605	1:100
CD80	BD Biosciences	564158	BV650	1:50
PD-L1	ThermoFisher Scientific	15-5983-42	PE Cy5	1:100
CD88	BioLegend	344318	PE dazzle 594	1:50
CD11c	BioLegend	337228	PE dazzle 594	1:200
CD14	BioLegend	301814	PE Cy7	1:200
CD16	BioLegend	302026	AF700	1:100
CD83	BioLegend	305312	APC	1:50
Live	BioLegend	423106	Zombie NIR	1:1000

Table 6: Antibody panel used for ex vivo analysis of APC populations frequencies, activation markers and chemokine receptors after vaccination with YF17D

	Company	Catalog Number	Fluorophore	Dilution
Axl	R&D Systems	AB2859N.025	PE	1:100
CCR2	BD Biosciences	750472	BUV661	1:100
CD123	Invitrogen	45-1239-42	PerCP Cy5.5	1:100
CD135	BioLegend	344208	PE Cy7	1:50
CD14	BioLegend	301836	BV650	1:200
CD141	BioLegend	344116	BV785	1:50
CD16	BioLegend	302036	BV570	1:100
CD163	BD Biosciences	746549	BV480	1:50
CD19	BioLegend	302206	BV421	1:100
CD1c	BioLegend	331520	APC Cy7	1:50
CD20	BioLegend	302304	FITC	1:100
CD301	Novus Biologicals	FAB4881T	AF594	1:50
CD33	BD Biosciences	740293	BUV395	1:50
CD40	ThermoFisher Scientific	8-409-42	eF450	1:100
CD5	BioLegend	364026	AF700	1:50
CD56	BioLegend	304604	FITC	1:50
CD83	ThermoFisher Scientific	46-0839-42	PerCP eF	1:50
CD86	BioLegend	105036	BV605	1:100
CD88	BioLegend	344310	APC	1:50
CD89	BioLegend	354106	APC	1:100
CX3CR1	BioLegend	341630	BV711	1:100
CXCR3	BD Biosciences	741866	BUV737	1:25
HLA-DR	BioLegend	307646	BV510	1:50
Live	eBioscience	65-0866-18	eFluor 506	1:1000
PD-L1	ThermoFisher Scientific	15-5983-42	PE Cy5	1:100
Siglec 1	BioLegend	346016	PE dazzle 594	1:50
TREM-1	BD Biosciences	564472	AF647	1:200
XCR1	BioLegend	372610	BV421	1:100
CD3	BioLegend	981002	FITC	1:100
Live	ThermoFisher Scientific		eF506	1:1000

Table 7: Antibody panel for whole PBMCs RNAFlow lymphocytes.

	Company	Catalog Number	Fluorophore	Dilution
CD56	BioLegend	355504	PE	1:50
CD3	eBioscience	48-0037-42	BV421	1:200
CD19	BioLegend	302237	BV650	1:200
CD86	BioLegend	105036	BV605	1:100
HLA-DR	BioLegend	307646	BV510	1:50
Live	BioLegend		Zombie Red	1:1000
RNA probe			APC	

Table 8: Antibody panel for whole PBMCs RNAFlow DCs and monocytes.

	Company	Catalog Number	Fluorophore	Dilution
CD3	eBioscience	48-0037-42	BV421	1:200
CD20	BioLegend	302329	BV421	1:200
CD56	BioLegend	362551	BV421	1:50
CD16	BioLegend	302026	AF700	1:100
CD14	BioLegend	301835	BV650	1:100
HLA-DR	BioLegend	307646	BV510	1:50
CD11c	BioLegend	301606	PE	1:100
CD86	BioLegend	105036	BV605	1:100
RNA probe			APC	

Table 9: Antibody panel for whole PBMCs DCs and monocytes.

	Company	Catalog Number	Fluorophore	Dilution
CD3	eBioscience	48-0037-42	BV421	1:200
CD20	BioLegend	302329	BV421	1:200
CD56	BioLegend	362551	BV421	1:50
CD16	BioLegend	302026	AF700	1:100
CD14	BioLegend	301814	PE Cy7	1:200
HLA-DR	BioLegend	307640	BV605	1:40
CD11c	eBioscience	17-0128-42	APC	1:100
CD141	BioLegend	344116	BV785	1:50
CD123	Invitrogen	45-1239-42	PerCP Cy5.5	1:100
CD1c	BioLegend	331520	APC Cy7	1:50
CD19	BioLegend	302237	BV650	1:200
Axl	R&D Systems	AB2859N.025	PE	1:100
Live	ThermoFisher Scientific		eF506	1:1000
Virus			Venus	

Table 10: Antibody panel for whole PBMCs lymphocytes.

	Company	Catalog Number	Fluorophore	Dilution
CD3	eBioscience	48-0037-42	BV421	1:200
CD19	BioLegend	302237	BV650	1:200
CD16	BioLegend	302026	AF700	1:100
CD56	BioLegend	355504	PE	1:50
CD14	BioLegend	301814	PE Cy7	1:200
CD4	eBioscience	17-0048-42	APC	1:100
CD86	BioLegend	105036	BV605	1:100
Live	BioLegend		Zombie Red	1:1000
Virus			Venus	

Table 11: Antibody panel for coculture between VeroB4/BHK21 cells and monocytes/mo-DCs.

	Company	Catalog Number	Fluorophore	Dilution
HLA-DR	BioLegend	307646	BV510	1:50
CD80	BD Biosciences	564158	BV650	1:50
CD83	BioLegend	305312	APC	1:50
CD86	BioLegend	105036	BV605	1:100
PD-L1	BioLegend	374506	PE Cy7	1:100
CD14	Miltenyi Biotec	130-113-150	PerCP	1:400
Live	BioLegend		Zombie NIR	1:100
YF17D			Venus	
CD45	BioLegend	304024	AF700	1:100
CD11c	BioLegend	337228	ECD	1:100
CD1a	eBioscience	48-0019-42	eF450	1:100

Table 12: Antibody panel for in vitro infection of tonsil cells DC and monocytes.

	Company	Catalog Number	Fluorophore	Dilution
YF17D			Venus	
CD3	eBioscience	48-0037-42	BV421	1:200
CD56	BioLegend	362551	BV421	1:50
CD19	BioLegend	302234	BV421	
HLA-DR	BioLegend	307646	BV510	1:50
CD86	BioLegend	105036	BV605	1:100
CD11c	BioLegend	337228	ECD	1:100
CD14	BioLegend	301814	PE Cy7	1:200
CD16	BioLegend	302026	AF700	1:100
CD83	BioLegend	305312	APC	1:50
Live	BioLegend		Zombie NIR	1:100
CD45	eBioscience	12-0458-42	PE	1:100

Table 13: Antibody panel for in vitro infection of tonsil cells lymphocytes.

	Company	Catalog Number	Fluorophore	Dilution
CD56	BioLegend	304604	FITC	1:40
CD14	BioLegend	367116	FITC	1:100
CD16	BioLegend	302006	FITC	1:100
CD4	BioLegend	317434	BV421	1:100
CD19	BioLegend	302230	PerCP Cy5.5	1:50
CXCR5	BioLegend	356908	APC	1:20
CD38	BioLegend	303506	PE	1:100
HLA-DR	BioLegend	307616	PE Cy7	1:100
CD8	BioLegend	302814	BV510	1:100
CD3	BioLegend	300460	BV605	1:200
CD20	BioLegend	302336	BV650	1:100
Live	BioLegend		Zombie Red	1:100
CD27	BioLegend	302814	AF700	1:100
PD-1	BioLegend	329954	APC Fire	1:50

Table 14: Antibody panel for ex vivo staining for YF17D vaccinees with Ki67.

	Company	Catalog Number	Fluorophore	Dilution
CD3	BioLegend	981002	FITC	1:100
CD56	BioLegend	304604	FITC	1:40
CD20	BioLegend	302304	FITC	1:100
CD19	BioLegend	302206	FITC	1:100
CD14	BioLegend	367116	FITC	1:100
CD16	BioLegend	302006	FITC	1:100
CD123	Invitrogen	45-1239-42	PerCP Cy5.5	1:100
AXL	R&D Systems	FAB2859N-025	PE	1:100
CD1c	BioLegend	331520	APC Cy7	1:50
CD141	BioLegend	344116	BV785	1:50
HLA-DR	BioLegend	307646	BV510	1:40
Live	BioLegend	423110	Zombie Red	1:1000
CD274	BioLegend	329718	PE Cy7	1:100
CD33	BioLegend	366606	APC	1:50
CD80	BD Biosciences	564158	BV650	1:50
CD86	BioLegend	305430	BV605	1:100
Ki67	BioLegend	350506	BV421	1:100
Live	ThermoFisher Scientific		UV455	1:100

Table 15: Antibody panel for ex vivo staining for COVID-19 patients with Ki67.

	Company	Catalog Number	Fluorophore	Dilution
CD3	BioLegend	981002	FITC	1:00
CD56	BioLegend	304604	FITC	1:40
CD20	BioLegend	302304	FITC	1:100
CD19	BioLegend	302206	FITC	1:100
CD14	BioLegend	301836	BV650	1:100
CD16	BioLegend	302025	AF700	1:100
CD123	Invitrogen	45-1239-42	PerCP Cy5.5	1:100
AXL	R&D Systems	FAB2859N-025	PE	1:100
CD1c	BioLegend	331520	APC Cy7	1:50
CD141	Miltenyi Biotec	130-110-259	APC	1:100
HLA-DR	BioLegend	307646	BV510	1:40
Live	BioLegend	423112	Zombie Green	1:1000
CD274	BioLegend	329718	PE Cy7	1:100
CD11c	BioLegend	337228	ECD	1:200
CD86	BioLegend	305430	BV605	1:100
Ki67	BioLegend	350506	BV421	1:100
CD15	BioLegend	301904	FITC	1:100

Table 16: Antibody panel for coculture of DC3/monocytes and T cells from COVID-19 patients.

	Company	Catalog Number	Fluorophore	Dilution
Live			Zombie Red	1:1000
CD3	BioLegend	981002	FITC	1:100
CD4	BioLegend	317436	BV650	1:100
CTV	ThermoFisher Scientific		eF450	
CD38	BioLegend	303506	PE	1:100
HLA-DR	BioLegend	307616	PE Cy7	1:100
CD45RA	BioLegend	304120	AF700	1:100
CD69	BioLegend	310938	BV605	1:100
PD-1	BioLegend	329954	APC Fire	1:50

Table 17: Antibody panel for progenitor panel of COVID-19 patients.

	Company	Catalog Number	Fluorophore	Dilution
CD115	BioLegend	347310	PerCP Cy5.5	1:50
CD117	BioLegend	313218	BV605	1:50
CD123	Invitrogen	45-1239-42	PerCP Cy5.5	1:100
CD127	BioLegend	351304	PE	1:200
CD135	BioLegend	313314	PE Cy7	1:50
CD14	Miltenyi Biotec	130-113-150	PerCP	1:400

CD141	BioLegend	344116	BV785	1:50
CD15	BioLegend	301904	FITC	1:100
CD16	BioLegend	302036	BV570	1:100
CD163	BD Biosciences	746549	BV480	1:50
CD19	BioLegend	302206	FITC	1:100
CD1c	BioLegend	331520	APC Cy7	1:50
CD20	BioLegend	302304	FITC	1:100
CD3	BioLegend	981002	FITC	1:100
CD33	BD Biosciences	740293	BUV395	1:50
CD34	BioLegend	343528	BV510	1:50
CD45RA	BioLegend	304120	AF700	1:100
CD56	BioLegend	304604	FITC	1:50
CD66b	BioLegend	305104	FITC	1:100
CD88	BioLegend	344310	APC	1:50
CD89	BioLegend	354106	APC	1:100
Live	eBioscience		UV455	1:1000
HLA-DR	BioLegend	307643	BV711	1:50
Ki67	BioLegend	350506	BV421	1:100
Siglec 1	BioLegend	346016	PE dazzle 594	1:50

Table 18: Antibody panel for ex vivo analysis of APC populations frequencies, activation markers and chemokine receptors for hospitalized COVID-19 patients.

	Company	Catalog Number	Fluorophore	Dilution
Axl	R&D Systems	AB2859N.025	PE	1:100
CCR2	BD Biosciences	750472	BUV661	1:100
CD123	Invitrogen	45-1239-42	PerCP Cy5.5	1:100
CD143	BioLegend	344208	PE Cy7	1:100
CD14	BioLegend	301836	BV650	1:200
CD141	BioLegend	344116	BV785	1:50
CD16	BioLegend	302036	BV570	1:100
CD163	BD Biosciences	746549	BV480	1:50
CD19	BioLegend	302206	FITC	1:100
CD1c	BioLegend	331520	APC Cy7	1:50
CD20	BioLegend	302304	FITC	1:100
CD15	BioLegend	301904	FITC	1:100
CD33	BD Biosciences	740293	BUV395	1:50
CD40	ThermoFisher Scientific	8-409-42	eF450	1:100
CD5	BioLegend	364026	AF700	1:50
CD56	BioLegend	304604	FITC	1:50
CD66b	BioLegend	305104	FITC	1:100
CD86	BioLegend	105036	BV605	1:100
CD88	BioLegend	344310	APC	1:50
CD89	BioLegend	354106	APC	1:100

CX3CR1	BioLegend	341630	BV711	1:100
CXCR3	BD Biosciences	741866	BUV737	1:25
HLA-DR	BioLegend	307646	BV510	1:50
Live	eBioscience	65-0866-18	eFluor 506	1:1000
PD-L1	ThermoFisher Scientific	15-5983-42	PE Cy5	1:100
Siglec 1	BioLegend	346016	PE dazzle 594	1:50
TREM-1	BD Biosciences	564472	AF647	1:200
XCR1	BioLegend	372610	BV421	1:100
CD3	BioLegend	981002	FITC	1:100

Table 19: Antibody panel for ex vivo staining for hospitalized COVID-19 patients with Ki67.

	Company	Catalog Number	Fluorophore	Dilution
Axl	R&D Systems	AB2859N.025	PE	1:100
CD3	BioLegend	981002	FITC	1:100
CD19	BioLegend	302206	FITC	1:100
CD20	BioLegend	302304	FITC	1:100
CD56	BioLegend	304604	FITC	1:50
CD15	BioLegend	301904	FITC	1:100
CD66b	BioLegend	305104	FITC	1:100
PD-L1	BioLegend	329718	PE Cy7	1:100
HLA-DR	BioLegend	307646	BV510	1:50
CD123	Invitrogen	45-1239-42	PerCP Cy5.5	1:100
CD141	BioLegend	344116	BV785	1:50
CD1c	BioLegend	331520	APC Cy7	1:50
Live			UV	1:1000
CD80	BD	564158	BV650	1:50
CD86	BioLegend	305430	BV605	1:100
CD5	BioLegend	364026	AF700	1:100
CD14	BioLegend	301814	PE Cy7	1:200
CD16	BioLegend	302036	BV570	1:100
CD33	BD	740293	BUV395	1:50
CD88	BioLegend	344310	APC	1:50
CD89	BioLegend	354106	APC	1:100
Ki67	BioLegend	350506	BV421	1:100
CD163	BD	746549	BV480	1:50

3.1.6 Buffers, solutions, and media

Table 20: Buffers, solutions, and media.

Solution	Component	Concentration	Company
MACS buffer	PBS EDTA FCS	 2 mM 2 % (v/v)	ThermoFisher Scientific
DC medium	RPMI 1640 Heat inactivated FCS Penicillin Streptomycin Non-essential amino acids GlutaMAX™ β-Mercaptoethanol Sodium pyruvate	 10 % 100 U/ml 100 µg/ml 1 % 2 mM 0.05 mM 1 mM	Gibco life technologies
Sorting medium	DC medium EDTA	 2 mM	
TNE buffer	TRIS HCL pH 8 NaCl EDTA	20 mM 150 mM 2 mM	Carl Roth Carl Roth Carl Roth
Sucrose 60%	Sucrose TNE buffer		Carl Roth
PEG 8000	PEG 8000		Carl Roth
Homemade permeabilization buffer	Saponin 1% BSA 0.01% Sodium azide	0.5 % 1 % 0.01 %	
BHK21/VeroB4 medium	DMEM Heat inactivated FCS Penicillin Streptomycin GlutaMAX™	 10 % 100 U/ml 100 µg/ml 2 mM	ThermoFisher Scientific
Primary DC medium	RPMI-1640 Panexin NTS Panexin NTA Sodium pyruvate GlutaMAX™ Penicillin Streptomycin	 5 % 5 % 1 mM 2 mM 100 U/ml 100 µg/ml	Gibco life technologies Pan-Biotech Pan-Biotech
Crystal Violet solution	Crystal Violet Sodium chloride Formaldehyde (37%) Ethanol	12.5 mM 137 mM 5 % 50 %	Fluka Sigma Aldrich
Freezing Medium	DMSO (dimethyl sulfoxide) FCS (fetal calf serum)	10 % 90 %	Sigma Aldrich

3.1.7 Reagents used for Smart-seqv2 RNA sequencing

Table 21: Reagents used for Smart-seqv2

Reagent	Company	Catalog Number
CD3 beads	Miltenyi Biotec	130-050-101
FcR Blocking Reagent, human	Miltenyi Biotec	130-059-901
RLT Buffer	Qiagen	1053393
Qiagen RNeasy Plus Microkit	Qiagen	74034
DEPC	Thermo	46-2224
RNA Pico Chip	Agilent Technologies	5067-1513
ERCC Spike in	ThermoFisher Scientific	4456740
Oligo-dT30VN, Desalted, 0,04 µmol, diss. 100 µM, QC: Mass Check, DNA OligoSequence: 5'- AAG CAG TGG TAT CAA CGC AGA GTA CTT TTT TTT TTT TTT TTT TTT TTT TTT TTT TVN -3', (No. Bases: 57)	Metabion international AG	Custom made
dNTP	Promega	U1515
Betaine	Sigma Aldrich	61962-50G
SuperScript™ II Reverse Transcriptase	Thermo	74034
RNasin® Plus Ribonuclease Inhibitors	Promega	N2611
Magnesium chloride solution	Sigma Aldrich	M1028-10X1ML
QuantiFluor® dsDNA System	Promega	E2670
TE buffer low EDTA	VWR	J75793
Agilent high-sensitivity DNA kit	Agilent Technologies	5067-4626
KAPA HiFi HotStart ReadyMix	Roche	7958935001
Agencourt AMPure XP, 60 mL	Beckman Coulter	A63881
TSO: /5Biosg/AAGCAGTGGTATCAAC-GCAGAGTGAATrGrG+G - 250 nmole RNA oligo, RNase-Free HPLC Purification	Qiagen	Custom made
ISPCR oligo (5′-AAGCAGTGGTATCAAC-GCAGAGT-3′	Qiagen	Custom made
Ethanol	AppliChem	A1613,1000PE
ILMN Tag DNA Enzyme & Buffer Small Kit	Illumina	20034197
I7 and i5 primers	Qiagen	Custom made

3.2   Methods

3.2.1.1 Primary cell and plasma acquisition

Blood samples for isolation of peripheral blood mononuclear cells (PBMC) from healthy donors were obtained either from the Thrombocyte donation center (LMU Klinikum, Munich, Germany) or from healthy donors recruited to the laboratory (with approval of the LMU ethics committee, no. 18-415). Blood was drawn using S-Monovette Sodium-Heparin (Sarstedt, Nürnbrecht, Germany).

PBMC from YF17D vaccinees were obtained from a larger cohort build by our collaboration partners at the Division of Infectious Diseases and Tropical Medicine and the Department of Clinical Pharmacology (Prof. Dr. Simon Rothenfusser), University Hospital (LMU, Munich, Germany).

Blood from YF17D vaccinees was drawn in the same fashion as described for healthy donors. All participants were healthy (aged 21 to 35 years) and had not been previously exposed to the wild type YFV and were not previously immunized. After giving informed consent, the patients received a single subcutaneous injection of the YF17D vaccine (Stamaril, Sanofi Pasteur, Lyon, France) at the Division of Infectious Diseases and Tropical Medicine at LMU Munich. Blood was sampled directly before vaccination and on days 3, 7, 14, and 28 after vaccination (with approval of LMU ethics committee no. 86-16, 229-12 and 592-16).

In collaboration with Dr. Christof Geldmacher and Tabea Eser, blood samples from outpatient COVID-19 patients were collected by the Division of Infectious Diseases and Tropical Medicine, University Hospital, LMU, Munich, Germany. Recruitment was done by providing information and contact details to households of Munich with at least one registered positive polymerase chain reaction (PCR) test for SARS-CoV-2 reported to the health department of Munich. Samples used in this study were collected between April 2020 and February 2021. PCR-positive individuals and their respective household members were enrolled, and blood samples were collected during household visits or at a central testing facility with approval from the LMU ethics committee (no. 20-692 and 20-371) [169].

Blood samples from hospitalized COVID-19 patients were collected in S-Monovette Lithium-Heparin tubes by the COVID-19 Registry of the LMU University Hospital Munich with approval from the LMU ethics committee (no. 20-24 and 592-16, CORKUM, WHO trial ID DRKS00021225) at the LMU Klinikum.

Between March 2020 and January 2021, blood samples were collected from consenting patients ($\geq$ 18 years) diagnosed with COVID-19 by means of a positive SARS-CoV-2 PCR result at the LMU Klinikum by the CORKUM biobank. Cryopreserved PBMC samples of 26 patients and fresh blood samples from 48 patients were obtained from the CORKUM biobank from which PBMC were prepared in our laboratory at the Institute of Immunology. As controls for this cohort, freshly prepared or cryopreserved PBMCs either from leukocyte reduction chambers after thrombocyte donations of healthy donors aged 22–54 years or from blood of healthy donors or patients with negative SARS-CoV-2 PCR results that were hospitalized for other reasons were used. The disease severity was graded according to the ordinal WHO scale. 1: no limitations of activity; 2: limitations of activity, 3: hospitalized, no oxygen; 4: oxygen by mask or nasal tube; 5: non-invasive ventilation; 6: invasive ventilation; 7: organ support (extracorporeal membrane oxygenation); 8: death [170]. Blood samples of recovered patients were also collected, including patients who were either discharged with $\leq$ WHO score 2 and > 21 days after diagnosis or who were recruited > 30 days after primary diagnosis and still hospitalized for other reasons [171].

Human tonsils were obtained from tonsillectomies and kindly provided by Dr. med. Christoph Reichel (Klinikum Großhadern, Klinik und Poliklinik für Hals-Nasen-Ohrenheilkunde).

3.2.2 Cell culture

Cell cultures were maintained at 37°C in a humidified incubator with 5% CO_2 atmosphere. All cell culture media used are listed in Table 20.

3.2.2.1 Cell lines

Cell lines were inspected daily under a bright-field microscope (Leica, DM IL LED) and split every 3 to 5 days when confluence was reached in ratios between 1:3 and 1:10 depending on the cell density. For splitting of the cells, adherent VeroB4 and BHK21 were washed with PBS and detached from the culture flask by incubation with 1 x trypsin/EDTA solution for 1 to 5 min at 37 °C. The enzymatic reaction was stopped by the addition of VeroB4/BHK21 medium. Cells were then centrifuged, resuspended in medium, and plated in a new flask at the appropriate density. The cell lines were cultured for a maximum of 15 passages. Only cells cultured for less than 10 passages were used for viral production and plaque assays.

3.2.2.2 Primary cell preparation and culture

Tonsil cells were isolated by mechanical disruption of the tonsil on a 0.45 µm filter using a syringe plug, after which they were washed with DC medium and filtered again through a 0.45 µm filter. Tonsil cells were either used directly or frozen in 10 % DMSO in FCS in liquid nitrogen.

PBMCs were isolated from blood by gradient centrifugation. Up to 15 ml blood was diluted 1:2 in PBS and overlayed on 15 ml Biocoll solution in a 50 ml Falcon tube. Centrifugation was performed at room temperature (RT), for 45 min at 1 500 rpm without breaks (acceleration = 1, deceleration = 0). The interphase containing PBMCs was harvested, washed once with PBS, and erythrolysis was performed using red blood lysis buffer (Sigma Aldrich, cat. # R7757-100ml) and incubation for 10 min at RT. The PBMCs were subsequently washed twice using MACS buffer.

Primary monocytes were isolated by magnetic activated cell sorting (MACS, Miltenyi Biotec) using a Classical Monocyte Isolation Kit or Pan Monocyte Isolation Kit. Alternatively, monocytes were isolated by cell sorting. Monocytes were cultured in DC medium containing low-dose GMCSF (200 U/ml) for up to 72 hours. For generation of mo-DCs, monocytes were isolated by magnetic cell sorting using CD14^{+} microbeads or Classical Monocyte Isolation Kit.

Primary DCs were sorted and cultured in primary DC medium. For pDC culture, 10 ng/ml IL-3 was added. Primary DCs could be cultured for up to 48 hours.

3.2.2.3 Generation of mo-DCs

Mo-DCs were generated from monocytes isolated from PBMC by magnetic activated cell sorting. The purity after MACS was checked by flow cytometric analysis by staining cells with anti-CD14 antibody. If the purity exceeded 95 %, monocytes were seeded at 2×10^6 cells per well in a 6-well plate in 2 ml DC medium containing 500 U/ml GMCSF and 500 U/ml IL-4. In smaller well-sizes, the same concentration of 10^6/ml medium was used. Cells were incubated at 37 °C for 4 days, and on day 4, 250 U/ml IL-4 was resupplied. On day 6, the mo-DCs were harvested and their differentiation status (indicated by expression of CD14^{low} CD1a$^+$ CD11c$^+$) and maturation (CD83, CD86) was examined using flow cytometry.

3.2.2.4 Coculture of APCs from COVID-19 patients with autologous CD4$^+$ T cells

To determine the functionality of APCs in COVID-19 patients, APCs were cocultured with autologous naïve CD4$^+$ T cells from COVID-19 patients and from healthy control patients that were stimulated with immobilized anti-CD3 antibody. Cells were sorted from PBMCs into DC3 (HLA-DR$^+$, CD88/89$^-$, CD16$^-$, CD56$^-$, CD66b$^-$, CD15$^-$, CD4$^-$, CD8$^-$, CD11c$^+$, CD5$^-$, CD1c$^+$), mo1 (HLA-DR$^+$CD88/89$^+$, CD14$^+$, CD16$^-$, CD56$^-$, CD66b$^-$, CD15$^-$) and CD4$^+$ T cells (CD4$^+$, CD45RA$^+$, CD8$^-$). T cells were labeled with Cell Trace Violet dye (CTV, ThermoFisher Scientific, cat. #C34557) according to the manufacturer's instructions. DC3 and monocytes were then cocultured with the T cells in 150 µl of DC medium on a 96-well flat-bottom plate coated with anti-CD3 antibody (10 µg/ml, BioLegend, cat. # 317325), whereby 7×10^3 DC3 or 5×10^4 monocytes were used per well at a ratio of APC:T cells of 1:2. As a positive control, human T-Activator CD3/CD28 beads (ThermoFisher Scientific, cat. #111.61D) were used to induce T cell proliferation. After 5 days of coculture, cells were harvested, stained, and measured using the CytoFLEX S flow cytometer (Beckman Coulter), and additionally supernatants from the cell culture were also collected and stored at -20°C [171].

3.2.2.5 Coculture of APCs with YF17D infected cell lines

To determine whether cellular contact with virus-infected cells improves viral uptake in APCs compared to free virus, mo-DCs and monocytes were cocultured with virus-infected BHK21 or VeroB4 cells. Cell lines were infected at a density of 5×10^4 cells in a

24-well plate with a multiplicity of infection (MOI) of 0.01 for 24 hours. The cells were subsequently washed, and either monocytes or mo-DCs (0.5 x 10^6) were added onto the cell layer directly or into a transwell separating them from the layer of infected cells (0.4 µM pore size, Corning, cat. #3470). As controls for no cell-to-cell contact, cell-free supernatant of infected BHK21 or VeroB4 was added on APCs in addition to different concentrations of free virus and stimuli such as R848 and LPS. Cells were incubated for 48 hours in the coculture with monocytes, and 36 hours with mo-DCs, before being harvested and stained for flow cytometric measurement with the CytoFLEX S flow cytometer.

3.2.3 Flow cytometry

Up to 5 million cells were incubated with Fc-receptor blocking reagent (Miltenyi Biotec, cat. # 130-059-901) diluted in 50 µl of MACS buffer for 30 min according to the manufacturer's instruction. Surface marker staining was performed in 50 µl PBS containing fluorescently labeled antibodies as indicated in chapter 3.1.5 and incubated for 30 min on ice. Afterward, cells were washed twice with MACS buffer. For biosafety reasons or intracellular staining, cells were fixed with BD Cytofix (BD Biosciences, cat. # 554655), then washed, and subsequently resuspended in MACS buffer. Ki67 was stained intracellularly using the Transcription Factor Staining Buffer Set (ThermoFisher Scientific, cat. # 00-5523-00) following the manufacturer's instructions. Samples were measured using the CytoFLEX S (Beckman Coulter), LSRFortessa, the Cytek Aurora (Cytek Biosciences), or the FACS Aria III cell sorter.

3.2.4 Fluorescence activated cell sorting

For sorting of primary human DC populations for cell culture experiments, T cells were excluded using CD3 magnetic bead isolation (Miltenyi Biotec) and the rest of the PBMCs were enriched for DCs using the Dynabeads enrichment kit (ThermoFisher Scientific). For sorting primary human monocytes, PBMCs after exclusion of T cells with CD3 beads were used (Miltenyi Biotec). Cells were directly sorted with a 100 µm nozzle into an FCS-coated 3 ml FACS tube filled with DC medium containing 2 mM EDTA. For sorting primary human DC populations for RNA sequencing analysis, T cells were separated via CD3 magnetic bead isolation, and the CD3 negative cell fraction was used for cell sorting. Cells were sorted using an 85 µm nozzle either directly into RLT lysis buffer for B cells

or into DCs medium containing 2 mM EDTA and then resorted directly into RLT lysis buffer. Cells were then vortexed, centrifuged (450 g, 4°C, 5 min), and then immediately stored at -80°C until further processing.

3.2.5 RNAFlow Assay for detection of YF17D RNA

The RNAFlow Assay (Affymetrix, eBioscience) was used to detect the viral RNA of YF17D. RNAFlow is an in-situ hybridization assay in which RNA targets are detected via flow cytometry and, due to branched-DNA technology, the fluorescence signal caused by binding to the desired RNA transcript is amplified, thereby increasing the detection sensitivity. The RNAFlow assay was performed according to the manufacturer's instructions except for the target probe hybridization step, in which the incubation with the target probes was prolonged from 2 hours incubation at 40°C to 3 hours of incubation at 40°C to increase the detection of viral RNA.

3.2.6 Microscopy

Brightfield microscopic images were taken with a Leica microscope (type DFC3000 G) using 40x magnification in a flat-bottom cell culture dish. For fluorescence microscopy, cells were transferred onto an 8-well chamber slide (Ibidi cat. # 80841), left to adhere for 10 hours, fixated using 4 % PFA in PBS, and stained with 4′,6-diamidino-2-phenylindole (DAPI)-containing mounting medium (Ibidi, cat. # 50011) and images were taken with an Olympus BX41 fluorescent microscope with 60x magnification.

3.2.7 Virus production

For YF17D virus propagation, the vaccine virus Stamaril was reconstituted and added onto 5×10^6 BHK21 cells in a volume of 2 ml Opti-MEM medium. After 1 hour of incubation, cells were seeded into a T75 flask in BHK21 medium and cultured for 60 hours. The supernatant was collected, aliquoted, and stored at -80 °C as a passage 0 stock. The viral titer was determined as described in chapter 3.2.8. The virus was subsequently further amplified by infecting 15 confluent T75 flasks (Greiner Bio-One, cat. #658175) of BHK21 cells with a virus titer of 0.1 MOI of passage 0 virus stock in 2 ml of Opti-MEM. Cells were incubated for 1 hour at RT and shaken every 15 minutes. DMEM with 10 % FCS was added to the cells, and cells were distributed into 25 flasks. As a medium control,

25 T75 flasks with uninfected BHK21 were treated with the same procedure described below. On day 4 when CPE reached 60 %, cells were scraped off and pooled with their supernatant. Next, the cell suspension was centrifuged at 2 200 g for 5 min at 4 °C. Now, either this passage 1 supernatant was filtered for cell debris and used directly for infection experiments, or supernatant was purified with a sucrose gradient.

For the sucrose-purification, the supernatant was pooled, and the cell pellets were homogenized using a dounce homogenizer, centrifuged again at 2 200 g for 5 min at 4 °C and the remaining supernatant was added to the previously collected supernatant. In a subsequent step, PEG 8000 was gradually added to the virus supernatant to achieve a 7 % (w/v) solution and shaken for 10 min to dissolve the PEG after which the solution was stirred overnight at 4 °C. The PEG supernatant was then centrifuged at 3 800 g for 78 min at 4 °C using a swing-out rotor. Supernatant was discarded, and pellets were resuspended in 1.8 ml of cold TNE buffer, thereby resulting in approximately 4-5 ml of virus PEG stock. The pellet was subsequently homogenized using a dounce homogenizer and pipetted at RT until it dissolved. Sucrose was diluted in TNE buffer, and a sucrose gradient was pipetted into Ultra-clear centrifuge tubes (Beckman Coulter, cat. # 344059) - first with 2 ml of 60 % sucrose, followed by 1 ml of 30 % sucrose and 2.5 ml of the virus solution or the medium control. The samples were then centrifuged using an SW41 rotor for 2 hours at 35 000 rpm at 4 °C without breaks. After ultracentrifugation, the virus layer situated between the 60 % sucrose and 30 % sucrose layers was recovered in addition to the virus-free medium control (Figure 5). If sample was too viscous for pipetting, TNE buffer was added until pipetting was possible, and the sample was aliquoted in aliquots á 2-5 μl and frozen at -80°C.

The sucrose control containing only the virus-free medium from exactly the same number of T75 flasks with BHK21 was treated in exactly the same way and used to compare for unspecific effects of the stock preparation. Heat inactivation of virus was performed by incubation at 56 °C for 1 h. The inability of the heat-inactivated stock to infect cells was confirmed by infection of susceptible cell lines such as VeroB4 or BHK21 and measurement of viral infection by flow cytometry using intracellular staining for anti-4G2 flavivirus antibody (Novus Biologicals, cat. # NBP2-52709AF647). YF17D-Venus stock was prepared in the same way (in the laboratory of Simon Rothenfusser, LMU Munich).
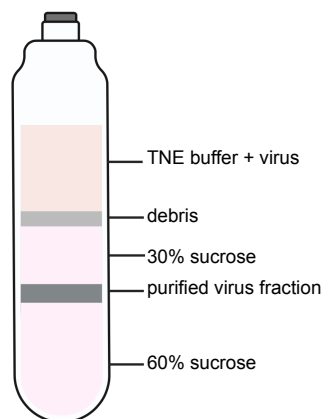
Figure 5: Sucrose gradient for YF17D viral purification.
Layers obtained after sucrose gradient centrifugation for purification of YF17D viral stock. The purified virus fraction is harvested and can subsequently be used for infection studies. Graphic generated using Biorender.

3.2.8   Determination of virus titer by plaque assay

Plaque assays were performed in order to determine the YF17D virus titer. VeroB4 cells were seeded at a concentration of 2 x 10^5 cells/well in 2 ml VeroB4 medium into a 6-well plate and incubated for 24 hours. Ten-fold serial dilutions of the respective virus were prepared in serum-free Opti-MEM. The supernatant from the VeroB4 cells was discarded and 1 ml of each dilution was added to the susceptible cells. To control for reproducibility, each dilution was performed in duplicate. After incubation at 37 °C for 1 hour, the virus was removed, and 2 ml 0.75 % agarose in VeroB4 medium was added to the cells. The semi-solid agarose layer inhibits the diffusion of released virus from infected cells and hence each infectious particle only spreads to neighboring cells. The cytopathic effect of the virus particles is then visible as a plaque. After 5 days for YF17D virus and up to 7 days for Venus-YF17D virus, the agarose layer was removed, and cells were fixated and stained with 1 ml of crystal violet solution for 1 h at RT. The plates were washed in tap water, dried, and the plaques were counted. Crystal violet stains living cells, and thus plaques appeared as clear spots in a purple-colored cell layer. To calculate the multiplicity of infection, the following formula was used:

$$virus\ titer\ \left(\frac{PFU}{ml}\right) = \frac{counted\ plaques * dilution\ factor}{volume\ of\ inoculum}$$

41

3.2.9 Stimulation of cells and inhibition of viral recognition pathways

Lipopolysaccharide (LPS) was used at a concentration of 10 ng/ml, R848 at 3 µM, BX795 at a 200 nM concentration in DMSO. Ruxolitinib was used at 1 µM in DMSO and added 4 hours prior to infection. DMSO controls were used for BX795 and Ruxolitinib experiments to control for unspecific effects of DMSO. To inhibit the type I interferon response, rabbit anti-IFN-α-polyclonal antibody (pAb), rabbit anti-IFN-β-pAb, and anti-IFNAR2-Ab (MMHAR-2, Acris) were used at concentrations of 2 000 U/ml, 5 000 U/ml, and 10 µg/ml respectively. The antibody cocktail was added to the cells 30 min prior to infection experiments. All inhibitors, stimulants and viruses were pipetted into the cell suspensions and mixed by gentle swirling of the plate to reduce unspecific activation of DCs and monocytes.

3.2.10 Determination of cytokine concentration

Cytokines were measured using the LEGENDplex human inflammation assay (cat. # 740809, BioLegend), the LEGENDplex T helper assay (cat. # 741028, BioLegend), and a personalized LEGENDplex assay according to the manufacturer's instructions but using half of all volumes described. FLT3L ELISA (cat. # DY308, R&D Systems) and GMCSF ELISA (cat. # 555126, BD) were performed with 1:2 diluted plasma. CXCL10/IP-10 (cat. # 550926, BD) was measured by ELISA using 1:20 diluted plasma. IFN-β was determined using the IFN-β DuoSet ELISA (R&D Systems, USA) following the manufacturer's protocol using 1:3 diluted medium supernatant.

3.2.11 Adapted Smart-seqv2

RNA was isolated from 1000 sorted cells using the Qiagen RNeasy Plus Microkit (Qiagen, Hilden, Germany) according to the manufacturer's instructions. The RNA was eluted in 10 µl DEPC water and the RNA quality was determined using the Bioanalyzer RNA 6000 pico assay (Agilent Technologies, Santa Clara, California, USA) according to the manufacturer's instructions. The library preparation was adapted from the Smart-seqv2 protocol [172] whereby 3.7 µl of isolated RNA were then transferred into a 96-well plate and 0.2 µl of 1:125 000 diluted ERCC spike-ins, 0.1 µl of Oligo-DT VN 30 Primer (100 mM), and 1 µl of dNTP Mix (10 mM) were added using the Mantis Liquid Handler (Formulatrix). The plate was vortexed, centrifuged, and immediately incubated at 72 °C

for 3 min and before being placed on a cooling rack. Subsequently, 5 µl reverse transcription master mix was added according to Table 22. The samples were mixed by gentle pipetting and incubated in a thermal cycler with a heated lid, as detailed in Table 23.

Table 22: Reverse transcription master mix.

Component	Volume µl /reaction	Volume µl/100 wells	Final concentration in 10 µl reaction volume
Superscript II reverse Transcriptase 200 U/µl	0.25	25	50 U
RNAse Inhibitor	0.25	25	10 U
Superscript II First-strand buffer	2	200	1x
DTT 100 mM	0.5	50	5 mM
Betaine 5 M	1.84	184	0.92 M
MgCl2 1 M	0.06	6	6 mM
TSO Primer 100 µM	0.1	10	1 µM
Total volume	5	500	

Table 23: Reverse transcription cycles.

Cycle	Temperature °C	Time	Purpose
1	42	90 min	RT and template switching
2-11 (10 cycles)	50	2 min	Unfolding of RNA secondary structure
	42	2 min	
12	70	15 min	Enzyme inactivation
13	4	Hold	Safe storage

Next, 15 µl of preamplification master mix (see Table 24) was added before the samples were vortexed and centrifuged, and PCR was performed in a thermal cycler according to the program in Table 25. For samples with 1 000 cells, 18 cycles were used whereas for 100 000 PBMCs, only 15 cycles were necessary.

Table 24: Preamplification master mix.

Component	Volume µl	Volume µl/100 wells	Final concentration
KAPA HIFI HotStart Ready Mix 2x	12.5	1250	1x
IS PCR Primer 10 µM	0.25	25	0.1 µM
Nuclease free water	2.25	225	
Total Volume	15	1 500	

Table 25: Preamplification cycles.

Cycle	Temperature °C	Time	Purpose
1	98	3 min	Denaturation
15-18	98	20 sec	Denature
	67	15 sec	Anneal
	72	6 min	Extend
20	72	5 min	Extend
21	4	Hold	Safe storage

Thereafter, a mixture of 21 µl AMPure XP Beads (Beckman Coulter, RT) and 15 µl DEPC water for a 0.6 x ratio was mixed with the sample and incubated for 10 min at RT, followed by incubation for 5 min on a magnetic stand. The supernatant was removed, and the beads were washed twice with 200 µl of freshly prepared 80 % ethanol. After removal of the ethanol, the beads were centrifuged and air-dried for exactly 5 min at RT, and the DNA was eluted with 10 µl TE buffer and transferred into a new plate. The size of the DNA library was measured using the Bioanalyzer high sensitivity DNA chip and DNA concentration was determined using QuantiFluor (Promega) according to the manufacturer's instructions.

After quantification, the DNA was diluted to a concentration of 1 ng/µl and 1 µl was mixed with 1.5 µl of the tagmentation master mix (see Table 26). The samples were incubated for 10 min at 55 °C and then kept on a cooling rack before 11.2 µl of KAPA HIFI enzyme and 4.4 µl of both i5 and i7 primers were added. PCR was performed according to the conditions outlined in Table 25. After the PCR, a cleanup of the DNA library was performed as previously with AMPure XP beads with a 0.75 x ratio, and again two washes with 80 % ethanol. The DNA was subsequently eluted in 10 µl TE buffer, quantified using a Bioanalyzer and QuantiFluor, and then sequenced with NextSeq1000 using 100 bp

paired-end sequencing by the LAFUGA Genzentrum in kind collaboration with Helmut Blum and Stefan Krebs.

Table 26: Tagmentation master mix.

Component	1 x [µL]	final conc (2.5 µL)
Tagmentation DNA buffer (2x)	1.25	1x
TDE1	0.25	
Total volume	1.5	

Table 27: PCR of tagmented library.

PCR stage	PCR condition	Number of cycles
Enzyme activation	72 °C, 3 min	1
Stripping of/ inactivation of TDE1	98 °C, 5 min	1
Denaturation	98 °C, 10 sec	
Annealing	62 °C, 30 sec	8
Extension	72 °C, 30 sec	
Final extension	72 °C, 5 min	1
Safe storage	10 °C, hold	

3.2.12 Data analysis

Statistical testing for significance was performed using GraphPad Prism (v9.1.0) or R (v1.4.1717) as indicated in the figure legends in chapter 4. In most cases, the Kruskal-Wallis test with Dunn's correction or ANOVA with Tukey's correction was performed and a P-value below 0.05 was considered statistically significant. The data was analyzed using ggplot2 (v3.3.5), complexHeatmap (v2.10.0), Rcis target (v1.14.0), fgsea (v1.20.0), GSEA (v.4.1.1) ggvenn (v0.1.9) and the corresponding detailed R scripts for analysis and visualization can be found in Appendix C. The data acquired from the flow cytometry experiments were analyzed using FlowJo (v10.7.1).

3.2.12.1 Calculation of absolute cell numbers

The rule of three was used to calculate cell numbers by either using cell counts from Trucount beads (kindly provided by Christof Geldmacher and Flora Deák) or with the clinical lab counts of a known population (e.g., known are cell numbers for monocytes = a[cells/liter]). The following formula was used for calculating the unknown cell number for population b[cells/liter], with the known percentages for a[percentage of living] and b[percentage of living] obtained from flow cytometric analysis.

45

$$b\left[\frac{cells}{liter}\right] = \frac{a[\frac{cells}{liter}] * b[percentage\ of\ living]}{a[percentage\ of\ living]}$$

3.2.12.2   Analysis of RNA sequencing data

Dual-indexed data obtained from RNA sequencing was demultiplexed from FASTq files using the Illumina demultiplex tool of the LAFUGA Gene Center (Munich), that was custom-written by Alexander Graf and allows one mismatch in the i5/i7 sequence. The adapter sequences were removed, and the reads were filtered for gene length. The quality of the reads was controlled with FastQC (v0.11.7), and reads were aligned to the human genome (UCSC hg38) using the RNA STAR seq mapper (v2.7.8a). The number of reads was counted using HTSeq-count (0.6.1p1) and differential gene expression analysis was performed using DESeq2 (v1.34.0) [173] to compare and normalize between the different samples. Here, normalization is done to the mean of ratios by creating a pseudo-reference for each gene across the samples which is equal to the geometric mean. The ratio of sample to reference is calculated for each gene and the median value of all ratios for a given sample is taken as the normalization factor. This method assumes that not all genes are differentially expressed and accounts for both the sequencing depth and the RNA composition of the sample. Due to its robustness for the identification of differentially expressed genes (DEGs) this method is commonly used for RNASeq analysis. Significance is tested via a likelihood ratio test, which is similar to an ANOVA, to compare the full model with all variances with the reduced model, with one variance missing to identify the effect of the given factor on gene expression. For individual time point comparisons, for example, between d0 and d7 after vaccination, the "contrast" function from the DESeq2 pipeline was used, which is applied to test if differences between groups are equal to zero via the Wald test and generates the log2 fold changes of the individual comparisons.

The data was transformed with variance stabilizing transformation (VST) for visualization using the fitted dispersion-mean relations and subsequently transforming the count data which is normalized by division by the size factors. This produces a matrix of values with homoscedasticity concerning their distribution, i.e., with a constant variance along the range of means.

4. Results

4.1 Infection of total PBMCs shows preferential infection in DCs and monocytes

Several studies have shown that viremia can be detected in the plasma and serum of patients after vaccination with YF17D and that mo-DCs and pDCs can be productively infected in vitro. However, it is not known which cells in the peripheral blood are preferentially infected. Experiments using humanized mice showed infection in peripheral B cells, pDCs, and macrophages [153]. To determine whether the same cells can be infected in vitro, total PBMCs were isolated from healthy donors and infected with YF17D.

4.1.1 Venus-fluorescence derived from Venus-YD17D reporter virus is suitable for detection of infected cells

Two different methods were compared to identify virus-infected cells. The first method is RNAFlow, in which an RNA probe that can bind specifically to YF17D plus-strand RNA is detected in infected cells by flow cytometry. Due to multiple amplifications of the fluorescence signal, this detection method is highly sensitive. However, following antibody staining, fixation, and permeabilization, the fluorescent RNA probe requires several hours of incubation at 40 °C, thereby limiting the number of antibodies that still function to conjugates with brilliant violet and non-tandem dyes and decreasing the signal of all surface antibodies used. The second method to detect viral infection is to use a YF17D reporter virus encoding Venus fluorescent protein. Venus is inserted after the first 25 amino acids of the capsid, after which the full YFV polyprotein follows (Venus-YF17D). Venus is then translated with the full polyprotein but contains cleaving sites to be cleaved off from viral proteins after translation to not interfere with the viral structure [168]. Infected cells can then be detected by flow cytometry due to the replication, transcription and translation of viral RNA which leads to the accumulation of the Venus protein.

Using Venus-YF17D to infect total PBMCs for 48 hours with an MOI of 1, YF + strand RNA was detected in DCs and monocytes by RNAFlow (Figure 6 A, B, blue). A higher rate of infection of monocytes and a lower rate of infection of DCs were detected using

47

RNAFlow staining of plus-strand RNA compared to Venus detection. Within the PBMCs, monocytes, DCs and NK cells were preferentially infected by Venus-YF17D. Low infection rates were found in B cells, and no infection was seen in T cells. This result was confirmed using RNAFlow except for NK cells which did not show a signal with this method. As RNAFlow did not achieve higher sensitivity of viral detection, limited the experimental design, and had high background staining, the Venus-YF17D detection was used for all subsequent experiments.
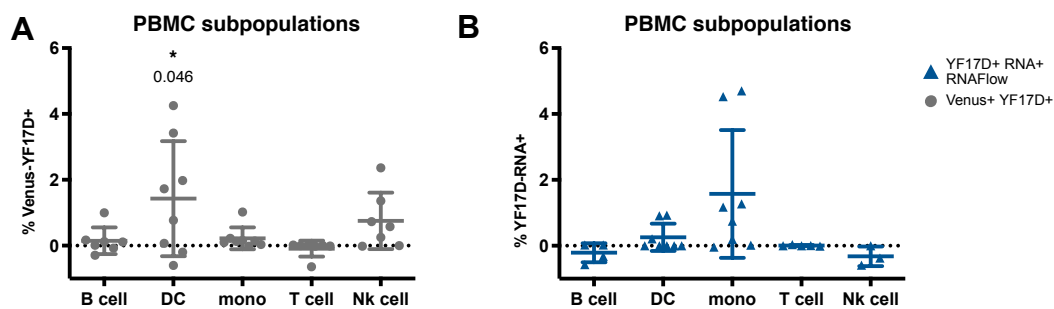
Figure 6: Detection of viral infection in PBMCs with RNAFlow and Venus signal.
A) Infection of total PBMCs for 48 h with MOI1 of Venus-YF17D. Percentage of infected cells within indicated subpopulations detected via Venus signal (gray, n = 8) and RNAFlow (blue, n = 8). 3 donors from the experiments shown in A and B were performed together with Magdalena Scheck from the laboratory of Simon Rothenfusser. Kruskal-Wallis-test with Dunn's correction was performed in GraphPad Prism. Significant p values (< 0.05) to the uninfected after correction; mean and SD are shown.

4.1.2 Infection of all DC and monocyte subsets from peripheral blood by YF17D

To identify which DC or monocyte subpopulations are productively infected, primary cells were sorted and infected for 48 hours with an MOI 10 of Venus-YF17D, and viral infection was measured by means of the Venus signal. All DC and monocyte subtypes could be infected with a high infection rate, mainly in the cDCs and monocytes and less infection found in tDCs and pDCs (Figure 7 A). As the DC3 subtype has been discovered recently, this experiment was repeated with DC subsets isolated from 3 additional donors including DC3 (Figure 7 B, C). These donors showed a higher rate of infection than previous ones, which could either be the result of using a new purified virus stock or donor-dependent. In this instance, all DC and monocyte subtypes again showed a Venus signal after 48 hours and DC3 were shown to also be infected. The cDCs showed the lowest Venus signal while the highest signal was found in monocytes and DC3.

Next, cytokines in the supernatant of the cultures were quantified and even though only a low cell number of 2 000 cells/condition was used, some cytokines could be detected in the distinct populations (Figure 7 D). As expected, IFN-α was mainly produced by pDCs and was induced by YF17D infection in pDCs even though this induction was not found to be statistically significant (p= 0.11). IFN-α was also induced in mo1, but not consistently in the other subpopulations whereas CXCL10 was primarily detected in supernatants of cDC1 and cDC2 in addition to tDCs, pDCs, and mo1 cultures. The amount of CXCL10 detected in the supernatant of infected cDC1 and cDC2 was significantly higher than in the uninfected controls. IL-10 was most highly secreted by mo int and mo2 but was not induced by infection with YF17D. IL-12p70 was found in similar concentrations in all populations except for mo int and IL-6 was highly secreted by all cDCs and monocytes. However, both were not induced by infection with YF17D. TNF-α was secreted after R848 stimulation by cDC1, cDC2, pDC, tDC and mo1 and constitutively secreted by mo int and mo2, but not induced by infection with YF17D.

Interestingly, DC3 showed a morphology similar to that of cDC2 after infection with multiple protruding dendrites, thereby differing from the morphology of monocytes (Figure 7 E).
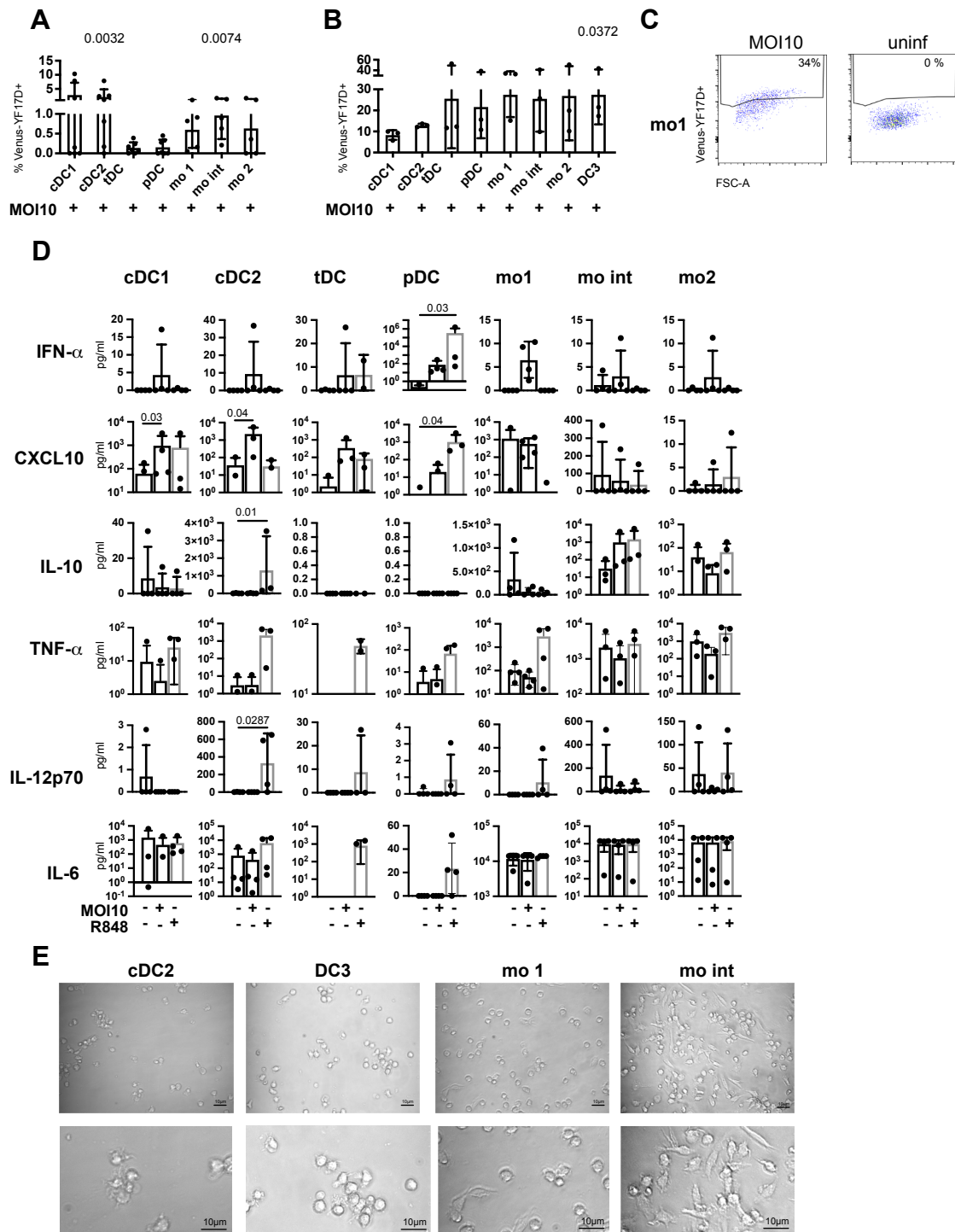
Figure 7: Infection of sorted DC and monocyte populations.
A) cDC1, cDC2, tDC, pDC, mo1, mo int and mo2 were sorted and infected with an MOI 10 of Venus-YF17D for 48 hours. Detection of Venus signal by flow cytometry shown (n = 5) B) Same as in A just with addition of DC3 sorted (n = 3). C) Representative dot plot from B showing Venus signal in mo1 in infected and uninfected control. D) Cytokines as measured in the supernatant from A either uninfected, infected with Venus-YF17D or stimulated with R848 for 48 h (n = 4 except for tDC R848 where n = 2). The Kruskal-Wallis-test with Dunn's correction was performed in GraphPad Prism. Significant p values (< 0.05) after correction; mean and SD are shown. E) Representative microscopic

images of infected cells DC3, mo1, and mo int from B. Upper panel 40x magnification, lower panel enlargement of 40x magnification.

4.1.3 YF17D MOI dependent activation of mo-DCs and monocytes

Publications show that YF17D is very slow to replicate and requires approximately 24 hours for one amplification cycle [174]. However, monocytes and DCs cannot be cultivated for extended periods. Therefore, the optimal time point of cell survival and viral detection for cell culture assays with monocytes and mo-DCs was first determined. A reduction in survival rate was observed after 48 hours for mo-DCs infected with an MOI 1 while monocytes could be cultivated for up to 72 hours (Figure 8 A). Only low percentages of infected cells were observed, with higher infection rates in mo-DCs compared to monocytes. The time points 36 and 48 hours after infection were chosen to detect activation of mo-DCs and monocytes respectively (see Figure 8 E, F, G). Different MOIs were tested, thereby indicating that the percentage of Venus$^+$ cells is dose-dependent in mo-DCs and less so in monocytes, which had a lower infection rate with MOI 10 compared to MOI 1 (Figure 8 C, D).

The expression of activation markers such as PD-L1, CD80, CD86, and HLA-DR was induced in monocytes with increasing MOI (statistically significant for CD80 and CD86 with MOI 1) but not to the level observed after stimulation with LPS or R848. CD83 was not highly expressed in monocytes but was induced in mo-DCs along with PD-L1, CD80 and HLA-DR with increasing virus dose (not significant, Figure 8 E, F, G). CD16 expression tended to be upregulated in monocytes, while CD14 showed a trend towards downregulation after YF17D infection. In mo-DCs, a mature phenotype with coexpression of CD83 and CD86 was only observed in a small percentage of DCs after infection with YF17D, but was seen in the majority of DCs with LPS and to a large extent also with R848 stimulation (Figure 8 E). Activation of mo-DCs or monocytes was not induced by heat-inactivated YF17D or a buffer containing the same amount of sucrose as the virus stock. Mo-DCs and monocytes also showed MOI-dependent secretion of IFN-β (significant in mo-DCs for MOI 10) comparable to the IFN-β response to LPS (Figure 8 H). Thus, YF17D infects mo-DCs at a low rate inducing a robust type I IFN response, but not full activation and maturation.
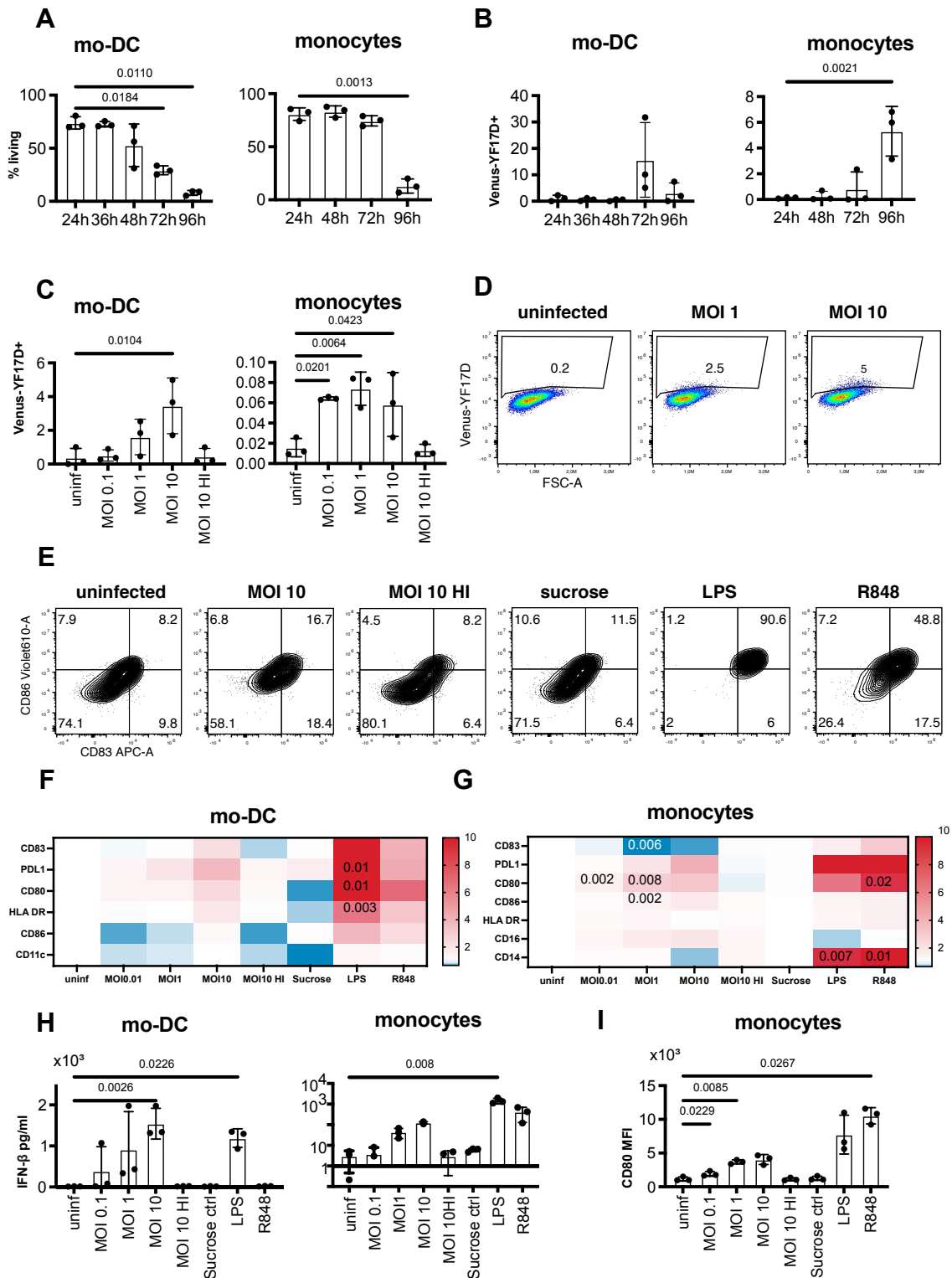
Figure 8: YF17D Venus infection of mo-DCs and monocytes.
A) Mo-DCs and monocytes were infected with an MOI 1 for 24 h, 36 h (only moDCs), 48 h, 72 h and 96 h. Percentage of living cells of total events measured B) and percentage of Venus-YF17D^{+} cells shown (n = 3). C) mo-DCs and monocytes were infected with different MOIs for 36 and 48 h respectively. Percentage of Venus-YF17D^{+} cells shown (n = 3). D) Representative dot plots of Venus signal in uninfected, MOI 1 and MOI 10 infected mo-DCs. E) Representative contour plots of maturation markers CD86 and CD83 in mo-DCs after infection or stimulation. (representative

of n = 3). F) MFI of activation and maturation markers CD83, PD-L1, CD90, HLA-DR, CD86, and DC marker CD11c in mo-DCs were normalized as fold-changes to uninfected controls of data shown in C (n = 3). 1 = white, downregulation = blue, upregulation = red. G) MFI of activation and differentiation markers CD83, PD-L1, CD80, CD86, HLA-DR, CD16, and CD14 in monocytes were normalized as fold-changes to uninfected controls of data shown in C (n = 3). 1 = white, downregulation = blue, upregulation = red. H) The IFN-β concentration in supernatants from mo-DCs and monocytes was measured. I) MFI of CD80 in monocytes shown. The Kruskal-Wallis-test with Dunn's correction was performed in GraphPad Prism. Significant p values (< 0.05) after correction; mean and SD are shown.

4.1.4 Direct cell-contact with virus-infected cells increased virus load in APCs

Although DCs and monocytes could be infected in vitro, the percentage of infected cells was quite low. Since viremia is found in YF17D vaccinated individuals, other cells than DCs and monocytes are likely to play a major role in the viral replication cycle in vivo. At the vaccination injection site, cells such as fibroblasts or epithelial cells could be the first target of YF17D and allow for local viral replication. Cocultures of APCs with cell lines susceptible to YF17D infections were performed to investigate if APCs can directly take up infectious viral particles from infected cells and thereby get infected or stimulated more efficiently. VeroB4 cells, which are deficient in interferon, allow high viral replication of YF17D.

Therefore, VeroB4 cells were infected with Venus-YF17D for 24 hours with an MOI of 0.01 and washed before APCs were added. After 48 hours of coculture, APCs were harvested and Venus fluorescence was detected by flow cytometry. As a control, supernatants from VeroB4 cells infected with an MOI of 0.01 were harvested after 72 hours and added to APCs for 48 hours. In parallel, APCs were infected in the absence of VeroB4 cells with YF17D MOI 1 as in previous experiments. Both monocytes and mo-DCs showed a higher percentage of Venus-YF17D$^+$ cells when cocultured with infected VeroB4 cells than supernatant of infected VeroB4 cells or with an MOI 1 of Venus-YF17D only (Figure 9 A). Transwell assays were performed to check if cellular contact was necessary for this effect, by separating VeroB4 and APCs using a size-selective membrane which allowed the transfer of YF17D and any cytokines secreted from the VeroB4 cells, but not direct cell-cell contact. A higher percentage of Venus-YF17D$^+$ cells was found in the conditions with direct cell contact compared to the conditions separated by transwells in monocytes and mo-DCs (Figure 9 B, E).

The same transwell experiments were performed using BHK21 cells, which are also IFN deficient and susceptible to YF17D infection, but are not derived from a primate – since

53

VeroB4 cells could release cytokines and growth factors that could influence the human APCs [175]. Here, cell contact also seemed to favor the YF17D infection of monocytes and mo-DCs (Figure 9 F, D). Consistent with the increased percentage of Venus-YF17D$^+$ cells, the PD-L1 expression of the APCs in direct contact with infected cells was also increased compared to the transwell condition where no direct contact with virus-infected cells was facilitated (shown for mo-DCs and VeroB4 Figure 9 C). The same effect was seen with CD80 and CD83 (mo-DCs: p = 0.048, p = 0.043, comparison infected coculture and infected transwell coculture) and a trend towards higher expression was observed for HLA-DR and CD86 (mo-DCs: p = 0.26, p = 0.22, comparison infected coculture and infected transwell coculture) in the direct contact conditions.
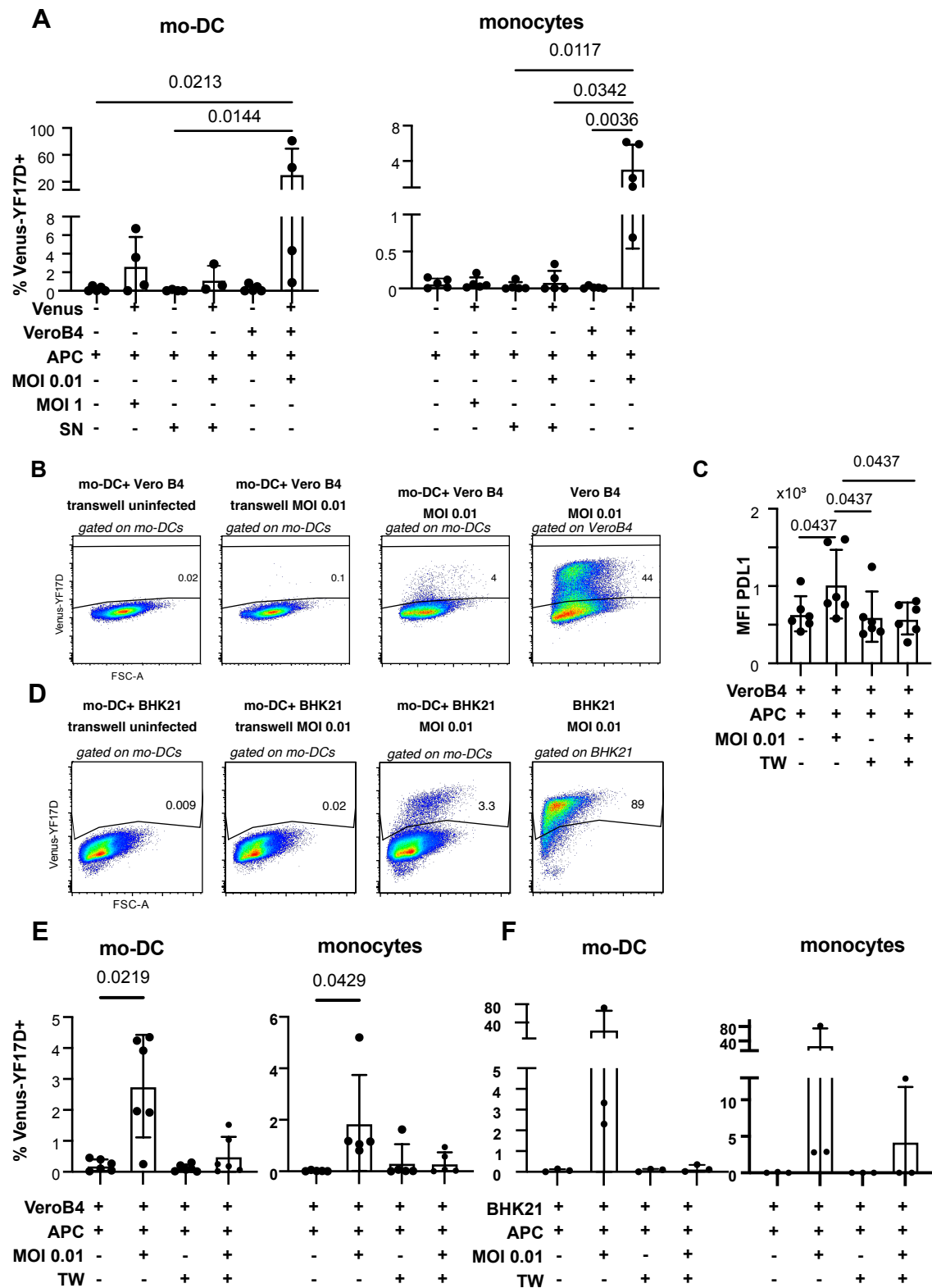
Figure 9: Coculture of infected cells with mo-DCs and monocytes.
A) VeroB4 cells were infected for 24 h with an MOI of 0.01 and cocultured for 48 h with mo-DCs or monocytes. Uninfected VeroB4 cells and monocytes/mo-DCs infected directly with an MOI 1 or with the supernatant from MOI 0.01 infected VeroB4 cells collected 72 h after infection were used as controls. The percentage of Venus-YF17D$^+$ cells is shown. The Kruskal-Wallis-test with Dunn's correction was performed in GraphPad Prism. Significant p values after

correction; mean and SD are shown. mo-DCs n = 4, monocytes n = 5. B) Transwell assays were performed with VeroB4 infected with an MOI of 0.01 for 24 hand cocultured with mo-DCs only separated by a transwell (= TW). VeroB4 cells were also infected and cultured with mo-DCs without transwell separation. As a control of infection, VeroB4 were gated within the co-culture. Representative pseudocolor plots showing the Venus-YF17D signal from n = 6 are illustrated. C) Expression of PD-L1 in mo-DCs of B. The Kruskal Wallis test with Dunn's correction was performed in GraphPad Prism. D) Representative pseudocolor plots showing Venus-YF17D signal using BHK21 cocultures from n = 3. E) Venus-YF17D positive cells from the experiments from B, transwell = TW. F) Venus-YF17D+ cells from experiments from D. The generation of mo-DCs, harvesting of cells and flow cytometric measurement of the results were supported by Yaren Canten during her internship under my supervision.

When examining microscopic images of sorted mo-DCs and BHK21 after the coculture, a wide distribution of Venus signal across the whole cytoplasm is found in both BHK21 and mo-DCs and the signal is not localized in intracellular vesicles (Figure 10 A, B), thereby suggesting that Venus fluorescence indicates replication and viral gene expression and is not due to the internalization of particulate material from infected cells via endocytosis or phagocytosis. These results show that contact with infected cells leads to more efficient infection of DCs and monocytes than exposure to the infectious virus alone.
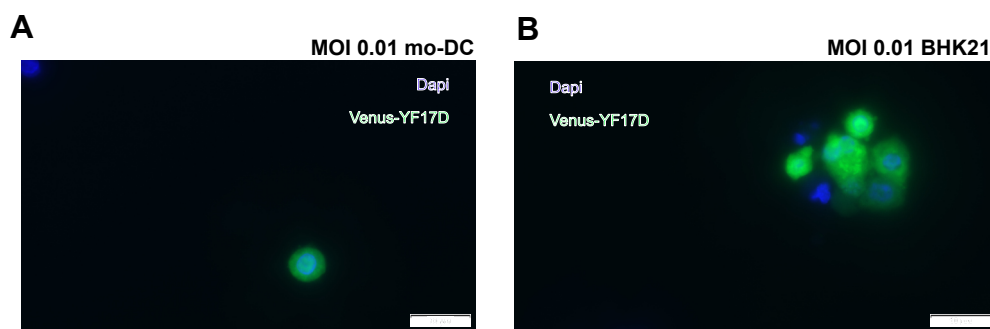
Figure 10: Microscopic images of Venus-YF17D infected coculture.
A) Sorted mo-DC after coculture with YF17D-virus infected BHK21 cells. Green is Venus-YF17D, blue is DAPI. B) BHK21 after infection with an MOI of 0.01 with Venus-YF17D. Representative images from 3 experiments are shown. The generation of mo-DCs, harvesting of cells, and flow cytometry measurement of the results were supported by Yaren Canten during her internship under my supervision.

4.2 Type I interferon controls viral replication in DCs and monocytes

Given the strong attenuation of YF17D in DCs and monocytes, analyzing the pathways involved in viral sensing and the control of viral replication in these cell types could help determine how viral infection is sensed and controlled in these cell types. Therefore, the

TBK1 inhibitor BX795, JAK1/JAK2 inhibitor Ruxolitinib and IFNAR blocking antibodies were used to check type I IFN induction (via TBK1) and signaling pathways involved in the control of viral replication. Previous studies had shown that IFN-incompetent cell lines such as BHK21 and VeroB4 are highly susceptible to viral infection with YF17D [151, 152, 176], which was also seen in our experiments. Furthermore, IFNAR knockout mice were also shown to be susceptible to infection with YF17D, thereby indicating the critical role of IFNAR signaling in the control of viral replication [150].
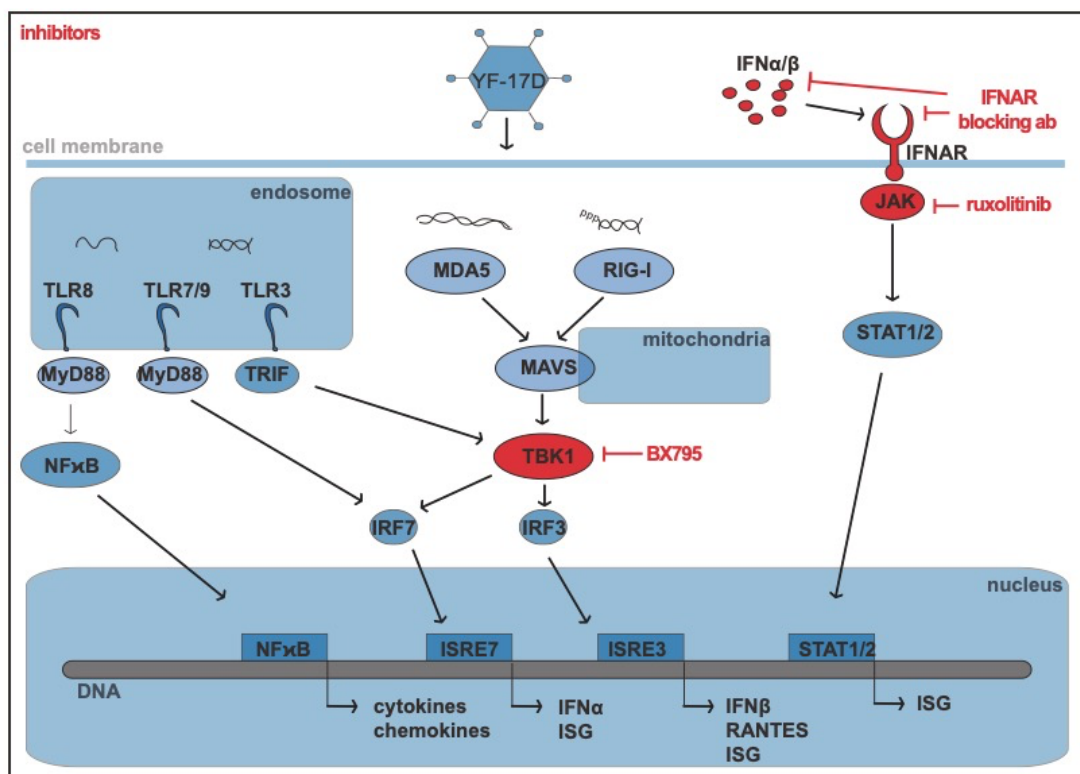
Figure 11: Viral sensing in host cells.
Inhibitors used to check pathways for viral sensing of YF17D. BX795 acts as a TBK1 inhibitor, which is involved in viral sensing via MDA5/RIG-I. Ruxolitinib inhibits the JAK/STAT pathway and IFNAR blocking antibodies block the IFNAR receptor.

4.2.1 Inhibition of type I IFN pathway increases viral infection in monocytes and mo-DCs

Using IFNAR blocking antibodies significantly increased the percentage of Venus-YF17D$^+$ mo-DCs and monocytes after infection with MOI 1 for 36 and 48 hours, respectively (Figure 12 A, B). This indicated that IFNAR signaling restricts YF17D viral repli-

cation. Using BX795 (BX), a TBK1 inhibitor that blocks type I IFN induction downstream of the viral sensors RIG-I/MDA5 and TLR3, a trend towards a higher infection rate in monocytes (Figure 12 B) but not mo-DCs was observed. However, this difference was not significant (monocytes: $p = 0.19$, mo-DCs: $p = 0.99$). The JAK1/JAK2 kinase inhibitor Ruxolitinib also did not consistently increase the percentage of Venus-YF17D$^+$ cells but a trend towards higher infection could be seen (monocytes: $p = 0.2$, mo-DCs $p= 0.99$). There was high donor-variability in response to Ruxolitinib and BX795 with clear effects only being observed in cells derived from some of the donors (see example in Fig. 12 B). Looking at IFN-β production, a significant increase of IFN-β secretion in infected monocytes and mo-DCs compared to the uninfected controls was visible (Figure 12 D) and heat-inactivated virus failed to induce IFN-β secretion. With IFNAR blocking antibodies, IFN-β secretion was the same for all conditions with and without virus in monocytes (Figure 12 C) and mo-DCs (data not shown). The inhibitor Ruxolitinib, however, significantly reduced the IFN-β secretion in response to YF17D in monocytes.

This indicates that the JAK/STAT pathway, which is essential for IFNAR signaling and the positive IFN feedback loop, could be relevant for the YF17D-induced secretion of IFN-β. Looking at LPS stimulation, all monocytes and mo-DCs were able to produce large amounts of IFN-β, thereby confirming the functionality of the cells with regard to IFN production and release in response to stimulation (Figure 12 D).
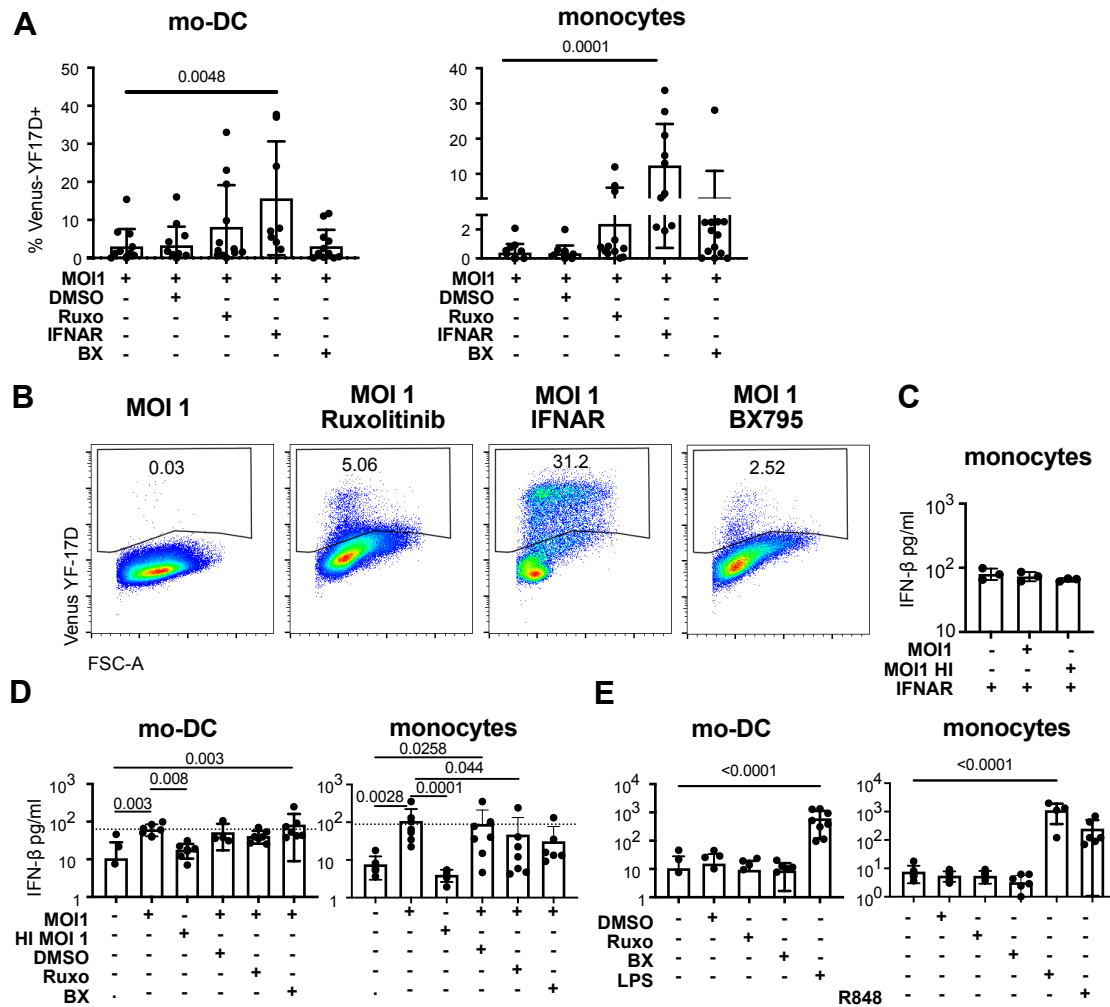
Figure 12: IFNAR signaling controls viral replication of YF17D in mo-DCs and monocytes.
A) Percentage of Venus-YF17D$^+$ mo-DCs (n = 12) and monocytes (n = 10) shown after infection with MOI1, with or without the use of inhibitors Ruxolitinib (Ruxo), BX795 (BX), and IFNAR blocking antibodies (IFNAR). DMSO was used as a control for Ruxolitinib and BX795. B) Representative dot plots of monocytes from A. C) IFN-β secretion of monocytes after treatment with IFNAR blocking antibodies in infected and uninfected monocytes. D) IFN-β secretion of mo-DCs and monocytes from A. E) IFN-β secretion of mo-DCs and monocytes from A with LPS and R848 as positive controls. Generation of mo-DCs, infection, and flow cytometry analysis of 6 of the 12 donors shown in this figure A, D, and E were performed by Yiqi Huang in our lab as part of her Master thesis. Her data was reanalyzed by me and combined with the data derived from the present research. The Kruskal-Wallis-test with Dunn's correction was done in GraphPad Prism. Significant p values (< 0.05) after correction; mean and SD are shown.

4.2.2 Activation of mo-DCs is increased after YF17D infection in conditions with BX795 and Ruxolitinib

As shown previously, activation of APCs can be induced by infection with YF17D, and upregulation of activation markers such as CD80, CD83, PD-L1, and HLA-DR seem to be dependent on the MOI used. Upregulation of these activation markers may depend on

59

the autocrine/paracrine effect of type I IFN that is produced after YF17D infection and may therefore require IFNAR signaling through the JAK/STAT pathway. Since the inhibitors were dissolved in DMSO, a DMSO control was used to check for unspecific effects of the carrier. In mo-DCs, no significant upregulation of HLA-DR, PD-L1, or CD83 was detected in conditions with YF17D virus ($p = 0.122$, p= > 0.99, p = >0.99 respectively, Figure 13 A). However, there was significant upregulation of CD86 after infection and of HLA-DR in the infected cells treated with Ruxolitinib or BX795 and significant upregulation of CD86 and CD83 in the infected cells treated with BX795 in comparison to uninfected cells. Although the upregulation of CD86 by YF17D was reduced by treatment with Ruxolitinib, this reduction was not significant. With IFNAR blocking antibodies, there was a trend towards lower but not higher activation marker expression being detectable in the infected condition, even though the percentage of infected cells was much higher than in the infected conditions without IFNAR blocking antibodies.

Figure 13: Activation marker expression in mo-DCs after infection with YF17D and treatment with different inhibitors.

A) Fold induction of the MFIs of HLA-DR, PD-L1, CD86, and CD83 to uninfected controls in mo-DCs is shown. The conditions used were infection with MOI1 of Venus-YF17D, infection of MOI1 of heat-inactivated Venus-YF17D (HI MOI1), treatment with Ruxolitinib (Ruxo), BX795 (BX), IFNAR blocking antibodies (IFNAR), and DMSO. (n= 4-9). SD and significant p values (p < 0.05) are shown and were calculated with Kruskal-Wallis with Dunn's correction or one-way ANOVA with Bonferroni correction using GraphPad Prism. Columns show mean and whiskers show standard deviation. B) Fold induction of the MFIs of the markers from A) and treatments from A) shown without infection.

In monocytes, CD86, PD-L1, and CD80 (but not HLA-DR and CD83) were significantly upregulated after infection with Venus-YF17D (Figure 14 A). The expression of CD80 and CD86 was found to be significantly reduced in the infected monocytes treated with Ruxolitinib compared to infection without Ruxolitinib treatment (Figure 14 A). The expression of CD80 and CD86 was also slightly reduced by IFNAR blockade although this change was not significant. All cells were responsive to LPS and R848 stimulation and

neither DMSO nor the inhibitors on their own had any effect on the expression of activation in mo-DCs or monocytes (Figure 14 B, Figure 13 D). Taken together, these results show that activation of DCs and monocytes by YF17D infection in vitro was generally weak compared to other stimuli and was not entirely dependent on the autocrine/paracrine effect of type I IFN.
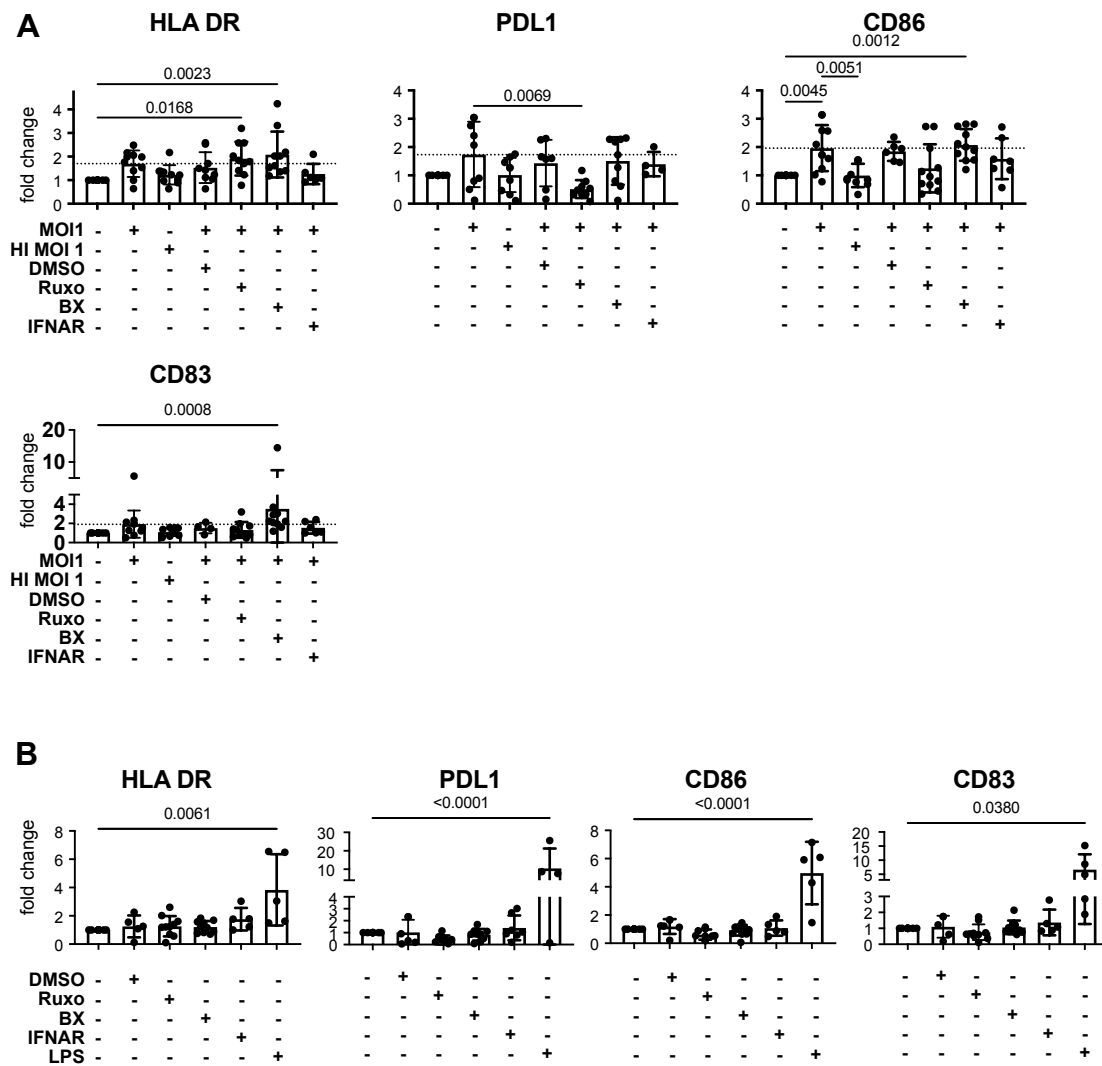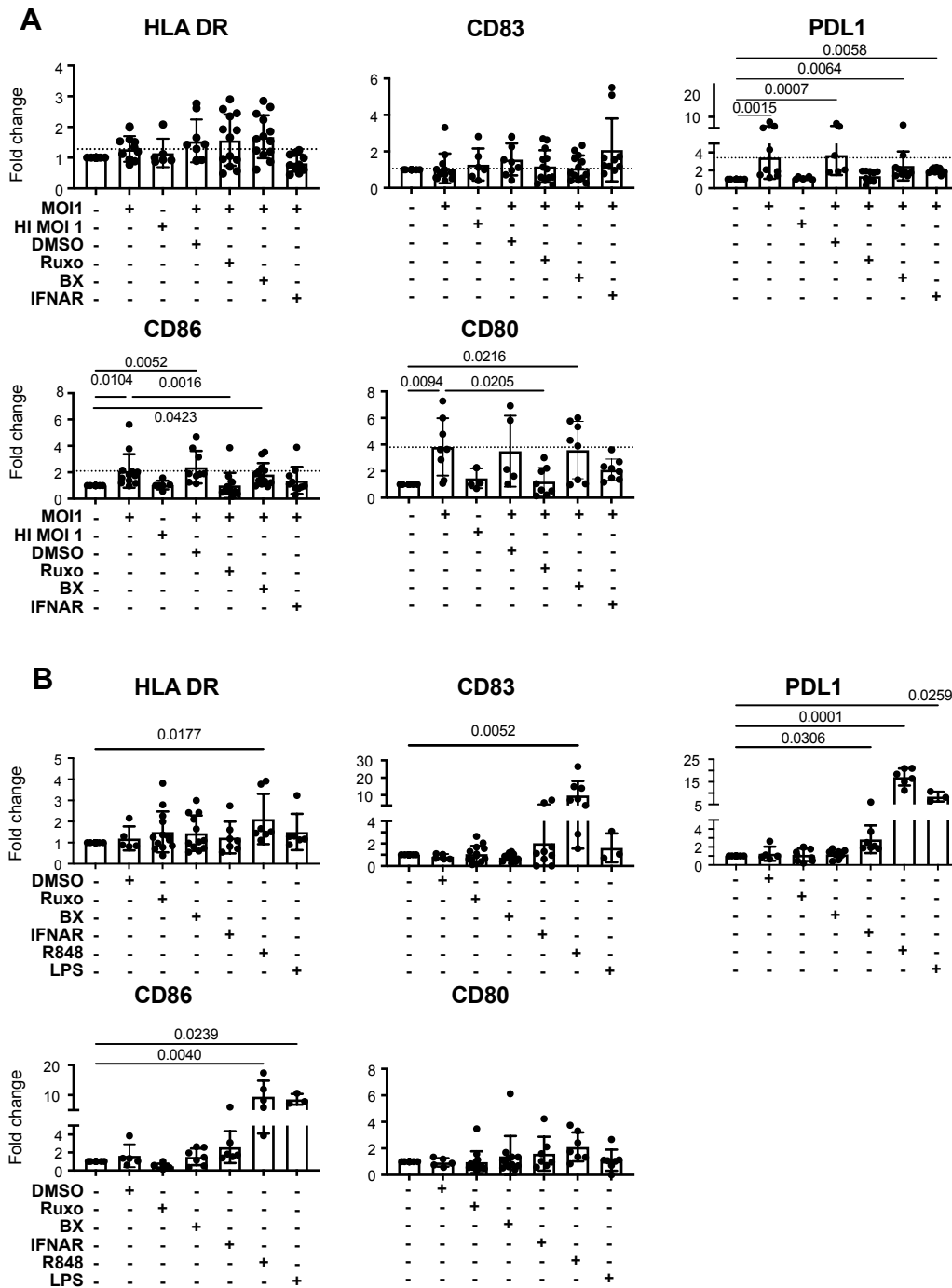
Figure 14: Activation marker expression in monocytes after infection with YF17D and treatment with different inhibitors.
A) Fold induction of the MFIs of HLA-DR, PD-L1, CD86, CD83, and CD80 to uninfected controls in monocytes is shown. Conditions used were infection with MOI1 of Venus-YF17D, infection of MOI1 of heat-inactivated Venus-YF17D (HI MOI1), treatment with Ruxolitinib (Ruxo), BX795 (BX), IFNAR blocking antibodies (IFNAR) and DMSO, n = 3-12. Signficant p values are shown and were calculated with Kruskal-Wallis with Dunn's correction or one-way ANOVA with Bonferroni correction using GraphPad Prism. Columns show mean and whiskers show standard deviation. B) Controls from A without infection.

4.2.3 Venus-YF17D$^+$ cells show higher expression of CD86 than uninfected cells

Based on these results, it was important to determine whether viral infection directly activates the infected cells. Hence, the MFI of costimulatory molecule CD86 was compared between Venus-YF17D$^+$ and Venus-YF17D$^-$ cells within each condition. A significantly higher expression of CD86 in infected cells than in uninfected bystander cells in mo-DCs and monocytes was observed. However, the difference between infected and uninfected cells was almost abrogated by IFNAR blocking antibody in mo-DCs, and was also reduced in monocytes (Figure 15 A, B). Thus, infected cells are more activated than uninfected cells in the same culture, and IFNAR signaling may contribute to this effect.
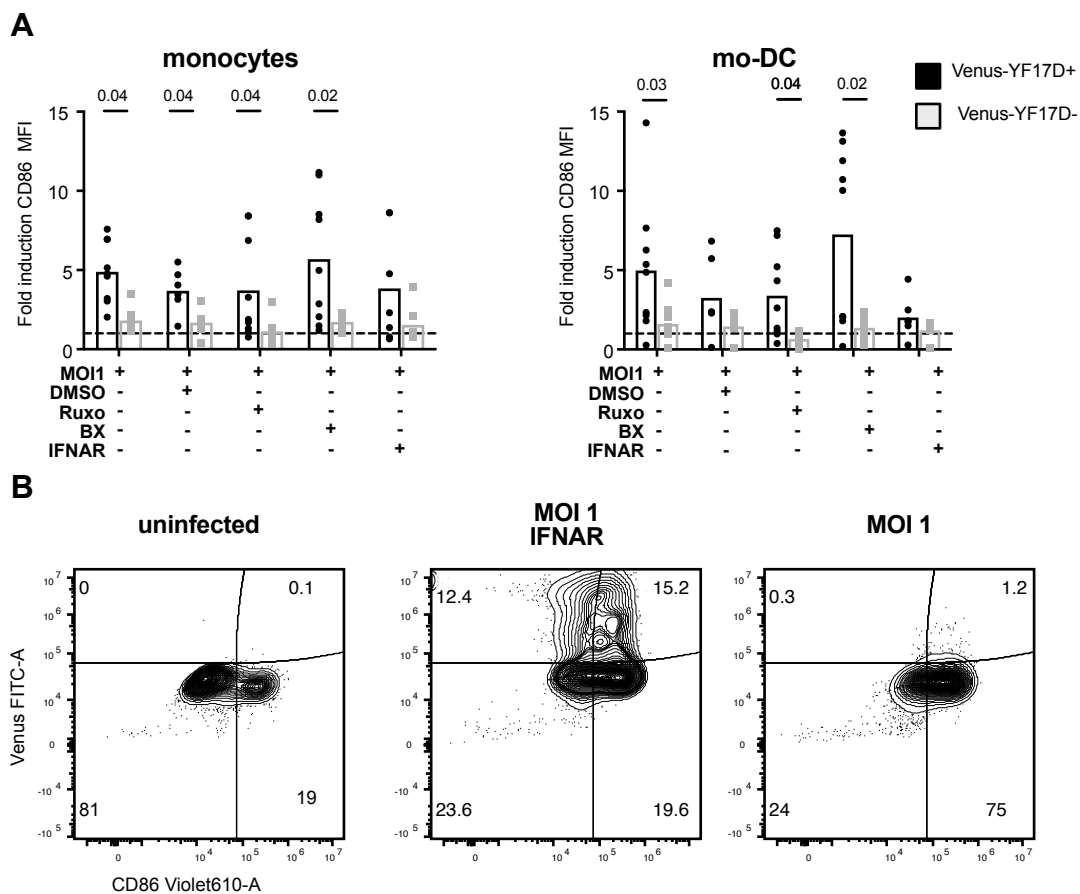
Figure 15: Activation of infected and uninfected cells.
A) MFIs of CD86 were normalized to uninfected cells for Venus-YF17D$^+$ and Venus-YF17D$^-$ cells within the conditions as indicated. Paired t-test was performed between Venus-YF17D$^+$ (black) and Venus-YF17D$^-$ (gray), n=6-10. B) Representative contour plots of Venus-YF17D and CD86 expression in mo-DCs in uninfected cells, infected cells treated with IFNAR blocking antibodies and infected cells only. MOI of 1 was used. B) Representative contour plots of A showing uninfected condition, condition infected with an MOI1 and treated with IFNAR or not.

4.2.4 Low rate of infection in tonsil tissue by YF17D

Since DCs differ in their functionality depending on where they are located in the human body, it is important to determine whether higher infection rates could be achieved in DCs located in human secondary lymphoid tissue than in DCs from the blood. Human tonsils were kindly provided by Dr. Schubert (Klinikum der LMU München), and total cells isolated from tonsils were infected with Venus-YF17D. Venus-YF17D$^+$ cells were detected, and the Venus signal was mainly found in NK cells, monocytes, pDC, and some signal was also observed in CD45$^-$ cells and cDCs (Figure 16 A, B). However, the infection rate of cells isolated from tonsils was not higher than the infection rates that were previously detected in PBMCs. A slight trend towards an increase of Venus-YF17D$^+$ infected total tonsil cells could be seen when using Ruxolitinib, but this was not statistically significant (p = 0.6, Figure 16 C, D, E). Gating on monocytes, pDCs, cDCs, and NK cells within the tonsil cells, infection rates were not significantly changed by treatment with Ruxolitinib or BX795.
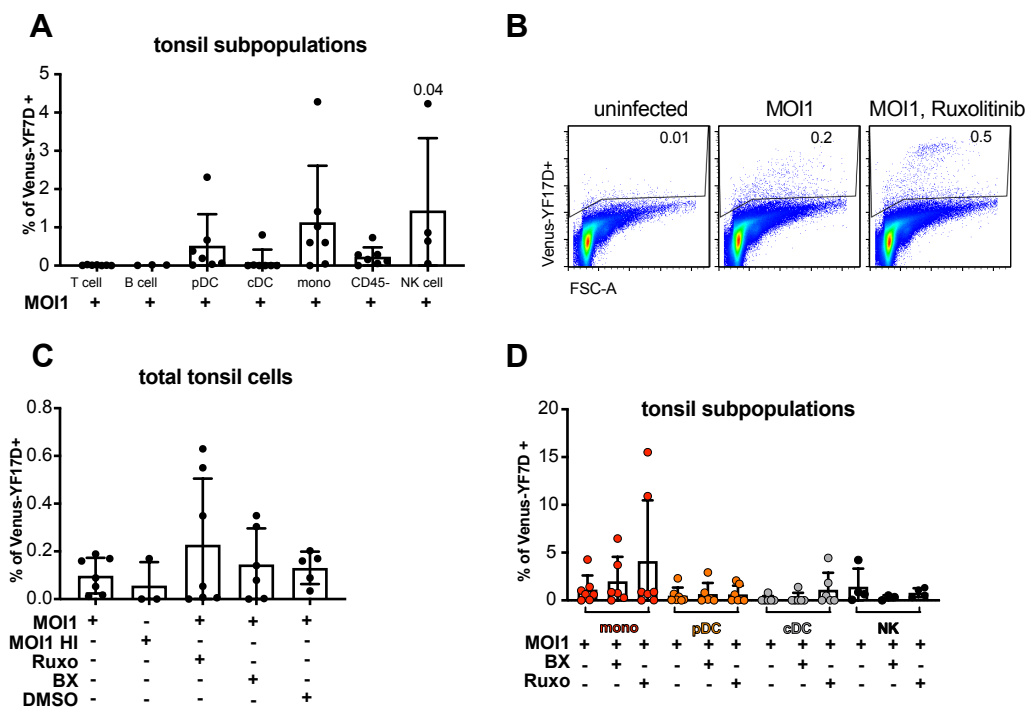
Figure 16: Infection of tonsil cells with Venus-YF17D.
A) Tonsil cells were infected with an MOI 1 of Venus-YF17D for 48 h and Venus signal was measured using flow cytometry. The % of Venus-YF17D$^+$ cells within gated T, B, NK cells as well as pDC, cDC and monocytes (mono), and CD45$^-$ cells are shown (n = 7). B) Representative dot plot of uninfected, infected, and infected and Ruxolitinib treated tonsil cells as gated on single living cells. C) Single living cells after infection with Venus-YF17D. Inhibitors Ruxolitinib and BX795 were used in addition to a DMSO control. D) Gated on mono, pDCs, cDCs and NK cells, the percentages of Venus-YF17D$^+$ cells are shown as described in C. Significant p values ($p < 0.05$) are shown and were calculated with the Kruskal-Wallis with Dunn's correction or one-way ANOVA with Bonferroni correction using GraphPad Prism. Columns show mean, and whiskers show standard deviation.

Summarizing the data so far, YF17D preferentially infects DCs, monocytes and NK cells from total PBMCs. Interestingly, all sorted DC subsets (cDC1, cDC2, DC3, tDC, pDC) and all monocytes (mo1, mo int, mo2) support viral replication in vitro. APCs reacted to direct contact with YF17D with modest upregulation of activation markers (mostly in the infected cells themselves), low viral infection rates, and secretion of cytokines such as IFN-β, IFN-α, and CXCL10. Additionally, the viral infection seemed to be controlled by the cell's interferon response and inhibition of the IFNAR increased the percentage of infected cells.

4.3 Innate immune response to YF17D ex vivo shows activation and proliferation of antigen-presenting cells

4.3.1 Design of the YF17D vaccination study

The next set of experiments focused on determining how peripheral blood APCs react to YF17D infection in vivo, after vaccination. Similarly to what was observed in vitro, APCs could potentially show an upregulation of activation and maturation markers. This activation could either be directly caused by a low-rate viral infection, by recognizing material such as nucleic acids derived from virus-infected cells, or by cytokines released in response to the vaccination. Time-dependent changes in the frequencies of APC subsets in the blood and ongoing proliferation could indicate active participation and increased turnover of specific subsets. Therefore, healthy volunteers were recruited and vaccinated with the live-virus vaccine YF17D. Blood was taken before vaccination and on days 3, 7, 14, and 28 after vaccination (Figure 17) before multi-parametric flow cytometry was performed to analyze the response of APC subsets to YF17D vaccination.
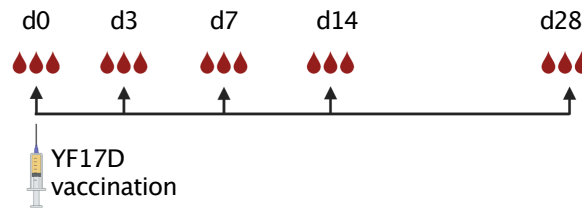
Figure 17: Design of the YF17D vaccination study.
YF17D vaccination study. Healthy volunteers needing YF17D vaccination for travel reasons were recruited. Blood was taken before vaccination (d0) and on days 3 (d3), 7 (d7), 14 (d14) and 28 (d28) after vaccination.

4.3.2 Early relative reduction of cDCs and expansion of pDCs after YF17D vaccination

The gating strategy was performed as shown in Figure 18. After gating on living single cells and excluding neutrophils, HLA-DR$^+$ cells were separated from HLA-DR$^-$ and lineage marker expressing cells (CD3, CD14, CD16, CD19, CD20, CD56). The lineage markers in this case also included monocyte markers. The HLA-DR$^+$ Lin$^-$ DC fraction was regated for HLA-DR^{high} cells without exclusion of CD123$^+$ pDCs, which characteristically express lower amounts of HLA-DR than cDCs. Next, pDCs and tDCs were identified by CD123 expression, and tDCs were defined as Axl$^+$ or CD33$^+$. CD123$^-$ CD33$^+$ cDCs were separated into cDC1 by CD141 expression and into cDC2 by CD1c expression and DC3 were not included in this gating strategy. When examining the composition of the DC gate, a relative reduction of cDC1 and cDC2 on days 3 and 7 after vaccination was observed, which coincided with an increase of pDC frequency (Figure 18 B). tDCs also showed a significant expansion, albeit only on day 14 when pDC and cDC frequencies had already normalized. Based on the cell numbers of these populations per liter of blood, as calculated with clinical data on blood counts, mostly consistent numbers of pDCs and cDCs/l blood were found with a slight decrease of cDC1 and cDC2 on day 7 after vaccination. The relative expansion of tDCs within the DC gate was also accompanied by an absolute increase of tDC numbers per liter of blood on day 14 compared to day 0.
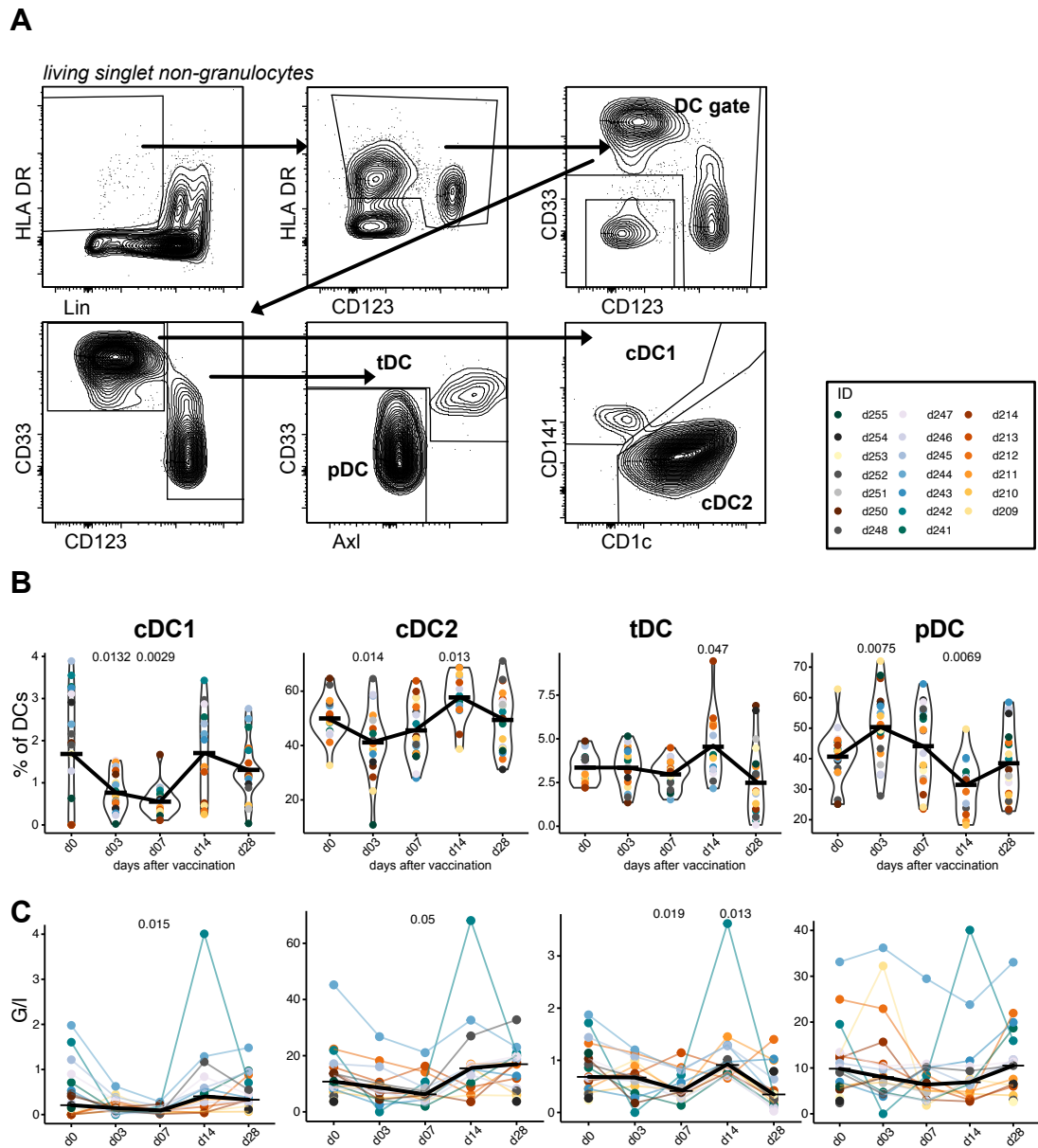
Figure 18: Gating strategy and cDC frequencies for the YF17D vaccination study.
A) Cells were gated as living singlets and CD16^{high} SSC-A^{high} granulocytes were excluded. Lineage (CD3, CD14, CD16, CD19, CD20, CD56)- cells were gated for HLA-DR^{high} cells, and DCs were identified as CD33+ or CD123+. Separation with CD123 identified within the CD123+ fraction CD33+Axl+ tDCs and CD33-Axl- pDCs. CD123- cells were gated as CD141+ cDC1 and CD1c+ cDC2. B) Frequencies of cDC1, cDC2, tDC and pDC of total DC gate. Donors are colored as indicated. The violin plots show distribution, and the median is indicated by a black line (n = 20). C) Frequencies of cDC1, cDC2, tDC and pDC were calculated per liter blood from lymphocyte and monocyte blood counts. Significant p values of changes compared to d0 are shown as calculated in R using the Kruskal-Wallis test and Dunn's multiple testing.

4.3.3 Ki67+ staining shows increased proliferation of cDCs and tDCs after YF17D vaccination

To determine whether the changes in DC subset composition in the blood were associated with proliferation, which might indicate enhanced turnover of specific subsets, intracellular Ki67 was measured as a marker of cells that are proliferating or have recently undergone proliferation. The percentage of Ki67+ cells was significantly increased in cDC1 and cDC2 on days 3 and 7 after vaccination, while only around 0-10 % of the cells showed a Ki67 signal before vaccination. tDCs behaved similarly to cDCs, with a significant increase of Ki67+ cells on days 3 and 7 after vaccination. On the other hand, in pDCs, no significant increase in proliferation was detected, thereby indicating that tDCs have a more similar cellular turnover to cDCs than pDCs (Figure 19A). An increase of Ki67+ proliferating T cells between days 7 and 14 after YF17D vaccination was described in the literature [120]. Therefore, gating on proliferating T cells was used as an internal positive control. An isotype control to the Ki67 antibody was used to set the gate in each population (Figure 19 B, C). In monocytes, which were gated as HLA-DR+ Lin+ CD33+ cells here, no significant increase of Ki67+ cells was found (Figure 19 D). Furthermore, FLT3L, which is essential for DC development and expansion, was not significantly increased in the plasma after vaccination with YF17D (Figure 19 E). Circulating cDC subsets and tDCs thus showed a transiently increased proliferative response after vaccination, which was followed by relative and absolute expansion of these subsets potentially indicating increased turnover and regeneration.

A

B **C** **D** **E**
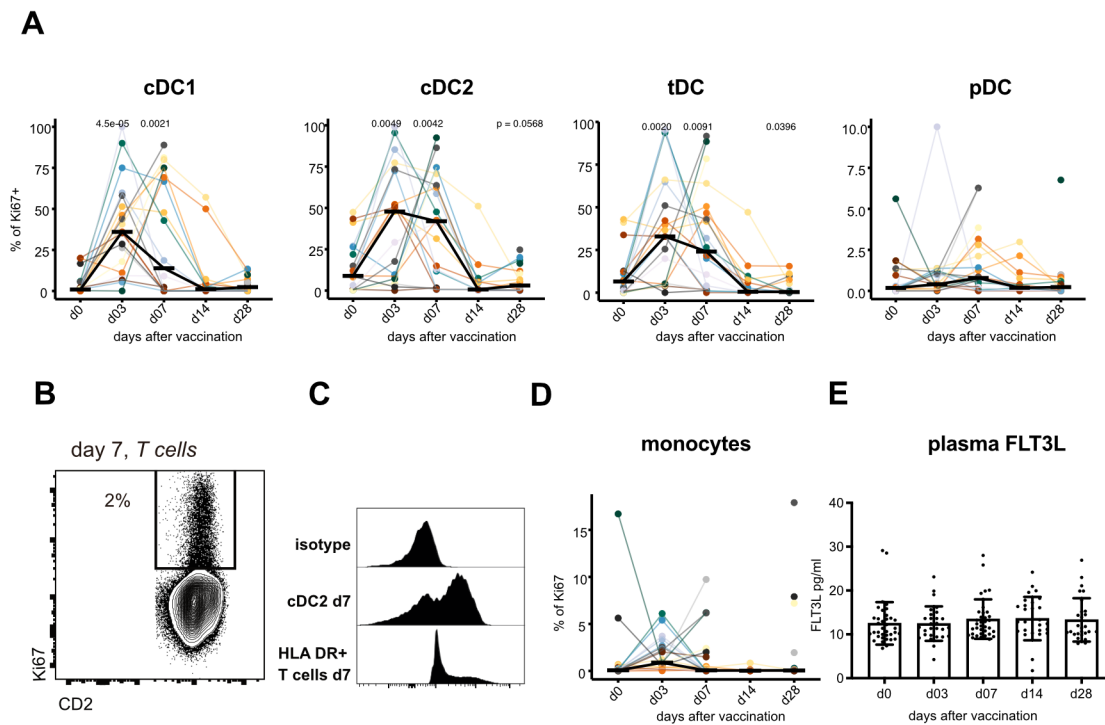
Figure 19: Ki67+ DC and monocytes.
A) The percentage of Ki67+ cells within cDC1, cDC2, tDC and pDC is shown. The black line shows the median and individual donors are indicated by colors and time points that are connected for each donor (n = 20). B) Representative dot plot for Ki67 signal in T cells on day 7 after vaccination. C) Representative histogram of Ki67 staining. The isotype control, cDC2 and HLA-DR+ T cells are shown on day 7 after vaccination. D) The percentage of Ki67+ cells within the monocytes is shown whereby the black line shows the median, and individual donors are indicated by colors and time points are connected for each donor. Significant p values are shown as calculated in R using the Kruskal-Wallis test and Dunn's multiple testing. E) Concentration of FLT3L in plasma of YF17D donors shown (n = 30).

4.3.4 Expansion of intermediate monocytes after YF17D vaccination.

Samples from an additional cohort comprising of 10 donors were measured using a more extensive multi-parameter panel to also analyze the frequencies of DC3 and monocyte subsets, their activation markers, and chemokine receptors in addition to the other DC subpopulations. Due to the need to identify CD14+ DC3, the separation of monocytes from DCs was done using CD88/CD89 and CD16 instead of CD14, followed by the usual DC gating. The CD5+ cDC2 were then separated from the CD5- DC3 and DC3 were differentiated into CD163- CD14-, CD163+ CD14- and CD14+ fractions. cDC1, cDC2, pDC, and tDC were gated as shown previously (Figure 20 A). A significant increase of mo int and decrease of mo1 was observed on day 7 after vaccination (Figure 20 B), thereby confirming previous findings in this laboratory of Livia Habenicht and other published data [125, 177, 178].

69
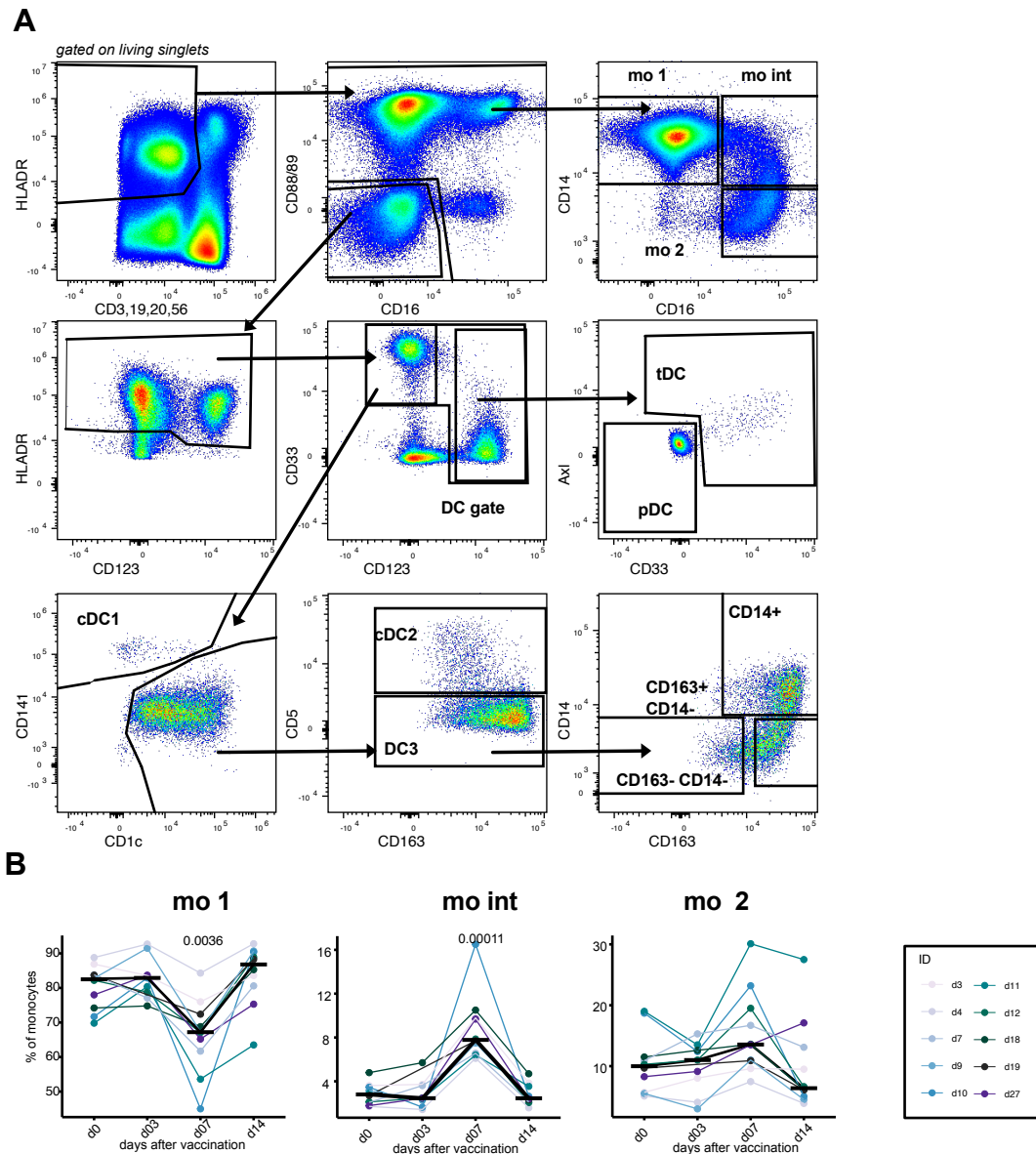
Figure 20: Gating strategy for YF17D vaccination study for activation markers and chemokine receptors.
A) Gating strategy for ex vivo analysis of APC population frequencies, activation markers and chemokine receptors after vaccination with YF17D. B) Frequencies of mo1, mo int, and mo2 are shown as a proportion of total monocytes (n = 10). The black line indicates the median. Significant p values are shown as calculated in R using the Kruskal-Wallis test and Dunn's multiple testing.

4.3.5 No significant expansion of CD14$^+$ DC3

While the DC3 frequency of all living cells was slightly increased on day 7 (not significant, p = 0.32), the percentage of DC3 within total DCs stayed consistent after vaccination with YF17D (Figure 21 A, B, C). Subpopulations in the DC3 population can be defined by distinct expression of CD163 and CD14, with the CD14$^+$ cells being associated with

inflammatory responses, for example in patients with systemic lupus erythematosus (SLE) [15]. After vaccination with YF17D, no significant changes were seen in the DC3 composition. However, there was a tendency towards a higher percentage of CD14$^+$ DC3 on day 7 after vaccination in the majority of donors (not significant, p = 0.12, Figure 21 D).
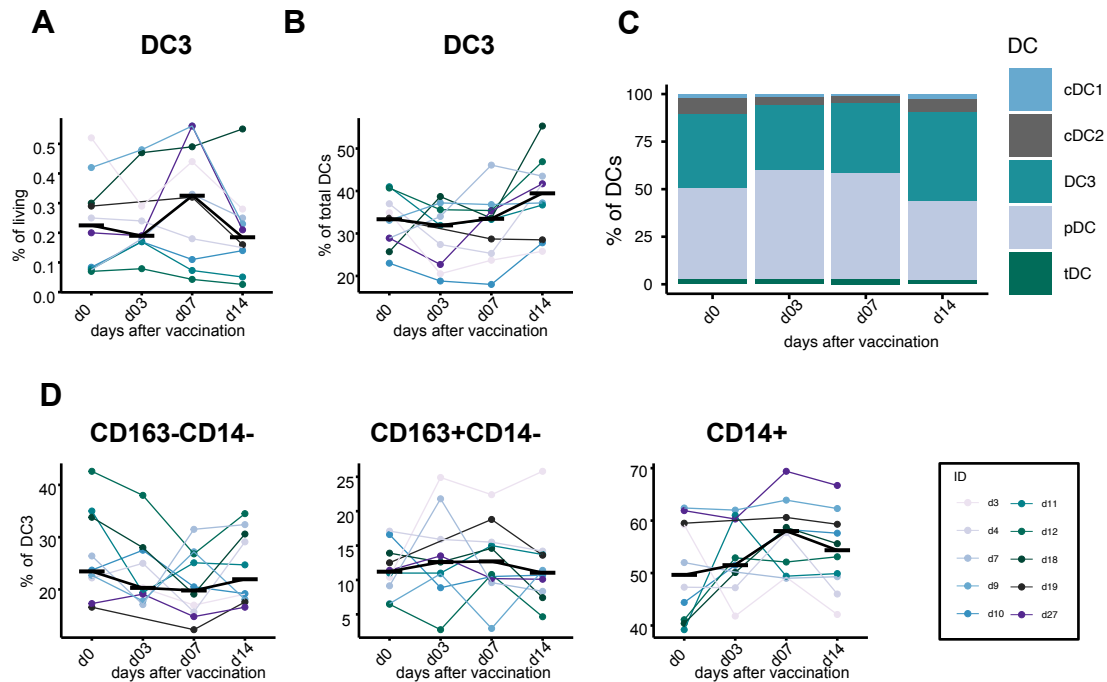
Figure 21: DC3 frequency changes after vaccination with YF17D.
A) Frequency of DC3 of total living cells shown. B) Frequency of DC3 of total DCs is shown. C) The distribution of cDC2, cDC2, DC3, tDC and pDC of total DCs is shown. D) The frequency of DC subtypes as gated by expression of CD163 and CD14 of total DC3 is shown. The black line indicates the median. Significant p values are shown as calculated in R using the Kruskal-Wallis test and Dunn's multiple testing.

4.3.6 UMAP analysis identifies a separate Siglec 1 expressing cluster in DC3 and monocytes

To confirm the manual DC gating strategy, an unbiased analysis of all merged DCs from the 10 vaccinees and 4 time points was performed by UMAP, and the manual gates were overlayed. The UMAP showed clear separation of cDCs and pDCs whereby tDCs were positioned between cDCs and pDCs, as expected. cDC1 (cluster 1) showed a clear separation by expression of CD141 while pDCs (cluster 7) and tDCs (cluster 6) separated by CD123 expression. Differentiation between cDC2 (cluster 2) and DC3 (clusters 3, 4, 5) was possible using CD5. However, the populations formed a continuum from CD5^{high}

cDC2 towards CD5^{low} DC3 while the DC3 subpopulations gated according to CD163 and CD14 expression also formed a continuum (Figure 22 A, B). Looking at the different time points, the composition of DC3 changed between early time points (d0, d3) and d7 after vaccination with a separate cluster appearing (Figure 22 C). This cluster was marked by high Siglec 1 expression on day 7 after vaccination (Figure 22 D). As Siglec 1 is a c-type lectin that is induced by type I IFN the appearance of DC3 and monocytes clusters with high Siglec 1 expression may indicate a strong response to type I IFN after vaccination.
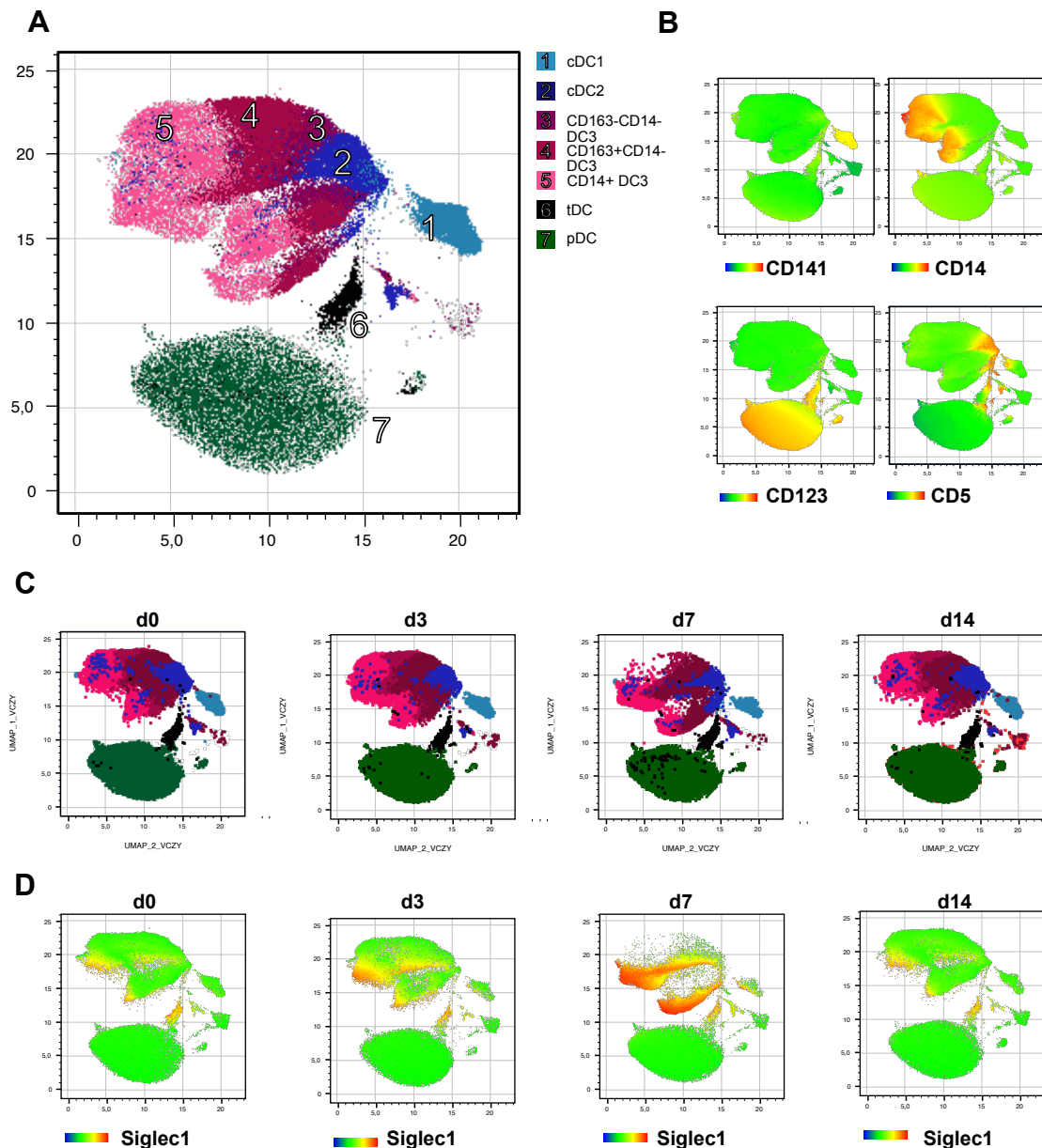
Figure 22: UMAP of merged donors before and after vaccination with YF17D.
A) All DCs from n = 10 vaccinees and time points d0, d3, d7 and d14 were merged and used for UMAP clustering. Gating from Figure 20 was overlayed and cDC1, cDC2, CD163$^-$CD14$^-$ DC3, CD163$^+$CD14$^-$DC3, and CD14$^+$DC3, tDC

and pDC were identified. B) The expression of CD141, CD14, CD123 and CD5 are shown in the UMAP dimension. C) UMAP was separated by time points d0, d3, d7 and d14. D) Expression of Siglec 1 on d0, d3, d7, and d14.

4.3.7 No evidence for tDCs diversification or differentiation towards cDC after YF17D vaccination

Before investigating potential tDC differentiation as fold-changes or diversification after vaccination, it was important to ensure that the gating strategy of tDCs includes the pre-DCs as identified by See et al. (2017) [30]. Recent publications compared transcriptomic data of pre-DCs from See et al. with AS DCs from Villani et al. (2017) [16] and found that they described overlapping populations [161, 179]. However, as the gating strategies defined in these papers differ concerning the markers used, a comparison of the gating strategies in 6 healthy donors within one panel was performed, containing all relevant identifying markers. See et al. gated on CD33 and CD45RA intermediates, followed by a strict gate on CD123^{high} CD45RA^{high} (purple gating strategy). Villani et al. gated on CD141^{-} Axl^{+} Siglec 1^{+} cells (orange gating strategy). When applying the gates used by Villani et al. on the pre-DC gates as in See et al., approximately 93 % of the pre-DCs were found in the first CD141^{low} gate and 65 % in the Axl^{+} Siglec 1^{+} gate. On the other hand, applying the gates used by See et al. to the AS DCs gated as done by Villani et al., approximately 97 % of the AS DCs were found in the CD33^{int} CD45RA^{int} gate and about 73 % in the CD123^{high} CD45RA^{high} gate (Figure 23 A). This shows that the gating strategies identify overlapping populations but not precisely the same cells, with some cells being excluded with either gating strategy.

Since a single exclusively identifying marker has not yet been defined, and tDCs are described in the literature as a heterogeneous population containing cDC1 and cDC2-like subpopulations, a similar gating strategy to Villani et al. with an initial exclusion of CD33^{+} CD123^{-} cDCs and subsequent gating within the CD123^{+} cells on both Axl and CD33 positive cells, not excluding single positives (pink gating strategy), was adopted. This approach led to a high overlap of our tDC gating with both that of the gating of See et al. and Villani et al. The same expression of surface markers stained in all three populations was found, with high CD123, CD2, Siglec 1, CD33, and Axl expression and intermediate CD45RA and low CD1c and CD141 expression (Figure 23 B).

73
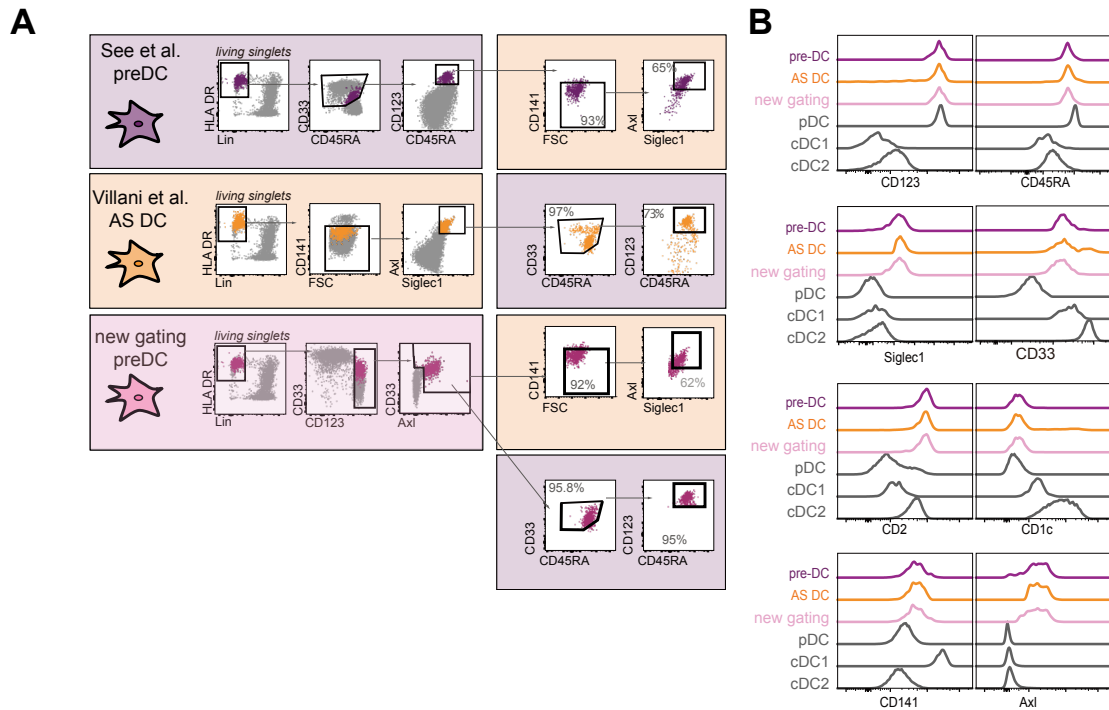
Figure 23: Comparison of tDC/AS DC and pre-DC gating strategies.
A) The gating strategy from See et al. (2017) [30] and Villani et al. (2017) [16] were compared within one sample. Additionally, tDCs were gated using CD33+ Axl+. The color of the cells indicates the primary gating, e.g., purple cells were gated using the See et al. gating strategy (orange = Villani, pink = new gating). The boxes indicate the gating e.g., a purple box refers to See et al. gating while purple cells in an orange box indicate that cells that have been pre-gated with See et al. are now regated using the Villani et al. gating. B) Histograms of different cell signature markers as expressed in the pre-DC/AS DC/ new gated DCs of a representative donor (n = 5).

With the established gating strategy and overlay onto the UMAP, tDCs were identified as a stable population connecting pDCs and cDCs before and 3, 7, and 14 days after vaccination (see Figure 22 C). On day 7, some tDCs could be found within the pDC projection of the UMAP. However, this analysis did not reveal any evidence for diversification of tDCs or differentiation towards cDC, which was described for in vitro cultured tDCs [30].

4.3.8 Upregulation of costimulatory molecules CD83, CD86 and PD-L1 after vaccination with YF17D in APC subsets

The expression levels of activation, maturation markers, and chemokine receptors were compared within the different APC populations at different time points before and after vaccination. The costimulatory molecule CD86 was significantly upregulated on day 7 in most populations and day 3 in tDCs and pDCs, whereas the maturation marker CD83 was

also upregulated in most populations on day 7, but cDC1, cDC2, tDCs, and mo2 already showed an early upregulation on day 3. PD-L1 expression, which is relevant in APCs for the regulation of T cell responses, was also upregulated significantly in all populations on day 7. HLA-DR was predominantly upregulated in monocytes and only significantly upregulated in mo1 on day 7 after vaccination. Looking at the expression of Axl and Siglec 1, which can be used to identify tDCs but have also been shown to be induced by type I IFN [180], the surface expression is significantly and strikingly upregulated in most populations on day 7 (Figure 24 A, B).

CXCR3, which can mediate chemotaxis in response to IFN-induced cytokines such as CXCL9, CXCL10, and CXCL11 [181], was also upregulated significantly in pDCs on day 7 after vaccination and there was a trend towards higher expression in the other APC populations. CX3CR1 was upregulated significantly in pDCs, and in other populations, a trend towards high expression on day 14 was also visible. In this context it is important to note, that CX3CR1 is associated with survival and patrolling ability of monocytes [58] while CCR2 is crucial for the recruitment of monocytes to the infection site via the CCR2-CCL2 axis. CCR2 was significantly downregulated in mo1 and pDCs and only significantly upregulated in mo2 on day 7 after vaccination. While the expression of TREM1 showed a trend towards higher expression on day 3 after vaccination, this did not prove to be significant.

CD40 expression, another costimulatory molecule, was induced in tDCs on day 7 but there was only a trend towards higher expression in the other APC subsets. Overall, an induction of activation and maturation markers can be seen on day 7 after vaccination in all APC subsets coinciding with upregulation of the potentially IFN-induced markers Axl and Siglec 1. On the other hand, chemokine receptors did not show consistent up or down-regulation and seemed to be modulated on days 7 and 14. The upregulation of CXCR3 and downregulation of CCR2 in several monocyte and DC subpopulations could promote migration to sites of IFN-induced chemokine expression.
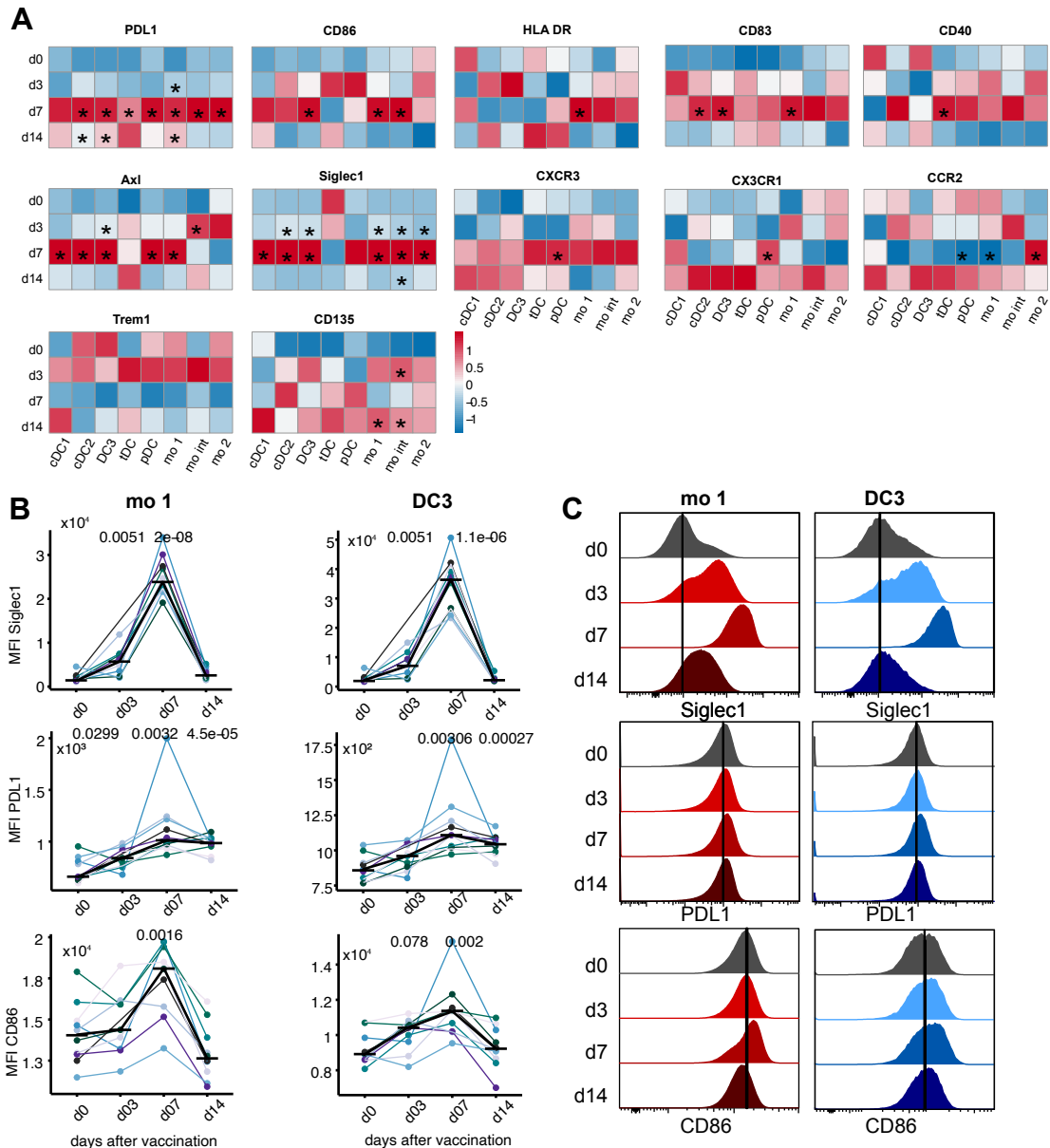
Figure 24: Activation marker and chemokine receptor expression on APCs after vaccination with YF17D.
A) Heatmap of the MFI of markers as indicated on days 0, 3, 7, and 14 after vaccination. The data is scaled for each column and significant p values are indicated by asterisks (* p < 0.05). Red = high expression, blue = low expression.
B) MFIs of Siglec 1, PD-L1, and CD86 over time in mo1 and DC3 of vaccinees. The black line indicates the median.
Significant p values are shown as calculated in R using the Kruskal-Wallis test and Dunn's multiple testing. C) Histograms of merged donors on days 0, 3, 7, and 14 after vaccination showing the Siglec 1, PD-L1 and CD86 expression in mo1 and DC3.

4.4 Transcriptomic response of innate immune cells to YF17D vaccination

The next step was to perform a transcriptome analysis in all human APC populations before and after YF17D vaccination to identify common and cell-type-specific transcriptomic responses at different time points. In this way, it can be determined how cells in the peripheral blood respond to YF17D vaccination, which gene signatures are up- and downregulated, and potentially identify the transcription factors initiating these responses. For this purpose, 1 000 cells were sorted of all DC subpopulations (cDC1, cDC2, DC3, tDC, and pDCs) in addition monocytes, (mo1, mo int, mo2) and B cells as well as 100 000 total PBMCs from the frozen PBMC samples collected from 4 study participants before and on days 3, 7, 14, and 28 after vaccination (gating strategy found in Figure 25 A). RNA sequencing was performed as described in the methods that were adapted for this purpose from the Smart-seqv2 protocol published by Picelli et al. (2014) [172] (Figure 25 B).
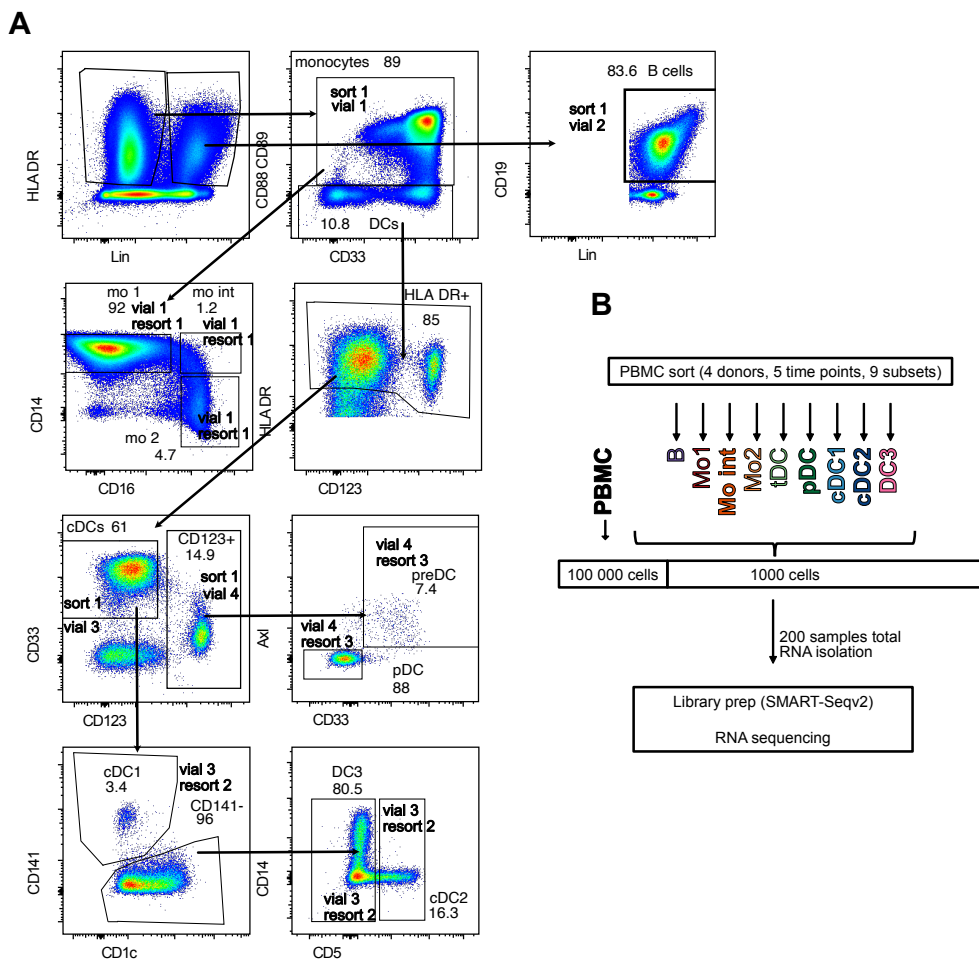
Figure 25: Sorting strategy for sequencing experiment.
A) B cells were gated as HLA-DR$^+$ Lin$^+$ CD19$^+$ and directly sorted. Monocytes were sorted as HLA-DR$^+$ Lin$^-$ CD88/89$^+$ and then resorted into CD14$^+$ CD16$^-$ mo1, CD14$^+$ CD16$^+$ mo int and CD14$^-$CD16$^+$ mo2. DCs were sorted as HLA-DR$^+$ Lin- CD88/89$^-$ and then regated for HLA-DR^{high} and separated into CD33$^+$ cDCs and CD123$^+$ cells. Then cDCs were subsequently resorted into CD141$^+$ cDC1, CD141$^-$CD1c$^+$CD5$^+$ cDC2 and CD1c$^+$CD5$^-$ DC3. CD123$^+$ cells were re-sorted into Axl$^+$ CD33$^+$ tDC or double negative pDC. B) Experimental design of the bulk-sequencing experiment whereby 1 000 cells of DC and monocyte populations and 100 000 cells of total living PBMCs were sorted directly into RLT buffer, RNA was isolated, and RNA libraries were prepared following the adapted Smart-seqv2 protocol. The libraries were subsequently sequenced.

4.4.1 PCA shows clustering of distinct APC populations

Principal component analysis (PCA) of all genes after filtering across all sequenced samples was used to analyze how the individual sorted APC populations cluster together. While PC2 mostly separates between B cells and DCs, monocytes, and PBMCs, PC1 separates between the individual DC and monocyte populations (Figure 26). Whereas pDCs cluster to the left of PC1, monocytes are found on the right. tDCs connect cDC1 and pDCs, then cDC2 follow and DC3 make the connection towards mo1, then mo int and mo2. Each sorted APC population clusters independently of the time point analyzed, showing that the inter-population difference is larger than the intra-population differences between the time points. Interestingly, at early time points, DC3 show closer proximity to monocytes, while at later time points, they are closer to DC2. Complete PBMCs clustered between tDCs, monocytes, and PBMCs were a bit lower on the PC2 axis but still far away from B cells and were widely spread between the DC and monocyte populations.
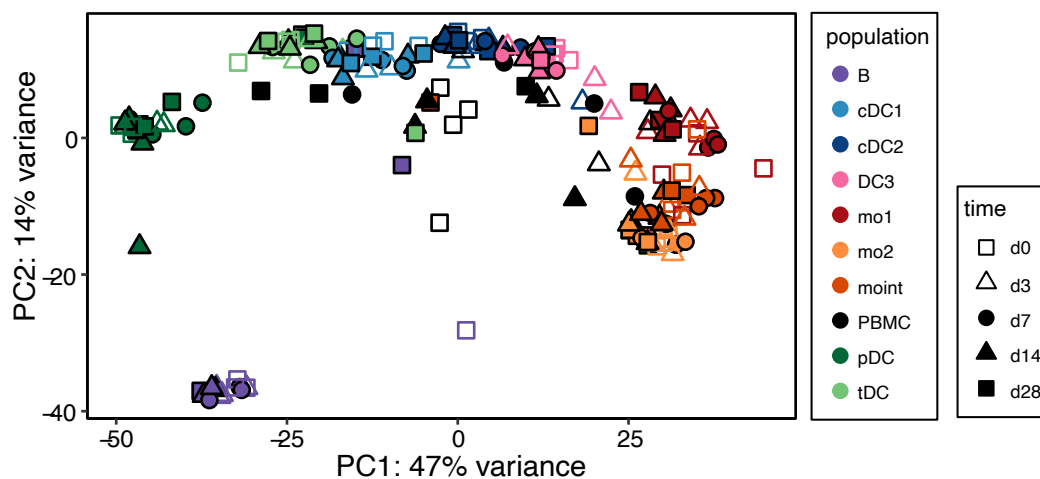
Figure 26: PCA analysis of VST transformed RNASeq data after pre-filtering.
Sorted populations are indicated by colors and the symbol indicates the time after vaccination.

Looking at the distinct DC subpopulations, the expression of the top 25 signature genes of each DC population from Villani et al. (2017) and for DC3 from both Villani et al. and Dutertre et al. (2019) [15, 16] were examined, which had been identified by comparing the different DC subsets in the steady-state and extracting sets of highly expressed population-specific genes. These gene lists were then used to extract the VST transformed expression values of the sorted APC subsets which were visualized using heatmaps (Figure 27).

A high expression of the respective signature genes in each sorted cell population across the different time points after vaccination was found, proving the identity of the sorted DC subpopulations. cDC2 signature genes were highly expressed in both cDC2 and DC3, indicating the close connection of the CD5$^+$ and CD5$^-$ CD1c$^+$ cells. However, from the DC3 signature genes, differences to cDC2 are visible due to genes also expressed by monocytes like *CD14*, *S100A8*, *S100A9*, which are not found in cDC2. This shows the similarity of DC3 to both cDC2 and to monocytes in the peripheral blood. Interestingly, even though DC3 signature genes were highly expressed in mo1, only low expression was found in mo2 and mo int. An examination of the pDC signature genes showed that most were also expressed in tDCs, although the overall expression was lower. The tDC gene signature contained several genes distinguishing them from pDCs such as *SIGLEC6*, *SIGLEC1*, *AXL*, and *CD5*. Overall, most signature genes were consistently expressed in the vaccinees over time, thereby indicating that the cell identity was maintained. However, the tDC-signature gene *SIGLEC1* was upregulated in DC and monocyte populations at time points 3 and 7 days after vaccination, which corresponds to the finding of increased surface expression of Siglec 1 in monocyte and DC subsets.
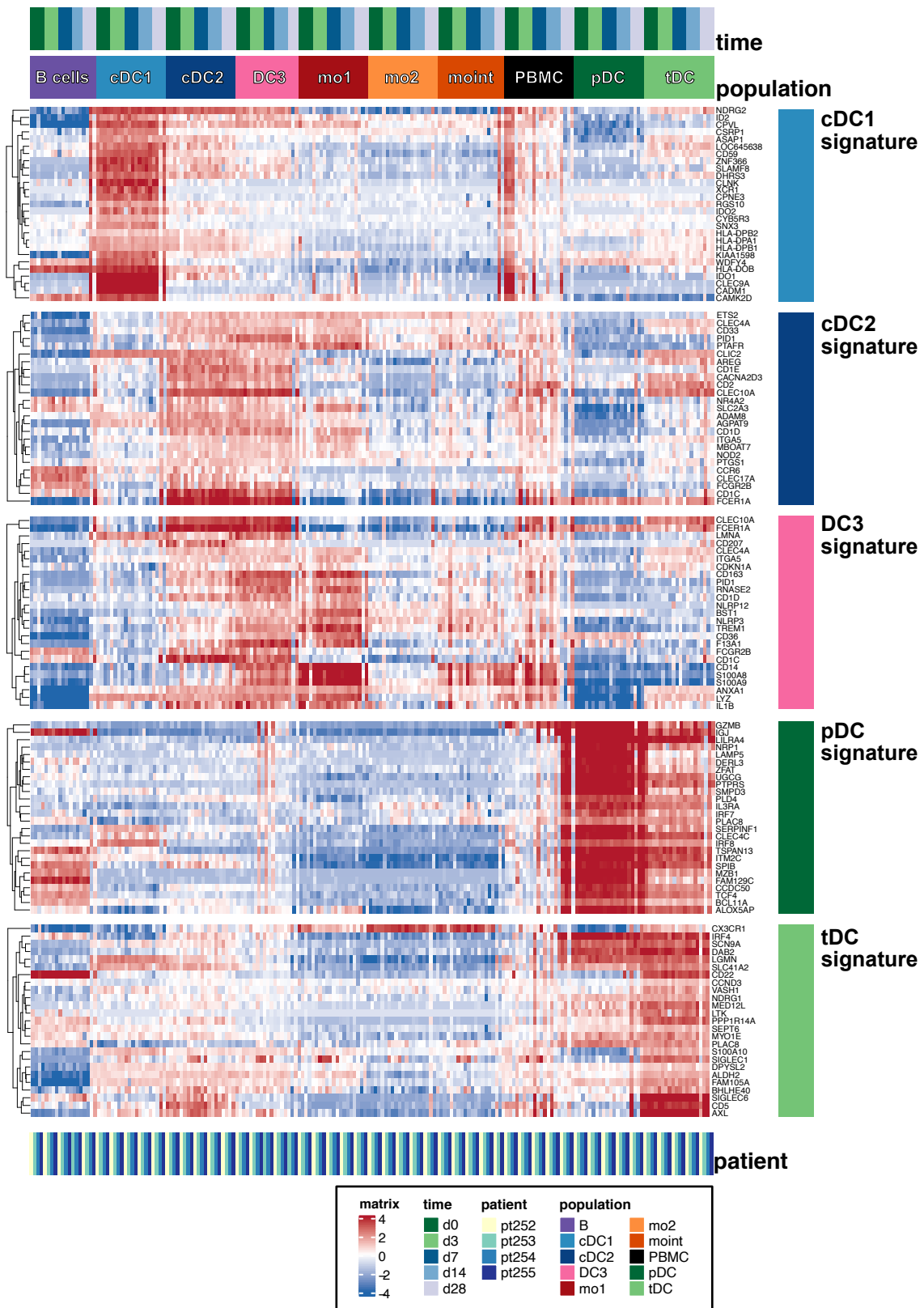
Figure 27: Expression of DC subtype-specific gene signatures.
Signatures were generated from Villani et al. (2017) and Dutertre et al. (2019) [15, 16] and used to annotate the dataset. 25 highly expressed genes were selected and used to visualize the VST transformed expression values obtained from the sequencing.

4.4.2 The peak of the innate immune response is on day 7 after vaccination

An examination of the significantly up- and downregulated genes in the individual populations over time (adjusted $p < 0.05$), identified the peak of the innate immune response on day 7 after vaccination in most populations, except for pDCs, where surprisingly the largest number of up- and downregulated genes was observed on day 28 after vaccination (Figure 28). Mo1 showed the highest number of up- and downregulated genes at all time points from day 3 up until day 28 after vaccination. Mo int and mo2 however showed only minor changes on day 3 after vaccination. Overall, the peak transcriptome response seems to be on day 7 after vaccination in most APC populations, with mo1 showing the greatest changes after vaccination, followed by DC3, mo2, cDC2, tDC, cDC1, pDC, B cells and lastly by mo int.
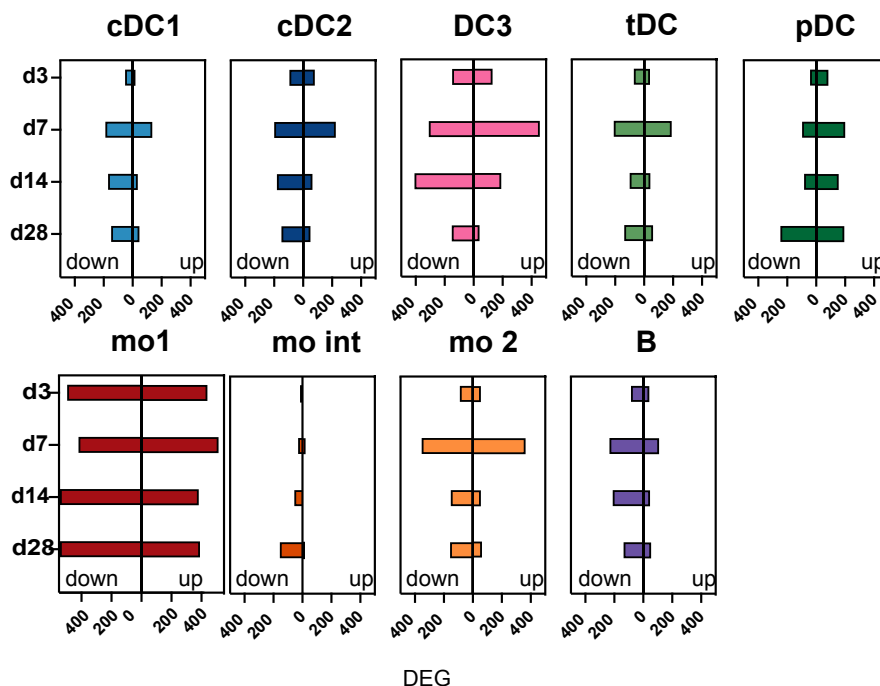
Figure 28: Significantly up or downregulated DEGs compared to day 0.
DESeq2 was used to find the up- and downregulated genes adjusted $p < 0.05$ of each population and each time point compared to day 0. The number of up- and downregulated DEGs are shown and the color indicates the population.

4.4.3 Interferon signature genes upregulated on day 7 after vaccination

The next analysis concerned the overall transcriptomic type I IFN response to YF17D vaccination since previous publications showed high induction of ISGs in total PBMCs [118, 130] and since upregulation of surface expression of Axl and Siglec 1 was found in the APC subsets, which could be a sign of a strong IFN response.

Looking at the individual populations, upregulation of IFN stimulated genes, which were annotated with a signature list from an IFN signature of SLE patients and vaccinees (including YF17D vaccination) [182, 183], was seen at 3 and 7 days after vaccination. Although one, sometimes two patients showed a high IFN response already on day 3, the overall peak response was on day 7 after vaccination. The highest induction of this specific ISG signature gene set was found in mo1, mo int, mo2, cDC2, DC3, followed by cDC1, B cells, and total PBMCs, and the lowest induction of these ISGs was identified in pDCs and tDCs. The genes *OAS1*, *OAS3*, *OASL*, *RSAD2*, *IFIT3*, *IFIT1*, and *EIF2AK2* were highly upregulated in all APC populations, which indicates a concerted ISG response after vaccination (Figure 29).
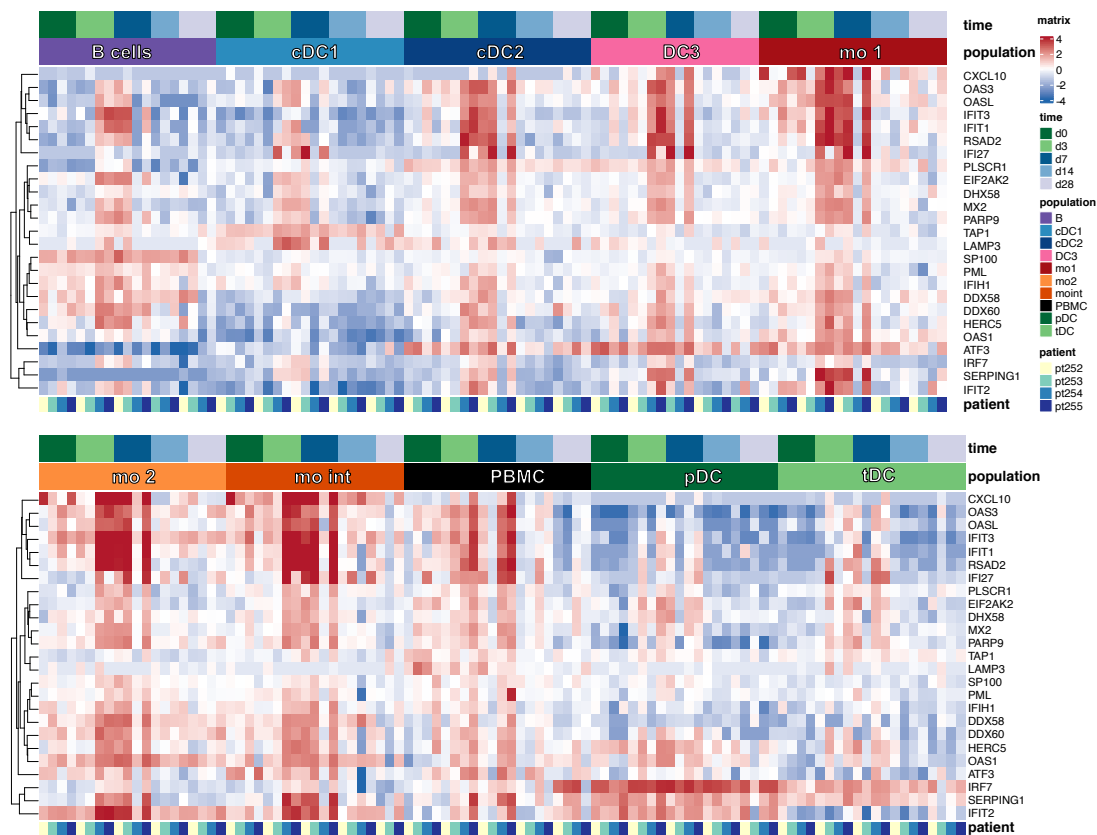
Figure 29: Expression of IFN I signature gene set.
Type I IFN signature genes [182, 183] are differentially expressed in the different populations and over time after vaccination with YF17D. Heatmap of VST transformed data of type I IFN gene set.

To analyze the expression of PRRs in APCs, a self-curated set of PRR genes (adapted from KEGG pathway data) was used which showed that cell-type-dependent expression occurred and that most PRR-associated genes were not differentially expressed over time. *TLR7* and *TLR9* were mostly expressed in pDCs, and *TLR9* was also expressed in tDCs (Figure 30 A). On the other hand, *TLR3* expression was restricted to cDC1. Interestingly, some PRR genes were differentially expressed over time, such as *DDX58*, *DHX58*, *NLRP1*, *STAT1,* and *STAT2* which showed higher expression on day 7 after vaccination in cDCs and monocytes (Figure 30 A, B) consistent with their induction by IFNs. The expression of *DDX58* encoding the cytosolic RNA sensor RIG-I that is involved in YF17D recognition is shown as an example in Figure 30 B. *AIM2*, which encodes an IFN-inducible DNA sensor that activates the inflammasome [184], was induced on day 7 after vaccination in monocytes, but was highly expressed in both B cells and cDC1 at all time points.
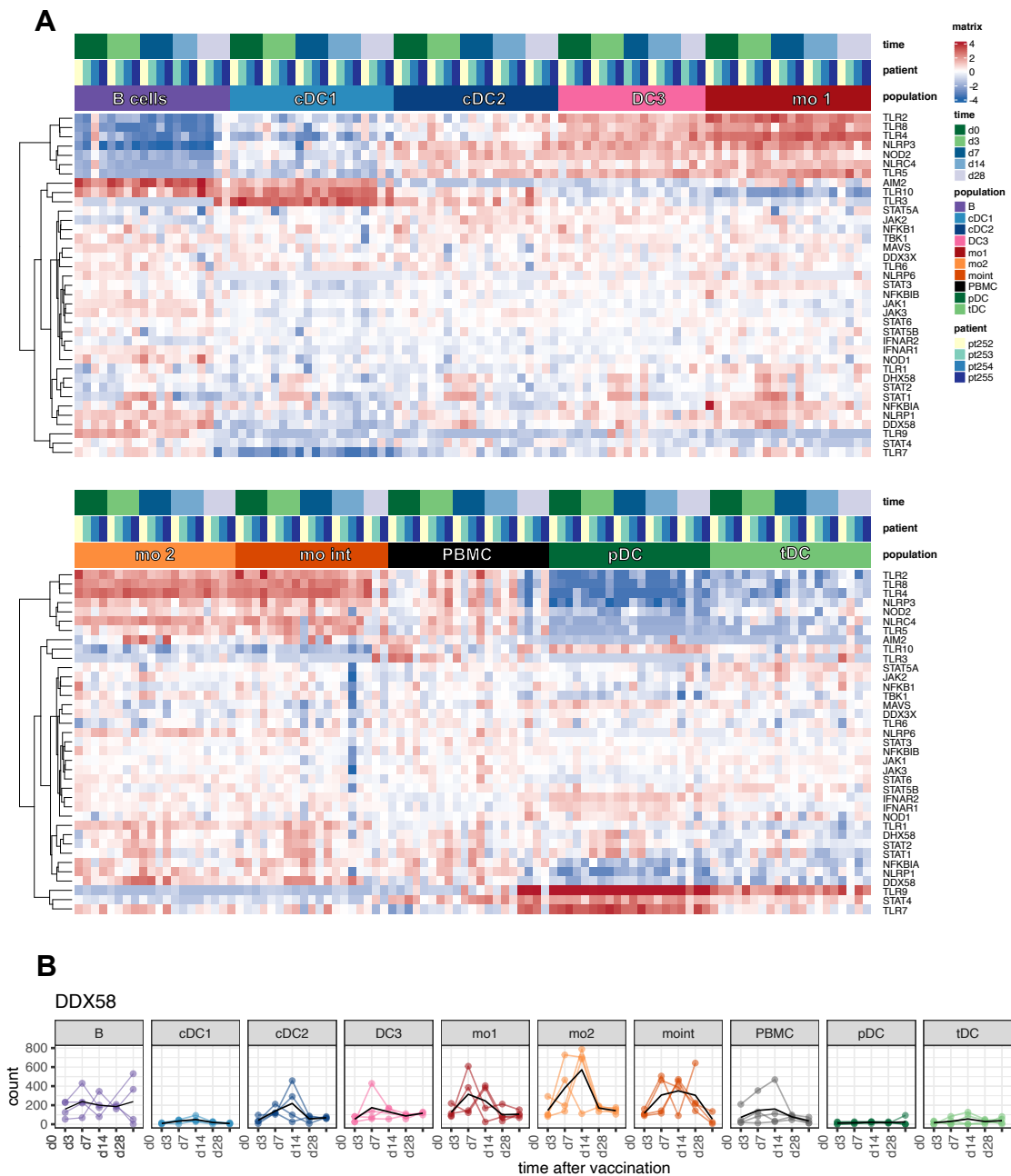
Figure 30: Expression of PRR associated genes in the different populations and over time after vaccination with YF17D.

A) Heatmap of VST transformed data of PRR associated genes. B) Normalized counts in different populations of *DDX58* expression over time.

4.4.4 DC3 and cDC2 show similar transcriptomic changes after vaccination with YF17D

DC3 share properties of monocytes and cDC2, but are distinct from monocytes and cDCs with regard to their ontogeny. Therefore, it was interesting to investigate their response

to viral infection such as after YF17D vaccination, and compare their response to that of cDC2 or monocytes. Since the signature gene expression profile of DC3 as well as the PCA analysis showed the closest similarity of DC3 with cDC2 and mo1, the DEGs were compared between day 7 (peak immune response) and day 0 (before vaccination) of DC3, cDC2, and mo1 to show which of the DEGs expressed after vaccination are overlapping or specific for the populations. The highest number of DEGs was found in DC3 and mo1. However, the highest overlap within these DEGs was between DC3 and cDC2, with 101 distinct genes being significantly up- or downregulated on day 7 after vaccination in both DC3 and cDC2 (Figure 31 A). In the comparison between DC3 and mo1, only 56 of the same genes were significantly differentially expressed. Thus, the transcriptome response to vaccination is more similar between cDC2 and DC3 than between DC3 and mo1. Altogether, 89 DEGs were found in all three populations (Figure 31 B) mainly encompassing IFN regulated genes such as *IFI6*, *IFI44L*, *IFIT1*, *MX2*, *OAS1,* and *STAT1*. A total of 530 DEGs were specific to DC3, for example, *IRF8* which is essential for cDC1 and pDC development and is relevant for antiviral responses by enhancing expression of IFN-α and IFN-β and inducing pro-inflammatory genes [185]. *TCF4*, a transcription factor relevant for pDC development, was also surprisingly found to be upregulated in DC3 after vaccination (Figure 31 C). The genes overlapping between cDC2 and DC3 encompassed some genes involved in antigen presentation via MHC I molecules such as *CLEC4C*, *PSME1*, *PSME2*, *PSMB9, HLA-A,* and *B2M* (Figure 31 D) that were upregulated on day 7 after vaccination in DC3. Interestingly, some genes were downregulated on day 7 in both cDC2 and DC3, including *IMPDH2*, which is involved in de novo guanine nucleotide biosynthesis and therefore relevant for RNA and DNA synthesis, and *CLTC*, the clathrin heavy chain relevant for endocytosis. On the other hand, *IL1R2*, a non-signaling receptor of IL-1, showed long-lasting downregulation in cDC2 and DC3 after vaccination up until the last time point measured.
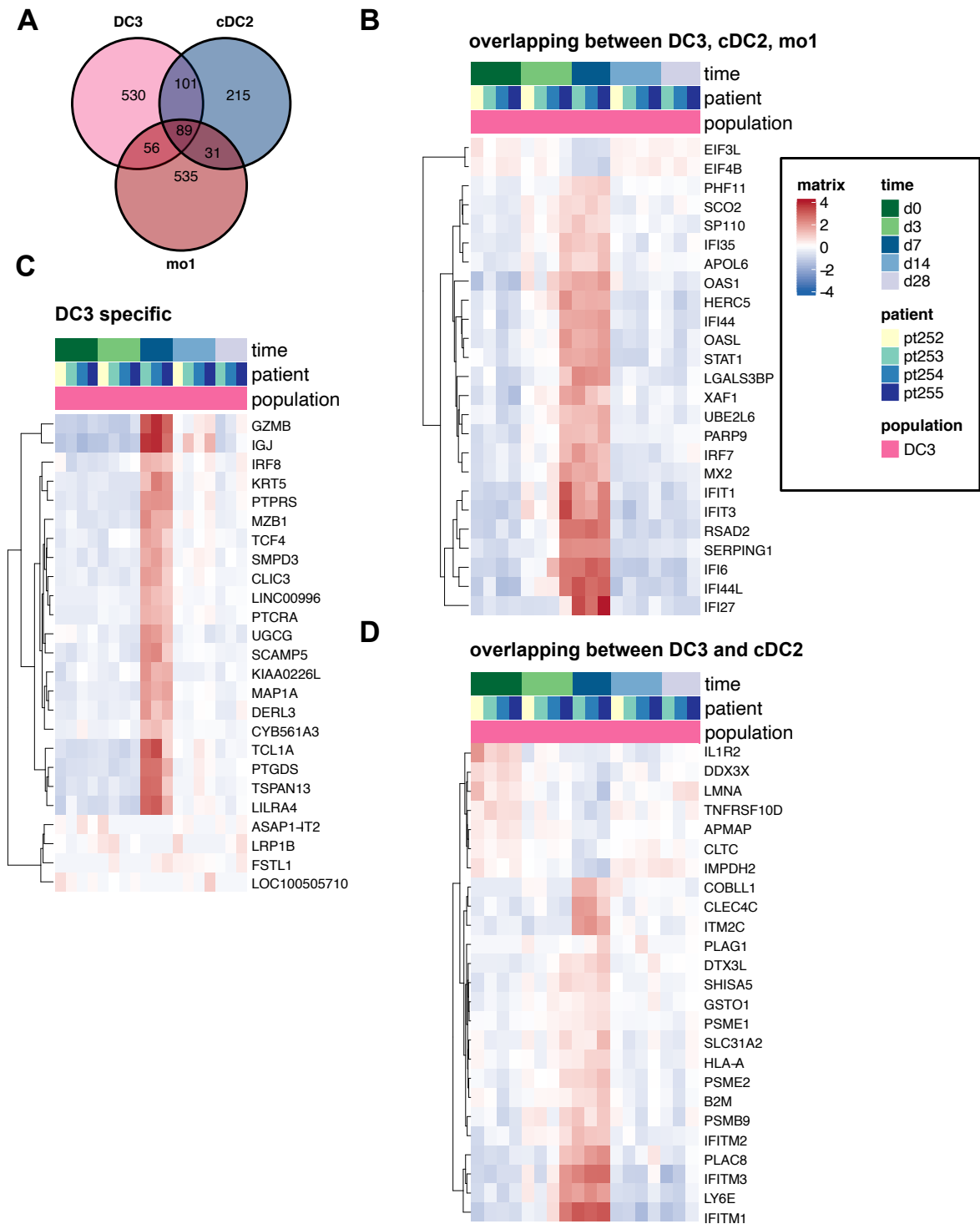
Figure 31: Comparison of immune response of cDC2, DC3 and mo1.
A) Venn diagram showing similarities and differences of DEGs (padj. >0.05) expressed on d7 compared to d0 in cDC2, DC3 and mo1. B) The top 25 of the 89 overlapping genes between DC3, cDC2 and mo1 are shown. C) The top 25 of the DC3 specific genes are shown. D) The top 25 of the 101 overlapping genes between DC3 and cDC2 are shown.

4.4.5 Gene set enrichment analysis shows the importance of interferon pathways for antiviral response in DC3

To further elucidate the immune response to YF17D vaccination in the DC3 population, all DEGs up- or downregulated in DC3 on day 7 compared to day 0 were used for gene set annotation analysis annotating to the KEGG pathway, the Hallmark gene sets, the Reactome and the Blood Transcriptional Modules (BTM) according to Li et al. (2014) [183]. Gene set enrichment analysis showed a strong upregulation of gene sets connected to the type I IFN responses (e.g., *IFITM3*, *IFI6*, *IFITM2*, *IRF8*, *STAT1*, *IFIT3*) and "antigen processing and crosspresentation" (e.g., *PSME2*, *PSMB2*, *HLA-A*, *HLA-F*, *B2M*, *PSME1*, *PSMA6*, *TAP1*, *TAP2*, *MYD88, SEC22B, SEC61B*) derived from the Reactome, Hallmark and BTM gene sets. The BTM annotation also described "antiviral signatures" (e.g., *SERPING1*, *HERC5*, *DHX58*, *DDX60*, *C1QB*) and an "innate antiviral response" (e.g., *OASL*, *IRF7*, *IFIT1*, *OAS1*, *RSAD2*) in addition to "viral sensing" (e.g., *IFI35*, *BST2*, *USP18*, *TLR7*, *TNFSF13B*, *ZBP1*) and "antigen presentation" (e.g., M95.0 *IRF8*, *ITGA4*, *SELL*, *AIF1*, *CD53*, *GIMAP6*, *FGL2*) to be enriched in the DC3 on day 7 after vaccination (Figure 32 A, B, C, D, E). On the other hand, "resting DC cell surface signature" (e.g., *IL1R2*, *ITGAX*, *IL1R1*, *HLA-DQB1*, *SERINC5*) as well as two of the "enriched in antigen presentation" modules (M71 e.g., *RTN1*, *HLA-DPB1*, *PTGS2*, *HLA-DRA, CD74;* M95.1 e.g., *FYB, CD53, HLA-DRA, ITGB2, ICAM1*) showed a negative normalized enrichment score (NES). Hence, MHC I antigen presentation generally seems to be favored over MHC II presentation in DC3 on day 7 after vaccination with YF17D. Since the BTM analysis, which is based on immune perturbations in PBMCs, has the most fitting modules for the dataset, the most interesting modules in DC3 were compared over time, using the individual DEGs from comparing each time point after vaccination with d0 (Figure 32 F) for GSEA. Many of the modules regulating DC activation and antiviral immune responses were positively enriched on day 3 and day 7 after vaccination, such as "activated dendritic cells", "antiviral IFN signature" and "innate antiviral response".
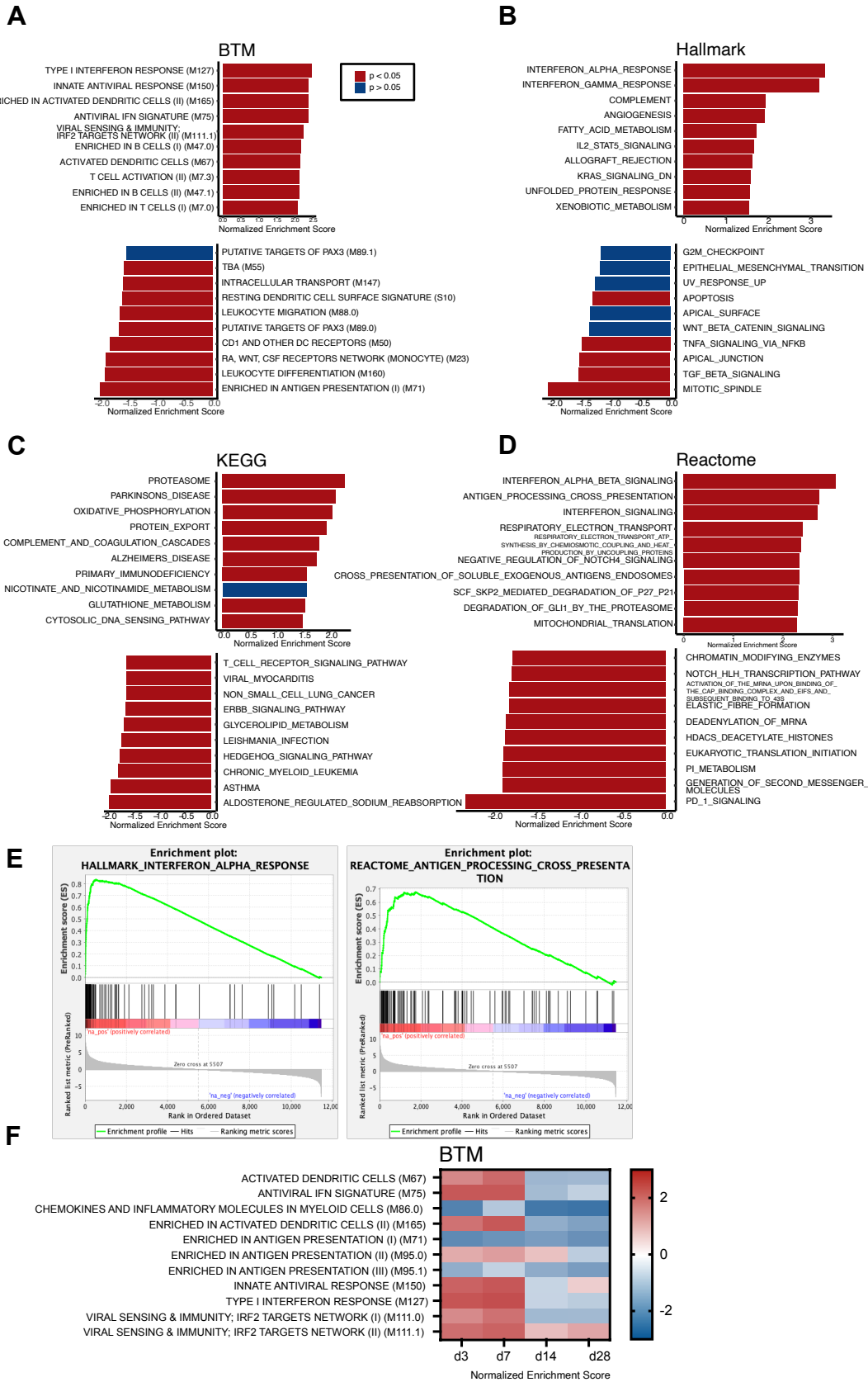
Figure 32: GSEA of DC3 DEG between d0 and d7 after vaccination.
A) BTM, B) Hallmark, C) KEGG pathway, and D) Reactome enrichment analysis. The 10 gene sets with the highest and lowest NES rank are shown. E) Visualization of exemplary Hallmark and Reactome enrichment analysis. F) GSEA of BTM modules of DC3 DEG between d0 and d3, d0 and d7, and d0 and d14 are displayed. The NES of selected BTMs of interest over time are shown.

To analyze the regulation of gene expression in DC3, k-means clustering of all genes that were differentially regulated over time (with the DESeqv2 reduced model) was performed and 10 gene clusters and 5 sample clusters were identified, which largely corresponded to the analysis time points, with d14 and d28 clustering together. The gene clusters were annotated by GSEA using the Hallmark gene sets and were also analyzed for enrichment of transcription factor binding motifs using the Rcis target package in R (Figure 33). Gene cluster 1 was enriched in genes found in Hallmark "IL2 STAT5 signaling" and "IL6 JAK STAT3 signaling" gene sets. Genes in this cluster were most highly expressed by DC3 on day 7 and, in one patient, already on day 3 after vaccination (sample cluster 5 and cluster 4). This cluster also contained genes involved in the interferon response such as *SIGLEC1*, *IFITM1*, *ISG15,* and *IRF7*, which was previously highlighted as being a relevant transcription factor for the regulation of the immune response to YF17D [118, 126]. Consistently, binding sites for transcription factors Stat1/Stat2, Irf1/2/7/9 were enriched in gene cluster 1. Gene cluster 6 was enriched in genes found in the Hallmark gene sets "IL2 STAT5 signaling", "TGF-β signaling", and "KRAS signaling up" and these genes were also upregulated for most donors on day 7 and on day 3 in one donor (pt255). This cluster was enriched for genes containing binding motifs for XBP1 and ATF2 as well as E2F1 indicating increased stress response and cell cycle/proliferation in DC3 at the time point of peak response. Gene cluster 8 contained genes upregulated on day 7 and was enriched in interferon response genes including *IRF4*, *IRF8*, *TLR9*, *TLR7*, *LAMP4,* and others. This cluster was enriched for binding sites of *GMEB2* (involved in glucocorticoid-mediated gene induction) and *CREB1*, which was shown to have an antiapoptotic and anti-inflammatory function in myeloid cells [186]. Gene clusters containing genes downregulated early or late after vaccination were also identified and warrant further investigation.
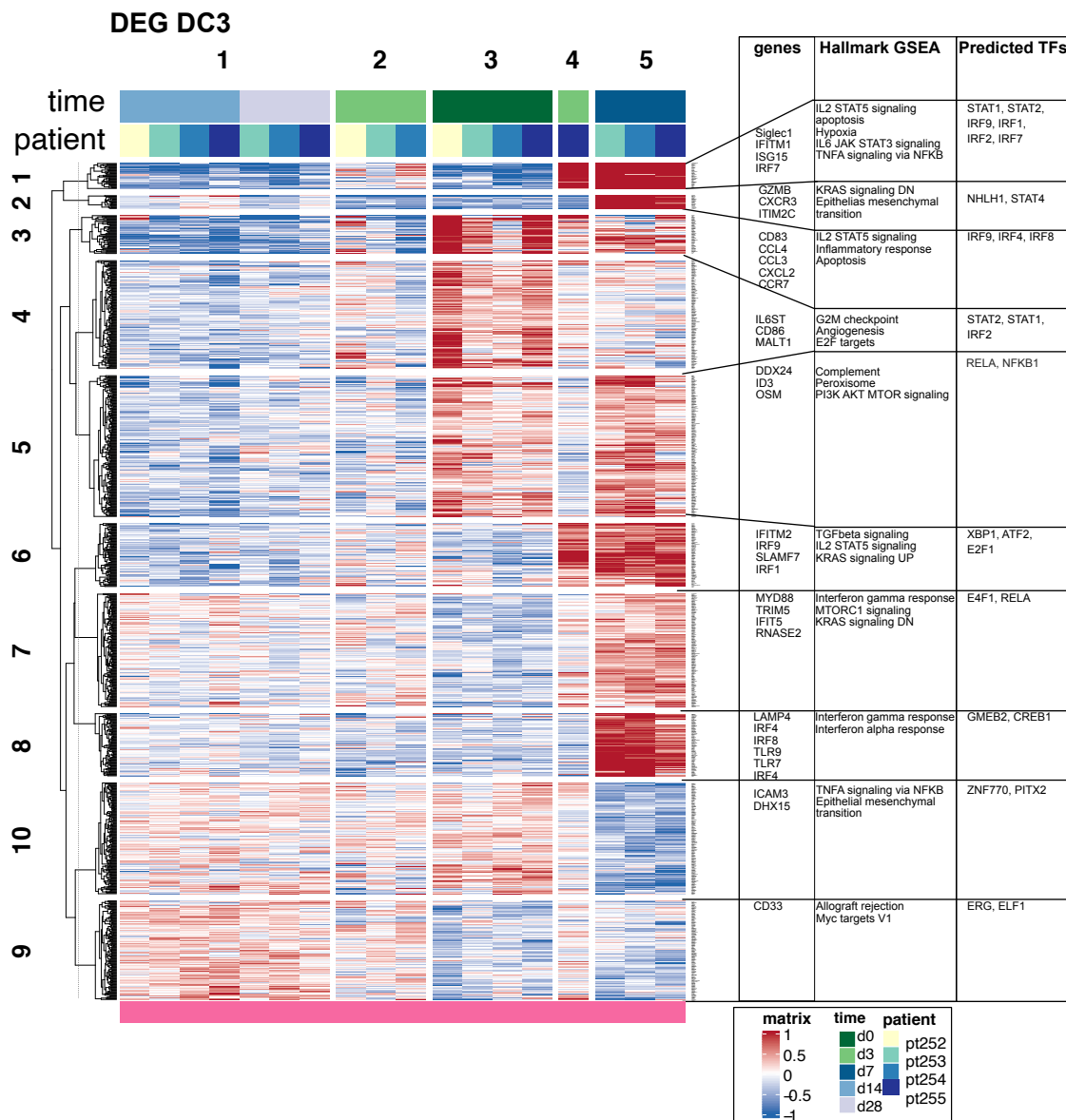
Figure 33: Clustering of DEGs of DC3 over time.
Both rows and columns are clustered using k-means clustering as indicated by the number and separation of the heatmap. The clusters were subsequently annotated for selected Hallmark functional pathways enriched in the major clusters and the known transcription factors (TFs) that bind to motifs enriched in the major clusters (selected for highest enrichment scores for each cluster).

These results show that in all APC populations, a strong upregulation of ISGs is one hallmark of the innate immune response to YF17D vaccination, with its peak on day 7. This ISG response consists of population-specific ISGs, and a common gene signature found across APC subsets in the peripheral blood (e.g., *OAS1*, *OAS3*, *OASL*, *RSAD2*, *IFIT3*, *IFIT1*, *EIF2AK2*). Direct comparison of DC3, cDC2, and mo1 showed a high similarity of the transcriptomic response after vaccination between DC3 and cDC2 with concerted

induction of MHC I antigen presentation genes. In contrast, the genes differentially regulated after vaccination in DC3, cDC2, and mo1 mostly comprise ISGs. GSEA then showed that the primary immune response of DC3 is the interferon responses, DC activation signatures, and antigen processing/MHC I presentation signatures.

4.5 Comparison of the DC and monocyte response in YF17D vaccinees and COVID-19 patients

YF17D is a very useful model to study viral infections in humans since it is a controlled live virus infection leading to life-long immunity. Viral infections with SARS-CoV-2 emerged in 2019 and, due to its highly contagious nature, SARS-CoV-2 has led to a global pandemic and millions of people dying of the associated disease COVID-19. The outcomes of a SARS-CoV-2 infection range from asymptomatic infections to mild, moderate and severe disease progression. Host factors, such as age, sex, comorbidities, and the immune response have a significant influence on the disease progression after infection. In patients with severe disease progression, the immune response appears to be dysregulated, leading to grave inflammatory responses and subsequent tissue damage in the lung and in other organs in some cases. On the other end of the spectrum, the infection is well controlled by the immune system and progresses with no or with only mild symptoms, which is more akin to the immune response observed after YF17D vaccination, although long-term protective immunity has not been proven and is unlikely to develop after SARS-CoV-2 infection. Additionally, convalescent COVID-19 patients can show productive reinfection [187]. It was therefore interesting to compare the innate immune response, especially the response of DC and monocyte subsets to YF17D vaccination and SARS-CoV-2 infection. The hypothesis is that there are similarities (especially concerning the mild form of SARS-CoV-2 induced disease) and also significant differences in how the immune system reacts to YF17D vaccine virus compared to SARS-CoV-2, which could already manifest in the first innate immune response to the viruses with consequences for adaptive immunity. It was thus decided to directly compare the innate immune response in patients with mild COVID-19 and the dysregulated immune response seen in patients with severe COVID-19 with the well-regulated and balanced immune response to YF17D in vaccinees from the cohort described in part 4.3.1-3.

4.5.1 Design of the COVID-19 outpatient study

To analyze the innate immune response to SARS-CoV-2 with a focus on circulating DC and monocyte subpopulations, multi-parametric flow cytometry was performed on PBMCs of COVID-19 patients at several time points after symptom onset in collaboration with AG Geldmacher. This study was conducted at the Division of Infectious Diseases and Tropical Medicine (LMU) by Dr. Christoph Geldmacher, whereby I established the antibody panel for flow cytometric analysis of DC and monocyte subsets including intra-cellular staining for Ki67. The sample preparation, staining, and flow cytometric meas-urements were performed by Tabea Eser. In a collaborative effort, the resulting raw data were kindly provided by AG Geldmacher, after which I performed analysis using FlowJo software and further data analysis in R in addition to visualization and interpretation of the data.

In this study, patients were directly recruited after their diagnosis at the test center. The patients and their household contacts were longitudinally followed with nasal swaps and SARS-CoV-2 diagnostic PCR for several months. All of the patients in this study pre-sented with mild COVID-19 symptoms (blue) and were quarantined at home without the need for hospitalization (mild, n = 39). Seven hospitalized COVID-19 patients (severe =S, n = 7, median 5 days after diagnosis) were included in this study as a separate group. A control group was recruited via household contacts of the COVID-19 outpatients and age-matched volunteers (healthy = H, n = 15, Figure 34 A). Blood samples were collected at several time points, between 0 and over 60 days after symptom onset. One patient that did not show any symptoms was excluded from the study. While the day of infection was unknown, the usage of the time after symptom onset facilitated the analysis of the kinetics of the immune response in a similar fashion to what was done in YF17D vaccinees. An almost identical antibody panel, just lacking antibodies against monocyte markers, was previously used on PBMCs from YF17D vaccinees, thereby allowing for a comparison of DC frequencies and activation status between the COVID-19 patients and the YF17D vaccinees. In this instance, the DC3 population was not analyzed separately.

A
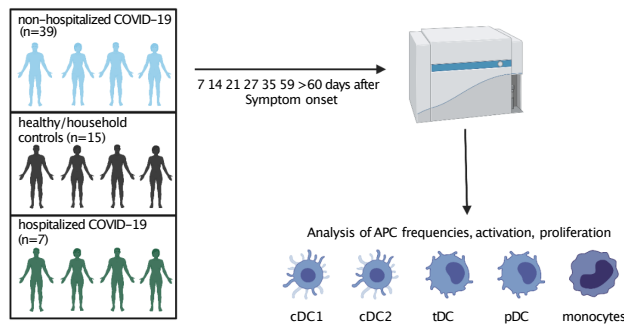
B
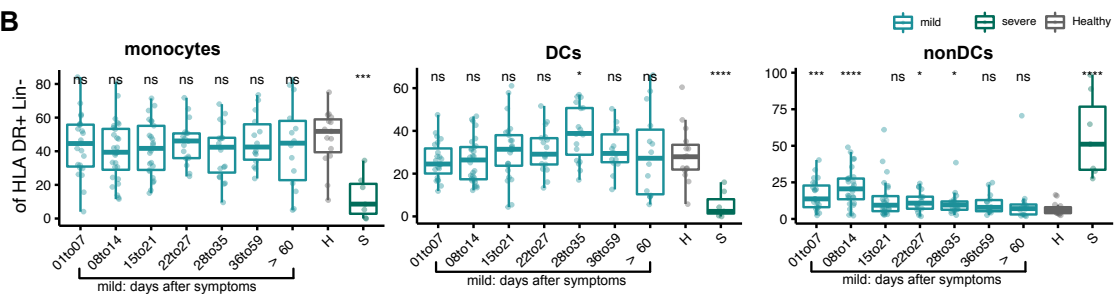
C
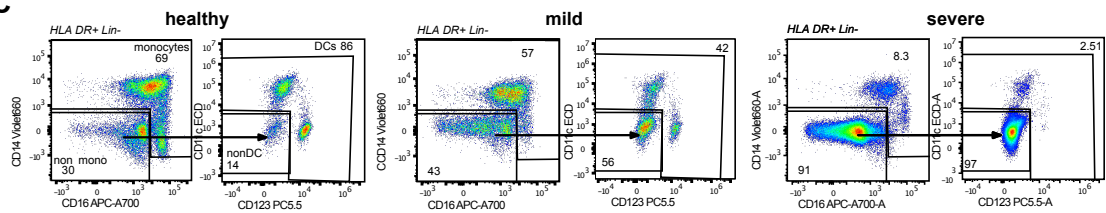
Figure 34: The design of the COVID-19 study in outpatients.
A) Design of the study. PBMCs were collected at multiple time points from non-hospitalized COVID-19 patients with a mild disease progression (n = 39), hospitalized, COVID-19 patients with severe disease progression (S, n = 7), and healthy controls (H, n = 15). DC and monocyte frequencies and activation status was measured and the data for the outpatient cohort with a mild disease progression was summarized for grouped time points after symptom onset. Graphical abstract done with Biorender. B) Monocyte (Lin⁻ HLADR⁺ CD14⁺ or CD16⁺), DC (Lin⁻ HLA-DR⁺ CD14/CD16⁻ CD11c⁺ or CD123⁺), and nonDC (Lin⁻ HLA-DR⁺ CD14/CD16⁻ CD11c/CD123⁻) frequency of HLA-DR⁺ Lin⁻ cells in mild patients (blue), healthy controls (gray) and severely affected, hospitalized COVID-19 patients (green). The horizontal lines show the median and the box plots show the upper and lower quartiles, while whiskers indicate 1.5 IQR. Significance (*p < 0.05, ** p > 0.01, *** p > 0.001, ****p > 0.0001) indicated by asterisks. Significant p values are shown as calculated in R using the Kruskal-Wallis test and Dunn's multiple testing and comparing with healthy controls. C) Dot plot of representative COVID-19 patients showing the reduction of monocytes and DCs and increase of nonDCs. The numbers indicate percentages of the cells within the respective gates.

4.5.2 Increase of population lacking DC and monocyte markers in severe COVID-19 patients

A relative reduction of the percentages of monocytes and DCs of total HLA-DR$^+$ Lin $^-$ (CD3, 19, 20, 56, 66b) was observed in the COVID-19 patients with severe disease progression compared to the healthy control group (Figure 34 B, C). Concomitantly, a population lacking typical monocyte and DC markers as well as T, B, NK cell and granulocyte markers (CD3$^-$, CD14$^-$, CD16$^-$, CD19$^-$, CD20$^-$, CD56$^-$, CD66b$^-$, CD123$^-$, CD11c$^-$, CD1c$^-$, CD141$^-$) but expressing CD86$^{+/-}$ and HLA-DR$^+$ was found to be highly represented in those patients (Figure 34 B, C), which were termed "nonDCs" due to their lack of markers associated with DCs or any other specific cell lineage. This population is described in more detail in Chapter 4.6.3.

These differences in cell frequencies were statistically significant. In outpatients with mild disease progression, a significant increase of nonDCs was seen at early time points up to 14 days after symptom onset while this expansion was more pronounced in the hospitalized patients with severe COVID-19. Relative frequency of DCs was significantly reduced in severe COVID-19 and in mild disease there was a trend towards a lower frequency DCs (not significant).

Focusing on monocytes, in mild and severe COVID-19 disease, an increased percentage of intermediate monocytes up to 7 days after symptom onset and a reduction of nonclassical monocytes were observed. In patients with severe disease the percentage of classical monocytes was significantly reduced (Figure 35 A, B). Although pDC frequency within DCs decreased at early time points in both mild and severe disease, other changes in the DC compartment could not be observed in COVID-19 patients (Figure 35 D, E). The measurements of 20 patients were grouped into 3 time points after the onset of symptoms: 0 to 15 days (to 15), 16 to 30 days (to 30), and 31 to 70 days (>30). In this way, multiple time points for each patient can be connected and individual patients can be monitored over time, excluding all patients with missing samples at specific time points. A high variability in the frequencies of cDC1 and pDCs was found with some patients showing different dynamics over time (Figure 35 F).
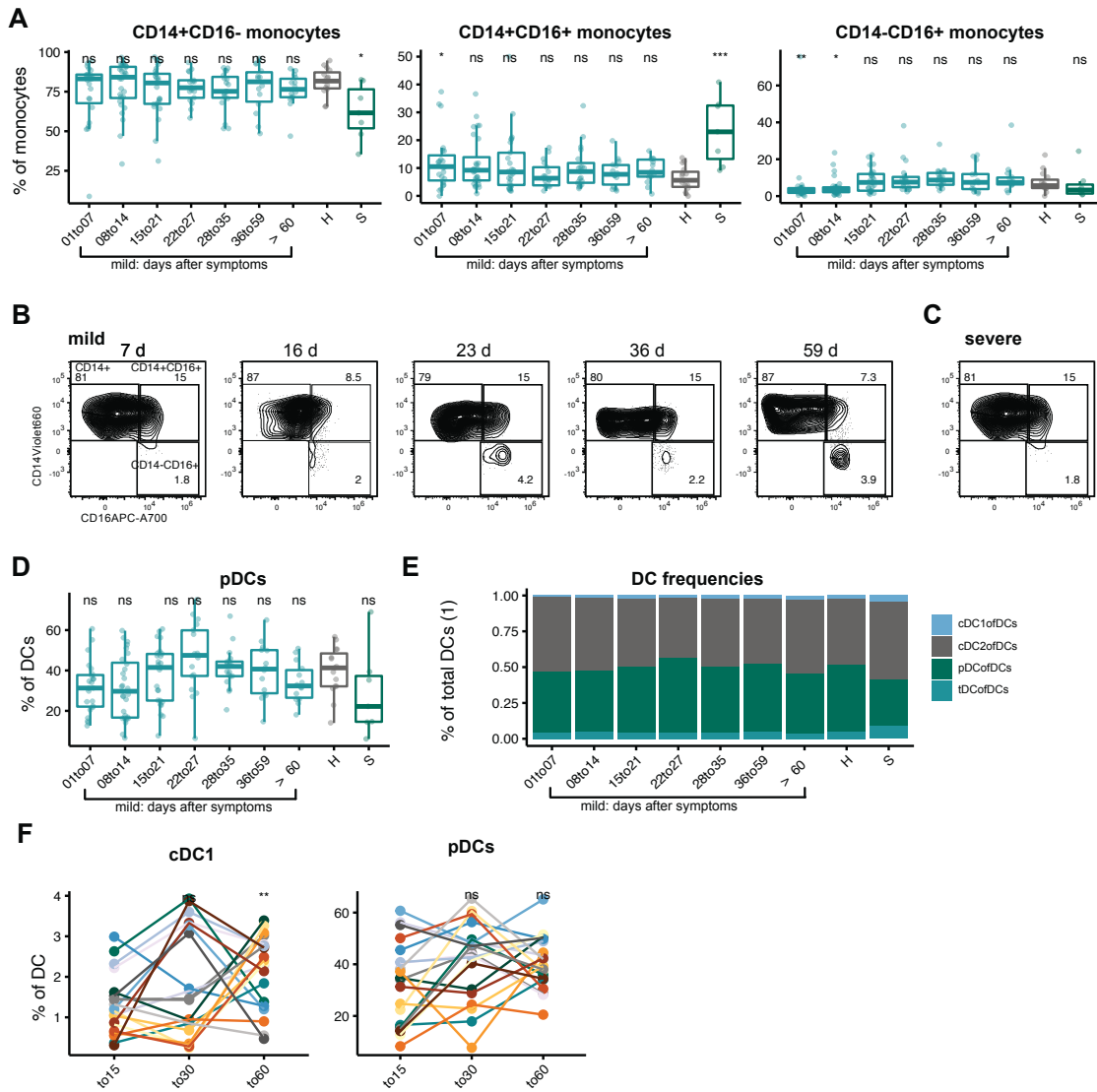
Figure 35: DC and monocyte frequencies from the COVID-19 study in outpatients.
A) Frequency of monocyte subsets defined by CD14 and CD16 expression of total monocyte cells in patients with mild disease progression (blue), healthy controls (gray), and hospitalized COVID-19 patients with severe disease progression (green). B) Representative contour plots showing monocyte subpopulations of a COVID-19 patient with mild disease progression at different time points after symptom onset. C) Representative contour plot showing monocyte subpopulations of a COVID-19 patient with severe disease progression 5 days after diagnosis. D) pDC frequency of total DCs in mild disease progression (blue), healthy controls (gray), and hospitalized COVID-19 patients with severe disease progression (green). E) DC subset composition in the indicated groups (mean). F) Longitudinal measurements of cDC1 and pDC frequencies of total DCs at grouped time points up to 15 days (to15), between 15 and 30 days (to30), and up to 60 days after symptom onset (to60). Each line connects the time points of one patient. Individual patients are indicated by different colors. Significance (*p < 0.05, **p > 0.01, ***p > 0.001, ****p > 0.0001) indicated by asterisks. Significant p values are shown as calculated in R using the Kruskal-Wallis test and Dunn's multiple testing and comparing with healthy controls (A, D) or with the first time point (F). Horizontal lines show the median, box plots show the upper and lower quartiles, and whiskers indicate 1.5 IQR (A, D).

Additionally, and coinciding with the fractional changes in DC composition, absolute counts of cDC1, cDC2 and pDCs were reduced at early time points after symptom onset (Figure 36). While there were changes in the absolute monocyte counts, with decreased

95

numbers up between day 15 up until day 35 compared to later time points, this reduction was not significant.
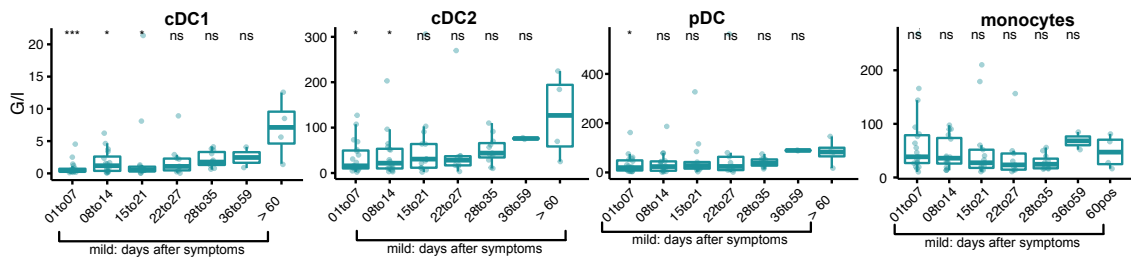
Figure 36: DC and monocyte cell counts from the COVID-19 study in outpatients.
Cell counts of cDC1, cDC2, pDC, and total monocytes per liter of blood as calculated using Trucount beads using the rule of three as described in Chapter 3.2.12. Significance (*p < 0.05, **p > 0.01, ***p > 0.001, ****p > 0.0001) indicated by asterisks. Significant p values are shown as calculated in R using the Kruskal-Wallis test and Dunn's multiple testing and comparing between early time points and a time point >60 days after symptom onset. Horizontal lines show the median, box plots show the upper and lower quartiles, and whiskers indicate 1.5 IQR.

4.5.3 Distinct activation and proliferation profile in mild compared to severe COVID-19 patients

Recruitment of immature immune cells into the circulation was observed after infection with SARS-CoV-2 by Schulte-Schrepping et al. (2020) [166]. Since an expansion of an HLA-DR$^+$ cell population lacking markers of differentiated DCs and monocytes was observed, the nonDCs, it seemed interesting to measure the proliferation of these cells. Ki67 is a marker expressed in proliferating cells and cells that have recently undergone proliferation. A general increase in Ki67$^+$ cells in the blood could indicate that actively proliferating progenitor cells appear prematurely in the circulation or that differentiated cells have recently been recruited from the bone marrow, thereby indicating increased cellular turnover. Therefore, Ki67 expression was measured in DCs and monocytes. The highest expression of Ki67 was observed in the nonDC fraction in both mild and severely affected COVID-19 patients. In patients with severe disease manifestations, pDCs and monocytes showed in increased frequency of Ki67$^+$ cells and in patients with mild disease, increased Ki67 expression was only seen in monocytes and also at late time points between days 22 and 35 after symptom onset (Figure 37 A, B, C). When looking at activation markers, increased expression of CD86 compared to healthy controls could be observed in the patients with a mild disease progression in nonDC, pDC, monocytes, cDC1, and cDC2. On the contrary, in patients with severe COVID-19, downregulation of CD86 was found in

96

monocytes, nonDCs, and cDC2, thereby showing distinct activation profiles between patients with severe and mild disease manifestations (Figure 37 D, E). Concerning PD-L1, stronger upregulation was seen in severe than in mild disease progression. While this was especially pronounced in classical monocytes, it was also observed in non-classical monocytes and pDC, cDC1, cDC2, and tDCs. The increased expression of PD-L1 in patients with a mild disease progression compared to healthy controls was also observed at late time points (up to 60 days) after symptom onset, thereby indicating effects lasting beyond the acute phase of the disease (Figure 37D, F). Looking at individual patients, different time courses in the expression of CD86 and PD-L1 were observed, with subgroups of patients expressing low amounts of either PD-L1 or CD86 from the earliest timepoint up to 15 days after symptom onset (Figure 37 G).
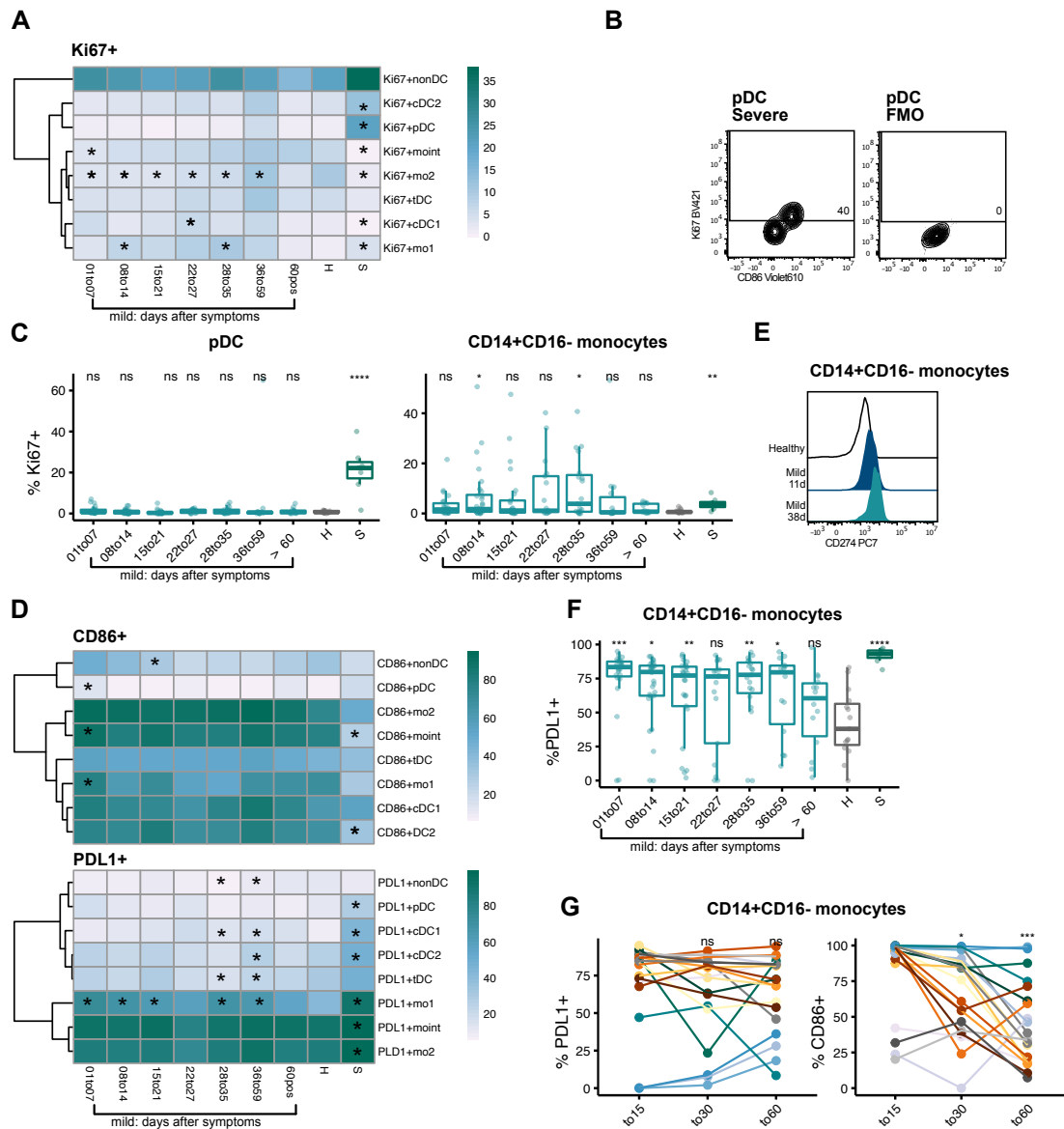
Figure 37: Activation markers of DCs and monocytes from the COVID-19 study in outpatients.
A) Heatmap showing the mean percentage of Ki67$^+$ cells of DC and monocyte subpopulations in patients with a mild disease progression, healthy controls (H), and hospitalized COVID-19 patients with a severe disease progression (S), unscaled. Dark green indicates high, and light blue indicates low expression. B) Representative contour plots showing Ki67 and CD86 expression in pDCs of a COVID-19 patient with severe disease progression. The FMO control for the channel used for Ki67 staining is shown on the right. C) Percentage of Ki67$^+$ pDC and Ki67$^+$ CD14$^+$CD16$^+$ monocytes in patients with a mild disease progression (blue), healthy controls (gray), and hospitalized COVID-19 patients with a severe disease progression (green). D) Heatmap showing the mean percentage of CD86$^+$ and PD-L1$^+$ cells of DC and monocyte subpopulations in patients with a mild disease progression, healthy controls (H), and hospitalized COVID-19 patients with a severe disease progression (S), scaled for each row. E) Representative histograms of PD-L1 expression in classical monocytes of a healthy donor and a COVID-19 patient with mild symptoms at 11 and 38 days after symptom onset. F) Percentages of PD-L1$^+$ CD14$^+$CD16$^+$ monocytes in mildly affected patients (blue), healthy controls (gray), and severely affected, hospitalized COVID-19 patients (green). G) Longitudinal measurements of the % of PD-L1 and CD86$^+$ mo 1 s at grouped time points up to 15 days (to15), between 15 and 30 days (to30), and up to 60 days (to60) after symptom onset). Each line connects the time points of one patient. Individual patients are indicated by different colors. Horizontal lines show the median, box plots show the upper and lower quartiles and whiskers indicate 1.5 IQR. Significant p values are shown as calculated in R using the Kruskal-Wallis test and Dunn's multiple testing and comparing with H. Significance (*$p < 0.05$, **$p > 0.01$, ***$p > 0.001$, ****$p > 0.0001$) indicated by asterisks. A, D Significance indicated by asterisks (*$p < 0.05$).

4.5.4 Distinct temporal shifts in patient populations: a distinct population of mild COVID-19 patients shows early downregulation of CD86

To better understand the different activation profiles between mildly and severely symptomatic COVID-19 patients, dimensionality reduction was performed using PCA with all scaled and centered data obtained from flow cytometric measurements such as innate population frequencies and their activation status. Severely symptomatic COVID-19 patients (dark green) clearly separated from the mild cases (light blue/green) in terms of PC1 and PC3 while the mild cases and healthy controls (orange) seemed to cluster together (Figure 38 A). Analysis of the PCA's rotation showed that parameters with the strongest influence on PC1 where the percentage of Ki67$^+$ pDC, percentage of PD-L1$^+$ cells, and percentage of CD86$^+$ cells. Other parameters with strong influence on PC3 were the percentages of DC subsets of total DCs.

Subsequently, the temporal dynamics of the innate immune response within the mildly affected COVID-19 patients were analyzed. This analysis was restricted to 20 patients, from whom longitudinal measurements with early, intermediate, and late time points were available. These patients were grouped as previously into 3 time periods after primary symptoms: 0 to 15 days (to 15), 16 to 30 days (to 30) and 31 to 70 days (>30). The data were normalized by calculating the delta between the first time point (0 to 15 days) to the intermediate (16 – 30 days) and the late time point (31 – 70 days). A positive difference

indicates downregulation, and a negative difference indicates upregulation at the intermediate and late time points compared to the early time point. With this normalized data k means clustering was performed, a centroid based unsupervised clustering algorithm, to cluster patients depending on their DC and monocyte response to SARS-CoV-2 infection. The average silhouette approach was used to choose the optimal number of clusters (k). The highest average silhouette width was obtained with 3 clusters (Figure 38 B). After k-means clustering of the 20 patients, cluster 1 encompassed 4 patients (median age=54, symptoms = 2), cluster 2 contained 13 patients (median age=36, symptoms = 2) and cluster 3 contained 3 patients (median age=30, symptoms =1) (Figure 38 C). The greatest difference between the clusters was seen in the change of CD86 and PD-L1 expression both at the intermediate and the late time point (indicated by dark green and dark blue rectangles above the heatmap). For example, PD-L1 expression in monocyte subsets was upregulated at the later timepoints in cluster 3 (color scale: yellow), while it was rather downregulated or unchanged at the later time points in clusters 1 and 2 (color scale: black, blue) (Figure 38 F).

PCA analysis of the non-normalized data also showed separation of these three clusters (Figure 38 D) with especially the earliest time point up to 15 days after symptom onset differing between the clusters and showing that the early immune response groups the patients together. Cluster 1 showed a consistent CD86 downregulation and high PD-L1 expression, while clusters 2 and 3 showed higher CD86 expression and cluster 3 very low early PD-L1 expression (Figure 38 F). The CD86 expression in cluster 1 was much lower than in the healthy control group (dotted line) and this change was still observed at later time points after symptom onset. In cluster 2, CD86 expression was only decreased at late time points, thereby showing a transient and early upregulation of CD86 in these patients. On the other hand, PD-L1 expression was high in clusters 1 and 2 while cluster 3 showed a decreased PD-L1 expression compared to healthy controls, which shows distinct activation profiles not only between severe and mild COVID-19 cases but also different profiles within the outpatient cohort with a mild disease progression. The cluster encompassing patients with the highest symptom score in this cohort were also the oldest patients and showed high expression of PD-L1 and low expression of CD86 throughout the observation period (Figure 38 E). While the correlation analysis of CD86 and PD-L1 with age did not show a significant correlation (data not shown), this cohort was age-matched

and lacked individuals with higher age groups. Therefore, the age effect on PD-L1 and CD86 expression should be reanalyzed in a different cohort of COVID-19 patients and healthy controls with a wide range of different ages. Cluster 1 also encompassed the patients with the lowest percentage of lymphocytes (Figure 38 G), which has been described to correlate with higher disease severity.
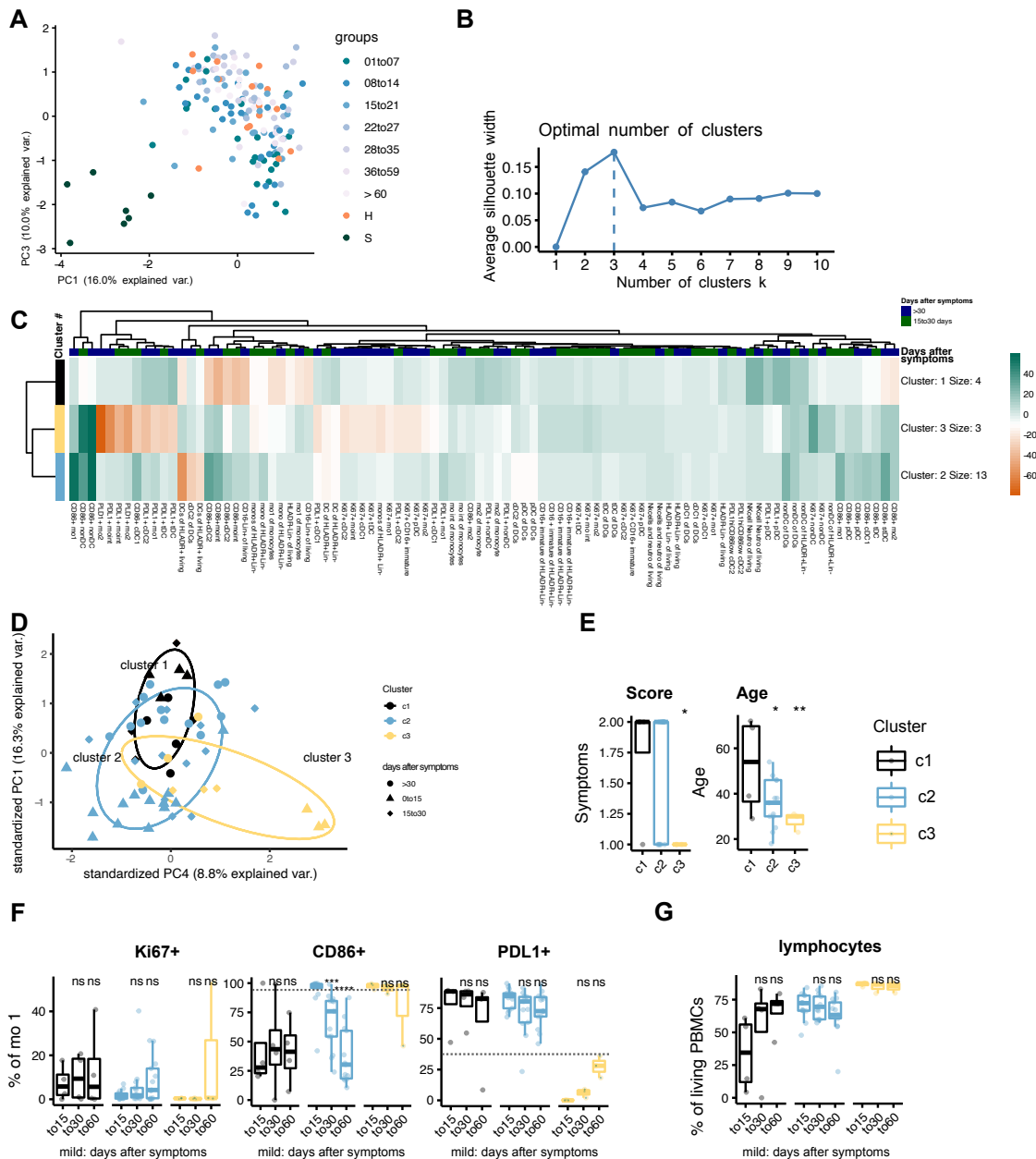
Figure 38: Clustering analysis from the COVID-19 study in outpatients.
A) PCA analysis of all mildly affected (time after symptom onset indicated by different blue colors), severely affected (dark green), and healthy donors (orange). B) Average silhouette width of different numbers of clusters k using the fviz_nbclust function on the dataset of 20 selected patients with a mild disease progression. The time points used for this analysis were 0 to 15 days after symptom onset, 16 to 30 days after symptom onset, and over 30 days after symptom onset. The latter time points were normalized with the first time point by calculating the delta. C) k-means clustering

of the normalized data from the 20 patients used in B. Time after symptom onset indicated by annotation in dark green (15 to 30 days) and dark blue (over 30 days). D) PCA analysis of data from B and C without the normalization to timepoint 0 to 15 days but with scaling and centering. Clusters obtained by k-means clustering (shown in B) are indicated by colors (black = cluster 1, blue = cluster 2, yellow = cluster 3) and time periods after symptom onset are indicated by symbols (triangles: 0 to 15 days, diamonds: 15 to 30 days, circles: over 30 days). E) Patients are separated by clusters identified in B) and patient age and disease score are shown. P values indicate comparison to cluster 1. F) Percentages of Ki67$^+$ CD86$^+$, and PD-L1$^+$ mo1. Dotted line shows the mean of the healthy control group. G) Percentages of lymphocytes within live PBMCs. Horizontal lines show the median, box plots show the upper and lower quartiles, and whiskers indicate 1.5 IQR (E, F, G). Significance (*$p < 0.05$, **$p > 0.01$, ***$p > 0.001$, ****$p > 0.0001$) indicated by asterisks. Significant p values are shown as calculated in R using the Kruskal-Wallis test and Dunn's multiple testing and comparing with first time point in F and G or comparing with cluster 1 in E.

4.5.5 Comparison to YF17D vaccination shows that the downregulation of CD86 in response to vaccination/infection is unusual

In order to put the innate immune response to SARS-CoV-2 infection into context with a well-regulated and efficient immune response, the data generated from the YF17D vaccination study was compared to that from the COVID-19 outpatient study.

Similar to infection with SARS-CoV-2, early expansion of intermediate monocytes was observed and has previously been described in the literature. However, after the YF17D vaccination, this expansion was much more pronounced (see Figure 20). Overall, no expansion of nonDCs as described in both mildly and severely affected COVID-19 patients could be seen after vaccination with YF17D (Figure 39). In the DC fraction, a significant expansion of pDCs and a slight reduction of cDC1 and cDC2 was observed 3 days after vaccination (see Figure 18 B, C), while in COVID-19 patients all DC subtypes were reduced in number (see Figure 36). Activation markers CD86 and PD-L1 were transiently upregulated after YF17D vaccination in DCs and monocytes (see Figure 24) which differed from what was seen in COVID-19 patients with more severe disease manifestations, where a downregulation of CD86 was observed (see Figure 37 D) but in a similar fashion to that detected in the outpatients with COVID-19 where most showed high expression of CD86. After vaccination with YF17D, a transiently increased percentage of Ki67$^+$ cells was found in cDCs and tDCs but not in pDCs or monocytes (see Figure 19). However, in COVID-19 patients with severe disease progression, proliferation of pDCs and monocytes was also observed. An increased frequency of Ki67$^+$ monocytes was also detected in the outpatient cohort with mild disease progression at later time points, thereby indicating increased turnover and regeneration of these cell types (see Figure 37).
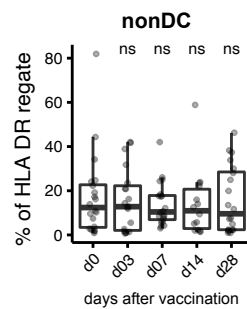
Figure 39: Frequency of nonDCs of HLA-DR⁺ Lin⁻ cells after YF17D vaccination.
Frequency of nonDCs of total HLA DR+ Lin- cells. Horizontal lines show the median, box plots show the upper and lower quartiles and whiskers indicate 1.5 IQR. Significance (*p < 0.05, **p > 0.01, ***p > 0.001, ****p > 0.0001) indicated by asterisks. Significant p values are shown as calculated in R using the Kruskal-Wallis test and Dunn's multiple testing and comparing with d0.

Thus, the response of DC and monocyte subsets to SARS-CoV-2 infection in outpatients with mild symptoms and especially in hospitalized patients with severe disease differs from the coordinated and transient response after YF17D vaccination.

4.6 Hospitalized COVID-19 patients show a dysregulated phenotype of DCs

To further characterize the dynamic changes in frequencies and activation status of DC and monocyte subsets in a larger cohort of patients with more severe disease manifestations, this time also including the DC3 subpopulation, PBMCs isolated from the blood of 65 patients with PCR-confirmed SARS-CoV-2 infection diagnosed at the LMU Klinikum between March 2020 and January 2021 were used for flow cytometric analysis. This cohort consisted of hospitalized COVID-19 patients with active disease as well as recovered patients. In addition, SARS-CoV-2 negative patients that were hospitalized for other health reasons were used as controls. Sample collection was performed by the CORKUM study group (Klinikum Großhadern and LMU) who kindly provided fresh blood samples, frozen PBMCs, and plasma samples. Samples from a group of healthy donors that were collected separately were analyzed as controls. T and B cell subpopulations were analyzed as well by Linus Rinke (AG Krug), thereby allowing for the correlation of innate and adaptive parameters. This data was published in PLOS Pathogens in 2021 [171]. The figures and figure legends (Figure 40 - Figure 50) are shown as they were used in the publication or as slightly modified versions from the publication, as indicated in the figure legends.

4.6.1 Design of the study with hospitalized COVID-19 patients

A total of 65 patients were included in this study cohort, which comprised 32 healthy patients and 39 with mild/moderate COVID-19 in addition to 18 patients with severe COVID-19 progression and 11 patients that were recovered from active disease, which means they were at a time point 30 days after the primary diagnosis and either released from the hospital or still hospitalized for other health reasons. The COVID-19 severity was scaled between a score of 0 (no COVID-19) and 8 (death of/with COVID-19) according to the WHO ordinal scale [170]. The maximal WHO score reached by each patient was defined as the WHOMax and positively correlated with maximal values of inflammation markers such as CRP, IL-6, and fibrinogen. The WHOMax also correlated positively with the maximal frequency of neutrophils and negatively with the minimal frequency of lymphocytes and monocytes (Figure 40). As lymphopenia and inflammation have been described as being characteristic of severe COVID-19 progression, this shows that the WHOMax score is an adequate representation of the patients' disease severity.
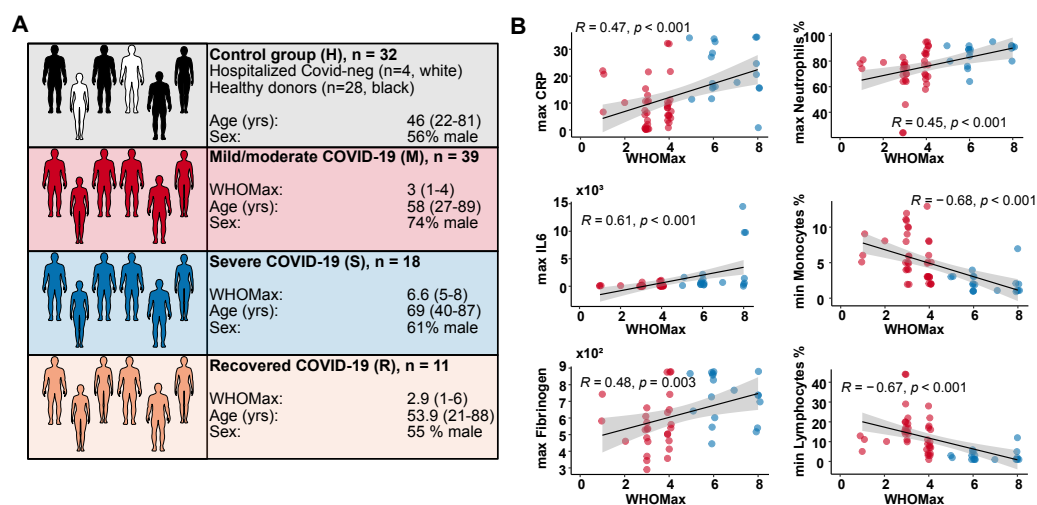
Figure 40: Study design of COVID-19 study in hospitalized patients.
(A) *The number, age, sex and maximal WHO ordinal scale (WHO max) reached are shown for the four different study groups. The control group (H) contained 28 healthy blood donors (black) and 4 SARS-CoV-2-negative patients (white). Patients with acute COVID-19 were grouped into mild/moderate (M, red, n=39) and severe (S, blue, n=18). A group of recovered patients was included for comparison (R, orange, n=11). (B) Correlation analysis of WHO max values with routine laboratory values (minimal and maximal values reached during hospitalization). CRP, C-reactive protein. Spearman's rank correlation coefficients, p-values and linear regression lines are shown.* The figure and figure legends have previously been published in PLOS pathogens [171].

4.6.2 Reduction of DCs and increase of nonDCs in the peripheral blood of COVID-19 patients

An examination of the peripheral blood showed that the relative frequencies of the neutrophils of total living cells increased significantly in COVID-19 patients with a severe disease progression (Figure 41 B). At the same time, monocyte frequencies and DC frequencies were reduced in a similar way as was observed in the previous cohort and as seen in the blood counts.
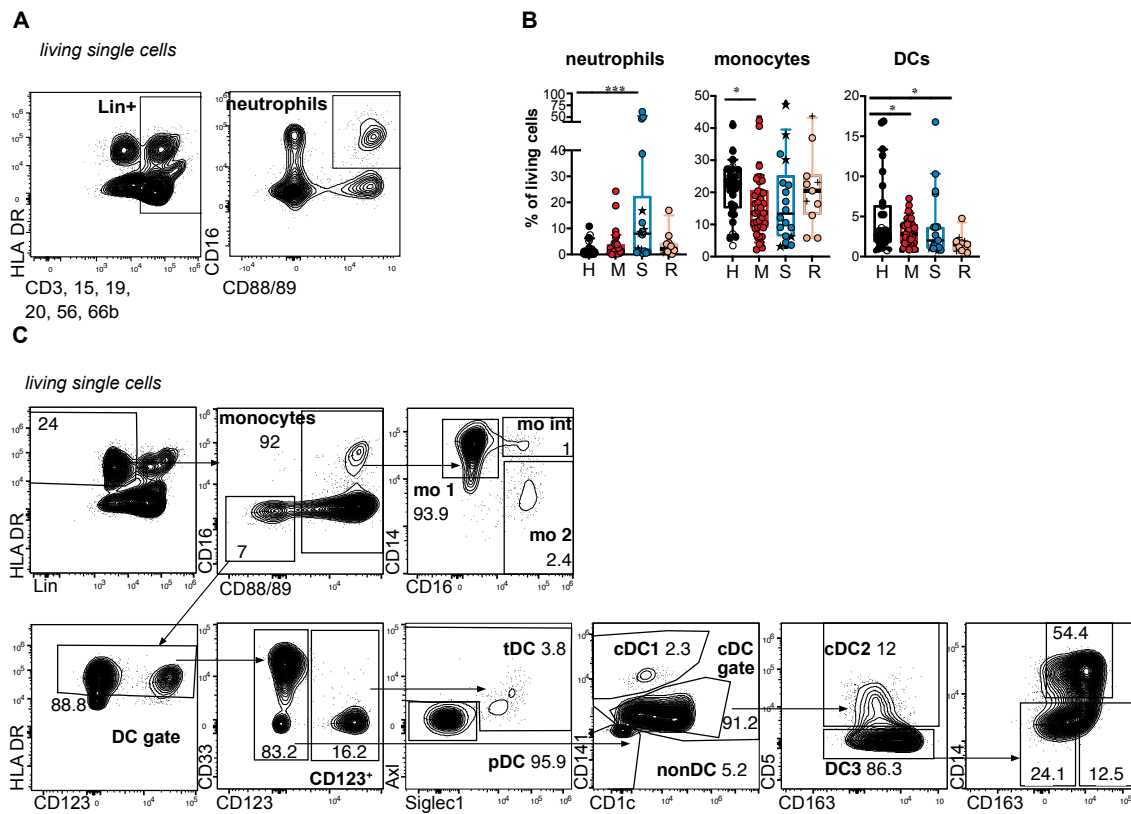
Figure 41: Gating strategy for COVID-19 study in hospitalized patients.
A) Gating strategy for neutrophils in the blood: Within the lineage (CD3, CD15, CD19, CD20, CD56, CD66b) positive cells neutrophils were gated as CD16⁺ and CD88/89⁺. B) Percentage of neutrophils (Lin⁺ CD88/89⁺ CD16⁺), monocytes (Lin⁻, HLADR⁺, CD88/CD89⁺) and DCs (Lin⁻, HLADR⁺, CD88/CD89⁻) of living PBMC. Healthy donors (=H, black symbols, n=28), hospitalized COVID-19 negative patients (=white symbols, n=4), acute COVID-19 patients with mild/moderate (=M, red symbols, n=39), severe (=S, blue symbols, n=18) disease at the first analysis timepoint and recovered patients (orange, n=11). In the severe group, patients that had received B cell-depleting therapy before diagnosis (n=5) are marked by a black star. Recovered patients that had already been analyzed during acute disease and were sampled again after recovery are indicated by a plus sign. C) Gating strategy for DC and monocyte subtypes in the blood: Within HLADR⁺ Lineage (CD3, CD15, CD19, CD20, CD56, CD66b), negative (Lin⁻) cells monocytes were gated as CD88/89 positive cells and separated into mo 1 (CD14⁺ CD16⁻ classical monocytes, mo int (CD14⁺ CD16⁺ intermediate monocytes, mo 2 (CD14ˡᵒ CD16⁺ non-classical monocytes). HLADR⁺ Lin⁻ CD88/89⁻ CD16⁻ cells were regated on HLADR positive cells (DC gate). Within the CD123⁺ DC fraction pDCs (Siglec1⁻ Axl⁻) and tDCs (Axl⁺ and/or Siglec1⁺) were distinguished. Within the CD123⁻ DC fraction cDC1 (CD141⁺ CD1cˡᵒ), cDC2 (CD141⁻, CD1c⁺,

CD5⁺), DC3 (CD141⁻CD1c⁺ CD5⁻ DCs) and "non-DC" (CD141⁻ CD1c⁻) were identified. DC3 were further separated into CD163⁻ CD14_, CD163⁺ CD14⁻ and CD163⁺ CD14⁺ DC3 subsets.
The figure and figure legend have previously been published by Winheim et al. in PLOS pathogens 2021 and have been slightly adapted [171].

In this cohort, a relative reduction of DC subsets was again seen in the peripheral blood in favor of HLA-DR⁺ DC marker-lacking nonDCs. DC3 frequencies were analyzed in addition to cDC1, cDC2, tDC, and pDC and were also found to be reduced in favor of nonDCs in the DC gate (HLA-DR⁺ Lin⁻CD88/89⁻ CD16⁻). This increase of nonDCs was most pronounced at early time points up until day 20 after diagnosis (Figure 42 A, B) but could also be seen as a trend in recovered patients over 60 days after the primary diagnosis. Upon excluding nonDCs and only looking at defined DC populations, both pDC and cDC1 frequencies were reduced significantly at the earliest time point measured, up to 3 days after diagnosis (Figure 42 C).
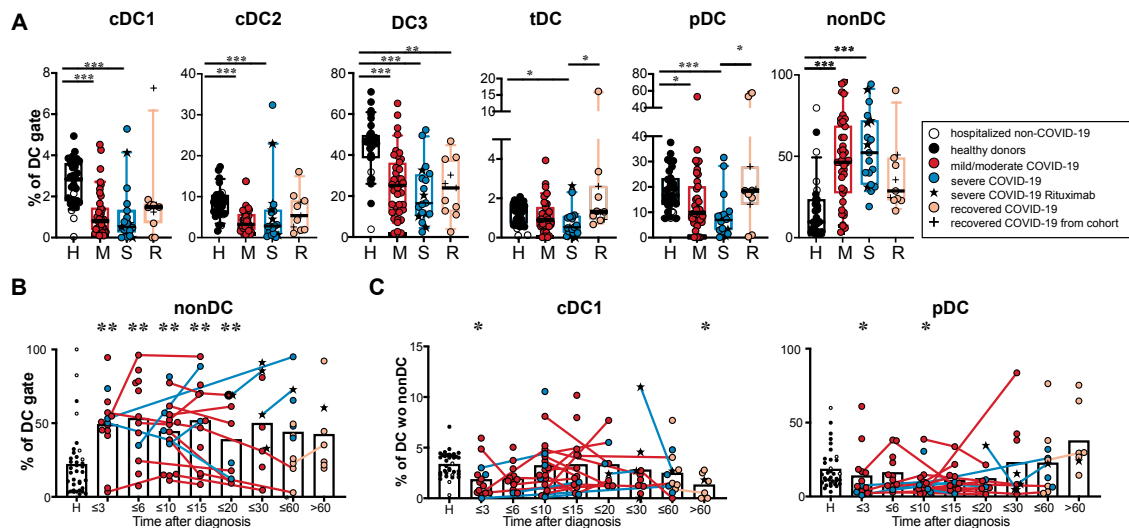
Figure 42: Shifts in DC composition.
*A) Relative frequencies of DC subsets and non-DCs within the DC gate are shown (Kruskal-Wallis test with Dunn's correction, n=97-100). B) Frequency of non-DCs within the DC gate at different grouped time points after diagnosis. C) Frequency of cDC1 and pDCs within the differentiated DC population (after excluding CD141– CD1c– non-DCs) at different grouped time points after diagnosis. [B and C] Connected lines represent multiple measurements of the same patient at different time points. Columns indicate the mean. Colors and symbols as in [Figure 41 A]. Comparison of the indicated time points with the healthy control group (Kruskal-Wallis test with Dunn's correction, n=124-127). Statistical significance in B, C, D, E is indicated by * p< 0.05, ** p> 0.01, *** p<0.001.*
The figure and figure legend have previously been published by Winheim et al. in PLOS pathogens 2021 and have been slightly adapted [171].

4.6.3 NonDCs do not express any of the characteristic progenitor markers

A similar population to nonDCs has previously been described in cancer patients and after malaria infection [188, 189] and has been defined as HLA-DR$^+$, lacking lineage, monocyte, and DC markers. UMAP clustering showed that nonDCs cluster separately from known DC populations (Figure 43 A). They lack expression of CD11c, CD1c, CD5, CD123, Axl, CD141, XCR1, CD163 but express HLA-DR in similar amounts to DCs and partly express CD86 (Figure 43 B, C). To analyze whether these cells fit progenitor cells that can be found in the blood and that could increase in COVID-19 patients due to the recruitment of immature cells, CD115, CD135, CD45RA, CD34 and CD117 expression was examined. These were negative for all but CD45RA with nonDCs partly expressing CD45RA in addition to showing Ki67 expression (Figure 43 E). nonDCs also lacked expression of CD127, which is a marker of innate lymphoid cells. When gating on innate lymphoid cells, and on different progenitor populations defined by CD117 and CD34 expression, no significant changes in frequencies in currently diseased or recovered COVID-19 patients compared to healthy controls could be found in these populations (Figure 43 F). These results show that nonDCs expanding in COVID-19 patients are not a previously described progenitor population and, based on their surface marker expression, cannot be identified as DCs or monocytes.
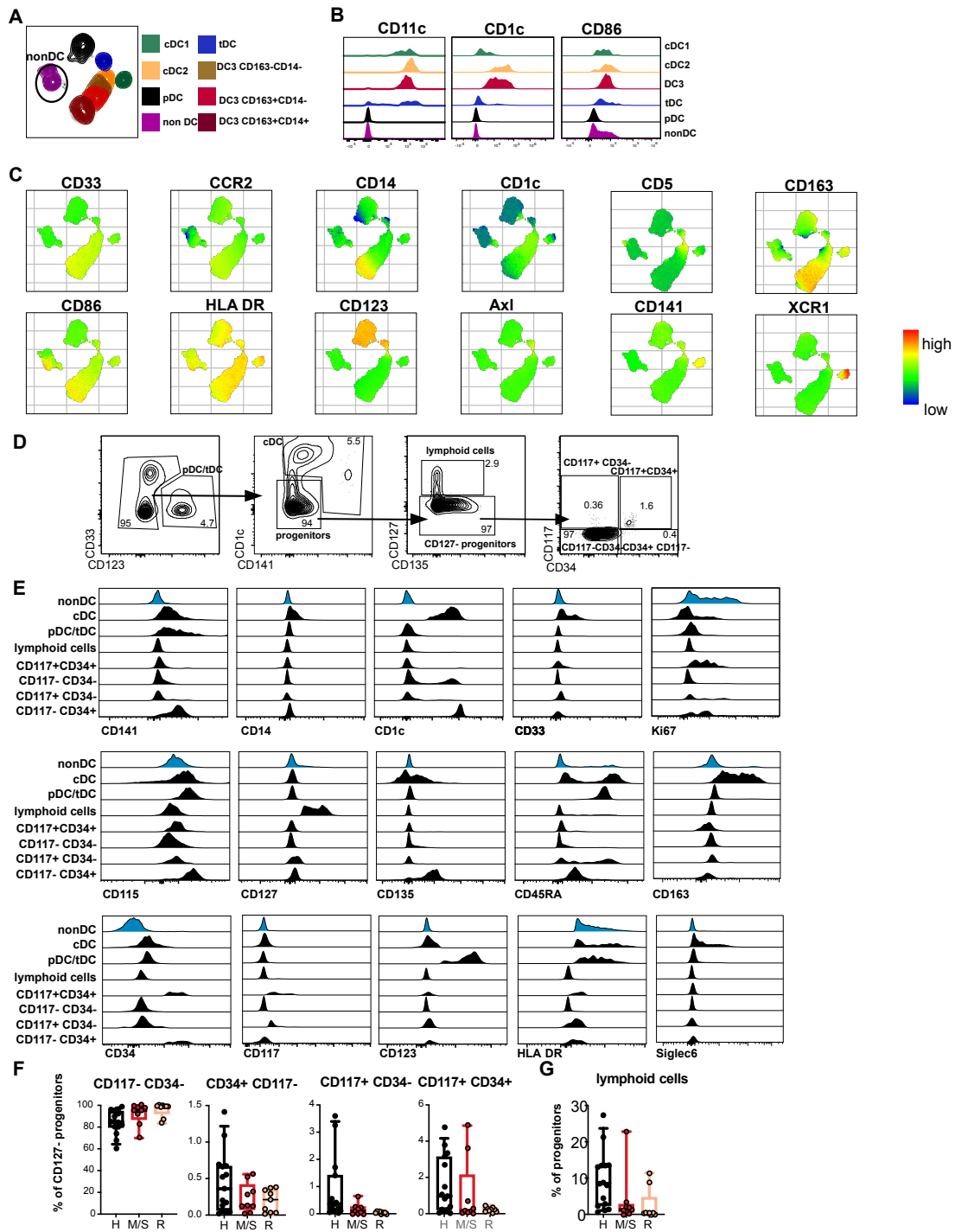
Figure 43: Characterization of HLA-DR⁺ nonDC population.

A) *UMAP clustering of one representative COVID-19 patient. Overlay of gated cDC1 (green, CD141⁺), cDC2 (orange, CD1c⁺, CD5⁺), DC3 (brown, red, dark red, CD1c⁺, CD5⁻, CD163⁺/⁻, CD14⁺/⁻), pDC (black, CD123⁺), tDC (blue, CD123⁺, Siglec1⁺, Axl⁺) and non-DC (purple, HLADR⁺, Lin⁻, CD141⁻, CD1c⁻) populations. B) Representative histograms of CD11c, CD1c and CD86 expression in cDC1, cDC2, DC3, tDC, pDC and non-DC in a patient with moderate COVID-19. C) Expression of several surface markers overlayed in the UMAP from [A]. Shown is the expression of CD33, CCR2, CD14, CD1c, CD5, CD163, CD86, HLADR, CD123, Axl, CD141, XCR1 indicated by color scale (red = high expression, green = intermediate, blue = low expression). D) Gating strategy for identification of progenitor populations in the blood. Cells are pregated on Lin⁻ (CD3, CD15, CD19, CD20, CD56, CD66b, CD88, CD89), HLADR⁺ living cells. pDCs and tDCs are excluded via gating on CD123⁻ cells followed by exclusion of cDCs by gating*

on CD1c⁻, CD141⁻ cells. These progenitors are then separated into lymphoid cells (CD127⁺) and CD127⁻ progenitors. Here, cells can be differentiated by their expression of CD117 and CD34 into four quadrants: CD117⁺ CD34⁻, CD117⁺ CD34⁺, CD117⁻ CD34⁺, CD117⁻ CD34⁻. E) Representative histograms of marker expression of non-DCs, cDCs, pDC/tDCs, lymphoid cells, CD117⁺ CD34⁺, CD117⁻ CD34⁻, CD117⁺ CD34⁻, CD117⁻ CD34⁺ progenitor cells, gated according to [D] of one COVID-19 patient. Expression of CD141, CD14, CD1c, CD33, Ki67, CD115, CD127, CD135, CD45RA, CD163, CD34, CD117, CD123, HLADR and Siglec6 is shown. F) Percentage of CD117⁻ CD34⁻, CD34⁺ CD117⁻, CD117⁺ CD34⁻, CD117⁺ CD34⁺ cells of total CD127⁻ progenitor cells. G) Percentage of CD127⁺ lymphoid cells of the progenitor cells are shown. Healthy donors (=H, black symbols, n=12), mild/moderate and severe COVID-19 patients (=M/S, red, n=9) and recovered patients (=R, orange, n=9).

The figure and figure legend have previously been published by Winheim et al. in PLOS pathogens 2021 and have been slightly adapted [171].

4.6.4 Increase of CD163⁺CD14⁺ DC3 fraction correlates with inflammatory markers and COVID-19 disease severity

Looking at DC3 subpopulations, defined by CD163 and CD14 expression (Figure 44 D), a significant increase of CD163⁺ CD14⁺ DC3 could be seen in both mild and severely affected COVID-19 patients, but not in recovered patients (Figure 44 B). This increase was rather enduring in some patients, showing a significant increase up to 20 days after primary diagnosis. The frequency of CD163⁺ CD14⁺ cells within the DC3 normalized to that of healthy controls in most patients in the recovered group. Some hospitalized SARS-CoV-2-negative controls also showed high CD163⁺ CD14⁺ frequencies (Figure 44 white circles, C), thereby indicating that this increase is not only found in COVID-19 but also in other disease conditions (here patients with COPD, interstitial lung disease and other diseases). CD163⁺ CD14⁺ DC3 were previously shown to accumulate in SLE patients, where inflammation is a key factor to pathogenesis. Therefore, it was interesting to correlate this DC3 subpopulation with the COVID-19 disease score and inflammatory markers. A significant positive correlation of CD163⁺ CD14⁺ DC3 with disease severity (WHOMax) and the CRP values was found. At the same time, CD163⁺ CD14⁻ DC3 negatively correlated with these parameters (Figure 44 E). Weak correlations were also found with IL-6 concentration in the serum (Figure 44 F). These results show that the shift from CD163⁺ CD14⁻ to CD163⁺ CD14⁺ DC3 was associated with disease severity and inflammation in COVID-19 patients.
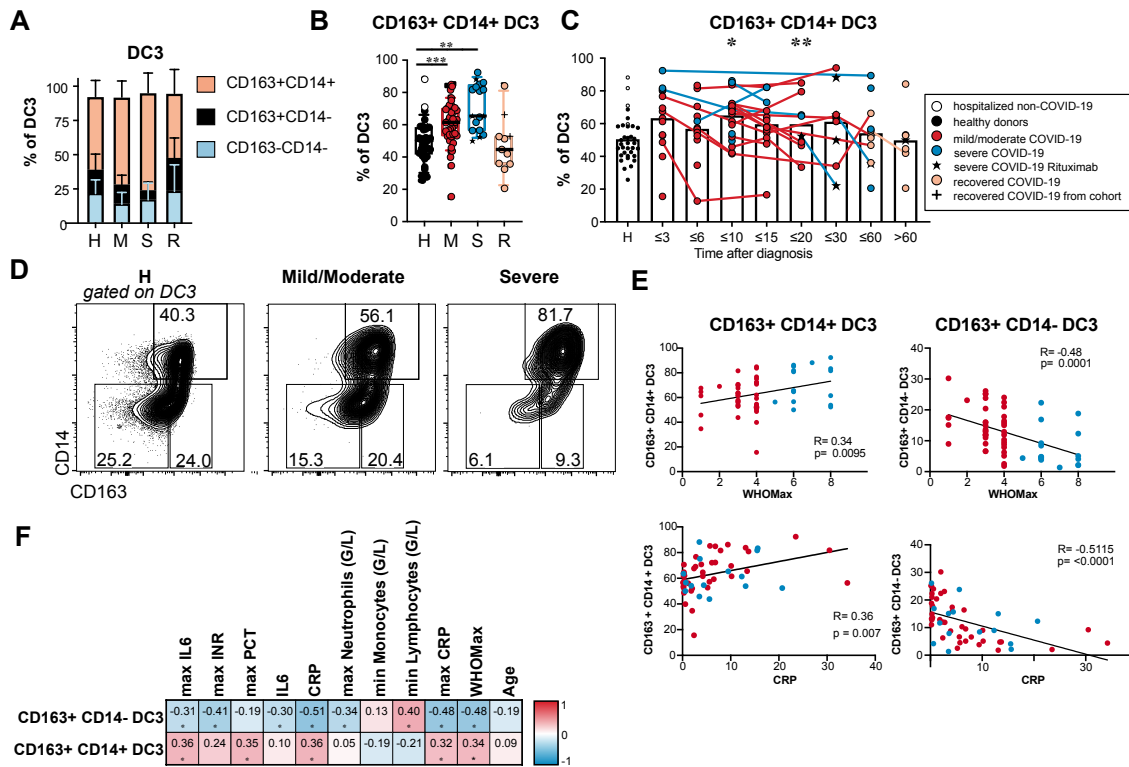
Figure 44: Increased percentage of CD163+ CD14+ cells in DC3 of COVID-19 patients.

(A, B) *Frequencies of DC3 subtypes identified by CD163 and CD14 expression are shown for healthy/non-COVID donors (H, n=31), patients with mild/moderate (M, n=39) and severe disease (S, n=18) at the first analysis timepoint and recovered patients (R, n=11). B) Results for individual patients are indicated by symbols as in Fig. 2 (Kruskal-Wallis test with Dunn's correction, n=99). C) Frequency of CD163+ CD14+ cells within DC3 in all patients of the cohort at different grouped time points after diagnosis. Connected lines represent multiple measurements of the same donor at different time points. Columns indicate the mean (Kruskal-Wallis test with Dunn's correction, n=124). *p<0.05, ** p> 0.01, *** p<0.001. D) CD14 and CD164 expression in DC3. Representative results of one healthy donor and two patients with moderate and severe COVID-19 are shown. E) Correlation of relative frequencies of CD163+ CD14+ and CD163+ CD14- DC3 with WHO max score (n=57) and CRP concentration in the plasma (n=55) at the same time point. Spearman's rank correlation coefficients, p-values and linear regression lines are shown. F) Correlation with inflammatory markers, blood cell counts, disease severity and age. Spearman correlation coefficients (-1 to 1) and adjusted p-values are shown.*

The figure and figure legend have previously been published by Winheim et al. in PLOS pathogens 2021 [171].

4.6.5 Non-classical monocytes are reduced in the peripheral blood and the reduction correlates with CX3CR1 expression

Monocytes may be recruited to sites of inflammation and have been shown to differentiate into macrophages or mo-DCs under certain stimulatory conditions. They are relevant for cytokine secretion and have been observed to accumulate in the lung of COVID-19 patients. A significant increase of mo1, and a significant decrease of mo2 (non-classical monocytes) was found in this cohort, which was most pronounced until 20 days after the

primary diagnosis (Figure 45 A, B, C). Although mo int appeared to be transiently increased up to 3 days after diagnosis, this was not statistically significant. The frequencies of monocyte subsets in the blood could be influenced by changes in migration, survival, regeneration, and differentiation processes. Mo2 frequencies were correlated with the expression of CCR2 and CX3CR1, which are chemokine receptors relevant for monocyte migration to tissues and survival (Figure 45 D). A negative correlation of mo2 frequency with CCR2 expression was detected, indicating that upregulation of CCR2 in mo2 could increase their migration to inflamed tissues with high expression of CCL2. In contrast, mo2 frequency correlated positively with CX3CR1 expression in mo2. At the same time, CX3CR1 expression, which was found to be important for the survival of mo2 [190, 191] also correlated with the time elapsed after diagnosis and could be a marker of recovery of mo2 (Figure 45 E).
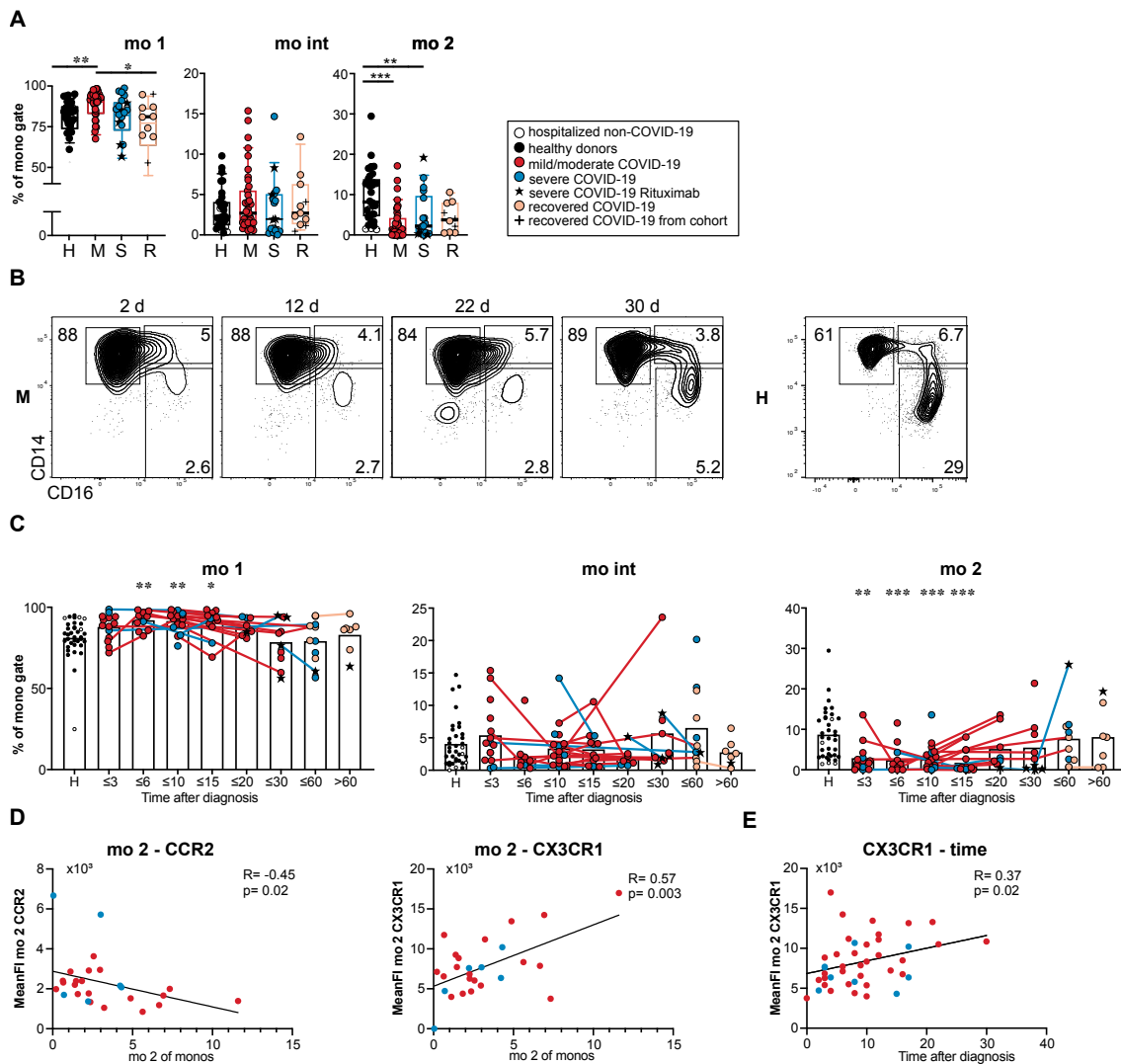
Figure 45: Monocyte frequency shifts in patients with SARS-CoV-2.
A) *Frequency of mo 1, mo int and mo 2 of all monocytes in healthy/non-COVID donors (H, n=31), patients with mild/moderate (M, n=39) and severe disease (S, n=18) at the first analysis timepoint and recovered patients (R, n=11).* B) Monocyte subpopulations at multiple time points (day 2, day 12, day 22, and day 30) in one moderate COVID-19 patient (CoV) compared to a healthy control patient (H). C) *Frequency of mo 1, mo int and mo 2 of all monocytes at different grouped timepoints after diagnosis. Connected lines represent multiple measurements of the same donor at different time points. Columns indicate the mean (Kruskal-Wallis test with Dunn's correction, n=124). * p<0.05, ** p> 0.01, *** p<0.001.* D) Correlation of H, M, and S patients mo 2 frequency with their expression of CCR2 and CXCR3. E) Correlation of the time since diagnosis with the CXCR3 expression of mo 2.
The figure and figure legend have previously been published by Winheim et al. in PLOS pathogens 2021 and have been slightly adapted [171].

4.6.6 cDCs and monocytes with a PD-L1^{hi} CD86^{lo} phenotype observed in patients with severe COVID-19 disease

The most striking phenotype differentiating between severe and mild COVID-19 patients and YF17D vaccinees was the differential expression of CD86 in severe COVID-19 patients. To support this finding, multi-parametric flow cytometry was performed on cryopreserved PBMC of a subcohort of 26 patients with COVID-19. 20 patients had a mild/moderate disease progression, 6 patients had a severe disease progression and 11 healthy donors were used as controls. The extensive antibody panel used for this analysis was similar to the one used for the YF17D cohort described in Chapter 4.3.8. Additionally, using cryopreserved samples allowed for direct comparisons of MFIs of activation markers while the previous data in the outpatient cohort was based on percentages of positive and negative cells determined in fresh samples. Looking at the MFIs, downregulation of CD86 was found in this cohort of hospitalized patients, especially in patients with severe disease, but also in patients with mild/moderate disease. Other activation markers such as HLA-DR were also downregulated while CD40 and PD-L1 were upregulated. Interestingly, both DC3 and cDC2 contained a distinct PD-L1^{hi} CD86^{lo} population in patients with severe COVID-19 disease (Figure 46 B). This population was significantly more frequent in patients with severe disease compared to healthy controls. A fraction of the hospitalized SARS-CoV-2-negative patients also exhibited this population but no one from the healthy group. These patients portrayed with COPD or interstitial lung disease and, therefore, this phenotype of PD-L1^{hi} CD86^{lo} expressing cells can also be found in other diseases that are linked with inflammatory responses. When excluding these hospitalized COVID-19 negative patients, a significant difference between recovered patients and healthy donors could be determined (DC3: p = 0.0173, cDC2: p =

0.0163) indicating a long-lasting change in the expression of CD86 and PD-L1 even after the acute disease had passed. CD163 was highly expressed in DC3 and monocytes of COVID-19 patients with severe COVID-19 disease progression. TREM1 was expressed at higher levels in mo1 and mo int and significantly upregulated in mo2 in the severe group. CD143 (ACE) expression was higher expressed in monocytes, tDCs, cDC2, and DC3 in COVID-19 patients compared to controls and was most highly expressed at early timepoints after diagnosis (Figure 46 A). Interestingly, CRP and IL-6 plasma levels correlated with CD143 expression (Figure 46 I). CCR2 was expressed at higher levels in all monocytes and DC populations except pDCs in COVID-19 patients. CXCR3 was highly expressed in COVID-19 patients in cDC2, DC3, and monocyte subsets but downregulated in pDCs, tDCs, and cDC1. On the other hand, the expression of CX3CR1 was reduced in cDC2, DC3, and monocytes in the diseased patients compared to healthy controls. These results suggest that in COVID-19 patients, circulating peripheral blood cDC and monocyte subpopulations are positioned to respond to inflammatory signals by migration.
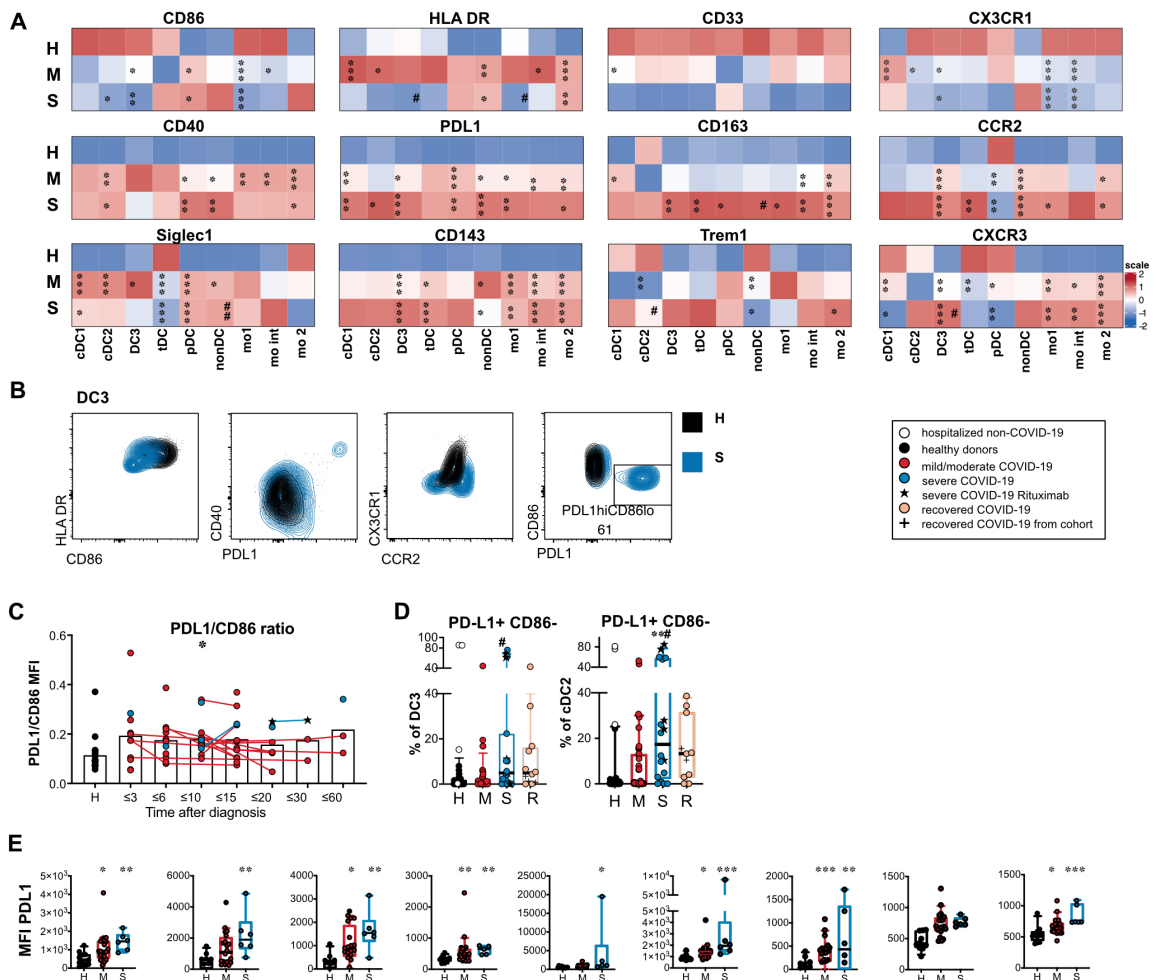
Figure 46: Phenotype alterations in circulating DC and monocyte subpopulations in COVID-19 patients compared to healthy controls.

A) *Expression heatmap of log$_{10}$ transformed median MFI values of surface markers in all DC and monocyte subpopulations in COVID-19 patients with mild/moderate (M, n=20) or severe disease (S, n=6) at the first analysis timepoint compared to healthy donors (H, n=11). The color indicates the scaled expression (z-score standardized) for each cell population (red = high expression, blue = low expression), * significant differences between patients and healthy donors, # significant differences between patients with mild/moderate and severe COVID-19 (ANOVA or Kruskal-Wallis test with Tukey's or Dunn's correction for multiple comparisons between H, M and S, * or # p<0.05, ** or ## p<0.01, *** or ### p<0.001). B) Representative results of the expression of HLADR, CD86, CD40, PD-L1, CX3CR1 and CCR2 in DC3 in a healthy control (black) and a patient with severe COVID-19 (blue). C) Ratio of PD-L1 and CD86 MFI values in DC3 at different grouped time points after diagnosis. Connected lines represent multiple measurements of the same donor at different time points. Columns indicate the mean (n=81, cohorts 2 and 3 combined). D) Frequency of the PD-L1^{hi} CD86^{lo} population in DC3 and cDC2 in healthy donors (H, black, n=28), non-COVID patients (H, white, n=4) and COVID-19 patients with mild/moderate (M, red, n=39) and severe (S, blue, n=18) disease. E) Expression of [...] [PD-L1] was measured as mean fluorescence intensity values in the indicated cell populations in COVID-19 patients with mild/moderate (M, n=20) or severe disease (S, n=6) at the first analysis timepoint compared to healthy donors (H, n=11). Results for individual patients are indicated by symbols, Box plots show the 25 to 75 percentile; whiskers show the 10 to 90 percentile, horizontal lines indicate the median (Kruskal-Wallis test with Tukey's or Dunn's correction, n=* p<0.05, ** p<0.01, *** p<0.001).*

The figure and figure legend have previously been published by Winheim et al. in PLOS pathogens 2021 and have been slightly adapted [171].

In this cohort, Ki67 was again measured to indicate current or recent proliferation. Recruitment of immature DCs from the bone marrow could explain the unusual PD-L1^{hi} CD86^{lo} phenotype of cDCs found in the peripheral blood. Subsequently, this phenotype should be observed in the fraction of Ki67^{+} cells. The expression of PD-L1 and CD86 was therefore compared on Ki67^{+} and Ki67^{-} DCs. Interestingly, CD86 and HLA-DR showed a higher expression and PD-L1 a lower expression in the Ki67^{+} cDC2 and DC3 (Figure 47 A, B). This suggests that the PD-L1^{hi} CD86^{lo} phenotype in DCs seems to be caused by external factors – for example inflammatory stimuli found in the blood of COVID-19 patients – and is not linked to increased migration of cells from the bone marrow.
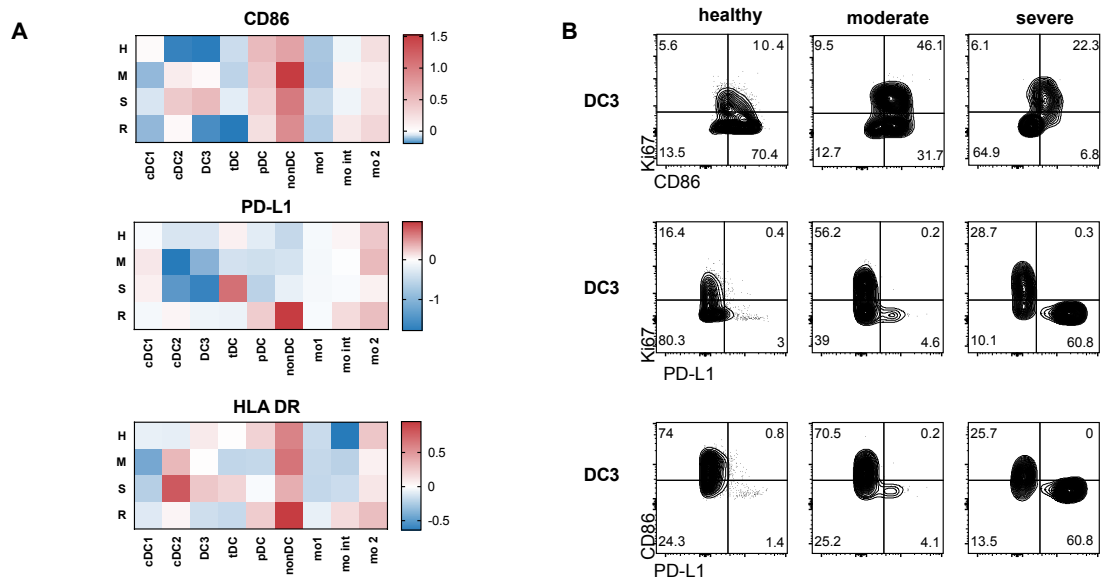
Figure 47: Ki67+ cells express high levels of CD86 and low PD-L1.
 A) *Log2 fold changes of median MFI values of CD86, PD-L1 and HLADR in Ki67+ versus Ki67− cells within the indicated populations are shown in the heatmaps indicated by the color scale.* B) *Representative results of Ki67, CD86 and PD-L1 expression in DC3 of a healthy control, and 2 COVID-19 patients with moderate and severe disease are shown.*
The figure and figure legend have previously been published by Winheim et al. in PLOS pathogens 2021 and have been slightly adapted [171].

Similar to what was previously observed in YF17D vaccinees, Siglec 1 was strongly up-regulated (mainly in DC3 and mo1) in most patients sampled at early time points after diagnosis (Figure 48 E) and then downregulated at later time points in longitudinally sampled patients. Interestingly, Siglec 1 expression in the COVID-19 patients correlated significantly with an IFN1/3 score that was calculated based on plasma concentrations of several IFN1-induced proteins in addition to IFNL1 (score kindly provided by Anne Hilgendorff and Benjamin Schubert, Figure 48 H). Unbiased mapping and clustering of the merged flow cytometric data showed a cluster of Siglec 1^{high} cells at early timepoints after sampling in DC3 and also mo1 (G, clustering done by Tobias Straub, LMU). Thus, a short-lived upregulation of IFN-inducible Siglec 1 was found at early time points after diagnosis regardless of the severity of COVID-19 while the PD-L1^{hi} CD86^{lo} HLA-DR^{lo} phenotype persisted after the acute phase of the disease and was more pronounced in severe disease.
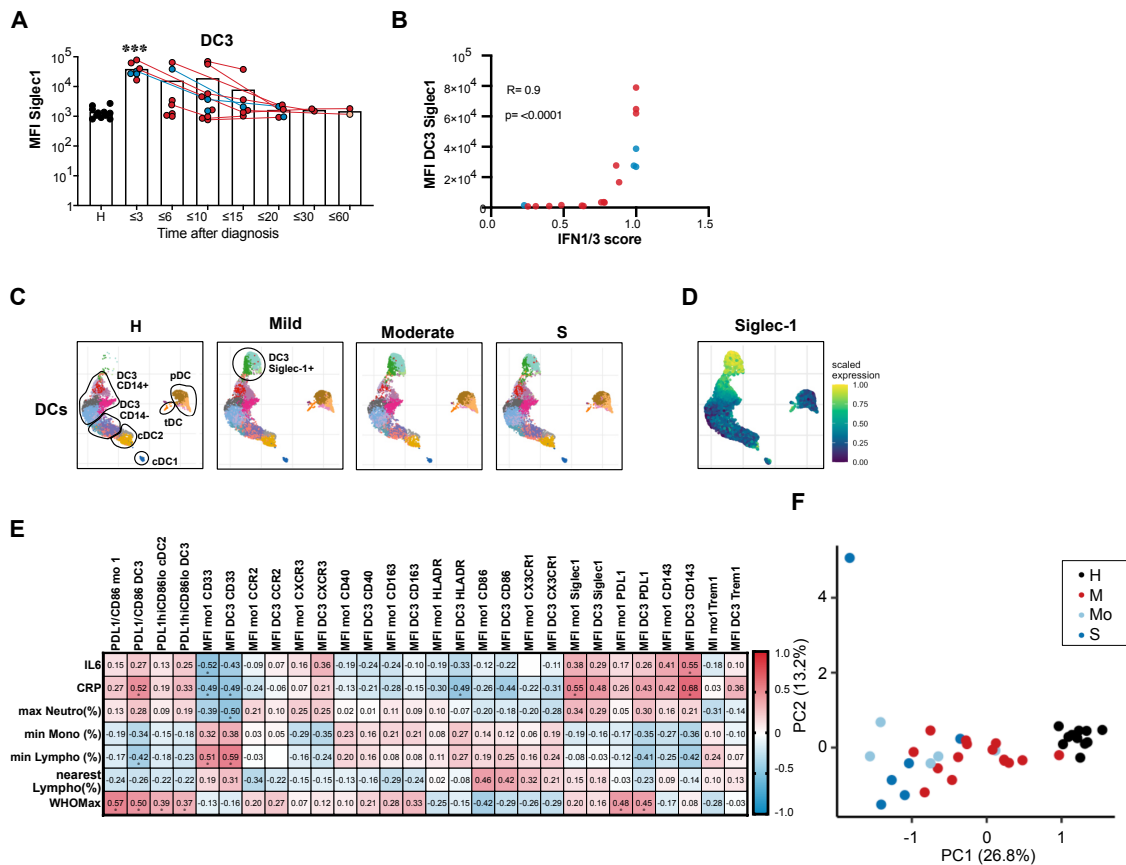
Figure 48: Siglec 1 expression and correlation of phenotypic alterations in circulating DC and monocyte subpopulations in COVID-19 patients.

A) *Siglec-1 expression (MFI) at different time points after diagnosis in DC3.* B) *Correlation of Siglec-1 expression (MFI) in DC3 with an IFN1 score derived from abundances of IFN1-induced plasma proteins. Spearman's rank correlation coefficient and p-value are shown (n=18).* [IFN1/3 score kindly provided by Anne Hilgendorff and Benjamin Schubert] C) *Clustering analysis was performed on pooled samples of 26 patients and 11 controls. UMAPs of reclustered DCs with Phenograph clusters indicated by colors are shown separately for the indicated groups (same number of cells). DC subpopulations are annotated according to marker expression in phenograph clusters [...].* [Clustering analysis kindly provided by Tobias Straub] D) *Siglec-1 scaled expression indicated by color overlayed on the UMAP embedding (moderate group).* E) *Spearman rank correlation coefficients (-1 to 1) for activation markers in mo 1 and DC3 with markers of inflammation and disease severity are shown and indicated by color scale (n=26-41). * adjusted p values below 0.05 (Benjamini-Hochberg procedure).* F) *Principal component analysis using extracted parameters from flow cytometric analysis of all DC and monocyte subpopulations with clinical groups indicated by colors.*

The figure and figure legend have previously been published by Winheim et al. in PLOS pathogens 2021 and have been slightly adapted [171].

4.6.7 DC3 and monocytes sorted from COVID-19 patients have reduced capacity to stimulate naïve CD4$^+$ T cells in vitro

Naïve CD4$^+$ T cells can be stimulated by DC3 and subsequently proliferate and produce cytokines IL-17 and IFN-γ. Upregulation of PD-L1, which can be involved in T cell regulation, and downregulation of costimulatory molecule and activation marker CD86 might reduce the ability of DC3 and monocytes to costimulate naïve CD4$^+$ T cells.

Therefore, the function of DC3 and monocytes sorted from COVID-19 patients was compared to cells sorted from healthy controls. After isolation of DC3 or mo1 from patients with COVID-19 and from healthy age-matched controls, the APCs were cocultured with CTV-labeled autologous naïve CD4$^+$ T cells on plates coated with anti-CD3 antibody to ensure a suboptimal TCR stimulation. Proliferation as indicated by CTV staining and CD69 expression of the T cells were significantly reduced in cocultures of DC3 or mo1 from COVID-19 patients compared to healthy controls. This reduced proliferation and activation was observed irrespective of glucocorticoid therapy (Figure 49 A, B, C). Control stimulation with anti-CD3/CD28 antibodies showed that the proliferation and CD69 expression of the T cells isolated from COVID-19 patients was not impaired in general compared to that of healthy controls. This indicates that the reduced T cell response in the coculture was not caused by a reduced ability of the patient's T cells to respond. Instead, it can be caused by the impaired costimulatory activity of the DC3 and monocytes, where low expression of CD86 was detected (Figure 49 D).

Looking at cytokines secreted from these cocultures, a trend towards reduced IFN-γ, TNF-α, IL-2, IL-4, IL-5, IL-9, IL-10, IL-13 and IL-17A was detected in cocultures of CD4$^+$ T cells and DC3 sorted from these patients (significant reduction found for IL-10, p = 0.003, Figure 49 E). The control stimuli of anti-CD3/CD28 antibodies showed comparable amounts of the majority of cytokines and increased amounts of IL-5 and IL-10 were produced by the CD4$^+$ T cells of such patients. Therefore, the patient's T cells ability to produce cytokines was not generally impaired. Thus, it was shown that in COVID-19 patients, circulating DC3 and monocytes are functionally impaired in their costimulation of CD4$^+$ T cells. Interestingly, the expression of PD-L1 as well as the PD-L1/CD86 ratio on mo1 correlated significantly with simultaneous PD-1 expression on CD8$^+$ T cells (PD-L1: R = 0.34; p = 0.02, PD-L1/CD86: R = 0.37; p = 0.01, DC3 PD-L1: R = 0.34; p = 0.02,

PD-L1/CD86: R = 0.37; p = 0.01, PD-1 expression data kindly provided by Linus Rinke). These results show that interactions of PD-1-expressing T cells with PD-L1-expressing monocytes or DCs could also occur in the patients with COVID-19 (Figure 49 F).
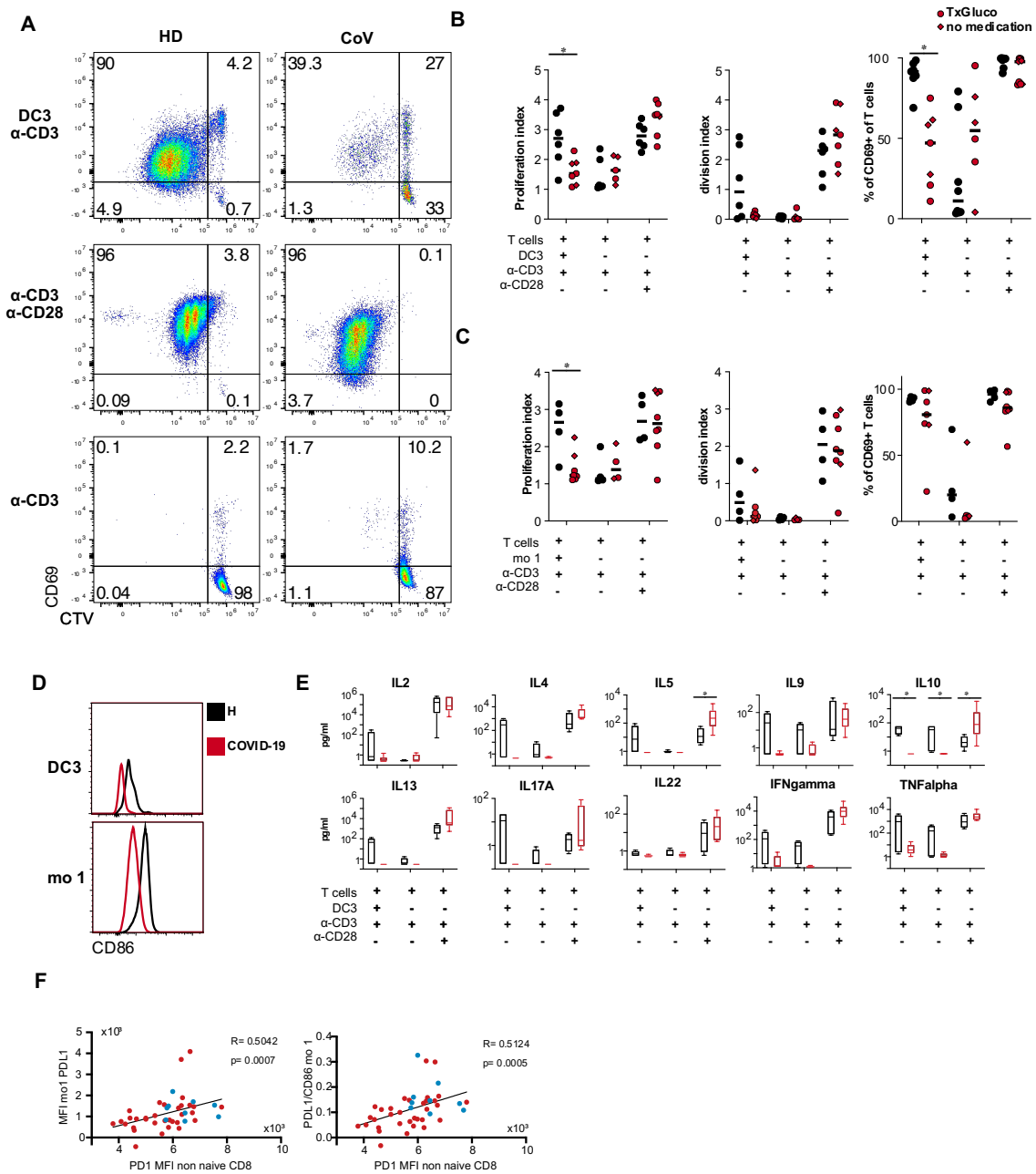
Figure 49: DC3 and monocytes from COVID-19 patients have reduced ability to stimulate naïve CD4 T cells.
A-D) *CTV-labeled autologous naïve CD4+ T cells were stimulated with immobilized anti-CD3 antibodies in the presence or absence of DC3 and mo 1 sorted from PBMC of healthy donors and COVID-19 patients at a 1:2 ratio for 5 days. Stimulation with anti-CD3/CD28-coated beads was used as a positive control. A) Representative dot plots showing proliferation of CD4+ T cells by CTV dilution and activation by CD69 expression (HD healthy donor, CoV COVID-19 patient). B) Proliferation index, division index and percentage of CD69+ T cells are shown for cocultures with DC3 from healthy controls (black symbols n=6) and COVID-19 patients (red symbols, n=7, circles: glucocorticoid therapy, diamonds: no glucocorticoid therapy). C) Proliferation index, division index and percentage of CD69+ T cells are*

Following this evaluation, innate parameters at early time points after primary diagnosis (day 0-10) were correlated with subsequent adaptive parameters at late time points (day 10-25, data kindly provided by Linus Rinke) in longitudinally sampled patients. CD8^{+} T cell activation showed correlations with the MFIs of HLA-DR, CD40, CCR2, and CXCR3 in both DC3 and monocytes (Figure 50 A). This APC phenotype was inversely correlated with anti-S1 antibody levels. CD163^{+} CD14^{+} DC3 frequencies of total DC3 and different inflammatory markers- such as CRP, IL-6 and the neutrophil/lymphocyte ratio – correlated positively with activated T_{fh} cells, antibody-secreting-cells and class-switched memory B cells but did not correlate with antibody titers. Therefore, this phenotype appears to be linked to inflammatory responses and the expansion of activated T_{fh} and B cells (Figure 50 B). An inverse correlation of the CD163^{+} CD14^{+} DC3 was found with the subsequent PD-1 expression in both CD4^{+} and CD8^{+} T cells. On the other hand, the expression of PD-L1 and CD40 on DC3 positively correlated with the expression of PD-1 on CD4^{+} T cells. When correlating an early innate with a late adaptive time point, no correlation of PD-L1 expression on mo1 and PD-1 expression on CD8^{+} T cells was visible, in contrast to positive correlations when examining the simultaneous PD-1 and PD-L1 expression as described in Figure 49 F. The majority of the patients analyzed in this cohort developed anti-SARS-CoV-2 S1 IgG antibodies and over time after diagnosis the antibody levels increased (Figure 50 C, data kindly provided by Paul Wratil).

Thus, the correlation analysis shows that the APC phenotypes are linked to multiple activated states of adaptive immune cells in the peripheral blood of patients with COVID-19.
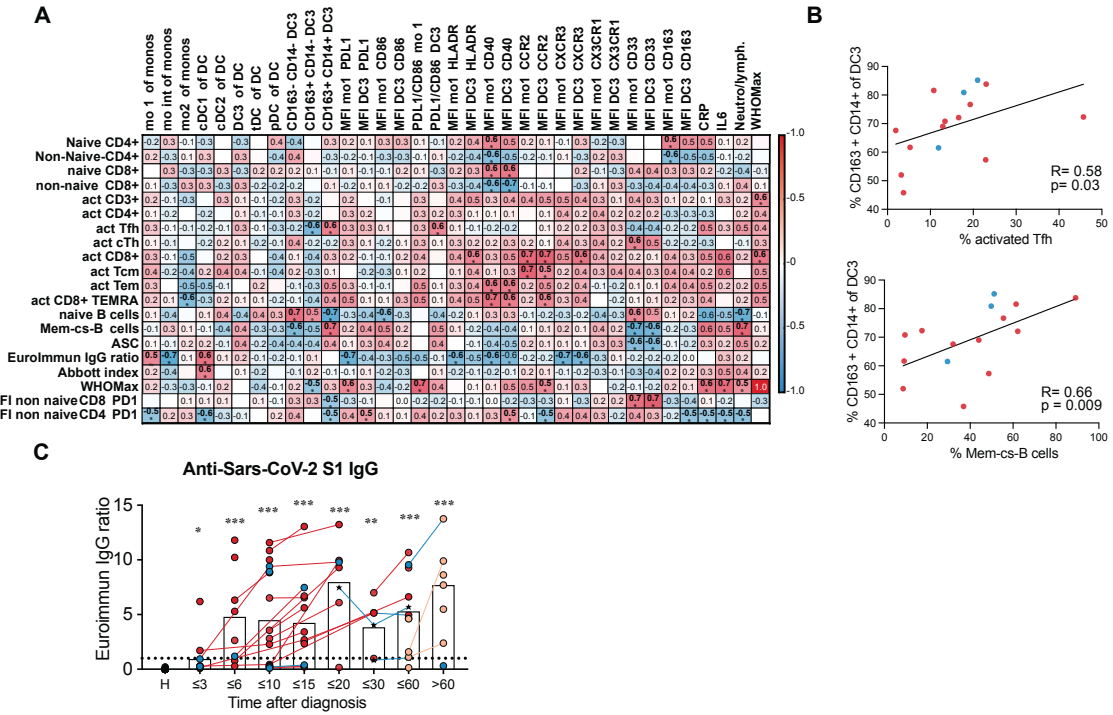
Figure 50: DC3 and monocyte phenotype correlates with Tfh and B cell activation.

A) *Correlation analysis of innate parameters up to 10 days after diagnosis (horizontal) with adaptive parameters at day 10 to 25 after diagnosis (vertical) in the same patients (n=9-17). Spearman's rank correlation coefficients (-1 to 1) are indicated by the color scale. * adjusted p values below 0.05.* B) *Correlation analysis of the percentage of CD163+ CD14+ cells within DC3 (until day 10) and the percentage of activated cells within Tfh-like cells or the percentage of class-switched memory B cells within CD19+ cells (day 10-25 after diagnosis, n=15). Spearman's rank correlation coefficient, p-value and linear regression line are shown. Mem c-s B: class-switched memory B cells; ASC: antibody secreting cells; T_{CM}: T central memory; T_{EM}: T effector memory; T_{EMRA}: T effector memory reexpressing CD45RA.* C) *anti-SARS-CoV-2 spike S1 IgG levels (Euroimmun IgG ratio) in plasma samples (n=105) of patients at different time points and in controls. The dotted line indicates the cutoff value for the antibody test. [...] Symbols indicate individual measurements [...]. Connected lines represent multiple measurements of the same donor at different time points. Columns indicate the mean. Data from each grouped time point were compared with data from the control group. Kruskal-Wallis test with Dunn's correction, *p<0.05, **p>0.01, ***p<0.001.* [Data on adaptive parameters kindly provided by Linus Rinke and IgG titers kindly provided by Paul Wratil] The figure and figure legend have previously been published by Winheim et al. in PLOS pathogens 2021 and have been slightly adapted [171].

In summary, this data showed that changes in the composition and phenotype of DCs and monocytes were linked with markers of inflammation and the activation of adaptive immune responses. In patients with a severe COVID-19 disease progression, all DC subpopulations were profoundly and persistently depleted while nonDCs, a cell population lacking both lineage and DC markers but expressing HLA-DR, were expanded. The frequency of CD163+ CD14+ DC3 was expanded and correlated with markers of systemic inflammation and T_{fh} and B cell activation. Classical monocytes and DC3 showed a dysregulated activation, marked by high expression of PD-L1 and CD40, but low expression of CD86 and were impaired in their ability to stimulate T cells.

119

5.   Discussion

5.1   The innate immune response to YF17D vaccination is marked by a pronounced and transient IFN response and efficient activation of multiple dendritic and monocyte subsets

This study aimed to identify the roles of DCs in viral infections. YF17D vaccination was used as a model of a well-regulated immune response to RNA virus infections, and healthy individuals were "infected" with the live-attenuated vaccine virus in a controlled manner through vaccination with YF17D. Analysis of APC subsets within PBMCs before and after vaccination allowed characterization of the overall innate immune response to this virus to showcase how an effective immune response is formed in humans. Understanding this innate immune response to the YF17D vaccine virus and how APCs interact with this virus in vitro can contribute insights into virus-host interactions, and how immune responses are regulated and induced. This research thereby provides an in-depth characterization of DC and monocyte subpopulations in the peripheral blood of people vaccinated against YF17D by flow cytometric analysis and RNASeq combined with in vitro data of YF17D infection of DCs and monocytes. This comprehensive analysis may help identify new strategies for the development of effective vaccines.

5.1.1   YF17D preferentially infects monocytes and DCs within total PBMCs

Previous publications have already shown the infection of DCs by YF17D in vitro and demonstrated (mainly using murine DCs) viral recognition via TLR2, 7, 8, 9, leading to expression of type I and III interferons and potential antigen presentation [151, 192]. Compared to wild-type YFV, enhanced viral replication of YF17D is found in cells infected in vitro and marks the difference between attenuated YF17D and wild-type strains [144]. The controlled viral replication in APCs is proposed to be one of the main factors behind the success of this vaccine as it would allow sufficient endogenous production of viral proteins for antigen presentation to induce a rapid and long-lasting adaptive immune response. Direct infection of APCs could hypothetically occur locally, but also in circulating APCs due to the viremia found after vaccination [124]. This infection of APCs could induce their optimal activation and presentation of viral antigens. Within total

PBMCs, preferential infection of DCs, monocytes, and NK cells can be identified by using FACS analysis of Venus-YF17D, confirming the results observed in humanized mice [153].

Interestingly, after isolation from PBMC all subsets of DCs – cDC1, cDC2, tDC, pDC, and recently identified DC3 – and all monocyte subsets from the peripheral blood could be infected by YF17D. The viral replication seemed to be highly restricted, with only approximately 2-20 % of APCs infected. The infection rate was highly variable and seemed to depend on the donors and possibly also on viral stocks – even if identical titers of viruses were compared. It has previously been described that the cells' receptiveness to certain innate stimuli can vary between individuals [193]. This interindividual variation could lead to an increased initial type I IFN and cytokine response, allowing for less viral replication and explaining this large range of infection rates. After infection, pDCs were the most potent producers of IFN-α, but most subsets produced the IFN-induced chemokine CXCL10 showing that direct infection of APCs does induce antiviral responses either in the infected cells or uninfected bystander cells.

Mo-DCs and classical monocytes were subsequently used as a model system to further elucidate virus-host responses. In monocytes and mo-DCs, infection with YF17D induced upregulation of distinct activation markers such as PD-L1, CD80, and HLA-DR. In mo-DCs, CD83 expression was also upregulated after YF17D infection. These effects were not observed with heat-inactivated virus, thereby excluding unspecific effects of the virus stock preparation. In addition, infected cells showed higher activation than uninfected bystander cells, indicating that direct infection of APCs activates monocytes and DCs or makes them more responsive to soluble factors inducing activation. This result also shows that in contrast to other viruses such as Zika virus, YF17D does not suppress the activation program [194]. However, full maturation of DCs as seen with control stimuli LPS and R848 was not initiated by YF17D infection, even at the highest viral concentrations used. This could indicate that direct viral infection by YF17D is only a suboptimal stimulus for APCs activation, and additional stimuli such as cytokines released by different cell types including effector lymphocytes, such as NK cells and T cells, most likely also play a role in the activation of APCs seen after YF17D vaccination. It could also be hypothesized that this restricted induction of APC activation is sufficient to trigger adaptive responses and may avoid overactivation and activation-induced cell death of DCs.

121

The detection of NK cell infection within PBMC was in agreement with the findings of Douam et al. (2017), who also found infected human NK cells in spleens of YF17D-infected humanized mice [153] although the biological significance of this result remains to be investigated in more detail.

In summary, a preferential infection of monocytes, DCs, and NK cells within total PBMCs by YF17D was observed in this research. While all subtypes of DCs and monocytes were shown to be susceptible to infection, the viral replication in APCs seems to be restrained and leads to limited activation of infected and bystander cells and secretion of cytokines.

5.1.2 Direct cell contact with virus-infected cells increases the amount of virus detected in DCs and monocytes

Direct infection of DCs and monocytes with YF17D leads to limited viral replication, with only 2 % to 20 % of cells infected. Therefore, and due to the overall scarcity of these subsets, the viremia found in vaccinees on day 7 is likely not the product of viral replication within DC and monocyte subpopulations alone but also of the infection of other cells that are less efficient at controlling viral replication. Regarding the cell tropism of YF17D, liver cells, fibroblasts, or endothelial cells could play a role in the viremia found in vaccinees. Besides the hypothesis that direct infection of APCs is one of the primary mechanisms activating these cells and allowing antigen presentation, the interaction of APCs with other virus-infected cells leading to increased uptake of viral components such as viral RNA or defective or intact viral particles could also play a significant role in driving the innate immune response and achieving presentation of viral antigens. For example, it was shown, that cDC1, which are highly resistant to Influenza virus infection, relied on viral antigens to be produced by neighboring cells and internalized them to elicit CD8^{+} T cell responses by cross-presentation [195]. The infection of non-immune cells can be recognized by APCs [196], which can take up antigens or even infectious virus from them, for example via exosomes [197, 198]. Similar observations have been made for DENV, a related flavivirus. pDCs have been shown to form an "interferogenic synapse" with DENV infected Huh-7.5.1 cells via $\alpha_L\beta_2$ integrin/ICAM-1, which allows the transfer of RNA and induces antiviral responses in pDCs [199]. A comparable study performed with

Discussion

DENV infected fibroblasts showed that crosstalk between fibroblasts and mo-DCs promoted IFN signaling in fibroblasts, DC maturation, and their ability to promote T cell responses [200]. Transfer of infectious virus between cells, e.g., via intraluminal endosomal vesicles that are secreted as exosomes, has also been described for other viruses [201].

Therefore, monocytes and mo-DCs were cocultured with cells highly susceptible to YF17D infection, such as VeroB4 and BHK21 cells. APCs cocultured with Venus-YF17D-infected cells showed a higher rate of Venus signal than APCs infected with a purified virus. This effect was only seen when the APCs had been in direct contact with virus-infected cells and was not found when they were separated by transwells. The increased Venus signal was accompanied by induction of activation markers, such as PD-L1 expression, on these cells. Microscopic images showed the Venus signal to be distributed across the whole cytoplasm of APCs and not localized in vesicles, thereby indicating viral infection rather than endocytosis of Venus-fluorescent material released from infected cells. The high intensity of the Venus signal detected in APCs after direct contact with virus-infected cells was also consistent with viral infection and replication.

In vaccinees, cells at the vaccination site such as fibroblasts or epithelial cells could potentially allow for viral replication. In such a case, APCs in the environment could be recruited and take up viral RNA or viral antigens. This uptake could be either from cells undergoing apoptosis, via extracellular vesicles, endosomes, or direct physical cell contact-mediated by, for example, ICAMs and integrins. While definite conclusions cannot be made from the limited data available, ICAM and integrin-mediated transfer are unlikely to be a major player in this system since non-human cell lines were used that might not be able to initiate receptor-based cell binding. However, performing coculture experiments with human fibroblasts, which were shown to support YF17D viral replication [128] and looking further at the interaction of the APCs and the virus-infected cells, would be essential to elucidate this further. In conclusion, the contact to virus-infected cells seems to be an additional mechanism for APCs to take up and produce YF17D viral antigens and could play a role in inducing efficient activation and antigen-presentation after vaccination with YF17D.

5.1.3   Infection by YF17D is highly restricted by type I IFN in DCs and monocytes

The type I IFN (IFN-β) response of monocytes and mo-DCs was greatly induced by infection with YF17D in vitro and dependent on the MOI. Using IFNAR in combination with IFN-α/β blocking antibodies, higher infection rates with YF17D were achieved in mo-DCs and monocytes which shows that the type I IFN response restricts viral infection or viral replication. On the other hand, Ruxolitinib inhibiting JAK1/JAK2 and thereby the JAK/STAT pathway increased the infection rate in monocytes significantly, but not consistently in mo-DCs, and BX795 blocking TBK1 downstream of RIG-I/MAVS did increase the percentage of infection in monocytes but these changes were not found to be significant. In monocytes, Ruxolitinib induced a significant reduction of IFN-β secretion and BX795 induced a trend towards fewer IFN-β, suggesting a role for TBK1 in IFN-β induction in monocytes and amplification of this response by IFNAR signaling. Additionally, Ruxolitinib reduced the infection-dependent upregulation of activation markers in mo-DCs (PD-L1) and monocytes (CD86, CD80).

Interestingly, previous research found reduced maturation of DCs and loss of response to stimuli such as LPS after treatment with Ruxolitinib [202]. However, in the experiments conducted within the framework of this thesis, a downregulation of activation markers was not seen in the Ruxolitinib control without infection, which indicates that the effects described are not simply caused by the use of the inhibitor but by inhibition of the pathway involved in the YF17D-dependent antiviral response. The inhibition of TBK1, downstream of RIG-I/MAVS, did not show the same effect. While both inhibitors were used at concentrations that inhibit their respective pathways and do not impair survival [203-205], incomplete inhibition may explain the results. Either partial activity of TBK1 is sufficient or TBK1-independent pathways compensate for reduced TBK-1 activity as multiple pathways are involved in the viral sensing of YF17D. From this data, it can be concluded that IFNAR signaling plays a major role in controlling viral replication, cytokine secretion, and cell activation in primary monocytes and DCs with involvement of the JAK/STAT pathway in vitro after infection with YF17D. The restriction of YF17D replication in APCs by type I IFN is consistent with the major role of IFNAR and type I IFN in preventing severe YF17D-associated viscerotropic or neurological disease [128]. Additionally, an in vitro study showed that the addition of IFN-β to YF17D susceptible

cells significantly reduced their infection with YF17D [128] which highlights the relevance of type I IFN in the control of viral replication.

The transcriptome analysis of different sorted APC populations ex vivo after vaccination further helps to elucidate the pathways involved – either in direct viral sensing or the systemic immune response to YF17D vaccination. Gene expression of all analyzed TLRs did not change within the APC populations over time after vaccination but – as expected – population-specific expressions were found with *TLR9* predominantly expressed in pDCs and tDCs as well as low expression in B cells and *TLR7* expression being restricted to pDCs. On the other hand, *TLR3* expression was limited to cDC1 as previously described [7]. *DDX58* (RIG-I) and *IFIH1* (MDA5), both IFN-induced genes, were upregulated on days 3 and 7 in all monocyte subsets, most highly in mo2 and in DC3 and cDC2. However, *TBK1* expression was not induced. Enhanced expression of *DDX58* – already at early time points on day 3 after vaccination – indicated an increased possibility to engage the RIG-I receptor in these cell types. This upregulation of *DDX58* was only found in monocytes and cDC2 and DC3, suggesting increased sensitivity of these populations to IFNs and the potential involvement of these subsets in sensing the vaccine virus via RIG-I. Indeed, it was reported that RIG-I is required for type I IFN induction in infected pDCs [167] and it is known that the non-vaccine yellow fever virus encodes a 2'O-methyltransferase which inhibits recognition of the viral RNA by RIG-I, demonstrating active evasion of this viral sensor [206]. Interestingly, a study investigating the mo-DC response to YF17D infection in vitro by microarray found that the IFN signaling response was the central pathway to be upregulated, and *DDX58* was also induced with a 3.5 x fold change [207] (Appendix 2, published by Kwek et al. 2018, data reanalyzed). This shows that RIG-I expression is upregulated in DCs after viral infection in vitro.

Ex vivo, *STAT1* and *STAT2* expression were upregulated in all peripheral blood APC subsets supporting the in vitro data showing the relevance of the JAK/STAT pathway in the context of YF17D infection. *STAT4* – which can be induced by IL-12- is highly expressed only in pDCs and total PBMCs and not influenced by YF17D vaccination. While direct infection and viral sensing in circulating APCs are possible, the changes observed in the transcriptome of peripheral blood APCs most likely reflect a systemic type I IFN response and the overall inflammatory state found after vaccination.

In conclusion, the data generated from in vitro infection experiments shows a robust control of YF17D infection by IFNAR with involvement of downstream signaling via the JAK/STAT pathway. Interestingly, the same pathways are activated in all DC and monocytes subsets after vaccination ex vivo, showing a systemic immune response across all APC subsets. Upregulation of *DDX58* in monocytes, cDC2, and DC3 after vaccination, and in mo-DCs in vitro [207] indicates an increased availability and thereby potential amplification of this viral sensing pathway after vaccination.

5.1.4 Strong IFN response in vaccinees

After vaccination, a strong IFN response in the transcriptome of APC populations was observed. This finding is in contrast to other flaviviruses such as Zika, where ISGs are downregulated after viral infection [208]. Multiple flaviviruses use antagonists to counteract this interferon-induced antiviral state, such as DENV [209] and WNV [210]. There is also evidence that YF17D inhibits IFN-I signaling via interactions between host STAT2 and viral NS5 protein after primary activation through IFN-I [148]. However, even though some inhibition of the IFN signaling might be induced by YF17D NS5, the IFNAR receptor signaling pathway greatly limits YF17D infection in DCs and monocytes in vitro.

A strong upregulation of ISGs was found in the transcriptome of all APC populations analyzed after vaccination with YF17D. The peak of the interferon response was found on day 7 which is the point in time when peak viremia and cytokine responses have also been described [130, 138]. Siglec 1 and Axl, which are both associated with IFN responses [180, 208], were also found to be upregulated on the cell surface in all APC populations on day 7, except for tDCs where both are expressed constitutively. This upregulation of *SIGLEC1* was also seen in the transcriptome. While it is part of the tDC signature genes, expression of *SIGLEC1* was also induced on day 7 in cDCs and monocytes, but not in B cells, pDCs or tDCs. The upregulation of *OAS1*, *OASL*, and *IRF7* found in total PBMCs by Querec et al. after YF17D vaccination was observed in all APC populations except for *IRF7*, which was constitutively expressed in tDCs and pDCs and did not show upregulation in these populations. *IRF7* has previously been described as being a master transcription factor upregulated prior to the adaptive immune response in YF17D

vaccinees [118, 126], which can now be confirmed. In addition to *IRF7*'s temporal up-regulation after vaccination in all cDC populations, monocytes, and B cells, Rcis enrichment analysis also showed that IRF7 is most likely a transcription factor involved in the regulation of DC3 responses, binding to motifs enriched in a cluster of DEGs upregulated in DC3 on day 7 (in one patient already on day 3) relevant for IL6-JAK-Stat signaling, IL2-STAT5 signaling as well as TNF-α signaling and containing genes such as *SIGLEC1* and *ISG15*. Interestingly, when examining the IFN signature of the distinct APCs, some cell-type-specific changes could be detected. *CXCL10* expression seemed to mostly be restricted to monocyte subpopulations and DC3 and was not upregulated in B cells, cDC1, pDCs, or tDCs. This indicates that monocytes and DC3 could be the major cell populations mediating inflammatory cytokine responses. Upregulation of *LAMP3*, involved in DC maturation and antigen processing [211], on the other hand, was mostly restricted to cDC1 and cDC2. Other genes such as *OAS1*, *OAS3*, *RSAD2*, *IFIT3*, *IFIT1*, and *EIF2AK2* were upregulated in unison on day 7 after vaccination in all populations analyzed. They form a common IFN regulated gene signature that is concertedly induced across different APC subsets after vaccination with YF17D.

Additionally, the main transcriptomic response overall was detected on day 7, with most DEGs found in all sorted populations. In B cells, where a later peak response was expected, only a low number of DEGs was detected with a peak on day 7. This could indicate that in the 1 000 sorted B cells YF17D-specific activated plasmablasts and plasma cells are overlooked due to their low frequency [111, 113]. The changes that are detected in the B cells here are most likely only the systemic effects of the general inflammatory response within the whole B cell fraction and are largely restricted to the IFN response.

It would be highly interesting to see if this transient and concerted IFN signature by all APC populations is only found after YF17D vaccination, or if it is a conserved immune response that drives immunity across viral infections and vaccinations. A study from 2014 by Li et al. compared the transcriptomic immune response to multiple vaccines [183]. The individual transcriptomic profiles were compared by using multiple RNASeq and microarray datasets published on the transcriptomic response of PBMCs to influenza (live attenuated vaccine LAIV, and inactivated protein vaccine TIV), YF17D, and vaccinations against Neisseria meningitides (MPSV4 and MCV4). The authors found a partial overlap between the live-attenuated vaccines YF17D and LAIV in some interferon-related genes.

127

However, high upregulation of IFN-α response genes (as seen in their BTM modules) was only found after YF17D and not in the other vaccinations.

Therefore, the study describes a distinct transcriptomic profile after YF17D vaccination, possibly explaining the high level of effectiveness of YF17D compared to other vaccinations. A follow-up study also identified that there was almost no overlap between the transcriptomic response of total PBMCs to YF17D vaccination compared to mRNA vaccination with BNT162b2 against SARS-CoV-2 infection [212]. Interestingly, the IFN response of the YF17D vaccinees also positively correlated with subsequent antibody titers, indicating its relevance for the adaptive immune response [183]. Furthering the understanding of the immune response to YF17D and adapting it to the development of new vaccinations could help reproduce the efficacy in inducing life-long protection against reinfection of the YF17D vaccination in the context of other viral agents.

Summarizing this data, a strong induction of a well-regulated and transient interferon response seems to be one of the major mechanisms of innate immune cells triggered by YF17D vaccination, with its peak on day 7 and effects found in all APC populations. A common gene signature of certain IFN induced genes is concertedly induced in all DCs, monocytes, and B cells. However, some changes in gene expression are only found in a subset of APCs, proving that in addition to this common gene signature, each APC population also shows its own unique signature.

5.1.5 Induction of activation and maturation markers after YF17D vaccination

Similar to what was seen after in vitro infection with YF17D, DCs and monocytes also showed upregulation of activation markers on the cell surface ex vivo after vaccination analyzed by flow cytometry. Especially costimulatory molecules CD86 and CD83 were significantly upregulated in DC3 and mo1 while expression of HLA-DR seemed to only be induced in mo1. The most substantial upregulation was found in Siglec 1 in all populations but tDC and pDC on day 7 which correlated with the overall IFN response. PD-L1 expression peaked on day 7 but was still significantly more highly expressed on day 14 than before vaccination in contrast to CD86, which returned to baseline after 14 days. PD-L1 can have multiple roles in DCs and monocytes. It is associated with the overall

activation of DCs and monocytes and is induced by IFN-γ or microbial stimulation. Additionally, PD-L1 can interact with PD-1 on T cells and therefore have a regulative function by suppressing T cell receptors and CD28 signaling. This negative regulatory effect can be overcome by strong CD28 signals delivered by costimulatory molecules CD80 and CD86 on APCs [213]. Therefore, the ratio of PD-L1 and CD80/CD86 on the APCs plays an important role in T cell activation and regulation. PD-L1 can also be upregulated on cDC1 after antigen uptake and reduces T cell-induced cytotoxicity [214] and by reverse signaling can be involved in dermal DC chemokine-mediated migration and cytotoxic T cell priming [215]. The upregulation of PD-L1 on circulating APCs was likely the result of the overall inflammatory response in vaccinees. The longer-lasting upregulation of PD-L1 in cDC2, DC3, and mo1 when CD86 was already at baseline levels could signify T cell regulation following T cell activation.

The analysis of chemokine receptor expression revealed differential regulation of CCR2, which is relevant for monocyte transmigration via the CCL2-CCR2 axis, with transient upregulation in mo2 and downregulation in mo1. This could indicate an increased ability of mo2 (patrolling the vascular endothelium) and decreased ability of mo1 to exit the circulation and migrate to tissues in response to CCR2 ligands on day 7 after vaccination. The significance of this finding is unclear at present. Downregulation of CCR2 on the surface of classical monocytes at this time point could also be a consequence of prolonged receptor engagement and internalization or monocyte maturation. CCR2 gene expression was also reduced after vaccination in mo1 (data not shown).

In conclusion, flow cytometry data shows upregulation of activation markers and IFN induced surface markers after vaccination with YF17D, with its peak on day 7 correlating with the peak transcriptomic response.

5.1.6 Expansion of mo int after YF17D vaccination

The peak activation marker upregulation and the peak of the main transcriptomic changes after YF17D on day 7 coincide with prominent changes in the monocyte composition. The intermediate $CD14^+$ $CD16^+$ population increased significantly, doubling in frequency. These monocytes are known to be more inflammatory than classical $CD14^+$ $CD16^-$ monocytes. After infection with YF17D in vitro, they secreted higher amounts of

TNF-α and IL-10 than the other populations. Previous studies have identified them as being the primary producers of TNF-α and, overall, highly efficient at secreting cytokines [54]. Several studies have shown mo1 to differentiate into mo int under inflammatory conditions [60]. Thus, this population could promote overall inflammation by secretion of different cytokines and is most likely differentiated from mo1, which actually showed a concomitant reduction in frequency.

cDC1, cDC2, and DC3 frequencies were reduced in absolute numbers and in relative percentage of total DCs on days 3 and 7 after vaccination and then replenished. Relative pDC frequency of total DCs increased concertedly. The changes in DC composition could indicate their migration to the site of inflammation or recruitment to lymph nodes. Recruitment of recently differentiated cells from the bone marrow could then replenish the DC compartment. At the times of reduction of cDC subsets, an increased percentage of Ki67$^+$ expression of these cDC subsets was also found, indicating regeneration from proliferative precursors or by the expansion of differentiated cDCs. pDCs that were not reduced in the peripheral blood did not show much expression of Ki67. tDCs behaved similarly to cDCs, with proliferation found on days 3 and 14 followed by an absolute expansion of tDC frequencies on day 14 after vaccination.

Whether tDCs are direct precursors of cDCs as suggested by See et al. (2017), who observed acquisition of cDC phenotypes after culture of tDCs [30], cannot be concluded from this data. There was no significant upregulation of cDC markers found in tDCs after vaccination with YF17D (data not shown). However, costimulatory molecules such as CD86 and PD-L1, as well as proliferation marker Ki67, were regulated similarly in tDCs and cDCs. Recruitment of tDCs from the bone marrow and differentiation into cDCs could potentially be one way to replenish the cDC compartment on days 3 and 7, although the peak of absolute numbers of tDCs on day 14, when cDC frequencies have normalized, suggests that this is not the case. In vitro, no direct differentiation of tDCs into cDCs after stimulation with YF17D was observed (data not shown) but multiple stimuli could be needed to induce differentiation in tDCs. In mice, pDCs differentiated into cells sharing transcriptomic profiles with tDC and cDC2 after MCMV infection in vivo, proving that tDCs could be an intermediate differentiation state in viral infections [35]. Whether the same process happens after YF17D infection remains elusive and cannot be answered with the bulk transcriptomic data provided here since no intermediary developmental

stages were analyzed. To answer this question, single-cell sequencing could put different stages of differentiation into context with fully differentiated cells at varying time points after vaccination and show the potential cell trajectories.

5.1.7   DC3 differ from mo1 in their transcriptomic response to YF17D

DC3 have recently been identified as a novel population involved in inflammatory processes and showing similarities to monocytes and cDC2. While the ontogeny of DC3 has shown separation from monocytes and cDC2, the surface expression of CD163 and CD14, as well as the transcriptomic expression profile, shows DC3 are highly similar to classical monocytes and cDC2 [17, 18]. Their close connection was verified by looking at DC3, cDC2, and monocyte signature genes identified by Villani et al. (2017) and Dutertre et al. (2019) in the transcriptome before and after vaccination [15, 16]. The DC3 signature genes were constitutively expressed and not affected by the vaccination. Genes used for the DC3 signature were either highly expressed in cDC2 or mo1, and there was much less overlap with mo int and mo2. Additionally, all cDC2 signature genes were also found to be highly expressed in DC3. Genes solely identifying DC3 have not been described in the literature as of yet but could be further elucidated using the dataset presented here in future analyses.

DC3 have been described as pro-inflammatory and were found to accumulate in SLE patients and produce a large number of cytokines upon stimulation with the plasma of these patients [15]. Looking at YF17D vaccination as a model of self-limited virus infection can serve to explain the function of DC3 in viral infections and their connection to monocytes and cDCs. The total amount of DEGs detected after vaccination was highest in mo1 and DC3. However, genes differentially expressed in DC3 on day 7, the peak of the innate immune response, overlapped more with day 7 DEGs of cDC2 rather than mo1. This indicates a similarity of DC3 and cDC2 in their response to systemic viral infection. The DEGs expressed on day 7 after vaccination in all three populations mainly encompassed ISGs including *STAT1*, *OASL,* and the master transcription factor *IRF7*. Interestingly, these were highly expressed in most APC populations analyzed, indicating that all subsets show a parallel and conserved gene signature induced by YF17D vaccination. On the other hand, genes that are specific to each population – between cDC2, DC3 and mo1 – could also be detected. For DC3, these were a total of 530 genes. *GZMB* was DC3

specific and upregulated on day 7 after vaccination. This gene codes for the protein granzyme B, which is usually found in NK cells and T cells, and can cleave caspases and therefore induce apoptosis. Another DC3 specific gene is *LILRA4*, also upregulated on day 7, which functions as a coreceptor that limits immune responses to viral infections and has previously been shown to reduce IFN production in pDCs upon viral infections [216]. *SCAMP5* was also specifically upregulated in DC3 on day 7. It is involved in the calcium-triggered secretion of cytokines such as CCL5 [217]. It can be concluded that while DC3 frequency in the peripheral blood is not significantly modulated after vaccination with YF17D, their responsiveness to the vaccine indicates that they might play an important role in the innate immune response. They respond to IFN by upregulation of IFN induced genes, promoting inflammatory responses, and entering an antiviral state. Additionally, they seem to have specific functions and could contribute to the cytokine environment found after YF17D vaccination by, for example, secretion of CXCL10 or other cytokines that can be modulated by *SCAMP5*.

Since DC3 were infectable with YF17D in vitro, direct activation by the virus could also occur in vivo, which could happen, for example, in the peripheral blood or in the infected tissue such as skin, where DC3 also seem to be found [218]. GSEA demonstrated that Reactome modules involved in antigen processing and cross-presentation – consisting of genes encoding members of the proteasome and MHC class I antigen presentation and trafficking of the endoplasmic reticulum (e.g., *PSME2*, *PSMB2*, *HLA-A*, *HLA-F*, *B2M*, *PSME1*, *PSMA6*, *TAP1*, *TAP2*, *MYD88, SEC22B, SEC61B*) – are upregulated in DC3 on day 7 after vaccination. One of three BTM modules for enrichment in antigen presentation (M95.0) containing several genes involved in cell adhesion was also upregulated on days 3, 7, and 14 compared to day 0 in DC3. The other two BTM modules for antigen processing consist of genes involved in the presentation of extracellular antigens on MHC II and show a low enrichment score in DC3 on day 7 compared to day 0. Genes involved in MHC I antigen presentation are already upregulated on day 3 and peak on day 7 after vaccination in DC3 (additional data shown in Appendix 3), most likely due to the fact that many of these genes are induced by IFNs. Interestingly, when looking at overlapping DEGs between cDC2 and DC3 many genes involved in antigen processing and MHC I presentation were shown to be upregulated in DC3 and cDC2 such as *CLEC4C*, *PSME1*,

132

PSME2, *PSMB9*, *HLA-A* and *B2M*. Overall, it is likely that both DC3 and cDC2 can contribute to antigen processing and presentation on MHC I after YF17D vaccination. MHC I antigen presentation of viral antigens either involves endogenous peptides that can be presented after a direct viral infection or antigens derived from virus-infected cells that can be taken up by DCs for cross-presentation to activate CD8^{+} T cells [219]. While cDC1 are the main cross-presenters, some publications show that both cDC2 and pDCs can also cross-present [28, 220]. Although the cross-presentation ability of DC3 has not yet been studied, DC3 were shown to promote a tissue-resident phenotype in activated CD8^{+} T cells [18].

Some of the DC3 specific and cDC/DC3 genes are actually highly expressed in pDCs and tDCs, which could indicate contamination of the bulk transcriptomic data. While a purity of 98-99 % after cell sorting was achieved, minor contamination with pDCs cannot be fully excluded. However, pDCs and tDCs do not show any upregulation of the genes found to be upregulated in cDC/DC3, such as *TCF4, CLEC4C, COBLL1, GZMB* and *LILRA4* (Appendix 4) after vaccination. Additionally, they show a much higher expression of these pDC/tDC associated genes than DC3. Therefore, if contamination is the reason for these genes being detected as induced in cDC2 and DC3, it would have had to have happened specifically for the day 7 samples. However, all samples from one individual donor (including all time points) were sorted on one day, gating was kept strictly the same and the samples were treated the same for RNASeq. Therefore, an error in the gating strategy or sample handling cannot explain this finding of changes in the day 7 samples. Contamination of pDCs and tDCs as defined in the gating strategy (CD33^{-} CD123^{+}) limited to day 7 after vaccination is therefore highly improbable. It is possible that pDCs or tDCs upregulate CD33 and CD1c in response to vaccination and at the same time downregulate CD123, leading to possible inclusion in cDC2 or DC3 gates at this time point. However, this was not seen in the flow cytometric data where pDCs and tDCs were always well separated from cDC2 and DC3 and did not show such an upregulation. Further analysis using single-cell sequencing could identify whether DC3 indeed express markers usually associated with pDC functions while maintaining their DC3 identity.

DC3 showed signs of proliferation in their transcriptome. One gene cluster putatively regulated by E2F, a regulator of cell cycle progression, consisted of genes involved in proliferation and apoptosis (e.g., *CDC40, ETS1, DSN1, FASTK, CUL4B*) and was upregulated on days 3 and 7. This supports the observation concerning increased proliferation (detected by Ki67 staining) found in the DC compartment.

Overall, DC3 seem to be greatly involved in the innate immune response to YF17D: on the one hand, as potential antigen presenters using MHC I and potentially initiating CD8^{+} T cell responses, and, on the other hand as potential inducers of inflammation through cytokine secretion and by upregulation of ISGs.
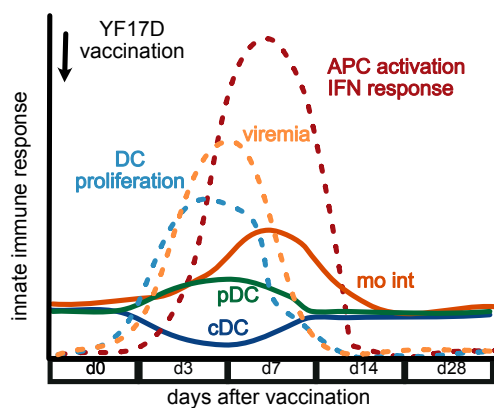
Figure 51: Graphical abstract showing timing of innate immune response after YF17D vaccination.
The proliferation of DCs coincides with a decrease of cDCs in the peripheral blood and a slight expansion of pDCs on days 3 and 7. Peak viremia between days 5 and 7 is followed by an expansion of mo int and overall APC activation and induction of ISGs on day 7.

From the data generated by this study, the following model can be proposed. Early replication of YF17D in susceptible cells at the injection site recruits APCs to the site of infection and, after one week, causes plasma viremia. Local APCs are infected but control viral replication via their IFN response. These cells get activated, secrete cytokines promoting inflammation, and can take up antigens for antigen presentation in the draining lymph node. Inflammatory cytokines in the plasma and possibly viral stimulation by virus particles and viral components in the blood during the transient viremia then lead to the concerted, transient, and multifactorial peak innate immune response assembled by all APC subsets on day 7 after vaccination that can shape the subsequent adaptive immunity. Overall, this coordinated and transient innate immune response is possibly the reason why YF17D vaccination is so potent and leads to persistent immune memory and long-lasting protection against reinfection.

134

5.2 COVID-19 patients show a dysregulated DC response with long-lasting changes

After analyzing the well-regulated and highly efficient innate immune response to YF17D infection, the next aim was to compare this to a real viral infection causing disease. SARS-CoV-2 infection can lead to mild or moderate symptoms in some patients and severe disease manifestations such as severe pneumonia and multi-organ failure leading to death in others. One major factor that influences the disease severity and progression is a dysregulated immune response. Therefore, analyzing the innate immune responses (focusing on DCs and monocytes) to Sars-CoV-2 in non-hospitalized patients with a mild progression of COVID-19 and in hospitalized patients with more severe disease and comparing this to immune responses to YF17D vaccination can be relevant for identifying causes of a dysregulated immune response.

5.2.1 Reduced DC frequencies in COVID-19

First of all, changes in the DC composition were observed. Differentiated DC subsets were reduced in frequency as well as in absolute number in the peripheral blood while $Lin^- HLA-DR^+ Ki67^+ CD86^{+/-} CD45RA^{+/-}$ cells that do not express typical DC and monocyte markers ("nonDC") were increased in the DC gate of the peripheral blood of COVID-19 patients both in non-hospitalized patients with mild disease progression and even more so in severely ill COVID-19 patients. While in non-hospitalized patients, DC depletion was not long-lasting and their frequency normalized 10-20 days after the onset of primary symptoms, hospitalized patients showed this phenotype even after recovery from acute disease. Increased proliferation accompanied the depletion of DC subsets in the peripheral blood, as seen by the Ki67 signal which indicates attempts of the hematopoietic system to restore the DCs. The reduction of DCs in the peripheral blood observed here is consistent with the findings of other studies [161, 221] and may indicate emigration of DCs from the blood or indicate premature cell death, as has already been described for pDCs in COVID-19 patients [222].

CXCR3 and CCR2 were upregulated and CX3CR1 downregulated in DC3 and monocytes of COVID-19 patients which suggests that they might be recruited to the infected lung and reacting to a chemokine gradient. Inflammatory chemokines CCL2, CCL3, and

CCL4 were increased in the airways of COVID-19 patients with severe symptoms [223]. cDC2 also upregulated these markers, while cDC1 and pDCs did not show this upregulation. This potential migration of cDC2 compared to cDC1 is supported by data showing preferred influx of cDC2 into the lungs and overall reduced numbers of pDCs located in the airways of COVID-19 patients [162].

Although expansion of mo int was found in COVID-19 patients with mild disease, it was only detected in one of the two cohorts with hospitalized patients. The blood samples from patients with severe COVID-19 were usually collected at later time points after infection than those of the patients with mild disease, and late sample collection after primary symptoms could explain this discrepancy since multiple publications found an expansion of mo int in severe COVID-19 [161, 166].

Mo2, on the other hand, were reduced in the severely affected COVID-19 patients and the mildly affected patients at early time points, thereby confirming the findings of previous studies [161, 166]. A positive correlation of mo2 frequency with CX3CR1 and a negative correlation of mo2 frequency with CCR2 expression in these cells showed that CCR2$^+$ mo2 could preferentially be recruited into the lung. The relevance of the CCR2-CCL2 axis for monocyte migration is confirmed by the publication of Szabo et al. (2021) that both showed recruitment of CD16$^+$ cells into the lung and increased expression of CCL2 in airway myeloid cells [223, 224]. There, the non-classical monocytes could favor inflammatory processes [50, 59].

The reduction of mo2 has also been used as a predictive factor for more severe disease manifestations [225]. Non-classical monocytes express higher levels of CX3CR1 than classical monocytes and CX3CR1 was shown to promote survival [190, 191]. Therefore, increased cell death could contribute to the preferential reduction of circulating non-classical monocytes, which may be more dependent on this signal for survival. The recovery of the non-classical monocyte fraction was observed at later time points (15-20 days after diagnosis) and was accompanied by an increase of CX3CR1 expression over time, which indicates a relevant role of this receptor for regulating the number of non-classical monocytes in the blood.

Interestingly, an expansion of CD163$^+$ CD14$^+$ DC3 that correlated with systemic inflammation and accumulation of activated T$_{fh}$ and B cells was detected in COVID-19 patients

with severe disease progression. However, whether this DC3 population directly influences T_{fh} and B cell activation or if both are influenced by the systemic inflammation found in COVID-19 patients cannot be concluded from these results.

5.2.2 Dysregulated phenotypic changes in COVID-19

COVID-19 patients suffering from a severe form of the disease showed a dysregulated activation of APCs expressing low CD86 and high PD-L1. This phenotype was found in unbiased k-means clustering in a subgroup of non-hospitalized patients and was associated with more severe disease manifestations and older age in this group. However, age neither correlates with PD-L1 nor with CD86 expression [171] and the expression level of both molecules grouped the patients according to disease severity in PCA. Similar changes of APC phenotype have previously been described. Several studies found down-regulation of HLA-DR on monocytes [163] and PD-L1^{high} neutrophils [166], and Kvedaraite et al. (2021) also found reduced expression of CD86 and HLA-DR in DCs and monocyte subsets [161].

DC3 and mo1 isolated from the hospitalized patients also showed impaired ability to induce efficient proliferation and differentiation of autologous naïve CD4$^+$ T cells while the T cells were easily stimulated by CD3/CD28 beads showing that not the T cells, but the APCs of COVID-19 patients seem to be dysfunctional and less able to costimulate naïve T cells. Studies showing that DCs isolated from the peripheral blood of COVID-19 patients are less responsive to TLR stimulation and cytokines provide further evidence for the dysfunction of circulating DCs in COVID-19 [163]. The altered phenotype of DCs and classical monocytes with low CD86, low HLA-DR, and high PD-L1 expression was only detected in Ki67$^-$ cells and not in the proliferating cells. Therefore, it is improbable that these phenotypic and functional changes are already imprinted in precursors of DCs and monocytes. Instead, this phenotype could be caused by circulating inflammatory mediators such as CRP, IL-6, and other pro-inflammatory cytokines, which correlated with the PD-L1^{hi} CD86^{lo} HLADR^{lo} phenotype in monocytes and cDCs, thereby supporting this hypothesis [171]. In COVID-19 patients, dysfunctional DCs that cannot adequately prime T cell responses could lead to insufficient adaptive immune responses and delay clearance of the SARS-CoV-2 virus. Nevertheless, T cell activation and sufficient antibody responses were achieved in this cohort. However, T cell responses detected in the blood

137

were highly variable between individual COVID-19 patients [160, 226-228] in contrast to the more homogeneous responses that can usually be observed in viral infections or after vaccinations [120, 229].

Transient high expression of Siglec 1 in DC3 and monocytes could be detected in the blood of COVID-19 patients at early time points and correlated with the IFN1/3 score generated from plasma proteins. Several other studies also found increased Siglec 1 in the plasma and expressed on monocytes [225, 230, 231]. Surprisingly, Siglec 1 was recently found to facilitate entry of SARS-CoV-2 by enhancing SARS-CoV-2 infection of ACE2-expressing HEK 293T cells when in contact with them in so called trans-infections [232]. The same study also described the expression of Siglec 1 on DCs, monocytes, and alveolar macrophages in steady-state [232] and concluded that the presence of Siglec 1^{high} cells at the site of infection could support SARS-CoV-2 infection. Therefore, viral infection could be favored by a strong IFN response and high expression levels of Siglec 1 on APCs migrating to the site of infection.

While some studies showed an impaired type I IFN response in patients with severe disease [164], others showed that these patients sustain high levels of IFN-α for a long time compared to mildly affected patients [160]. In this cohort, the IFN response was only transient in COVID-19 patients and, while the induction of Siglec 1 could potentially accelerate disease progression, it was not significantly positively or negatively correlated with disease severity. This finding stands in contrast to the observations made in a previous study that found high Siglec 1 expression to be correlated with mild disease manifestations [231]. Siglec 1 expression on monocytes in COVID-19 patients has been propagated as a biomarker for early diagnosis of COVID-19 [230]. The data presented here that show high expression levels of Siglec 1 after vaccination with YF17D and in COVID-19 patients now suggests that Siglec 1 could be used for the general diagnostics of viral infections or of other diseases inducing type I IFN responses.

Additionally, Siglec 1 expression was found on activated monocytes with high HLA-DR expression and high cross-presentation ability [233]. Siglec 1 could mark cells with higher antigen presentation ability, or it could be functionally involved in antigen uptake and presentation. Therefore, the function of Siglec 1 on APCs in the context of viral infections should be analyzed further.

Discussion

In summary, this data showed that depletion, phenotypic alterations associated with impaired costimulatory function, and enhanced turnover of circulating DCs in COVID-19 patients are long-lasting in patients with a severe disease progression and persist even in some milder COVID-19 cases. The consequences of these alterations of DCs and monocytes are still unknown. Potentially, these alterations could dampen the inflammatory responses in COVID-19 patients and reduce the overactivation of the immune system. However, together with the previously described lymphopenia, these changes could make patients more susceptible to secondary infections, which are recognized to occur frequently in COVID-19 patients [234, 235].
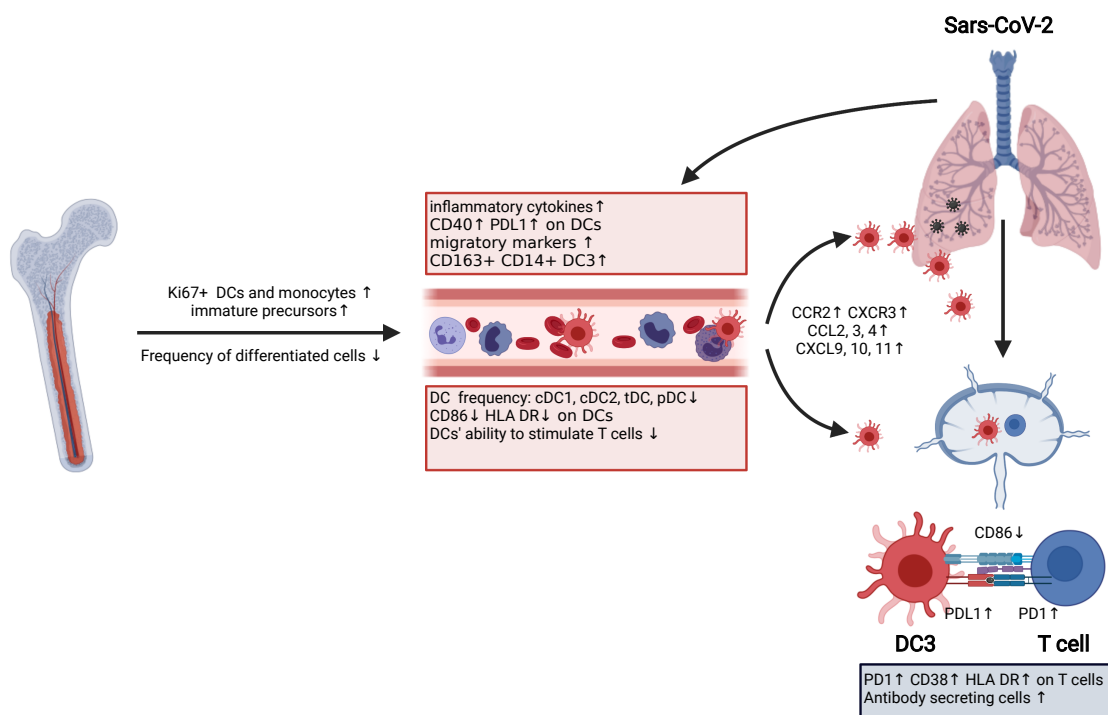
Figure 52: Graphical abstract to summarize the innate immune response to COVID-19 in COVID-19 patients with a severe disease progression.
Ki67[+] DCs, monocytes, and immature precursor populations are recruited from the bone marrow and increase in frequency in the peripheral blood compared to fully differentiated populations. The overall inflammatory response is measurable in the peripheral blood through increases in pro-inflammatory cytokines. Correlating with inflammation, CD14^{+} DC3 increase and phenotypic changes of DCs and monocytes are observed with increased expression of CD40 and PD-L1 and with decreased expression of CD86 and HLA-DR. The functionality of DCs and monocytes to stimulate CD4^{+} T cell responses is also decreased. Migratory molecules are upregulated in monocytes, DC3, and cDC2 and it is likely that these populations are recruited to the lung as a site of infection by a chemokine gradient. Figure generated using BioRender.

5.2.3 Comparison of DC and monocyte response to YF17D vaccination and to Sars-CoV-2 infection

Comparing the well-regulated and balanced response of circulating DC and monocyte subsets to YF17D vaccination and SARS-CoV-2 infection, several differences and some similarities were found which are summarized in Table 28. First of all, relative cDC frequencies were changed in both situations with an early relative and absolute reduction of cDCs in the peripheral blood in all cohorts examined. After YF17D vaccination, this reduction of cDCs was only transient at early time points while in COVID-19 patients with severe disease progression it was long-lasting. pDCs were also reduced in COVID-19 patients, which was not observed after YF17D vaccination. The reduction of DCs in the peripheral blood could be caused by the exit from the circulation and migration to the site of inflammation and/or recruitment to the lymph nodes for antigen presentation. Increased proliferation of DCs as measured by Ki67 signal followed these reductions and seemed to be able to replenish the DC compartment after vaccination, whereas in severe COVID-19 DC depletion and proliferation occurred simultaneously and for longer time periods, thereby indicating delayed regeneration. In COVID-19 patients where pDC numbers were also reduced, they were found to proliferate in some patients, which was not observed in the YF17D cohort. Interestingly, in COVID-19 patients nonDCs – a population lacking DC and monocyte markers but expressing HLA-DR and CD86 – were found to be expanded which was not the case in YF17D vaccinees. Due to the high Ki67$^+$ signal in this population, even in healthy individuals, they could be an immature precursor population that is expanded and released prematurely into the circulation in response to SARS-CoV-2 infection. Similar cells have already been identified in cancer and severe malaria cases [188, 189]. The increase of these nonDCs could be a sign of the enhanced and dysregulated myelopoiesis found in COVID-19 patients [166] but not after vaccination with YF17D.

Mo int, marked by expression of CD14$^+$CD16$^+$, showed a transient expansion after YF17D vaccination and in mildly affected COVID-19 patients on day 7. However, in the severe COVID-19 cases, only some patients showed an increase of intermediate monocytes. Mo2 were reduced in the peripheral blood of COVID-19 patients, confirming previous studies [161, 166], but this was not a characteristic observed after YF17D vaccina-

tion. One of the main differences between severe COVID-19 patients and YF17D vaccinees was the altered phenotype of DCs and monocytes. Expansion of CD14$^+$ DC3 was found in COVID-19 patients correlating with disease activity and inflammation but was not seen after YF17D vaccination. Upregulation of Siglec 1 on the surface of blood monocytes and DC3 was found to be a sensitive marker of the systemic type I IFN response in response to YF17D vaccination and in the early phase of COVID-19 that should be further investigated as a biomarker in viral infection and vaccination. Activation markers CD86 and PD-L1 were both upregulated in circulating APCs after vaccination with YF17D at the peak of the innate immune response and subsequently downregulated. In non-hospitalized COVID-19 patients, this activation pattern was also observed in most cases except for a few patients with more pronounced symptoms that showed downregulation of CD86 while maintaining high expression of PD-L1. In hospitalized COVID-19 patients with more severe disease, the downregulation of CD86 and upregulation of PD-L1 in cDC2, DC3 and monocytes were apparent. This altered phenotype observed in several DC and monocyte subsets is a sign of a dysregulated innate immune response in COVID-19 associated with inflammation and disease severity, as was already proposed for classical monocytes [166, 225, 236]. Therefore, the specific expression pattern of cell surface activation markers could be useful to predict immune response outcomes to viral infections and vaccinations.

Table 28: Comparison of innate immune response to YF17D vaccination and to SARS-CoV-2 in mild and severe COVID-19 cases.

No = blue, yes= red, not analyzed= gray. Time points refer to ♦days after vaccination. * days after symptom onset. # days after the first diagnosis.

	YF17D ♦	Mild COVID-19 *	Severe COVID-19 #
Reduction of cDCs	Yes, on day 7	Yes, up to day 14	Yes, in some recovered >30 days
Reduction of pDCs	No	Yes, up to day 7	Yes, up to day 10
Expansion of mo int	Yes, on day 7	Yes, up to day 7	No, only in some patients
Reduction of mo2	No	Yes, up to 14 days	Yes, up to 15 days
Expansion of nonDCs	No	Yes, up to 35 days	Yes, up to 20 days
Upregulation of PD-L1 expression	Yes, on day 7	Yes, up to 60 days	Yes, even in some recovered >30 days
Downregulation of CD86	No, upregulation on day 7	No, up- in most, downregulation in some patients	Yes, in some recovered > 30 days
Proliferation of cDCs	Yes, on day 7	Yes, in some cDC1 at late timepoints	Yes, in some recovered > 30 days

Discussion

Proliferation of pDCs	No	No	Yes
Proliferation of monocytes	No	Yes	Yes
Reduced ability to stimulate T cells	Not analyzed	Not analyzed	Yes
Transient Siglec 1 expression in DC3 and monocytes	Yes	Not analyzed	Yes, up to 15 days
Expansion of CD14+ DC3	No	Not analyzed	Yes, up to 20 days

In summary, YF17D vaccination induces a transient coordinated response of blood APCs with the peak on day 7 after vaccination, while the responses in COVID-19 are long-lasting and show unusual phenotypes of monocytes and DCs accompanied by functional impairment.

The fact that only peripheral blood and no other tissue such as the local site of vaccination or infection and secondary lymphoid tissue could be analyzed in humans is a limitation of the study. However, multiple innate immune parameters measured, such as APC frequencies, activation status, and plasma cytokines showed strong correlations with the disease severity of COVID-19 patients. These findings highlight the important role of systemic innate immune responses in the pathophysiology of this disease and suggest that the analysis of peripheral blood APCs can be used to predict disease outcomes. The in-depth characterization of the response of circulating DC and monocyte subpopulations to viral infection and vaccination presented here furthers the understanding of virus-host interactions and defines key features of innate immune responses leading to protective immunity as well as indicators of dysregulated innate immune responses.

VI. Appendix A: Figures
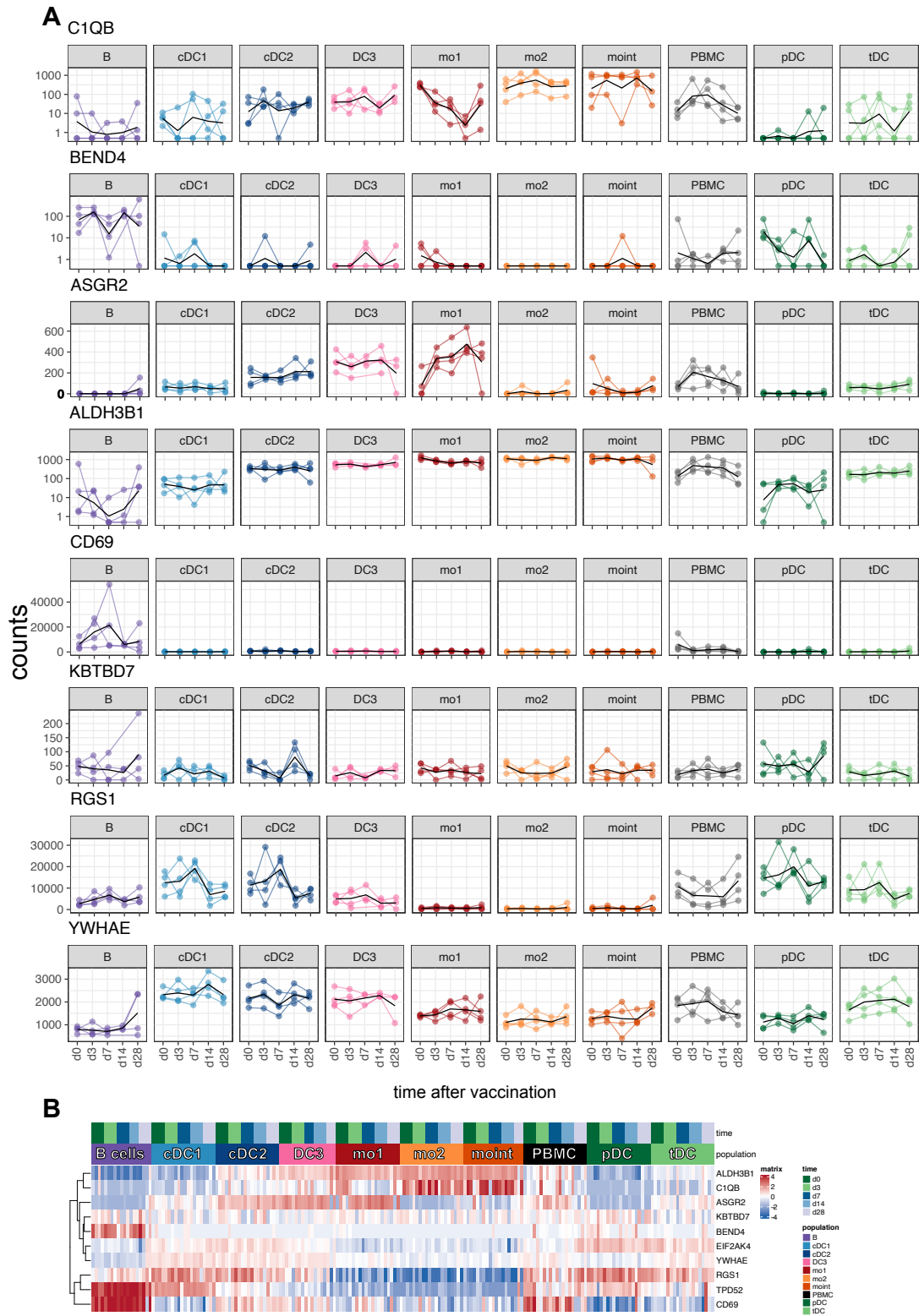
Appendix 1: Gene expression in patients over time after vaccination with YF17D.
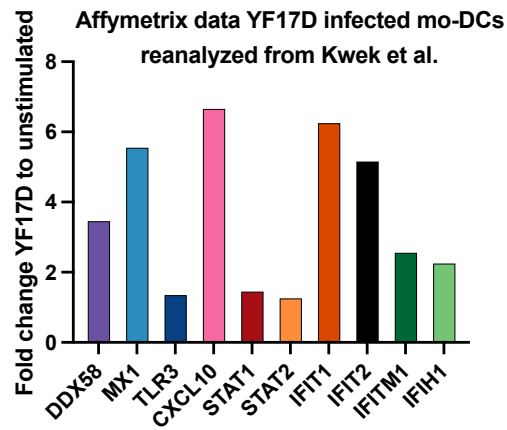
Appendix 2: Affymetrix data from Kwek et al. (2018)
Kwek et al. (2018) [207] infected mo-DCs with an MOI1 of YF17D for 24 hours, RNA was isolated using Qiagen mini kit and then microarray was performed using Gene 2.0 ST Array (Affymetrix). Shown are the fold changes to uninfected controls as reanalyzed by me.
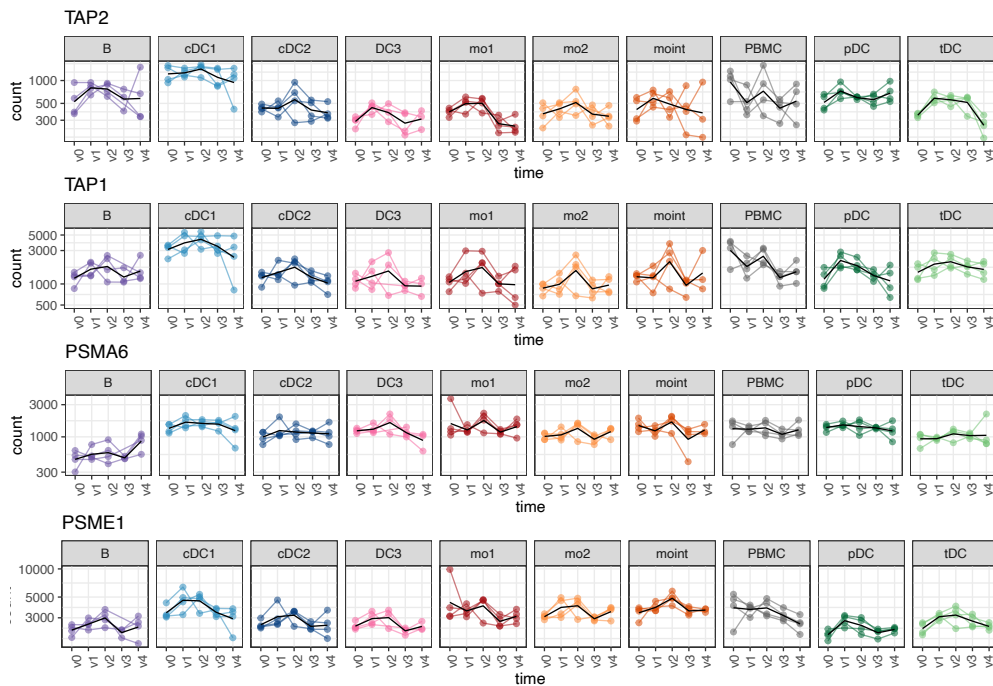
Appendix 3: Genes involved in antigen processing and presentation.
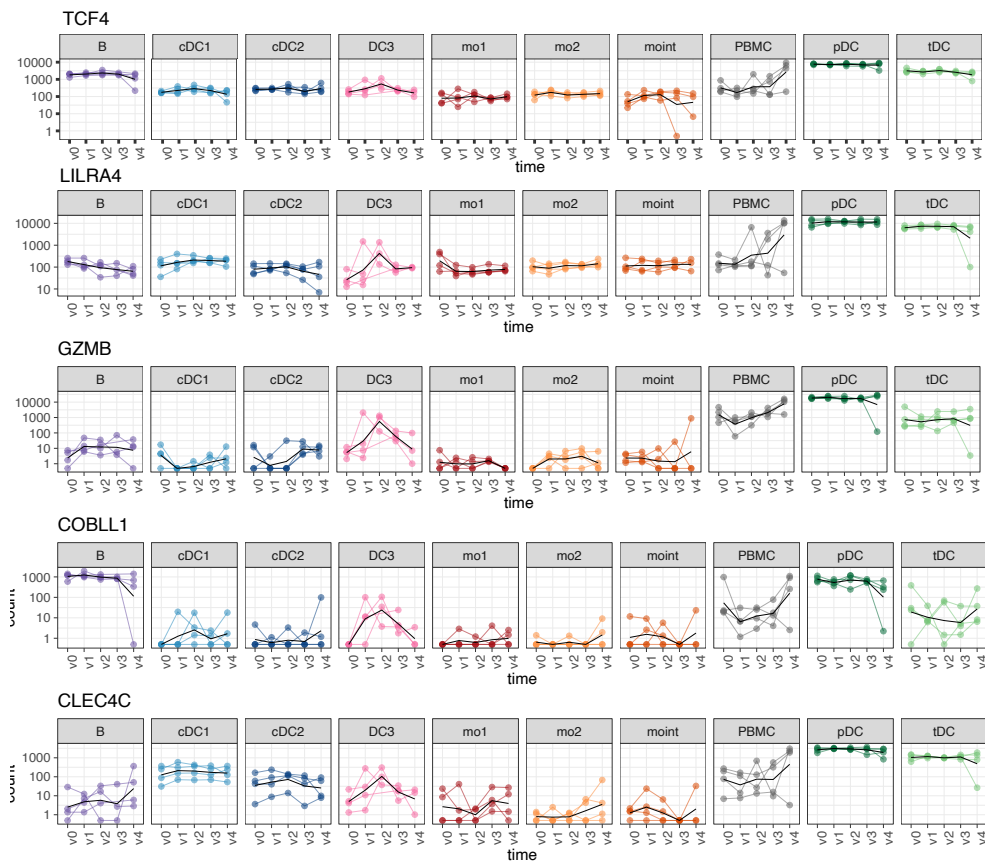
Appendix 4: Genes expressed by DC3 and usually associated with pDC functions.

VII. Appendix B: Supplementary table

Table 29: Characteristics of study participants.

0= Male, 1= Female. For one of the healthy donors of the COVID-19 outpatient study the data of age was not collected. The characteristics of the cohort consisting of hospitalized COVID-19 patients can be found in [171].

Patient ID	Age	Gender	Cohort
d3	25	1	YF Aurora Panel
d4	26	1	YF Aurora Panel
d7	23	1	YF Aurora Panel
d9	23	1	YF Aurora Panel
d10	35	0	YF Aurora Panel
d11	24	1	YF Aurora Panel
d12	29	1	YF Aurora Panel
d18	21	1	YF Aurora Panel
d19	21	1	YF Aurora Panel
d27	23	0	YF Aurora Panel
d209	33	0	YF Ki67 Panel
d210	30	1	YF Ki67 Panel
d211	22	1	YF Ki67 Panel
d212	22	1	YF Ki67 Panel
d213	22	1	YF Ki67 Panel
d214	25	1	YF Ki67 Panel
d241	31	1	YF Ki67 Panel
d242	26	0	YF Ki67 Panel
d243	22	1	YF Ki67 Panel
d244	24	1	YF Ki67 Panel
d245	24	1	YF Ki67 Panel
d246	25	1	YF Ki67 Panel
d247	27	1	YF Ki67 Panel
d248	32	1	YF Ki67 Panel
d250	35	1	YF Ki67 Panel
d251	32	0	YF Ki67 Panel
d252	23	0	YF Ki67 Panel, RNASeq
d253	22	1	YF Ki67 Panel, RNASeq
d254	25	1	YF Ki67 Panel, RNASeq
d255	27	0	YF Ki67 Panel, RNASeq
1	29	0	H Outpatient COVID-19
2	61	1	H Outpatient COVID-19
3	30	1	H Outpatient COVID-19
4	?	1	H Outpatient COVID-19
5	24	1	H Outpatient COVID-19

6	26	1	H Outpatient COVID-19
7	25	1	H Outpatient COVID-19
8	23	1	H Outpatient COVID-19
9	55	0	H Outpatient COVID-19
10	28	0	H Outpatient COVID-19
11	50	1	H Outpatient COVID-19
12	20	1	H Outpatient COVID-19
13	61	0	H Outpatient COVID-19
14	23	0	H Outpatient COVID-19
15	26	0	H Outpatient COVID-19
16	87	0	S Outpatient COVID-19
17	64	1	S Outpatient COVID-19
18	82	0	S Outpatient COVID-19
19	72	0	S Outpatient COVID-19
20	85	0	S Outpatient COVID-19
21	90	1	S Outpatient COVID-19
22	78	0	S Outpatient COVID-19
23	31	1	M Outpatient COVID-19
24	23	0	M Outpatient COVID-19
25	18	0	M Outpatient COVID-19
26	39	1	M Outpatient COVID-19
27	31	1	M Outpatient COVID-19
28	61	0	M Outpatient COVID-19
29	23	1	M Outpatient COVID-19
30	30	1	M Outpatient COVID-19
31	29	1	M Outpatient COVID-19
32	49	1	M Outpatient COVID-19
33	26	1	M Outpatient COVID-19
34	32	1	M Outpatient COVID-19
35	30	1	M Outpatient COVID-19
36	54	1	M Outpatient COVID-19
37	25	0	M Outpatient COVID-19
38	25	0	M Outpatient COVID-19
39	48	0	M Outpatient COVID-19
40	46	1	M Outpatient COVID-19
41	30	1	M Outpatient COVID-19
42	50	0	M Outpatient COVID-19
43	38	1	M Outpatient COVID-19
44	33	0	M Outpatient COVID-19
45	36	0	M Outpatient COVID-19
46	49	0	M Outpatient COVID-19

47	46	0	M Outpatient COVID-19
48	30	1	M Outpatient COVID-19
49	32	0	M Outpatient COVID-19
50	31	1	M Outpatient COVID-19
51	30	0	M Outpatient COVID-19
52	56	1	M Outpatient COVID-19
53	55	0	M Outpatient COVID-19
54	59	0	M Outpatient COVID-19
55	30	1	M Outpatient COVID-19
56	38	1	M Outpatient COVID-19
57	36	1	M Outpatient COVID-19
58	72	0	M Outpatient COVID-19
59	69	1	M Outpatient COVID-19
60	51	0	M Outpatient COVID-19
61	48	1	M Outpatient COVID-19

VIII. Appendix C: R Markdown code

i. Connected Datapoints over time Loop

Elena Winheim

9/20/2021

```
# First put in the Excel table you want to use to generate your Graphs
setwd("~/RData")
library(readxl)
library(ggplot2)
library(tidyverse)
library(ggpubr)
YF_Round1 <- read_excel("Aurora_YF_Round1.xlsx")



# Here you can put the donor ID and a specific color together, this is
then saved as cols2 and can be used for any figure #superhelpful
cols2 <- c("d3" = "#ece2f0", "d4" = "#d0d1e6", "d7" = "#a6bddb","d9" =
"#67a9cf", "d10" = "#3690c0","d11" = "# 02818a", "d12" = "# 016c59", "
d18" = "# 014636", "d19" = "#252525", "d28" = "#fff7bc")
#extra colors if needed , "1146R02" = "#fee391", "1147K01" = "#fec44f"
, "1148F02" = "#fe9929","1152P02" = "#ec7014", "1153H01" = "#cc4c02",
"3785T01" = "#993404" , "3785T02" = "#662506", "4739P01" = "#bdbdbd",
"4739P02" = "#525252")


# This is a function that will plot everything within the excel table
that you are using. This one is specifically for connected points over
time. The samples are grouped and colored by the "ID" of the donors. C
olor is decided on by cols2. We are also showing all significant p val
ues (careful! no correction for multiple testing done here in the loop
). You can decide between different testing, by method =. Additionally
, you can decide which group is the one everything is compared to with
ref.group=.

plot_for_loop_connection <- function(df, .x_var, .y_var) {
 # convert strings to variable
  x_var <- sym(.x_var)
  y_var <- sym(.y_var)
  # unquote variables using !!
  ggplot(df, aes(x = !! x_var, y = !! y_var)) +
    geom_point(aes(color=ID)) +
  geom_line(aes(group = ID, color=ID))+
    labs(x = x_var, y = y_var) +
    theme_classic(base_size = 8)+
    theme(
      axis.text.x = element_text(color="black", angle = 45,hjust = 1),
      axis.ticks = element_line(color = "black"), axis.text.y =element
_text(color= "black"),
```

150

```
      element_line(size=0.5)
    ) +
    scale_color_manual(values = cols2) +
  stat_compare_means(label = "p.format", method = "kruskal.test", data
= YF_Round1,
                    ref.group = "v0", size = 2)


}

#run the function on all columns against column 3 (time point) and sav
e the plots as plot_list
plot_list <- colnames(YF_Round1) %>%
  map( ~ plot_for_loop_connection(YF_Round1, colnames(YF_Round1)[3], .
x))


# view all plots but not if it is too many otherwise you will go mad
# plot_list

#save all plots as a pdf
pdf("YF_Aurora_Round1_connected_20210920.pdf", width=3, height=1.5)
invisible(lapply(plot_list, print))
dev.off()

## quartz_off_screen
##                     2
```

Input tidy data:

FCS name	ID	time point	cDC1 | Freq. of DC parent gate
3_v0.fcs	d3	v0	1,68
3_v1.fcs	d3	v1	0,65
3_v2.fcs	d3	v2	0,67
3_v3.fcs	d3	v3	1,41
4_v0.fcs	d4	v0	2,96
4_v1.fcs	d4	v1	1,33
4_v2.fcs	d4	v2	0,95
4_v3.fcs	d4	v3	1,53
7_v0.fcs	d7	v0	3,26
7_v1.fcs	d7	v1	3,47
7_v2.fcs	d7	v2	1,19

Output looks like this with one figure for each column of the input excel table
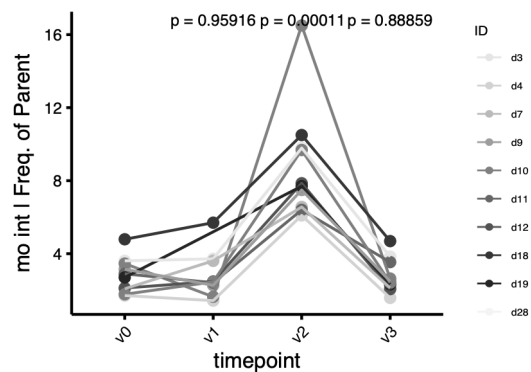
ii.   Stacked graphs

Elena Winheim

9/27/2021

```
# First put in the Excel table you want to use to generate your Graphs
library(readxl)
library(ggpubr)
library(tidyverse)
library(ggplot2)
library(rlang)
setwd("~/RData")
YF_Round1 <- read_excel("Aurora_YF_Round1_v2.xlsx")

# now select the datapoints from which you want to make a stacked grap
h

YF_DConly <- select(YF_Round1, "time point", "ID", "cDC1 | Freq. of DC
parent gate", "cDC2 | Freq. of DC parent gate", "DC3 | Freq. of DC par
ent gate", "pDC | Freq. of DC parent gate", "tDC | Freq. of DC parent
gate")

# make long dataframe out of DC data
library("tidyr")
DC.long <- pivot_longer(data = YF_DConly,
                        cols = -c(time point, ID),
                        names_to = "DC",
                        values_to = "value")

#make stacked plot and save as PDF
pdf("Aurora_stackedDC_YF_20210927.pdf", width=3.8, height=1.5)
ggplot(DC.long, aes(fill = DC, y= value, x = time point))
ggplot(DC.long, aes(fill=DC, y=value, x=time point)) +
```

```
    geom_bar(position="fill", stat="identity")+
    scale_fill_manual(values = c("#67a9cf",
                                 "#636363",
                                 "#1c9099",
                                 "#bdc9e1",
                                 "#016c59"))+
  theme_classic(base_size=8)+
  theme(
      axis.text.x = element_text(color="black", angle = 45,hjust = 1),
      axis.ticks = element_line(color = "black"), axis.text.y =element
_text(color= "black"),
      element_line(size=0.5))
```

Output:
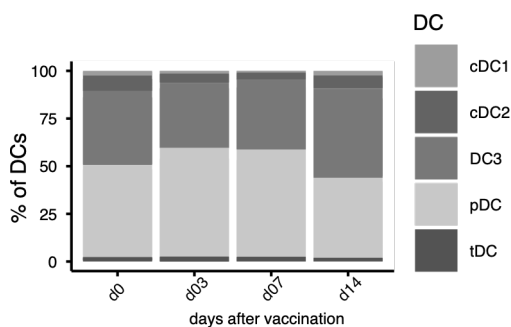
iii.   Heatmap activation markers

Elena Winheim

9/27/2021

```
setwd("~/RData")
library(readxl)
library(ggplot2)
library(tidyverse)

## ── Attaching packages ──────────────────────────────────── tidyv
erse 1.3.1 ──

## ✓ tibble  3.1.4     ✓ dplyr   1.0.7
## ✓ tidyr   1.1.3     ✓ stringr 1.4.0
## ✓ readr   2.0.1     ✓ forcats 0.5.1
## ✓ purrr   0.3.4

## ── Conflicts ───────────────────────────────────────── tidyverse_c
onflicts() ──
## x dplyr::filter() masks stats::filter()
## x dplyr::lag()    masks stats::lag()

library(ggpubr)
setwd("~/RData")
```

153

```
YF_Round1 <- read_excel("Aurora_YF_Round1_v2.xlsx")
YF_PDL1 <- select(YF_Round1, "time point", "ID", "mo1 | PE-Cy5-A :: PD
L1)","mo int | PE-Cy5-A :: PDL1)", "mo2 | PE-Cy5-A :: PDL1)", "cDC1 |
PE-Cy5-A :: PDL1)", "cDC2 | PE-Cy5-A :: PDL1)", "DC3 | PE-Cy5-A :: PDL
1)", "tDC | PE-Cy5-A :: PDL1)", "pDC | PE-Cy5-A :: PDL1)")


PDL1.long <- pivot_longer(data = YF_PDL1,
                    cols = -c(time point, ID),
                    names_to = "Class",
                    values_to = "value")



new.PDL1 <- aggregate(x= PDL1.long$value,
           by =list(PDL1.long$time point, PDL1.long$Class),
           FUN = mean, na.rm= TRUE)

new.wide3 <- pivot_wider(new.PDL1, names_from = Group.2, values_from =
x)
rownames(new.wide3) <- new.wide3$Group.1 # making new rownames

## Warning: Setting row names on a tibble is deprecated.

rc <- colorspace::rainbow_hcl(nrow(new.wide3))
new.wide3t <- t(new.wide3)
new.wide3t <- new.wide3t[-1,]
library(pheatmap)
str(new.wide3t)

##  chr [1:8, 1:4] "419.0000" " 745.7000" " 869.5000" "1227.800" " 724
.5000" ...
##  - attr(*, "dimnames")=List of 2
##   ..$ : chr [1:8] "cDC1 | PE-Cy5-A :: PDL1)" "cDC2 | PE-Cy5-A :: PD
L1)" "DC3 | PE-Cy5-A :: PDL1)" "mo int | PE-Cy5-A :: PDL1)" ...
##   ..$ : chr [1:4] "v0" "v1" "v2" "v3"

mode(new.wide3t) = "numeric"
newer.wide <- t(new.wide3t)


pdf("YF_Aurora_HeatmapPDL1_20210927.pdf", width=4, height=4.5)
pheatmap(newer.wide,  cluster_rows = FALSE, scale = "column",
         col = colorRampPalette(c("#f6eff7", "#67a9cf", "#016c59"))(50
))
```
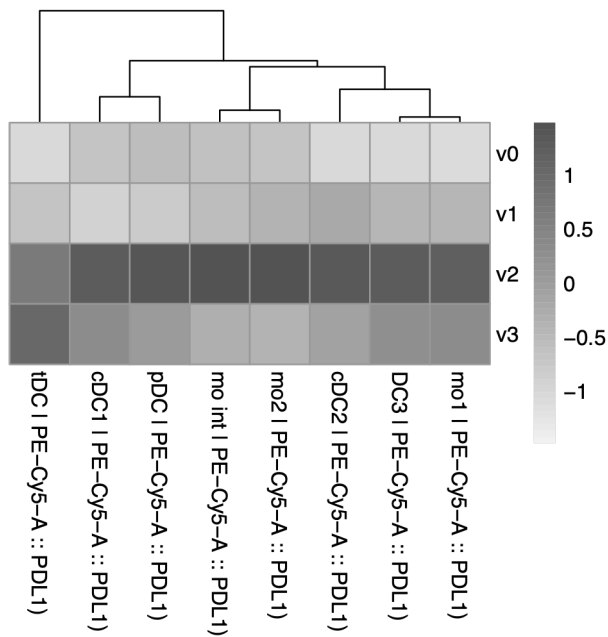
iv.   DC3 DESeq2 Analysis

Elena Winheim

10/8/2021

This is the markdown for DC3

```
library("readxl")
library("DESeq2")

library("pheatmap")
library("RColorBrewer")
library("DEGreport")
library("genefilter")

library("ggvenn")

library("prob")
```

First we are putting in the HT read counts for each sample that we are comparing

```
directory <- "/Users/Elena/RData/SeqRData"
sampleFiles <- list.files(directory)

#############################################################################
##
######### put in the excel table describing experimental setup########
#############################################################################
##
```

```
setwd("/Users/Elena/RData/SeqRData")
coldata_DC3 <- read_excel("Column_DC3.xlsx")
rownames(coldata_DC3) <- coldata_DC3$name # making new rownames

coldata_DC32 <-coldata_DC3[,-1]
rownames(coldata_DC32) <- coldata_DC3$name # making new rownames

## Warning: Setting row names on a tibble is deprecated.

##############################################################################
##
###################### put in the rest of the samples ##############
##
##############################################################################
##


args <- commandArgs(TRUE)
path <- as.character(args[1])
myoutname <-as.character(args[2])



##Read files names
files <- list.files(path="/Users/Elena/RData/SeqRData/DC3", pattern="*
.tabular")


print(files)

##  [1] "252_DC3_v0.tabular" "252_DC3_v1.tabular" "252_DC3_v3.tabular"
##  [4] "253_DC3_v0.tabular" "253_DC3_v1.tabular" "253_DC3_v2.tabular"
##  [7] "253_DC3_v3.tabular" "253_DC3_v4.tabular" "254_DC3_v0.tabular"
## [10] "254_DC3_v1.tabular" "254_DC3_v2.tabular" "254_DC3_v3.tabular"
## [13] "254_DC3_v4.tabular" "255_DC3_v0.tabular" "255_DC3_v1.tabular"
## [16] "255_DC3_v2.tabular" "255_DC3_v3.tabular" "255_DC3_v4.tabular"

##Read files names
files <- list.files(path="/Users/Elena/RData/SeqRData/DC3", pattern="*
.tabular")


print(files)

##  [1] "252_DC3_v0.tabular" "252_DC3_v1.tabular" "252_DC3_v3.tabular"
##  [4] "253_DC3_v0.tabular" "253_DC3_v1.tabular" "253_DC3_v2.tabular"
##  [7] "253_DC3_v3.tabular" "253_DC3_v4.tabular" "254_DC3_v0.tabular"
## [10] "254_DC3_v1.tabular" "254_DC3_v2.tabular" "254_DC3_v3.tabular"
## [13] "254_DC3_v4.tabular" "255_DC3_v0.tabular" "255_DC3_v1.tabular"
## [16] "255_DC3_v2.tabular" "255_DC3_v3.tabular" "255_DC3_v4.tabular"
```

```
##############################################################################
# trimm file extension########
##############################################################################

labs <- paste("", gsub("\\.tabular", "", files, perl=TRUE), sep="")

 ##############################################################################
####################
##Load all files
##############################################################################
##################
print(sprintf("######### START ######### %s", format(Sys.time(),"%b_%d
_%Y_%H_%M_%S_%Z")))

## [1] "######### START ######### Okt_18_2021_11_15_39_CEST"

cov <- list()
for (i in labs) {
filepath <- file.path("/Users/Elena/RData/SeqRData/DC3",paste(i,".tabu
lar",sep=""))
cov[[i]] <- read.table(filepath,sep = "\t", header=F, stringsAsFactors
=FALSE)
colnames(cov[[i]]) <- c("ENSEMBL_GeneID", i)
}
print(sprintf("######### END ######### %s", format(Sys.time(),"%b_%d_%
Y_%H_%M_%S_%Z")))

## [1] "######### END ######### Okt_18_2021_11_15_39_CEST"

 ##############################################################################
###
## construct one data frame from list of data.frames using reduce func
tion
##############################################################################
##

print(sprintf("######### merge ######### %s",
format(Sys.time(),"%b_%d_%Y_%H_%M_%S_%Z")))

## [1] "######### merge ######### Okt_18_2021_11_15_39_CEST"

df_DC3 <-Reduce(function(x,y) merge(x = x, y = y, by ="ENSEMBL_GeneID"
), cov)
print(sprintf("######### merge END ######### %s", format(Sys.time(),"%
b_%d_%Y_%H_%M_%S_%Z")))

## [1] "######### merge END ######### Okt_18_2021_11_15_41_CEST"

print(sprintf("Exported merged table within work directory in txt and
Rdata format with file name merged_%s_%s", make.names(format(Sys.time(
),"%b_%d_%Y_%H_%M_%S_%Z")), myoutname))

## [1] "Exported merged table within work directory in txt and Rdata f
ormat with file name merged_Okt_18_2021_11_15_41_CEST_NA"
```

157

```
write.table(df_DC3,paste(path, myoutname,".txt",sep=""), sep="\t", quo
te= F, row.names = F)

###########################################################################
###################
#########remove first five columns from df_DC3 since it is summary fro
m htSeq########
###########################################################################
##################

df_DC3 <- df_DC3[-c(1:5),]
head(df_DC3)

##      ENSEMBL_GeneID 252_DC3_v0 252_DC3_v1 252_DC3_v3 253_DC3_v0 253_D
C3_v1
## 6              A1BG          8         20         17         15
24
## 7          A1BG-AS1          0         15         42         38
41
## 8              A1CF          0          0          0          0
0
## 9               A2M          0          8         10          1
0
## 10          A2M-AS1          1         14         54         20
6
## 11            A2ML1          3          0          0          1
0
##      253_DC3_v2 253_DC3_v3 253_DC3_v4 254_DC3_v0 254_DC3_v1 254_DC3_v
2 254_DC3_v3
## 6            21         44         39         59         47          2
2         13
## 7            29         31         92         39         65          1
9         44
## 8             0          0          0          0          0
0          0
## 9             3         93         13          8          2
1         14
## 10           13          8         15         22         17          1
7         20
## 11            0          0          0          0          0
6          0
##      254_DC3_v4 255_DC3_v0 255_DC3_v1 255_DC3_v2 255_DC3_v3 255_DC3_v
4
## 6            28         25         29         22         26          3
0
## 7            21         23         36         48         21          2
6
## 8             0          0          0          0          0
0
## 9             7         55          3          3          1
8
## 10           22         12         20         12         11
```

```
8
## 11            0          0          0          0          0
0
```

```
##############################################################################
##########
# i need to remove the ensembl gene ID column and make it into row nam
e########
##############################################################################
##########
df_DC32 <-df_DC3[,-1]
rownames(df_DC32) <- df_DC3$ENSEMBL_GeneID # making new rownames
```

Filtering

```
nrow(df_DC32 )
```

```
## [1] 33121
```

```
keep <- rowSums(df_DC32) >= 50
df_DC32  <- df_DC32[keep,]
nrow( df_DC32 )
```

```
## [1] 13138
```

```
dds_DC32 <- DESeqDataSetFromMatrix ( countData = df_DC32,colData = col
data_DC32, design = ~ time + patient)
```

```
dds_DC3 = DESeq(dds_DC32, test = "LRT", reduced = ~  patient)
```

```
##############################################################################
##########
#####################running DESeq2 reduced formulas################
#############
##############################################################################
##########
vsd_DC3_time <- vst(dds_DC3_time)
```

```
resultsNames(dds_DC3)
```

```
## [1] "Intercept"            "time_v1_vs_v0"          "time_v2_vs_v
0"
## [4] "time_v3_vs_v0"        "time_v4_vs_v0"          "patient_pt25
3_vs_pt252"
## [7] "patient_pt254_vs_pt252" "patient_pt255_vs_pt252"
```

```
vsd_DC3 <- vst(dds_DC3)
```

filtering

```
pcaData <- plotPCA(vsd_DC3, intgroup = c("time", "patient"), returnDat
a = TRUE)
pcaData
```

159

```
##                       PC1          PC2      group time patient        name
## 252_DC3_v0 -0.7724672 20.3643447 v0:pt252   v0   pt252 252_DC3_v0
## 252_DC3_v1 -2.3676216  6.4294291 v1:pt252   v1   pt252 252_DC3_v1
## 252_DC3_v3 -6.5261386 -0.3951017 v3:pt252   v3   pt252 252_DC3_v3
## 253_DC3_v0 -2.6943056  4.0045300 v0:pt253   v0   pt253 253_DC3_v0
## 253_DC3_v1 -3.9919436 -1.9511554 v1:pt253   v1   pt253 253_DC3_v1
## 253_DC3_v2 19.9846616 -3.6652224 v2:pt253   v2   pt253 253_DC3_v2
## 253_DC3_v3 -7.0976715 -6.0431628 v3:pt253   v3   pt253 253_DC3_v3
## 253_DC3_v4 -7.2405928 -5.3529134 v4:pt253   v4   pt253 253_DC3_v4
## 254_DC3_v0 -6.4332450  1.9210470 v0:pt254   v0   pt254 254_DC3_v0
## 254_DC3_v1 -3.3581790 -8.9562697 v1:pt254   v1   pt254 254_DC3_v1
## 254_DC3_v2 20.0959318 -6.4122027 v2:pt254   v2   pt254 254_DC3_v2
## 254_DC3_v3 -7.0453162 -6.6185431 v3:pt254   v3   pt254 254_DC3_v3
## 254_DC3_v4 -8.1156657 -6.5412245 v4:pt254   v4   pt254 254_DC3_v4
## 255_DC3_v0 -2.6491467 15.3751867 v0:pt255   v0   pt255 255_DC3_v0
## 255_DC3_v1  9.3346343  4.1750613 v1:pt255   v1   pt255 255_DC3_v1
## 255_DC3_v2 18.6466682 -0.1430842 v2:pt255   v2   pt255 255_DC3_v2
## 255_DC3_v3 -6.0719915 -6.7105362 v3:pt255   v3   pt255 255_DC3_v3
## 255_DC3_v4 -3.6976109  0.5198174 v4:pt255   v4   pt255 255_DC3_v4
```

```
percentVar <- round(100 * attr(pcaData, "percentVar"))
'
setwd(("~/RData/SeqRData/Results/DC3"))
pdf("Seq_DC3_PCA.pdf", width=6, height=5)'

## [1] "\nsetwd((\"~/RData/SeqRData/Results/DC3\"))\npdf(\"Seq_DC3_PCA
.pdf\", width=6, height=5)"

ggplot(pcaData, aes(x = PC1, y = PC2, color = patient, shape = time))
+
  geom_point(size =3) +
  xlab(paste0("PC1: ", percentVar[1], "% variance")) +
  ylab(paste0("PC2: ", percentVar[2], "% variance")) +
  coord_fixed() +
  ggtitle("PCA with VST data")+
          theme_classic()+
  scale_color_manual(values=c("#006837",  "#41ab5d" ,"#4eb3d3", "#0840
81"))+
  scale_shape_manual(values = c(0, 2, 16, 17, 15))
```


PCA with VST data
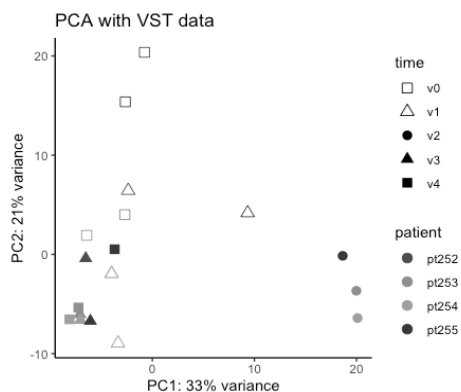
```
res_DC3 <- results(dds_DC3, alpha=0.05)
```

MA plot to check distribution

```
res_DC3_shrink <- lfcShrink(dds_DC3, alpha = 0.05, coef=2, type ="ashr
")
```

```
## using 'ashr' for LFC shrinkage. If used in published research, plea
se cite:
##     Stephens, M. (2016) False discovery rates: a new deal. Biostati
stics, 18:2.
##     https://doi.org/10.1093/biostatistics/kxw041
```

```
'res_DC3_shrink'
```

```
## [1] "res_DC3_shrink"
```

```
'setwd(("~/RData/SeqRData/Results/DC3"))
pdf("Seq_DC3_MA.pdf", width=4, height=4)'
```

```
## [1] "setwd((\"~/RData/SeqRData/Results/DC3\"))\npdf(\"Seq_DC3_MA.pd
f\", width=4, height=4)"
```

```
plotMA(res_DC3_shrink, ylim=c(-3,3))
```
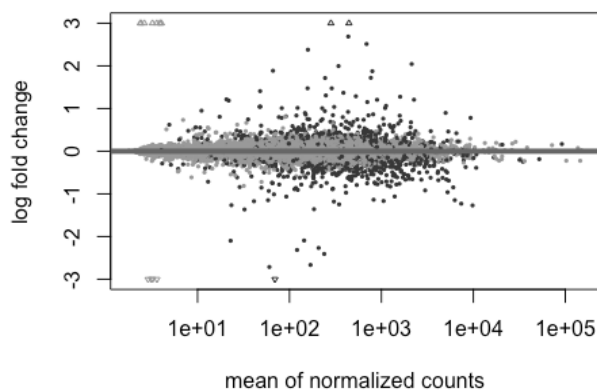


```
resSig_DC3 <- subset(res_DC3, res_DC3$pvalue< 0.05)
'resSig_DC3'
```

```
## [1] "resSig_DC3"
```

```
write.csv(resSig_DC3, "resSig_DC3.csv", quote=F)
topGene_DC3 <- rownames(res_DC3)[which.min(res_DC3$padj)]
write.csv(topGene_DC3, "topgenes_DC3.csv", quote=F)
```

```
res_DC3 = results(dds_DC3, alpha= 0.05)
summary(res_DC3)
```

MA plots

```
res_DC3_v0v1_shrink <-  lfcShrink(dds_DC3, contrast=c("time", "v1", "v
0"), alpha = 0.05, type ="ashr")
```

```
'setwd(("~/RData/SeqRData/Results/DC3"))
pdf("Seq_DC3_MA_v0v1.pdf", width=4, height=4)'
```

```
## [1] "setwd((\"~/RData/SeqRData/Results/DC3\"))\npdf(\"Seq_DC3_MA_v0
v1.pdf\", width=4, height=4)"
```

```
plotMA(res_DC3_v0v1_shrink, ylim=c(-2,2))
```
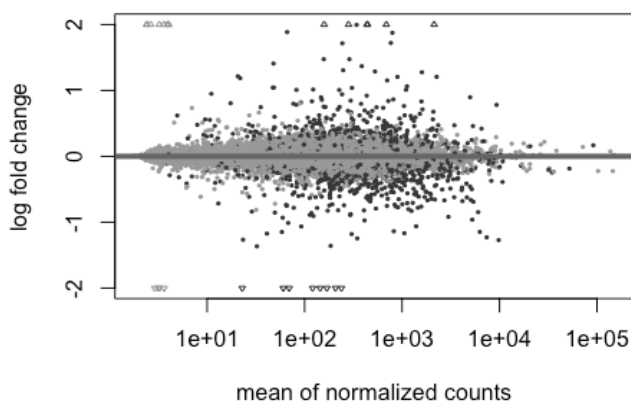

FDR correction: [237]

save res_sig

```
setwd(("~/RData/SeqRData/Results/DC3"))
resSig_DC3 <- subset(res_DC3, res_DC3$pvalue< 0.05)
write.csv(resSig_DC3, "resSig_DC3.csv", quote=F)

resSig_DC3_v0v1 <- subset(res_DC3_v0v1, res_DC3_v0v1$pvalue< 0.05)
write.csv(resSig_DC3_v0v1, "resSig_DC3_v0v1.csv", quote=F)

resSig_DC3_v0v2 <- subset(res_DC3_v0v2, res_DC3_v0v2$pvalue< 0.05)
write.csv(resSig_DC3_v0v2, "resSig_DC3_v0v2.csv", quote=F)


resSig_DC3_v0v3 <- subset(res_DC3_v0v3, res_DC3_v0v3$pvalue< 0.05)
write.csv(resSig_DC3_v0v3, "resSig_DC3_v0v3.csv", quote=F)


resSig_DC3_v0v4 <- subset(res_DC3_v0v4, res_DC3_v0v4$pvalue< 0.05)
write.csv(resSig_DC3_v0v4, "resSig_DC3_v0v4.csv", quote=F)
```

Top Genes and DEG report

```
'
setwd(("~/RData/SeqRData/Results/DC3"))'
```

Appendix

```
## [1] "\nsetwd((\"~/RData/SeqRData/Results/DC3\"))"

'pdf("Seq_DC3_Top25.pdf", width=8, height=4)'

## [1] "pdf(\"Seq_DC3_Top25.pdf\", width=8, height=4)"

DEGreport::degPlot(dds = dds_DC3, res = res_DC3, n = 25, xs = "time",
group = "patient") # dds object is output from DESeq2
```
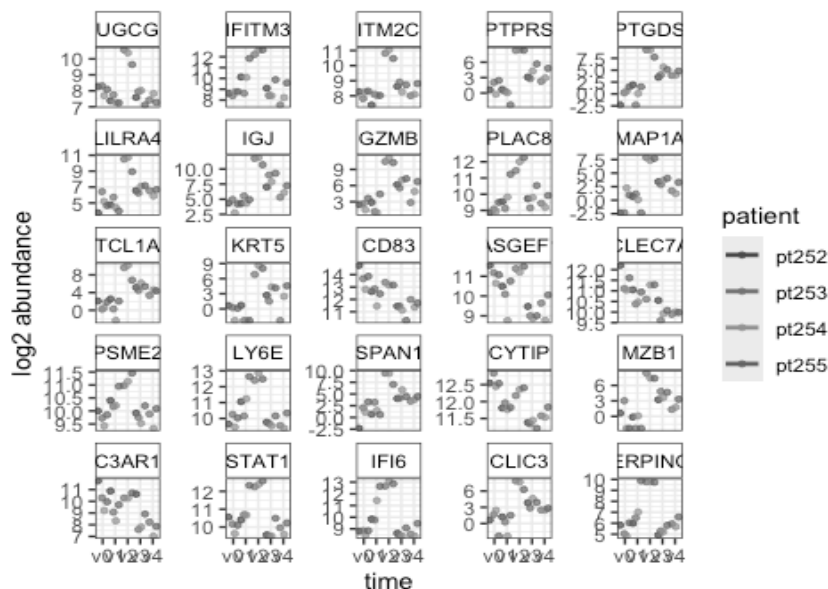


```
dev.off()

## null device
##              1

'setwd(("~/RData/SeqRData/Results/DC3"))
pdf("Seq_DC3_top25_v0_v4.pdf", width=8, height=4)'

resreport <- degResults(dds = dds_DC3, name = "test", org = NULL,
                        do_go = FALSE, group = "patient", xs = "time",
                        path_results = NULL)
```

v.   Signature heatmaps

```
Elena Winheim
10/4/2021
IFNSigbig <- c("ATF3",  "CXCL10", "DDX58", "DDX60",
"DHX58", "EIF2AK2", "HERC5", "IFI27", "IFIH1", "IFIT1",
"IFIT2", "IFIT3", "IRF7", "LAMP3", "MX2", "OAS1", "OAS3",
"OASL", "PARP9", "PLSCR1", "PML", "RSAD2", "SERPING1",
"SP100", "TAP1")
vsd_Full <- vsd_full[,
order(vsd_full$time,vsd_full$population)]

mat  <- assay(vsd_Full)
```
163

```
mat  <- mat - rowMeans(mat)
anno <- as.data.frame(colData(vsd_Full)[,
c("time","patient")])
ha_Full = HeatmapAnnotation(time= vsd_Full$time, col =
list(time = c("v0" = "#006837", "v1" = "#78c679", "v2" =
"#045a8d", "v3" = "#74a9cf", "v4"  = "#d0d1e6"),  patient
= c("pt252" = "#ffffcc", "pt253" = "#7fcdbb", "pt254" =
"#2c7fb8", "pt255" = "#253494"), population= c( "cDC1" =
"#2b8cbe", "cDC2" = "#084081", "DC3" = "#f768a1", "tDC" =
"#74c476", "pDC" = "#006837", "mo1" = "#a50f15", "moint" =
"#d94801", "mo2" = "#fd8d3c", "B" = "#6a51a3", "PBMC" =
"#000000")),
                        patient = vsd_Full$patient,
population=vsd_Full$population, population=  anno_block(
labels = c("d0", "d3", "d7", "d14", "d28")))

pdf("Seq_pDC_Heatmap_IFN_signature_KMeans.pdf", width = 40,
height=7)
library(ComplexHeatmap)
Heatmap((mat[ IFNSigbig, ]),cluster_columns = FALSE,
top_annotation=ha_Full, column_km = 5)
```

vi.   RCis Target

```
if (!requireNamespace("BiocManager", quietly=TRUE))
    install.packages("BiocManager")
# To support paralell execution:
BiocManager::install(c("doMC", "doRNG"))
# For the examples in the follow-up section of the tutorial:
BiocManager::install(c("DT", "visNetwork"))
BiocManager::install("RcisTarget")
####### input of data
geneSet1 <- rownames(Kmeans_Dc31)
library("RcisTarget")
geneLists <- list(geneSetName=c(Kmeans_Dc310_row))

featherURL <-
"https://resources.aertslab.org/cistarget/databases/homo_sapiens/hg19/
refseq_r45/mc9nr/gene_based/hg19-tss-centered-10kb-
7species.mc9nr.feather"

motifRankings <- importRankings("hg19-tss-centered-10kb-
7species.mc9nr.feather")
# Load the annotation to human transcription factors
data(motifAnnotations_hgnc)
motifRankings
data(motifAnnotations_hgnc)
motifAnnotations_hgnc[199:202,]
motifs_AUC <- calcAUC(geneLists, motifRankings)
```

164

```
motifAnnotations_hgnc'
# 2. Select significant motifs, add TF annotation & format as table
'motifEnrichmentTable <- addMotifAnnotation(motifs_AUC,
                          motifAnnot=motifAnnotations_hgnc)'

# 3. Identify significant genes for each motif
# (i.e. genes from the gene set in the top of the ranking)
# Note: Method 'iCisTarget' instead of 'aprox' is more accurate, but
slower
motifEnrichmentTable_wGenes <-
addSignificantGenes(motifEnrichmentTable,
                                        geneSets=geneLists,

rankings=motifRankings,

                                        nCores=1,
                                        method="aprox")
motifEnrichmentTable_wGenes <- cisTarget(geneLists,
        motifRankings,
        motifAnnot=motifAnnotations_hgnc)
motifEnrichmentTable_wGenes_wLogo <-
addLogo(motifEnrichmentTable_wGenes)
resultsSubset <- motifEnrichmentTable_wGenes_wLogo[1:50,]
library(DT)

dtable<- datatable(resultsSubset[,-c("enrichedGenes", "TF_lowConf"),
with=FALSE],
        escape = FALSE, # To show the logo
        filter="top", options=list(pageLength=5))
html_test <- "RCIS_DC3_cluster10.html"
```

vii. GSEA analysis

```
if (!requireNamespace("BiocManager", quietly=TRUE))
    install.packages("BiocManager")
# To support paralell execution:
BiocManager::install(c("doMC", "doRNG"))
# For the examples in the follow-up section of the tutorial:
BiocManager::install(c("DT", "visNetwork"))
BiocManager::install("RcisTarget")


mcols(res.dds, use.names = TRUE) #this is important for results inter-
pretation

res.dds
rownames(res.dds)

res.dds$Gene_Name <- row.names(res.dds)                        # Apply
row.names function
res.dds
library("AnnotationDbi")
library("org.Hs.eg.db")
library(data.table)
res.dds$ENSEMBL = mapIds(org.Hs.eg.db,
                    keys=row.names(res.dds),
                    column="ENSEMBL",
                    keytype="SYMBOL",
                    multiVals="first")
```

165

```
RNK2 = data.table(ENSEMBL_ID = res.dds$ENSEMBL, stat = res.dds$stat)
#These are 2 columns from our deseq2 output that we need for GSEA
RNK

RNK2 = subset(RNK2, stat != "NA")
head(RNK)
RNK2
write.table(RNK2, "RNK_DESeq2_DC3_v0v4.rnk",quote=F,sep="\t",
row.names = F)
```

viii.   PCA analysis

```
#install.packages("readxl")
library("readxl")
setwd("~/RData")
PCA_geld <- read_excel("Geldmacher_New_PCA.xlsx")
str(PCA_geld)
PCA of only COVID data
PCAGeld <- prcomp(PCA_geld[,c(11:56)], center = TRUE,scale. =
TRUE)
#install.packages("remotes")
#remotes::install_github("vqv/ggbiplot")
library(ggbiplot)
g <- ggbiplot(PCAGeld,choices=c(1,3), var.axes=FALSE, groups =
PCA_geld$DaysSymptoms, x= "PC1", y= "PC2")+
  scale_color_manual(values = c("#02818a","#3690c0",
"#67a9cf","#a6bddb", "#d0d1e6", "#ece2f0", "#f6eff7", "#fc8d59",
"#014636"))+ #your colors here
   theme_classic()

Rot_cov <- PCAGeld$rotation

pdf("Geldmacher_PCACOVID.pdf", width=6, height=3)
print(g)
```
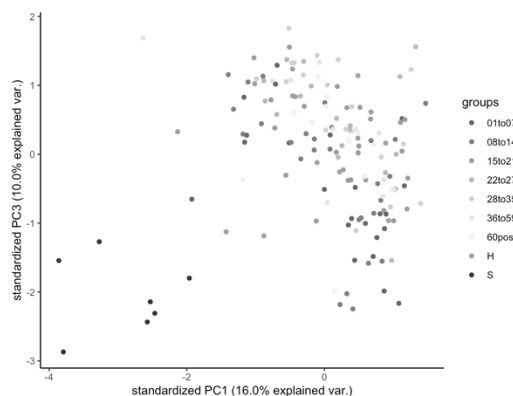
ix.   Venn diagram

Elena Winheim

10/24/2021

```
library(ggvenn)

DEgenes_DC3 <-rownames(resSig_DC3_time_v0v2)
DEgenes_cDC2 <- rownames(resSig_cDC2_time_v0v2)
DEgenes_mo1 <- rownames(resSig_mo1_time_v0v2)

x = list(DC3 = DEgenes_DC3,
         cDC2 = DEgenes_cDC2,
         mo1= DEgenes_mo1)

ggvenn(
  x,
  fill_color = c("#ca0020", "#92c5de", "#f4a582", "#0571b0"),
  stroke_size = 0.5, set_name_size = 4
  )
```
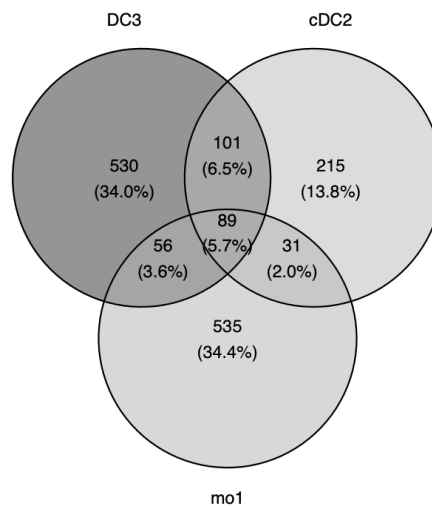
IX. References

1. Nussenzweig, M.C., R.M. Steinman, B. Gutchinov, and Z.A. Cohn, *Dendritic cells are accessory cells for the development of anti-trinitrophenyl cytotoxic T lymphocytes.* J Exp Med, 1980. **152**(4): p. 1070-84.

2. Van Voorhis, W.C., L.S. Hair, R.M. Steinman, and G. Kaplan, *Human dendritic cells. Enrichment and characterization from peripheral blood.* J Exp Med, 1982. **155**(4): p. 1172-87.

3. Steinman, R.M. and Z.A. Cohn, *Identification of a novel cell type in peripheral lymphoid organs of mice. I. Morphology, quantitation, tissue distribution.* J Exp Med, 1973. **137**(5): p. 1142-62.

4. MacDonald, K.P., D.J. Munster, G.J. Clark, A. Dzionek, J. Schmitz, and D.N. Hart, *Characterization of human blood dendritic cell subsets.* Blood, 2002. **100**(13): p. 4512-20.

5. Dzionek, A., A. Fuchs, P. Schmidt, S. Cremer, M. Zysk, S. Miltenyi, D.W. Buck, and J. Schmitz, *BDCA-2, BDCA-3, and BDCA-4: three markers for distinct subsets of dendritic cells in human peripheral blood.* J Immunol, 2000. **165**(11): p. 6037-46.

6. Haniffa, M., A. Shin, V. Bigley, N. McGovern, P. Teo, P. See, P.S. Wasan, X.N. Wang, F. Malinarich, B. Malleret, A. Larbi, P. Tan, H. Zhao, M. Poidinger, S. Pagan, S. Cookson, R. Dickinson, I. Dimmick, R.F. Jarrett, L. Renia, J. Tam, C. Song, J. Connolly, J.K. Chan, A. Gehring, A. Bertoletti, M. Collin, and F. Ginhoux, *Human tissues contain CD141hi cross-presenting dendritic cells with functional homology to mouse CD103+ nonlymphoid dendritic cells.* Immunity, 2012. **37**(1): p. 60-73.

7. Jongbloed, S.L., A.J. Kassianos, K.J. McDonald, G.J. Clark, X. Ju, C.E. Angel, C.J. Chen, P.R. Dunbar, R.B. Wadley, V. Jeet, A.J. Vulink, D.N. Hart, and K.J. Radford, *Human CD141+ (BDCA-3)+ dendritic cells (DCs) represent a unique myeloid DC subset that cross-presents necrotic cell antigens.* J Exp Med, 2010. **207**(6): p. 1247-60.

8. Crozat, K., R. Guiton, V. Contreras, V. Feuillet, C.A. Dutertre, E. Ventre, T.P. Vu Manh, T. Baranek, A.K. Storset, J. Marvel, P. Boudinot, A. Hosmalin, I. Schwartz-Cornil, and M. Dalod, *The XC chemokine receptor 1 is a conserved selective marker of mammalian cells homologous to mouse CD8alpha+ dendritic cells.* J Exp Med, 2010. **207**(6): p. 1283-92.

9. Ziegler-Heitbrock, L., P. Ancuta, S. Crowe, M. Dalod, V. Grau, D.N. Hart, P.J. Leenen, Y.J. Liu, G. MacPherson, G.J. Randolph, J. Scherberich, J. Schmitz, K. Shortman, S. Sozzani, H. Strobl, M. Zembala, J.M. Austyn, and M.B. Lutz, *Nomenclature of monocytes and dendritic cells in blood.* Blood, 2010. **116**(16): p. e74-80.

10. Nestle, F.O., X.G. Zheng, C.B. Thompson, L.A. Turka, and B.J. Nickoloff, *Characterization of dermal dendritic cells obtained from normal human skin reveals phenotypic and functionally distinctive subsets.* The Journal of Immunology, 1993. **151**(11): p. 6535-6545.

11. De Monte, A., C.-V. Olivieri, S. Vitale, S. Bailleux, L. Castillo, V. Giordanengo, J.L. Maryanski, E. Segura, and A. Doglio, *CD1c-Related DCs that Express CD207/Langerin,*
168

but Are Distinguishable from Langerhans Cells, Are Consistently Present in Human Tonsils. Frontiers in Immunology, 2016. **7**: p. 197.

12. Bigley, V., N. McGovern, P. Milne, R. Dickinson, S. Pagan, S. Cookson, M. Haniffa, and M. Collin, *Langerin-expressing dendritic cells in human tissues are related to CD1c+ dendritic cells and distinct from Langerhans cells and CD141high XCR1+ dendritic cells.* J Leukoc Biol, 2015. **97**(4): p. 627-34.

13. Sittig, S.P., G. Bakdash, J. Weiden, A.E. Sköld, J. Tel, C.G. Figdor, I.J.M. de Vries, and G. Schreibelt, *A Comparative Study of the T Cell Stimulatory and Polarizing Capacity of Human Primary Blood Dendritic Cell Subsets.* Mediators of Inflammation, 2016. **2016**: p. e3605643.

14. Yin, X., H. Yu, X. Jin, J. Li, H. Guo, Q. Shi, Z. Yin, Y. Xu, X. Wang, R. Liu, S. Wang, and L. Zhang, *Human Blood CD1c+ Dendritic Cells Encompass CD5high and CD5low Subsets That Differ Significantly in Phenotype, Gene Expression, and Functions.* The Journal of Immunology, 2017. **198**(4): p. 1553-1564.

15. Dutertre, C.A., E. Becht, S.E. Irac, A. Khalilnezhad, V. Narang, S. Khalilnezhad, P.Y. Ng, L.L. van den Hoogen, J.Y. Leong, B. Lee, M. Chevrier, X.M. Zhang, P.J.A. Yong, G. Koh, J. Lum, S.W. Howland, E. Mok, J. Chen, A. Larbi, H.K.K. Tan, T.K.H. Lim, P. Karagianni, A.G. Tzioufas, B. Malleret, J. Brody, S. Albani, J. van Roon, T. Radstake, E.W. Newell, and F. Ginhoux, *Single-Cell Analysis of Human Mononuclear Phagocytes Reveals Subset-Defining Markers and Identifies Circulating Inflammatory Dendritic Cells.* Immunity, 2019. **51**(3): p. 573-589 e8.

16. Villani, A.C., R. Satija, G. Reynolds, S. Sarkizova, K. Shekhar, J. Fletcher, M. Griesbeck, A. Butler, S. Zheng, S. Lazo, L. Jardine, D. Dixon, E. Stephenson, E. Nilsson, I. Grundberg, D. McDonald, A. Filby, W. Li, P.L. De Jager, O. Rozenblatt-Rosen, A.A. Lane, M. Haniffa, A. Regev, and N. Hacohen, *Single-cell RNA-seq reveals new types of human blood dendritic cells, monocytes, and progenitors.* Science, 2017. **356**(6335).

17. Cytlak, U., A. Resteu, S. Pagan, K. Green, P. Milne, S. Maisuria, D. McDonald, G. Hulme, A. Filby, B. Carpenter, R. Queen, S. Hambleton, R. Hague, H. Lango Allen, J.E.D. Thaventhiran, G. Doody, M. Collin, and V. Bigley, *Differential IRF8 Transcription Factor Requirement Defines Two Pathways of Dendritic Cell Development in Humans.* Immunity, 2020. **53**(2): p. 353-370 e8.

18. Bourdely, P., G. Anselmi, K. Vaivode, R.N. Ramos, Y. Missolo-Koussou, S. Hidalgo, J. Tosselo, N. Nunez, W. Richer, A. Vincent-Salomon, A. Saxena, K. Wood, A. Lladser, E. Piaggio, J. Helft, and P. Guermonprez, *Transcriptional and Functional Analysis of CD1c+ Human Dendritic Cells Identifies a CD163+ Subset Priming CD8+CD103+ T Cells.* Immunity, 2020. **53**(2): p. 335-352 e8.

19. Lennert, K. and W. Remmele, *Karyometric research on lymph node cells in man. I. Germinoblasts, lymphoblasts & lymphocytes.* Acta Haematol, 1958. **19**(2): p. 99-113.

20. Dress, R.J., C.A. Dutertre, A. Giladi, A. Schlitzer, I. Low, N.B. Shadan, A. Tay, J. Lum, M. Kairi, Y.Y. Hwang, E. Becht, Y. Cheng, M. Chevrier, A. Larbi, E.W. Newell, I. Amit, J. Chen, and F. Ginhoux, *Plasmacytoid dendritic cells develop from Ly6D+ lymphoid progenitors distinct from the myeloid lineage.* Nat Immunol, 2019. **20**(7): p. 852-864.

21. Siegal, F.P., N. Kadowaki, M. Shodell, P.A. Fitzgerald-Bocarsly, K. Shah, S. Ho, S. Antonenko, and Y.J. Liu, *The nature of the principal type 1 interferon-producing cells in human blood.* Science, 1999. **284**(5421): p. 1835-7.

22. Cella, M., D. Jarrossay, F. Facchetti, O. Alebardi, H. Nakajima, A. Lanzavecchia, and M. Colonna, *Plasmacytoid monocytes migrate to inflamed lymph nodes and produce large amounts of type I interferon.* Nat Med, 1999. **5**(8): p. 919-23.

23. Perussia, B., V. Fanning, and G. Trinchieri, *A leukocyte subset bearing HLA-DR antigens is responsible for in vitro alpha interferon production in response to viruses.* Nat Immun Cell Growth Regul, 1985. **4**(3): p. 120-37.

24. Santini, S.M., C. Lapenta, M. Logozzi, S. Parlato, M. Spada, T. Di Pucchio, and F. Belardelli, *Type I interferon as a powerful adjuvant for monocyte-derived dendritic cell development and activity in vitro and in Hu-PBL-SCID mice.* J Exp Med, 2000. **191**(10): p. 1777-88.

25. Krug, A., A.R. French, W. Barchet, J.A. Fischer, A. Dzionek, J.T. Pingel, M.M. Orihuela, S. Akira, W.M. Yokoyama, and M. Colonna, *TLR9-dependent recognition of MCMV by IPC and DC generates coordinated cytokine responses that activate antiviral NK cell function.* Immunity, 2004. **21**(1): p. 107-19.

26. Kadowaki, N., S. Ho, S. Antonenko, R.W. Malefyt, R.A. Kastelein, F. Bazan, and Y.J. Liu, *Subsets of human dendritic cell precursors express different toll-like receptors and respond to different microbial antigens.* J Exp Med, 2001. **194**(6): p. 863-9.

27. Jarrossay, D., G. Napolitani, M. Colonna, F. Sallusto, and A. Lanzavecchia, *Specialization and complementarity in microbial molecule recognition by human myeloid and plasmacytoid dendritic cells.* Eur J Immunol, 2001. **31**(11): p. 3388-93.

28. Tel, J., G. Schreibelt, S.P. Sittig, T.S. Mathan, S.I. Buschow, L.J. Cruz, A.J. Lambeck, C.G. Figdor, and I.J. de Vries, *Human plasmacytoid dendritic cells efficiently cross-present exogenous Ags to CD8+ T cells despite lower Ag uptake than myeloid dendritic cell subsets.* Blood, 2013. **121**(3): p. 459-67.

29. Cella, M., F. Facchetti, A. Lanzavecchia, and M. Colonna, *Plasmacytoid dendritic cells activated by influenza virus and CD40L drive a potent TH1 polarization.* Nat Immunol, 2000. **1**(4): p. 305-10.

30. See, P., C.A. Dutertre, J. Chen, P. Gunther, N. McGovern, S.E. Irac, M. Gunawan, M. Beyer, K. Handler, K. Duan, H.R.B. Sumatoh, N. Ruffin, M. Jouve, E. Gea-Mallorqui, R.C.M. Hennekam, T. Lim, C.C. Yip, M. Wen, B. Malleret, I. Low, N.B. Shadan, C.F.S. Fen, A. Tay, J. Lum, F. Zolezzi, A. Larbi, M. Poidinger, J.K.Y. Chan, Q. Chen, L. Renia, M. Haniffa, P. Benaroch, A. Schlitzer, J.L. Schultze, E.W. Newell, and F. Ginhoux, *Mapping the human DC lineage through the integration of high-dimensional techniques.* Science, 2017. **356**(6342).

31. Alcantara-Hernandez, M., R. Leylek, L.E. Wagar, E.G. Engleman, T. Keler, M.P. Marinkovich, M.M. Davis, G.P. Nolan, and J. Idoyaga, *High-Dimensional Phenotypic Mapping of Human Dendritic Cells Reveals Interindividual Variation and Tissue Specialization.* Immunity, 2017. **47**(6): p. 1037-1050 e6.

32. Grouard, G., M.C. Rissoan, L. Filgueira, I. Durand, J. Banchereau, and Y.J. Liu, *The enigmatic plasmacytoid T cells develop into dendritic cells with interleukin (IL)-3 and CD40-ligand.* J Exp Med, 1997. **185**(6): p. 1101-11.

33. Alculumbre, S.G., V. Saint-Andre, J. Di Domizio, P. Vargas, P. Sirven, P. Bost, M. Maurin, P. Maiuri, M. Wery, M.S. Roman, L. Savey, M. Touzot, B. Terrier, D. Saadoun, C. Conrad, M. Gilliet, A. Morillon, and V. Soumelis, *Diversification of human plasmacytoid predendritic cells in response to a single stimulus.* Nat Immunol, 2018. **19**(1): p. 63-75.

34. Leylek, R., M. Alcantara-Hernandez, Z. Lanzar, A. Ludtke, O.A. Perez, B. Reizis, and J. Idoyaga, *Integrated Cross-Species Analysis Identifies a Conserved Transitional Dendritic Cell Population.* Cell Rep, 2019. **29**(11): p. 3736-3750 e8.

35. Abbas, A., T.P. Vu Manh, M. Valente, N. Collinet, N. Attaf, C. Dong, K. Naciri, R. Chelbi, G. Brelurut, I. Cervera-Marzal, B. Rauwel, J.L. Davignon, G. Bessou, M. Thomas-Chollier, D. Thieffry, A.C. Villani, P. Milpied, M. Dalod, and E. Tomasello, *The activation trajectory of plasmacytoid dendritic cells in vivo during a viral infection.* Nat Immunol, 2020. **21**(9): p. 983-997.

36. Rodrigues, P.F., L. Alberti-Servera, A. Eremin, G.E. Grajales-Reyes, R. Ivanek, and R. Tussiwand, *Distinct progenitor lineages contribute to the heterogeneity of plasmacytoid dendritic cells.* Nat Immunol, 2018. **19**(7): p. 711-722.

37. Bar-On, L., T. Birnberg, K.L. Lewis, B.T. Edelson, D. Bruder, K. Hildner, J. Buer, K.M. Murphy, B. Reizis, and S. Jung, *CX3CR1+ CD8alpha+ dendritic cells are a steady-state population related to plasmacytoid dendritic cells.* Proc Natl Acad Sci U S A, 2010. **107**(33): p. 14745-50.

38. Zhang, H., J.D. Gregorio, T. Iwahori, X. Zhang, O. Choi, L.L. Tolentino, T. Prestwood, Y. Carmi, and E.G. Engleman, *A distinct subset of plasmacytoid dendritic cells induces activation and differentiation of B and T lymphocytes.* Proc Natl Acad Sci U S A, 2017. **114**(8): p. 1988-1993.

39. Matsui, T., J.E. Connolly, M. Michnevitz, D. Chaussabel, C.I. Yu, C. Glaser, S. Tindle, M. Pypaert, H. Freitas, B. Piqueras, J. Banchereau, and A.K. Palucka, *CD2 distinguishes two subsets of human plasmacytoid dendritic cells with distinct phenotype and functions.* J Immunol, 2009. **182**(11): p. 6815-23.

40. Bryant, C., P.D. Fromm, F. Kupresanin, G. Clark, K. Lee, C. Clarke, P.A. Silveira, H. Suen, R. Brown, E. Newman, I. Cunningham, P.J. Ho, J. Gibson, K. Bradstock, D. Joshua, and D. Hart, *A CD2 high-expressing stress-resistant human plasmacytoid dendritic-cell subset.* Immunol Cell Biol, 2016. **94**(5): p. 447-57.

41. Izquierdo-Useros, N., M. Lorizate, M.C. Puertas, M.T. Rodriguez-Plata, N. Zangger, E. Erikson, M. Pino, I. Erkizia, B. Glass, B. Clotet, O.T. Keppler, A. Telenti, H.G. Krausslich, and J. Martinez-Picado, *Siglec-1 is a novel dendritic cell receptor that mediates HIV-1 trans-infection through recognition of viral membrane gangliosides.* PLoS Biol, 2012. **10**(12): p. e1001448.

42. Meertens, L., A. Labeau, O. Dejarnac, S. Cipriani, L. Sinigaglia, L. Bonnet-Madin, T. Le Charpentier, M.L. Hafirassou, A. Zamborlini, V.M. Cao-Lormeau, M. Coulpier, D.

Misse, N. Jouvenet, R. Tabibiazar, P. Gressens, O. Schwartz, and A. Amara, *Axl Mediates ZIKA Virus Entry in Human Glial Cells and Modulates Innate Immune Responses.* Cell Rep, 2017. **18**(2): p. 324-333.

43. Ruffin, N., E. Gea-Mallorqui, F. Brouiller, M. Jouve, A. Silvin, P. See, C.A. Dutertre, F. Ginhoux, and P. Benaroch, *Constitutive Siglec-1 expression confers susceptibility to HIV-1 infection of human dendritic cell precursors.* Proc Natl Acad Sci U S A, 2019. **116**(43): p. 21685-21693.

44. Kuziel, W.A., S.J. Morgan, T.C. Dawson, S. Griffin, O. Smithies, K. Ley, and N. Maeda, *Severe reduction in leukocyte adhesion and monocyte extravasation in mice deficient in CC chemokine receptor 2.* Proc Natl Acad Sci U S A, 1997. **94**(22): p. 12053-8.

45. Geissmann, F., S. Jung, and D.R. Littman, *Blood monocytes consist of two principal subsets with distinct migratory properties.* Immunity, 2003. **19**(1): p. 71-82.

46. Tsou, C.L., W. Peters, Y. Si, S. Slaymaker, A.M. Aslanian, S.P. Weisberg, M. Mack, and I.F. Charo, *Critical roles for CCR2 and MCP-3 in monocyte mobilization from bone marrow and recruitment to inflammatory sites.* J Clin Invest, 2007. **117**(4): p. 902-9.

47. Florey, H.W. and R.H. Ebert, *The Extravascular Development of the Monocyte Observed In vivo.* Br J Exp Pathol., 1939. **20**(4): p. 342–356.

48. Richter, L., O.J.B. Landsverk, N. Atlasy, A. Bujko, S. Yaqub, R. Horneland, O. Oyen, E.M. Aandahl, K.E.A. Lundin, H.G. Stunnenberg, E.S. Baekkevold, and F.L. Jahnsen, *Transcriptional profiling reveals monocyte-related macrophages phenotypically resembling DC in human intestine.* Mucosal Immunol, 2018. **11**(5): p. 1512-1523.

49. Wong, K.L., J.J. Tai, W.C. Wong, H. Han, X. Sem, W.H. Yeap, P. Kourilsky, and S.C. Wong, *Gene expression profiling reveals the defining features of the classical, intermediate, and nonclassical human monocyte subsets.* Blood, 2011. **118**(5): p. e16-31.

50. Boyette, L.B., C. Macedo, K. Hadi, B.D. Elinoff, J.T. Walters, B. Ramaswami, G. Chalasani, J.M. Taboas, F.G. Lakkis, and D.M. Metes, *Phenotype, function, and differentiation potential of human monocyte subsets.* PLoS One, 2017. **12**(4): p. e0176460.

51. Wong, K.L., W.H. Yeap, J.J. Tai, S.M. Ong, T.M. Dang, and S.C. Wong, *The three human monocyte subsets: implications for health and disease.* Immunol Res, 2012. **53**(1-3): p. 41-57.

52. Mukherjee, R., P. Kanti Barman, P. Kumar Thatoi, R. Tripathy, B. Kumar Das, and B. Ravindran, *Non-Classical monocytes display inflammatory features: Validation in Sepsis and Systemic Lupus Erythematous.* Sci Rep, 2015. **5**: p. 13886.

53. Balboa, L., J. Barrios-Payan, E. Gonzalez-Dominguez, C. Lastrucci, G. Lugo-Villarino, D. Mata-Espinoza, P. Schierloh, D. Kviatcovsky, O. Neyrolles, I. Maridonneau-Parini, C. Sanchez-Torres, C. Sasiain Mdel, and R. Hernandez-Pando, *Diverging biological roles among human monocyte subsets in the context of tuberculosis infection.* Clin Sci (Lond), 2015. **129**(4): p. 319-30.

54. Belge, K.U., F. Dayyani, A. Horelt, M. Siedlar, M. Frankenberger, B. Frankenberger, T. Espevik, and L. Ziegler-Heitbrock, *The proinflammatory CD14+CD16+DR++ monocytes are a major source of TNF.* J Immunol, 2002. **168**(7): p. 3536-42.

55. Fingerle, G., A. Pforte, B. Passlick, M. Blumenstein, M. Strobel, and H.W. Ziegler-Heitbrock, *The novel subset of CD14+/CD16+ blood monocytes is expanded in sepsis patients.* Blood, 1993. **82**(10): p. 3170-6.

56. Michlmayr, D., P. Andrade, K. Gonzalez, A. Balmaseda, and E. Harris, *CD14+ CD16+ monocytes are the main target of Zika virus infection in peripheral blood mononuclear cells in a paediatric study in Nicaragua.* Nat Microbiol, 2017. **2**(11): p. 1462-1470.

57. Auffray, C., D. Fogg, M. Garfa, G. Elain, O. Join-Lambert, S. Kayal, S. Sarnacki, A. Cumano, G. Lauvau, and F. Geissmann, *Monitoring of blood vessels and tissues by a population of monocytes with patrolling behavior.* Science, 2007. **317**(5838): p. 666-70.

58. Ancuta, P., R. Rao, A. Moses, A. Mehle, S.K. Shaw, F.W. Luscinskas, and D. Gabuzda, *Fractalkine preferentially mediates arrest and migration of CD16+ monocytes.* J Exp Med, 2003. **197**(12): p. 1701-7.

59. Cros, J., N. Cagnard, K. Woollard, N. Patey, S.Y. Zhang, B. Senechal, A. Puel, S.K. Biswas, D. Moshous, C. Picard, J.P. Jais, D. D'Cruz, J.L. Casanova, C. Trouillet, and F. Geissmann, *Human CD14dim monocytes patrol and sense nucleic acids and viruses via TLR7 and TLR8 receptors.* Immunity, 2010. **33**(3): p. 375-86.

60. Patel, A.A., Y. Zhang, J.N. Fullerton, L. Boelen, A. Rongvaux, A.A. Maini, V. Bigley, R.A. Flavell, D.W. Gilroy, B. Asquith, D. Macallan, and S. Yona, *The fate and lifespan of human monocyte subsets in steady state and systemic inflammation.* J Exp Med, 2017. **214**(7): p. 1913-1923.

61. Lee, J., G. Breton, T.Y. Oliveira, Y.J. Zhou, A. Aljoufi, S. Puhr, M.J. Cameron, R.P. Sekaly, M.C. Nussenzweig, and K. Liu, *Restricted dendritic cell and monocyte progenitors in human cord blood and bone marrow.* J Exp Med, 2015. **212**(3): p. 385-99.

62. Lee, J., G. Breton, A. Aljoufi, Y.J. Zhou, S. Puhr, M.C. Nussenzweig, and K. Liu, *Clonal analysis of human dendritic cell progenitor using a stromal cell culture.* J Immunol Methods, 2015. **425**: p. 21-26.

63. Liu, K., G.D. Victora, T.A. Schwickert, P. Guermonprez, M.M. Meredith, K. Yao, F.F. Chu, G.J. Randolph, A.Y. Rudensky, and M. Nussenzweig, *In vivo analysis of dendritic cell development and homeostasis.* Science, 2009. **324**(5925): p. 392-7.

64. Fogg, D.K., C. Sibon, C. Miled, S. Jung, P. Aucouturier, D.R. Littman, A. Cumano, and F. Geissmann, *A clonogenic bone marrow progenitor specific for macrophages and dendritic cells.* Science, 2006. **311**(5757): p. 83-7.

65. Breton, G., J. Lee, Y.J. Zhou, J.J. Schreiber, T. Keler, S. Puhr, N. Anandasabapathy, S. Schlesinger, M. Caskey, K. Liu, and M.C. Nussenzweig, *Circulating precursors of human CD1c+ and CD141+ dendritic cells.* J Exp Med, 2015. **212**(3): p. 401-13.

66. Breton, G., S. Zheng, R. Valieris, I. Tojal da Silva, R. Satija, and M.C. Nussenzweig, *Human dendritic cells (DCs) are derived from distinct circulating precursors that are*

precommitted to become CD1c+ or CD141+ DCs. J Exp Med, 2016. **213**(13): p. 2861-2870.

67. Hambleton, S., S. Salem, J. Bustamante, V. Bigley, S. Boisson-Dupuis, J. Azevedo, A. Fortin, M. Haniffa, L. Ceron-Gutierrez, C.M. Bacon, G. Menon, C. Trouillet, D. McDonald, P. Carey, F. Ginhoux, L. Alsina, T.J. Zumwalt, X.F. Kong, D. Kumararatne, K. Butler, M. Hubeau, J. Feinberg, S. Al-Muhsen, A. Cant, L. Abel, D. Chaussabel, R. Doffinger, E. Talesnik, A. Grumach, A. Duarte, K. Abarca, D. Moraes-Vasconcelos, D. Burk, A. Berghuis, F. Geissmann, M. Collin, J.L. Casanova, and P. Gros, *IRF8 mutations and human dendritic-cell immunodeficiency.* N Engl J Med, 2011. **365**(2): p. 127-38.

68. Schlitzer, A., N. McGovern, P. Teo, T. Zelante, K. Atarashi, D. Low, A.W. Ho, P. See, A. Shin, P.S. Wasan, G. Hoeffel, B. Malleret, A. Heiseke, S. Chew, L. Jardine, H.A. Purvis, C.M. Hilkens, J. Tam, M. Poidinger, E.R. Stanley, A.B. Krug, L. Renia, B. Sivasankar, L.G. Ng, M. Collin, P. Ricciardi-Castagnoli, K. Honda, M. Haniffa, and F. Ginhoux, *IRF4 transcription factor-dependent CD11b+ dendritic cells in human and mouse control mucosal IL-17 cytokine responses.* Immunity, 2013. **38**(5): p. 970-83.

69. Cisse, B., M.L. Caton, M. Lehner, T. Maeda, S. Scheu, R. Locksley, D. Holmberg, C. Zweier, N.S. den Hollander, S.G. Kant, W. Holter, A. Rauch, Y. Zhuang, and B. Reizis, *Transcription factor E2-2 is an essential and specific regulator of plasmacytoid dendritic cell development.* Cell, 2008. **135**(1): p. 37-48.

70. Villar, J. and E. Segura, *Decoding the Heterogeneity of Human Dendritic Cell Subsets.* Trends Immunol, 2020. **41**(12): p. 1062-1071.

71. Helft, J., F. Anjos-Afonso, A.G. van der Veen, P. Chakravarty, D. Bonnet, and C. Reis e Sousa, *Dendritic Cell Lineage Potential in Human Early Hematopoietic Progenitors.* Cell Rep, 2017. **20**(3): p. 529-537.

72. Doulatov, S., F. Notta, K. Eppert, L.T. Nguyen, P.S. Ohashi, and J.E. Dick, *Revised map of the human progenitor hierarchy shows the origin of macrophages and dendritic cells in early lymphoid development.* Nat Immunol, 2010. **11**(7): p. 585-93.

73. Iwabuchi, R., S. Ikeno, M. Kobayashi-Ishihara, H. Takeyama, M. Ato, Y. Tsunetsugu-Yokota, and K. Terahara, *Introduction of Human Flt3-L and GM-CSF into Humanized Mice Enhances the Reconstitution and Maturation of Myeloid Dendritic Cells and the Development of Foxp3+CD4+ T Cells.* Front Immunol, 2018. **9**: p. 1042.

74. Maraskovsky, E., E. Daro, E. Roux, M. Teepe, C.R. Maliszewski, J. Hoek, D. Caron, M.E. Lebsack, and H.J. McKenna, *In vivo generation of human dendritic cell subsets by Flt3 ligand.* Blood, 2000. **96**(3): p. 878-84.

75. Greter, M., J. Helft, A. Chow, D. Hashimoto, A. Mortha, J. Agudo-Cantero, M. Bogunovic, E.L. Gautier, J. Miller, M. Leboeuf, G. Lu, C. Aloman, B.D. Brown, J.W. Pollard, H. Xiong, G.J. Randolph, J.E. Chipuk, P.S. Frenette, and M. Merad, *GM-CSF controls nonlymphoid tissue dendritic cell homeostasis but is dispensable for the differentiation of inflammatory dendritic cells.* Immunity, 2012. **36**(6): p. 1031-46.

76. Hashimoto, D., A. Chow, C. Noizat, P. Teo, M.B. Beasley, M. Leboeuf, C.D. Becker, P. See, J. Price, D. Lucas, M. Greter, A. Mortha, S.W. Boyer, E.C. Forsberg, M. Tanaka, N. van Rooijen, A. Garcia-Sastre, E.R. Stanley, F. Ginhoux, P.S. Frenette, and M. Merad,

Tissue-resident macrophages self-maintain locally throughout adult life with minimal contribution from circulating monocytes. Immunity, 2013. **38**(4): p. 792-804.

77. Ginhoux, F., M. Greter, M. Leboeuf, S. Nandi, P. See, S. Gokhan, M.F. Mehler, S.J. Conway, L.G. Ng, E.R. Stanley, I.M. Samokhvalov, and M. Merad, *Fate mapping analysis reveals that adult microglia derive from primitive macrophages.* Science, 2010. **330**(6005): p. 841-5.

78. Ginhoux, F. and M. Guilliams, *Tissue-Resident Macrophage Ontogeny and Homeostasis.* Immunity, 2016. **44**(3): p. 439-449.

79. Sallusto, F. and A. Lanzavecchia, *Efficient presentation of soluble antigen by cultured human dendritic cells is maintained by granulocyte/macrophage colony-stimulating factor plus interleukin 4 and downregulated by tumor necrosis factor alpha.* J Exp Med, 1994. **179**(4): p. 1109-18.

80. Luft, T., M. Jefford, P. Luetjens, H. Hochrein, K.A. Masterman, C. Maliszewski, K. Shortman, J. Cebon, and E. Maraskovsky, *IL-1 beta enhances CD40 ligand-mediated cytokine secretion by human dendritic cells (DC): a mechanism for T cell-independent DC activation.* J Immunol, 2002. **168**(2): p. 713-22.

81. Rubio, M.T., T.K. Means, R. Chakraverty, J. Shaffer, Y. Fudaba, M. Chittenden, A.D. Luster, and M. Sykes, *Maturation of human monocyte-derived dendritic cells (MoDCs) in the presence of prostaglandin E2 optimizes CD4 and CD8 T cell-mediated responses to protein antigens: role of PGE2 in chemokine and cytokine expression by MoDCs.* Int Immunol, 2005. **17**(12): p. 1561-72.

82. Luo, X.L. and M. Dalod, *The quest for faithful in vitro models of human dendritic cells types.* Mol Immunol, 2020. **123**: p. 40-59.

83. Sander, J., S.V. Schmidt, B. Cirovic, N. McGovern, O. Papantonopoulou, A.L. Hardt, A.C. Aschenbrenner, C. Kreer, T. Quast, A.M. Xu, L.M. Schmidleithner, H. Theis, L.D. Thi Huong, H.R.B. Sumatoh, M.A.R. Lauterbach, J. Schulte-Schrepping, P. Gunther, J. Xue, K. Bassler, T. Ulas, K. Klee, N. Katzmarski, S. Herresthal, W. Krebs, B. Martin, E. Latz, K. Handler, M. Kraut, W. Kolanus, M. Beyer, C.S. Falk, B. Wiegmann, S. Burgdorf, N.A. Melosh, E.W. Newell, F. Ginhoux, A. Schlitzer, and J.L. Schultze, *Cellular Differentiation of Human Monocytes Is Regulated by Time-Dependent Interleukin-4 Signaling and the Transcriptional Regulator NCOR2.* Immunity, 2017. **47**(6): p. 1051-1066 e12.

84. Reynolds, G., P. Vegh, J. Fletcher, E.F.M. Poyner, E. Stephenson, I. Goh, R.A. Botting, N. Huang, B. Olabi, A. Dubois, D. Dixon, K. Green, D. Maunder, J. Engelbert, M. Efremova, K. Polanski, L. Jardine, C. Jones, T. Ness, D. Horsfall, J. McGrath, C. Carey, D.M. Popescu, S. Webb, X.N. Wang, B. Sayer, J.E. Park, V.A. Negri, D. Belokhvostova, M.D. Lynch, D. McDonald, A. Filby, T. Hagai, K.B. Meyer, A. Husain, J. Coxhead, R. Vento-Tormo, S. Behjati, S. Lisgo, A.C. Villani, J. Bacardit, P.H. Jones, E.A. O'Toole, G.S. Ogg, N. Rajan, N.J. Reynolds, S.A. Teichmann, F.M. Watt, and M. Haniffa, *Developmental cell programs are co-opted in inflammatory skin disease.* Science, 2021. **371**(6527).

85. Tamoutounour, S., M. Guilliams, F. Montanana Sanchis, H. Liu, D. Terhorst, C. Malosse, E. Pollet, L. Ardouin, H. Luche, C. Sanchez, M. Dalod, B. Malissen, and S.

Henri, *Origins and functional specialization of macrophages and of conventional and monocyte-derived dendritic cells in mouse skin.* Immunity, 2013. **39**(5): p. 925-38.

86. Leon, B., M. Lopez-Bravo, and C. Ardavin, *Monocyte-derived dendritic cells formed at the infection site control the induction of protective T helper 1 responses against Leishmania.* Immunity, 2007. **26**(4): p. 519-31.

87. Sharma, M.D., P.C. Rodriguez, B.H. Koehn, B. Baban, Y. Cui, G. Guo, M. Shimoda, R. Pacholczyk, H. Shi, E.J. Lee, H. Xu, T.S. Johnson, Y. He, T. Mergoub, C. Venable, V. Bronte, J.D. Wolchok, B.R. Blazar, and D.H. Munn, *Activation of p53 in Immature Myeloid Precursor Cells Controls Differentiation into Ly6c+CD103+ Monocytic Antigen-Presenting Cells in Tumors.* Immunity, 2018. **48**(1): p. 91-106 e6.

88. Liao, C.T., R. Andrews, L.E. Wallace, M.W. Khan, A. Kift-Morgan, N. Topley, D.J. Fraser, and P.R. Taylor, *Peritoneal macrophage heterogeneity is associated with different peritoneal dialysis outcomes.* Kidney Int, 2017. **91**(5): p. 1088-1103.

89. Watchmaker, P.B., K. Lahl, M. Lee, D. Baumjohann, J. Morton, S.J. Kim, R. Zeng, A. Dent, K.M. Ansel, B. Diamond, H. Hadeiba, and E.C. Butcher, *Comparative transcriptional and functional profiling defines conserved programs of intestinal DC differentiation in humans and mice.* Nat Immunol, 2014. **15**(1): p. 98-108.

90. Patel, V.I., J.L. Booth, E.S. Duggan, S. Cate, V.L. White, D. Hutchings, S. Kovats, D.M. Burian, M. Dozmorov, and J.P. Metcalf, *Transcriptional Classification and Functional Characterization of Human Airway Macrophage and Dendritic Cell Subsets.* J Immunol, 2017. **198**(3): p. 1183-1201.

91. McGovern, N., A. Schlitzer, M. Gunawan, L. Jardine, A. Shin, E. Poyner, K. Green, R. Dickinson, X.N. Wang, D. Low, K. Best, S. Covins, P. Milne, S. Pagan, K. Aljefri, M. Windebank, D. Miranda-Saavedra, A. Larbi, P.S. Wasan, K. Duan, M. Poidinger, V. Bigley, F. Ginhoux, M. Collin, and M. Haniffa, *Human dermal CD14+ cells are a transient population of monocyte-derived macrophages.* Immunity, 2014. **41**(3): p. 465-477.

92. Goudot, C., A. Coillard, A.C. Villani, P. Gueguen, A. Cros, S. Sarkizova, T.L. Tang-Huau, M. Bohec, S. Baulande, N. Hacohen, S. Amigorena, and E. Segura, *Aryl Hydrocarbon Receptor Controls Monocyte Differentiation into Dendritic Cells versus Macrophages.* Immunity, 2017. **47**(3): p. 582-596 e6.

93. Tang-Huau, T.L., P. Gueguen, C. Goudot, M. Durand, M. Bohec, S. Baulande, B. Pasquier, S. Amigorena, and E. Segura, *Human in vivo-generated monocyte-derived dendritic cells and macrophages cross-present antigens through a vacuolar pathway.* Nat Commun, 2018. **9**(1): p. 2570.

94. Segura, E., M. Touzot, A. Bohineust, A. Cappuccio, G. Chiocchia, A. Hosmalin, M. Dalod, V. Soumelis, and S. Amigorena, *Human inflammatory dendritic cells induce Th17 cell differentiation.* Immunity, 2013. **38**(2): p. 336-48.

95. Lemaitre, B., E. Nicolas, L. Michaut, J.M. Reichhart, and J.A. Hoffmann, *The dorsoventral regulatory gene cassette spatzle/Toll/cactus controls the potent antifungal response in Drosophila adults.* Cell, 1996. **86**(6): p. 973-83.

96. Medzhitov, R., P. Preston-Hurlburt, and C.A. Janeway, Jr., *A human homologue of the Drosophila Toll protein signals activation of adaptive immunity.* Nature, 1997. **388**(6640): p. 394-7.

97. Hornung, V., A. Ablasser, M. Charrel-Dennis, F. Bauernfeind, G. Horvath, D.R. Caffrey, E. Latz, and K.A. Fitzgerald, *AIM2 recognizes cytosolic dsDNA and forms a caspase-1-activating inflammasome with ASC.* Nature, 2009. **458**(7237): p. 514-8.

98. Chang, S., A. Dolganiuc, and G. Szabo, *Toll-like receptors 1 and 6 are involved in TLR2-mediated macrophage activation by hepatitis C virus core and NS3 proteins.* J Leukoc Biol, 2007. **82**(3): p. 479-87.

99. Rolland, A., E. Jouvin-Marche, C. Viret, M. Faure, H. Perron, and P.N. Marche, *The envelope protein of a human endogenous retrovirus-W family activates innate immunity through CD14/TLR4 and promotes Th1-like responses.* J Immunol, 2006. **176**(12): p. 7636-44.

100. Dalod, M., R. Chelbi, B. Malissen, and T. Lawrence, *Dendritic cell maturation: functional specialization through signaling specificity and transcriptional programming.* EMBO J, 2014. **33**(10): p. 1104-16.

101. Takeuchi, O. and S. Akira, *Pattern recognition receptors and inflammation.* Cell, 2010. **140**(6): p. 805-20.

102. Seth, R.B., L. Sun, C.K. Ea, and Z.J. Chen, *Identification and characterization of MAVS, a mitochondrial antiviral signaling protein that activates NF-kappaB and IRF 3.* Cell, 2005. **122**(5): p. 669-82.

103. Kato, H., O. Takeuchi, S. Sato, M. Yoneyama, M. Yamamoto, K. Matsui, S. Uematsu, A. Jung, T. Kawai, K.J. Ishii, O. Yamaguchi, K. Otsu, T. Tsujimura, C.S. Koh, C. Reis e Sousa, Y. Matsuura, T. Fujita, and S. Akira, *Differential roles of MDA5 and RIG-I helicases in the recognition of RNA viruses.* Nature, 2006. **441**(7089): p. 101-5.

104. Sharma, S., B.R. tenOever, N. Grandvaux, G.P. Zhou, R. Lin, and J. Hiscott, *Triggering the interferon antiviral response through an IKK-related pathway.* Science, 2003. **300**(5622): p. 1148-51.

105. Honda, K. and T. Taniguchi, *IRFs: master regulators of signalling by Toll-like receptors and cytosolic pattern-recognition receptors.* Nat Rev Immunol, 2006. **6**(9): p. 644-58.

106. Su, C.M., L. Wang, and D. Yoo, *Activation of NF-kappaB and induction of proinflammatory cytokine expressions mediated by ORF7a protein of SARS-CoV-2.* Sci Rep, 2021. **11**(1): p. 13464.

107. Marie, I., J.E. Durbin, and D.E. Levy, *Differential viral induction of distinct interferon-alpha genes by positive feedback through interferon regulatory factor-7.* EMBO J, 1998. **17**(22): p. 6660-9.

108. Theiler, M. and H.H. Smith, *The Effect of Prolonged Cultivation in Vitro Upon the Pathogenicity of Yellow Fever Virus.* J Exp Med, 1937. **65**(6): p. 767-86.

109. Theiler, M. and H.H. Smith, *The Use of Yellow Fever Virus Modified by in Vitro Cultivation for Human Immunization.* J Exp Med, 1937. **65**(6): p. 787-800.

110. Silva, M.L., M.A. Martins, L.R. Espirito-Santo, A.C. Campi-Azevedo, D. Silveira-Lemos, J.G. Ribeiro, A. Homma, E.G. Kroon, A. Teixeira-Carvalho, S.M. Eloi-Santos, and O.A. Martins-Filho, *Characterization of main cytokine sources from the innate and adaptive immune responses following primary 17DD yellow fever vaccination in adults.* Vaccine, 2011. **29**(3): p. 583-92.

111. Wec, A.Z., D. Haslwanter, Y.N. Abdiche, L. Shehata, N. Pedreno-Lopez, C.L. Moyer, Z.A. Bornholdt, A. Lilov, J.H. Nett, R.K. Jangra, M. Brown, D.I. Watkins, C. Ahlm, M.N. Forsell, F.A. Rey, G. Barba-Spaeth, K. Chandran, and L.M. Walker, *Longitudinal dynamics of the human B cell response to the yellow fever 17D vaccine.* Proc Natl Acad Sci U S A, 2020. **117**(12): p. 6675-6685.

112. Poland, J.D., C.H. Calisher, T.P. Monath, W.G. Downs, and K. Murphy, *Persistence of neutralizing antibody 30-35 years after immunization with 17D yellow fever vaccine.* Bull World Health Organ, 1981. **59**(6): p. 895-900.

113. Huber, J.E., J. Ahlfeld, M.K. Scheck, M. Zaucha, K. Witter, L. Lehmann, H. Karimzadeh, M. Pritsch, M. Hoelscher, F. von Sonnenburg, A. Dick, G. Barba-Spaeth, A.B. Krug, S. Rothenfusser, and D. Baumjohann, *Dynamic changes in circulating T follicular helper cell composition predict neutralising antibody responses after yellow fever vaccination.* Clin Transl Immunology, 2020. **9**(5): p. e1129.

114. Kohler, S., N. Bethke, M. Bothe, S. Sommerick, M. Frentsch, C. Romagnani, M. Niedrig, and A. Thiel, *The early cellular signatures of protective immunity induced by live viral vaccination.* Eur J Immunol, 2012. **42**(9): p. 2363-73.

115. Sandberg, J.T., S. Ols, M. Lofling, R. Varnaite, G. Lindgren, O. Nilsson, L. Rombo, M. Kalen, K. Lore, K. Blom, and H.G. Ljunggren, *Activation and Kinetics of Circulating T Follicular Helper Cells, Specific Plasmablast Response, and Development of Neutralizing Antibodies following Yellow Fever Virus Vaccination.* J Immunol, 2021. **207**(4): p. 1033-1043.

116. Martins, M.A., M.L. Silva, A.P. Marciano, V. Peruhype-Magalhaes, S.M. Eloi-Santos, G. Ribeiro j, R. Correa-Oliveira, A. Homma, E.G. Kroon, A. Teixeira-Carvalho, and O.A. Martins-Filho, *Activation/modulation of adaptive immunity emerges simultaneously after 17DD yellow fever first-time vaccination: is this the key to prevent severe adverse reactions following immunization?* Clin Exp Immunol, 2007. **148**(1): p. 90-100.

117. Santos, A.P., D.C.S. Matos, A.L. Bertho, S.C.F. Mendonca, and R. Marcovistz, *Detection of Th1/Th2 cytokine signatures in yellow fever 17DD first-time vaccinees through ELISpot assay.* Cytokine, 2008. **42**(2): p. 152-155.

118. Gaucher, D., R. Therrien, N. Kettaf, B.R. Angermann, G. Boucher, A. Filali-Mouhim, J.M. Moser, R.S. Mehta, D.R. Drake, 3rd, E. Castro, R. Akondy, A. Rinfret, B. Yassine-Diab, E.A. Said, Y. Chouikh, M.J. Cameron, R. Clum, D. Kelvin, R. Somogyi, L.D. Greller, R.S. Balderas, P. Wilkinson, G. Pantaleo, J. Tartaglia, E.K. Haddad, and R.P. Sekaly, *Yellow fever vaccine induces integrated multilineage and polyfunctional immune responses.* J Exp Med, 2008. **205**(13): p. 3119-31.

119. Blom, K., M. Braun, M.A. Ivarsson, V.D. Gonzalez, K. Falconer, M. Moll, H.G. Ljunggren, J. Michaelsson, and J.K. Sandberg, *Temporal dynamics of the primary human T cell response to yellow fever virus 17D as it matures from an effector- to a memory-type response.* J Immunol, 2013. **190**(5): p. 2150-8.

120. Miller, J.D., R.G. van der Most, R.S. Akondy, J.T. Glidewell, S. Albott, D. Masopust, K. Murali-Krishna, P.L. Mahar, S. Edupuganti, S. Lalor, S. Germon, C. Del Rio, M.J. Mulligan, S.I. Staprans, J.D. Altman, M.B. Feinberg, and R. Ahmed, *Human effector and memory CD8+ T cell responses to smallpox and yellow fever vaccines.* Immunity, 2008. **28**(5): p. 710-22.

121. Akondy, R.S., M. Fitch, S. Edupuganti, S. Yang, H.T. Kissick, K.W. Li, B.A. Youngblood, H.A. Abdelsamed, D.J. McGuire, K.W. Cohen, G. Alexe, S. Nagar, M.M. McCausland, S. Gupta, P. Tata, W.N. Haining, M.J. McElrath, D. Zhang, B. Hu, W.J. Greenleaf, J.J. Goronzy, M.J. Mulligan, M. Hellerstein, and R. Ahmed, *Origin and differentiation of human memory CD8 T cells after vaccination.* Nature, 2017.

122. Akondy, R.S., N.D. Monson, J.D. Miller, S. Edupuganti, D. Teuwen, H. Wu, F. Quyyumi, S. Garg, J.D. Altman, C. Del Rio, H.L. Keyserling, A. Ploss, C.M. Rice, W.A. Orenstein, M.J. Mulligan, and R. Ahmed, *The yellow fever virus vaccine induces a broad and polyfunctional human memory CD8+ T cell response.* J Immunol, 2009. **183**(12): p. 7919-30.

123. Campi-Azevedo, A.C., L.R. Reis, V. Peruhype-Magalhaes, J.G. Coelho-Dos-Reis, L.R. Antonelli, C.T. Fonseca, C. Costa-Pereira, E.M. Souza-Fagundes, I.A. da Costa-Rocha, J.V.M. Mambrini, J.A.C. Lemos, J.G.L. Ribeiro, I.R. Caldas, L.A.B. Camacho, M.L.S. Maia, T.G. de Noronha, S.M.B. de Lima, M. Simoes, M.D.S. Freire, R.M. Martins, A. Homma, P.L. Tauil, P.F.C. Vasconcelos, A.P.M. Romano, C.M. Domingues, A. Teixeira-Carvalho, and O.A. Martins-Filho, *Short-Lived Immunity After 17DD Yellow Fever Single Dose Indicates That Booster Vaccination May Be Required to Guarantee Protective Immunity in Children.* Front Immunol, 2019. **10**: p. 2192.

124. Akondy, R.S., P.L. Johnson, H.I. Nakaya, S. Edupuganti, M.J. Mulligan, B. Lawson, J.D. Miller, B. Pulendran, R. Antia, and R. Ahmed, *Initial viral load determines the magnitude of the human CD8 T cell response to yellow fever vaccination.* Proc Natl Acad Sci U S A, 2015. **112**(10): p. 3050-5.

125. Martins, M.A., M.L. Silva, S.M. Eloi-Santos, J.G. Ribeiro, V. Peruhype-Magalhaes, A.P. Marciano, A. Homma, E.G. Kroon, A. Teixeira-Carvalho, and O.A. Martins-Filho, *Innate immunity phenotypic features point toward simultaneous raise of activation and modulation events following 17DD live attenuated yellow fever first-time vaccination.* Vaccine, 2008. **26**(9): p. 1173-84.

126. Hou, J., S. Wang, M. Jia, D. Li, Y. Liu, Z. Li, H. Zhu, H. Xu, M. Sun, L. Lu, Z. Zhou, H. Peng, Q. Zhang, S. Fu, G. Liang, L. Yao, X. Yu, L.N. Carpp, Y. Huang, J. McElrath, S. Self, and Y. Shao, *A Systems Vaccinology Approach Reveals Temporal Transcriptomic Changes of Immune Responses to the Yellow Fever 17D Vaccine.* J Immunol, 2017. **199**(4): p. 1476-1489.

127. Bastard, P., E. Michailidis, H.H. Hoffmann, M. Chbihi, T. Le Voyer, J. Rosain, Q. Philippot, Y. Seeleuthner, A. Gervais, M. Materna, P.M.N. de Oliveira, M.L.S. Maia, A.P. Dinis Ano Bom, T. Azamor, D. Araujo da Conceicao, E. Goudouris, A. Homma, G.

179

Slesak, J. Schafer, B. Pulendran, J.D. Miller, R. Huits, R. Yang, L.B. Rosen, L. Bizien, L. Lorenzo, M. Chrabieh, L.V. Erazo, F. Rozenberg, M.M. Jeljeli, V. Beziat, S.M. Holland, A. Cobat, L.D. Notarangelo, H.C. Su, R. Ahmed, A. Puel, S.Y. Zhang, L. Abel, S.J. Seligman, Q. Zhang, M.R. MacDonald, E. Jouanguy, C.M. Rice, and J.L. Casanova, *Auto-antibodies to type I IFNs can underlie adverse reactions to yellow fever live attenuated vaccine.* J Exp Med, 2021. **218**(4).

128.   Hernandez, N., G. Bucciol, L. Moens, J. Le Pen, M. Shahrooei, E. Goudouris, A. Shirkani, M. Changi-Ashtiani, H. Rokni-Zadeh, E.H. Sayar, I. Reisli, A. Lefevre-Utile, D. Zijlmans, A. Jurado, R. Pholien, S. Drutman, S. Belkaya, A. Cobat, R. Boudewijns, D. Jochmans, J. Neyts, Y. Seeleuthner, L. Lorenzo-Diaz, C. Enemchukwu, I. Tietjen, H.H. Hoffmann, M. Momenilandi, L. Poyhonen, M.M. Siqueira, S.M.B. de Lima, D.C. de Souza Matos, A. Homma, M.L.S. Maia, T.A. da Costa Barros, P.M.N. de Oliveira, E.C. Mesquita, R. Gijsbers, S.Y. Zhang, S.J. Seligman, L. Abel, P. Hertzog, N. Marr, R.M. Martins, I. Meyts, Q. Zhang, M.R. MacDonald, C.M. Rice, J.L. Casanova, E. Jouanguy, and X. Bossuyt, *Inherited IFNAR1 deficiency in otherwise healthy patients with adverse reaction to measles and yellow fever live vaccines.* J Exp Med, 2019. **216**(9): p. 2057-70.

129.   Pulendran, B., *Learning immunology from the yellow fever vaccine: innate immunity to systems vaccinology.* Nat Rev Immunol, 2009. **9**(10): p. 741-7.

130.   Querec, T.D., R.S. Akondy, E.K. Lee, W. Cao, H.I. Nakaya, D. Teuwen, A. Pirani, K. Gernert, J. Deng, B. Marzolf, K. Kennedy, H. Wu, S. Bennouna, H. Oluoch, J. Miller, R.Z. Vencio, M. Mulligan, A. Aderem, R. Ahmed, and B. Pulendran, *Systems biology approach predicts immunogenicity of the yellow fever vaccine in humans.* Nat Immunol, 2009. **10**(1): p. 116-125.

131.   Azamor, T., A.M.V. da Silva, J.G. Melgaco, A.P. Dos Santos, C. Xavier-Carvalho, L.E. Alvarado-Arnez, L.R. Batista-Silva, D.C. de Souza Matos, C. Bayma, S. Missailidis, A.P.D. Ano Bom, M.O. Moraes, and P.C. da Costa Neves, *Activation of an Effective Immune Response after Yellow Fever Vaccination Is Associated with the Genetic Background and Early Response of IFN-gamma and CLEC5A.* Viruses, 2021. **13**(1).

132.   Brett D. Lindenbach, H.-J.T., Charles M. Rice, *Flaviviridae: The Viruses and Their Replication.* Fields Virology, 2007. **5th Edition**: p. 1101-1133.

133.   Hahn, C.S., J.M. Dalrymple, J.H. Strauss, and C.M. Rice, *Comparison of the virulent Asibi strain of yellow fever virus with the 17D vaccine strain derived from it.* Proc Natl Acad Sci U S A, 1987. **84**(7): p. 2019-23.

134.   Chu, J.J. and M.L. Ng, *Infectious entry of West Nile virus occurs through a clathrin-mediated endocytic pathway.* J Virol, 2004. **78**(19): p. 10543-55.

135.   Gollins, S.W. and J.S. Porterfield, *Flavivirus infection enhancement in macrophages: an electron microscopic study of viral cellular entry.* J Gen Virol, 1985. **66 (Pt 9)**: p. 1969-82.

136.   Gollins, S.W. and J.S. Porterfield, *The uncoating and infectivity of the flavivirus West Nile on interaction with cells: effects of pH and ammonium chloride.* J Gen Virol, 1986. **67 (Pt 9)**: p. 1941-50.

137.   Lindenbach, B.D. and C.M. Rice, *trans-Complementation of yellow fever virus NS1 reveals a role in early RNA replication.* J Virol, 1997. **71**(12): p. 9608-17.

138.   Reinhardt, B., R. Jaspert, M. Niedrig, C. Kostner, and J. L'Age-Stehr, *Development of viremia and humoral and cellular parameters of immune activation after vaccination with yellow fever virus strain 17D: a model of human flavivirus infection.* J Med Virol, 1998. **56**(2): p. 159-67.

139.   Liang, H., M. Lee, and X. Jin, *Guiding dengue vaccine development using knowledge gained from the success of the yellow fever vaccine.* Cell Mol Immunol, 2016. **13**(1): p. 36-46.

140.   Querec, T.D. and B. Pulendran, *Understanding the role of innate immunity in the mechanism of action of the live attenuated Yellow Fever Vaccine 17D.* Adv Exp Med Biol, 2007. **590**: p. 43-53.

141.   Wu, S.J., G. Grouard-Vogel, W. Sun, J.R. Mascola, E. Brachtel, R. Putvatana, M.K. Louder, L. Filgueira, M.A. Marovich, H.K. Wong, A. Blauvelt, G.S. Murphy, M.L. Robb, B.L. Innes, D.L. Birx, C.G. Hayes, and S.S. Frankel, *Human skin Langerhans cells are targets of dengue virus infection.* Nat Med, 2000. **6**(7): p. 816-20.

142.   Khaiboullina, S.F., A.A. Rizvanov, M.R. Holbrook, and S. St Jeor, *Yellow fever virus strains Asibi and 17D-204 infect human umbilical cord endothelial cells and induce novel changes in gene expression.* Virology, 2005. **342**(2): p. 167-76.

143.   Woodson, S.E. and M.R. Holbrook, *Infection of hepatocytes with 17-D vaccine-strain yellow fever virus induces a strong pro-inflammatory host response.* J Gen Virol, 2011. **92**(Pt 10): p. 2262-71.

144.   Barba-Spaeth, G., R.S. Longman, M.L. Albert, and C.M. Rice, *Live attenuated yellow fever 17D infects human DCs and allows for presentation of endogenous and recombinant T cell epitopes.* J Exp Med, 2005. **202**(9): p. 1179-84.

145.   Deauvieau, F., V. Sanchez, C. Balas, A. Kennel, D.E.M. A, J. Lang, and B. Guy, *Innate immune responses in human dendritic cells upon infection by chimeric yellow-fever dengue vaccine serotypes 1-4.* Am J Trop Med Hyg, 2007. **76**(1): p. 144-54.

146.   Palmer, D.R., S. Fernandez, J. Bisbing, K.K. Peachman, M. Rao, D. Barvir, V. Gunther, T. Burgess, Y. Kohno, R. Padmanabhan, and W. Sun, *Restricted replication and lysosomal trafficking of yellow fever 17D vaccine virus in human dendritic cells.* J Gen Virol, 2007. **88**(Pt 1): p. 148-56.

147.   Sinigaglia, L., S. Gracias, E. Decembre, M. Fritz, D. Bruni, N. Smith, J.P. Herbeuval, A. Martin, M. Dreux, F. Tangy, and N. Jouvenet, *Immature particles and capsid-free viral RNA produced by Yellow fever virus-infected cells stimulate plasmacytoid dendritic cells to secrete interferons.* Sci Rep, 2018. **8**(1): p. 10889.

148.   Laurent-Rolle, M., J. Morrison, R. Rajsbaum, J.M.L. Macleod, G. Pisanelli, A. Pham, J. Ayllon, L. Miorin, C. Martinez, B.R. tenOever, and A. Garcia-Sastre, *The interferon signaling antagonist function of yellow fever virus NS5 protein is activated by type I interferon.* Cell Host Microbe, 2014. **16**(3): p. 314-327.

149.   Perelygin, A.A., S.V. Scherbik, I.B. Zhulin, B.M. Stockman, Y. Li, and M.A. Brinton, *Positional cloning of the murine flavivirus resistance gene.* Proc Natl Acad Sci U S A, 2002. **99**(14): p. 9322-7.

150.   Meier, K.C., C.L. Gardner, M.V. Khoretonenko, W.B. Klimstra, and K.D. Ryman, *A mouse model for studying viscerotropic disease caused by yellow fever virus infection.* PLoS Pathog, 2009. **5**(10): p. e1000614.

151.   Querec, T., S. Bennouna, S. Alkan, Y. Laouar, K. Gorden, R. Flavell, S. Akira, R. Ahmed, and B. Pulendran, *Yellow fever vaccine YF-17D activates multiple dendritic cell subsets via TLR2, 7, 8, and 9 to stimulate polyvalent immunity.* J Exp Med, 2006. **203**(2): p. 413-24.

152.   Dong, H.L., H.J. Wang, Z.Y. Liu, Q. Ye, X.L. Qin, D. Li, Y.Q. Deng, T. Jiang, X.F. Li, and C.F. Qin, *Visualization of yellow fever virus infection in mice using a bioluminescent reporter virus.* Emerg Microbes Infect, 2021. **10**(1): p. 1739-1750.

153.   Douam, F., G. Hrebikova, Y.E. Albrecht, J. Sellau, Y. Sharon, Q. Ding, and A. Ploss, *Single-cell tracking of flavivirus RNA uncovers species-specific interactions with the immune system dictating disease outcome.* Nat Commun, 2017. **8**: p. 14781.

154.   Zhu, N., D. Zhang, W. Wang, X. Li, B. Yang, J. Song, X. Zhao, B. Huang, W. Shi, R. Lu, P. Niu, F. Zhan, X. Ma, D. Wang, W. Xu, G. Wu, G.F. Gao, W. Tan, I. China Novel Coronavirus, and T. Research, *A Novel Coronavirus from Patients with Pneumonia in China, 2019.* N Engl J Med, 2020. **382**(8): p. 727-733.

155.   Huang, C., Y. Wang, X. Li, L. Ren, J. Zhao, Y. Hu, L. Zhang, G. Fan, J. Xu, X. Gu, Z. Cheng, T. Yu, J. Xia, Y. Wei, W. Wu, X. Xie, W. Yin, H. Li, M. Liu, Y. Xiao, H. Gao, L. Guo, J. Xie, G. Wang, R. Jiang, Z. Gao, Q. Jin, J. Wang, and B. Cao, *Clinical features of patients infected with 2019 novel coronavirus in Wuhan, China.* Lancet, 2020. **395**(10223): p. 497-506.

156.   Chen, G., D. Wu, W. Guo, Y. Cao, D. Huang, H. Wang, T. Wang, X. Zhang, H. Chen, H. Yu, X. Zhang, M. Zhang, S. Wu, J. Song, T. Chen, M. Han, S. Li, X. Luo, J. Zhao, and Q. Ning, *Clinical and immunological features of severe and moderate coronavirus disease 2019.* J Clin Invest, 2020. **130**(5): p. 2620-2629.

157.   Zheng, H.Y., M. Zhang, C.X. Yang, N. Zhang, X.C. Wang, X.P. Yang, X.Q. Dong, and Y.T. Zheng, *Elevated exhaustion levels and reduced functional diversity of T cells in peripheral blood may predict severe progression in COVID-19 patients.* Cell Mol Immunol, 2020. **17**(5): p. 541-543.

158.   Zheng, M., Y. Gao, G. Wang, G. Song, S. Liu, D. Sun, Y. Xu, and Z. Tian, *Functional exhaustion of antiviral lymphocytes in COVID-19 patients.* Cell Mol Immunol, 2020. **17**(5): p. 533-535.

159.   Gao, Y., T. Li, M. Han, X. Li, D. Wu, Y. Xu, Y. Zhu, Y. Liu, X. Wang, and L. Wang, *Diagnostic utility of clinical laboratory data determinations for patients with the severe COVID-19.* J Med Virol, 2020. **92**(7): p. 791-796.

160.   Lucas, C., P. Wong, J. Klein, T.B.R. Castro, J. Silva, M. Sundaram, M.K. Ellingson, T. Mao, J.E. Oh, B. Israelow, T. Takahashi, M. Tokuyama, P. Lu, A. Venkataraman, A. Park, S. Mohanty, H. Wang, A.L. Wyllie, C.B.F. Vogels, R. Earnest,

182

S. Lapidus, I.M. Ott, A.J. Moore, M.C. Muenker, J.B. Fournier, M. Campbell, C.D. Odio, A. Casanovas-Massana, R. Herbst, A.C. Shaw, R. Medzhitov, W.L. Schulz, N.D. Grubaugh, C. Dela Cruz, S. Farhadian, A.I. Ko, S.B. Omer, and A. Iwasaki, *Longitudinal analyses reveal immunological misfiring in severe COVID-19.* Nature, 2020. **584**: p. 463–69.

161.   Kvedaraite, E., L. Hertwig, I. Sinha, A. Ponzetta, I. Hed Myrberg, M. Lourda, M. Dzidic, M. Akber, J. Klingström, E. Folkesson, J.R. Muvva, P. Chen, S. Gredmark-Russ, S. Brighenti, A. Norrby-Teglund, L.I. Eriksson, O. Rooyackers, S. Aleman, K. Strålin, H.-G. Ljunggren, F. Ginhoux, N.K. Björkström, J.-I. Henter, and M. Svensson, *Major alterations in the mononuclear phagocyte landscape associated with COVID-19 severity.* Proc Natl Acad Sci U S A, 2021. **118**(6): p. e2018587118.

162.   Zhou, R., K.K. To, Y.C. Wong, L. Liu, B. Zhou, X. Li, H. Huang, Y. Mo, T.Y. Luk, T.T. Lau, P. Yeung, W.M. Chan, A.K. Wu, K.C. Lung, O.T. Tsang, W.S. Leung, I.F. Hung, K.Y. Yuen, and Z. Chen, *Acute SARS-CoV-2 Infection Impairs Dendritic Cell and T Cell Responses.* Immunity, 2020. **53**(4): p. 864-877 e5.

163.   Arunachalam, P.S., F. Wimmers, C.K.P. Mok, R.A.P.M. Perera, M. Scott, T. Hagan, N. Sigal, Y. Feng, L. Bristow, O. Tak-Yin Tsang, D. Wagh, J. Coller, K.L. Pellegrini, D. Kazmin, G. Alaaeddine, W.S. Leung, J.M.C. Chan, T.S.H. Chik, C.Y.C. Choi, C. Huerta, M. Paine McCullough, H. Lv, E. Anderson, S. Edupuganti, A.A. Upadhyay, S.E. Bosinger, H.T. Maecker, P. Khatri, N. Rouphael, M. Peiris, and B. Pulendran, *Systems biological assessment of immunity to mild versus severe COVID-19 infection in humans.* Science, 2020. **369**(6508): p. 1210-20.

164.   Hadjadj, J., N. Yatim, L. Barnabei, A. Corneau, J. Boussier, N. Smith, H. Péré, B. Charbit, V. Bondet, C. Chenevier-Gobeaux, P. Breillat, N. Carlier, R. Gauzit, C. Morbieu, F. Pène, N. Marin, N. Roche, T.A. Szwebel, S.H. Merkling, J.M. Treluyer, D. Veyer, L. Mouthon, C. Blanc, P.L. Tharaux, F. Rozenberg, A. Fischer, D. Duffy, F. Rieux-Laucat, S. Kernéis, and B. Terrier, *Impaired type I interferon activity and inflammatory responses in severe COVID-19 patients.* Science, 2020. **369**(6504): p. 718-24.

165.   Sánchez-Cerrillo, I., P. Landete, B. Aldave, S. Sánchez-Alonso, A. Sánchez-Azofra, A. Marcos-Jiménez, E. Ávalos, A. Alcaraz-Serna, I. de Los Santos, T. Mateu-Albero, L. Esparcia, C. López-Sanz, P. Martínez-Fleta, L. Gabrie, L. Del Campo Guerola, H. de la Fuente, M.J. Calzada, I. González-Álvaro, A. Alfranca, F. Sánchez-Madrid, C. Muñoz-Calleja, J.B. Soriano, J. Ancochea, and E. Martín-Gayo, *COVID-19 severity associates with pulmonary redistribution of CD1c+ DCs and inflammatory transitional and nonclassical monocytes.* J Clin Invest, 2020. **130**(12): p. 6290-6300.

166.   Schulte-Schrepping, J., N. Reusch, D. Paclik, K. Baßler, S. Schlickeiser, B. Zhang, B. Krämer, T. Krammer, S. Brumhard, L. Bonaguro, E. De Domenico, D. Wendisch, M. Grasshoff, T.S. Kapellos, M. Beckstette, T. Pecht, A. Saglam, O. Dietrich, H.E. Mei, A.R. Schulz, C. Conrad, D. Kunkel, E. Vafadarnejad, C.-J. Xu, A. Horne, M. Herbert, A. Drews, C. Thibeault, M. Pfeiffer, S. Hippenstiel, A. Hocke, H. Müller-Redetzky, K.-M. Heim, F. Machleidt, A. Uhrig, L.B. de Jarcy, L. Jürgens, M. Stegemann, C.R. Glösenkamp, H.-D. Volk, C. Goffinet, J. Raabe, K.M. Kaiser, M. To Vinh, G. Rieke, C. Meisel, T. Ulas, M. Becker, R. Geffers, M. Witzenrath, C. Drosten, N. Suttorp, C. von Kalle, F. Kurth, K. Händler, J.L. Schultze, A.C. Aschenbrenner, Y. Li, J. Nattermann, B.

Sawitzki, A.-E. Saliba, and L.E. Sander, *Severe COVID-19 is marked by a dysregulated myeloid cell compartment.* Cell, 2020. **182**: p. 1419–40.

167.   Bruni, D., M. Chazal, L. Sinigaglia, L. Chauveau, O. Schwartz, P. Despres, and N. Jouvenet, *Viral entry route determines how human plasmacytoid dendritic cells produce type I interferons.* Sci Signal, 2015. **8**(366): p. ra25.

168.   Yi, Z., L. Sperzel, C. Nurnberger, P.J. Bredenbeek, K.J. Lubick, S.M. Best, C.T. Stoyanov, L.M. Law, Z. Yuan, C.M. Rice, and M.R. MacDonald, *Identification and characterization of the host protein DNAJC14 as a broadly active flavivirus replication modulator.* PLoS Pathog, 2011. **7**(1): p. e1001255.

169.   Brand, I., L. Gilberg, J. Bruger, M. Gari, A. Wieser, T.M. Eser, J. Frese, M.I.M. Ahmed, R. Rubio-Acero, J.M. Guggenbuehl Noller, N. Castelletti, J. Diekmannshemke, S. Thiesbrummel, D. Huynh, S. Winter, I. Kroidl, C. Fuchs, M. Hoelscher, J. Roider, S. Kobold, M. Pritsch, and C. Geldmacher, *Broad T Cell Targeting of Structural Proteins After SARS-CoV-2 Infection: High Throughput Assessment of T Cell Reactivity Using an Automated Interferon Gamma Release Assay.* Front Immunol, 2021. **12**: p. 688436.

170.   WHO., *Novel Coronavirus: COVID-19 Therapeutic Trial Synopsis.* 2020 Draft February 18, 2020. WHO R&D Blueprint.

171.   Winheim, E., L. Rinke, K. Lutz, A. Reischer, A. Leutbecher, L. Wolfram, L. Rausch, J. Kranich, P.R. Wratil, J.E. Huber, D. Baumjohann, S. Rothenfusser, B. Schubert, A. Hilgendorff, J.C. Hellmuth, C. Scherer, M. Muenchhoff, M. von Bergwelt-Baildon, K. Stark, T. Straub, T. Brocker, O.T. Keppler, M. Subklewe, and A.B. Krug, *Impaired function and delayed regeneration of dendritic cells in COVID-19.* PLOS Pathogens, 2021. **17**(10): p. e1009742.

172.   Picelli, S., O.R. Faridani, A.K. Bjorklund, G. Winberg, S. Sagasser, and R. Sandberg, *Full-length RNA-seq from single cells using Smart-seq2.* Nat Protoc, 2014. **9**(1): p. 171-81.

173.   Love, M.I., W. Huber, and S. Anders, *Moderated estimation of fold change and dispersion for RNA-seq data with DESeq2.* Genome Biol, 2014. **15**(12): p. 550.

174.   Cong, Y., M.A. McArthur, M. Cohen, P.B. Jahrling, K.B. Janosko, N. Josleyn, K. Kang, T. Zhang, and M.R. Holbrook, *Characterization of Yellow Fever Virus Infection of Human and Non-human Primate Antigen Presenting Cells and Their Interaction with CD4+ T Cells.* PLoS Negl Trop Dis, 2016. **10**(5): p. e0004709.

175.   Desai, N.N. and J.M. Goldfarb, *Growth factor/cytokine secretion by a permanent human endometrial cell line with embryotrophic properties.* J Assist Reprod Genet, 1996. **13**(7): p. 546-50.

176.   Stoker, M. and I. Macpherson, *Syrian Hamster Fibroblast Cell Line Bhk21 and Its Derivatives.* Nature, 1964. **203**: p. 1355-7.

177.   Bovay, A., S. Nassiri, H. Maby-El Hajjami, P. Marcos Mondejar, R.S. Akondy, R. Ahmed, B. Lawson, D.E. Speiser, and S.A. Fuertes Marraco, *Minimal immune response to booster vaccination against Yellow Fever associated with pre-existing antibodies.* Vaccine, 2020. **38**(9): p. 2172-2182.

178.   Pulendran, B., J. Miller, T.D. Querec, R. Akondy, N. Moseley, O. Laur, J. Glidewell, N. Monson, T. Zhu, H. Zhu, S. Staprans, D. Lee, M.A. Brinton, A.A. Perelygin, C. Vellozzi, P. Brachman, Jr., S. Lalor, D. Teuwen, R.B. Eidex, M. Cetron, F. Priddy, C. del Rio, J. Altman, and R. Ahmed, *Case of yellow fever vaccine--associated viscerotropic disease with prolonged viremia, robust adaptive immune responses, and polymorphisms in CCR5 and RANTES genes.* J Infect Dis, 2008. **198**(4): p. 500-7.

179.   Günther, P., B. Cirovic, K. Baßler, K. Händler, M. Becker, C.A. Dutertre, V. Bigley, E. Newell, M. Collin, F. Ginhoux, A. Schlitzer, and J.L. Schultze, *A rule-based data-informed cellular consensus map of the human mononuclear phagocyte cell space.* bioRxiv, 2019: p. 658179.

180.   Oliveira, J.J., S. Karrar, D.B. Rainbow, C.L. Pinder, P. Clarke, A. Rubio Garcia, O. Al-Assar, K. Burling, S. Morris, R. Stratton, T.J. Vyse, L.S. Wicker, J.A. Todd, and R.C. Ferreira, *The plasma biomarker soluble SIGLEC-1 is associated with the type I interferon transcriptional signature, ethnic background and renal disease in systemic lupus erythematosus.* Arthritis Res Ther, 2018. **20**(1): p. 152.

181.   Metzemaekers, M., V. Vanheule, R. Janssens, S. Struyf, and P. Proost, *Overview of the Mechanisms that May Contribute to the Non-Redundant Activities of Interferon-Inducible CXC Chemokine Receptor 3 Ligands. Front Immunol,* 2017. **8**: p. 1970.

182.   Kotliarov, Y., R. Sparks, A.J. Martins, M.P. Mule, Y. Lu, M. Goswami, L. Kardava, R. Banchereau, V. Pascual, A. Biancotto, J. Chen, P.L. Schwartzberg, N. Bansal, C.C. Liu, F. Cheung, S. Moir, and J.S. Tsang, *Broad immune activation underlies shared set point signatures for vaccine responsiveness in healthy individuals and disease activity in patients with lupus.* Nat Med, 2020. **26**(4): p. 618-629.

183.   Li, S., N. Rouphael, S. Duraisingham, S. Romero-Steiner, S. Presnell, C. Davis, D.S. Schmidt, S.E. Johnson, A. Milton, G. Rajam, S. Kasturi, G.M. Carlone, C. Quinn, D. Chaussabel, A.K. Palucka, M.J. Mulligan, R. Ahmed, D.S. Stephens, H.I. Nakaya, and B. Pulendran, *Molecular signatures of antibody responses derived from a systems biology study of five human vaccines.* Nat Immunol, 2014. **15**(2): p. 195-204.

184.   Burckstummer, T., C. Baumann, S. Bluml, E. Dixit, G. Durnberger, H. Jahn, M. Planyavsky, M. Bilban, J. Colinge, K.L. Bennett, and G. Superti-Furga, *An orthogonal proteomic-genomic screen identifies AIM2 as a cytoplasmic DNA sensor for the inflammasome.* Nat Immunol, 2009. **10**(3): p. 266-72.

185.   Jefferies, C.A., *Regulating IRFs in IFN Driven Disease.* Front Immunol, 2019. **10**: p. 325.

186.   Wen, A.Y., K.M. Sakamoto, and L.S. Miller, *The role of the transcription factor CREB in immune function.* J Immunol, 2010. **185**(11): p. 6413-9.

187.   To, K.K., I.F. Hung, J.D. Ip, A.W. Chu, W.M. Chan, A.R. Tam, C.H. Fong, S. Yuan, H.W. Tsoi, A.C. Ng, L.L. Lee, P. Wan, E.Y. Tso, W.K. To, D.N. Tsang, K.H. Chan, J.D. Huang, K.H. Kok, V.C. Cheng, and K.Y. Yuen, *Coronavirus Disease 2019 (COVID-19) Re-infection by a Phylogenetically Distinct Severe Acute Respiratory Syndrome Coronavirus 2 Strain Confirmed by Whole Genome Sequencing.* Clin Infect Dis, 2021. **73**(9): p. e2946-e2951.

188.   Pinzon-Charry, A., C.S. Ho, R. Laherty, T. Maxwell, D. Walker, R.A. Gardiner, L. O'Connor, C. Pyke, C. Schmidt, C. Furnival, and J.A. Lopez, *A population of HLA-DR+ immature cells accumulates in the blood dendritic cell compartment of patients with different types of cancer.* Neoplasia, 2005. **7**(12): p. 1112-22.

189.   Pinzon-Charry, A., T. Woodberry, V. Kienzle, V. McPhun, G. Minigo, D.A. Lampah, E. Kenangalem, C. Engwerda, J.A. Lopez, N.M. Anstey, and M.F. Good, *Apoptosis and dysfunction of blood dendritic cells in patients with falciparum and vivax malaria.* J Exp Med, 2013. **210**(8): p. 1635-46.

190.   Collar, A.L., M. Swamydas, M. O'Hayre, M.S. Sajib, K.W. Hoffman, S.P. Singh, A. Mourad, M.D. Johnson, E.M. Ferre, J.M. Farber, J.K. Lim, C.M. Mikelis, J.S. Gutkind, and M.S. Lionakis, *The homozygous CX3CR1-M280 mutation impairs human monocyte survival.* JCI Insight, 2018. **3**(3).

191.   Landsman, L., L. Bar-On, A. Zernecke, K.W. Kim, R. Krauthgamer, E. Shagdarsuren, S.A. Lira, I.L. Weissman, C. Weber, and S. Jung, *CX3CR1 is required for monocyte homeostasis and atherogenesis by promoting cell survival.* Blood, 2009. **113**(4): p. 963-72.

192.   Fernandez-Garcia, M.D., L. Meertens, M. Chazal, M.L. Hafirassou, O. Dejarnac, A. Zamborlini, P. Despres, N. Sauvonnet, F. Arenzana-Seisdedos, N. Jouvenet, and A. Amara, *Vaccine and Wild-Type Strains of Yellow Fever Virus Engage Distinct Entry Mechanisms and Differentially Stimulate Antiviral Immune Responses.* MBio, 2016. **7**(1): p. e01956-15.

193.   Wurfel, M.M., W.Y. Park, F. Radella, J. Ruzinski, A. Sandstrom, J. Strout, R.E. Bumgarner, and T.R. Martin, *Identification of high and low responders to lipopolysaccharide in normal subjects: an unbiased approach to identify modulators of innate immunity.* J Immunol, 2005. **175**(4): p. 2570-8.

194.   Pardy, R.D., S.F. Valbon, B. Cordeiro, C.M. Krawczyk, and M.J. Richer, *An epidemic Zika virus isolate suppresses antiviral immunity by disrupting antigen presentation pathways.* Nat Commun, 2021. **12**(1): p. 4051.

195.   Silvin, A., C.I. Yu, X. Lahaye, F. Imperatore, J.B. Brault, S. Cardinaud, C. Becker, W.H. Kwan, C. Conrad, M. Maurin, C. Goudot, S. Marques-Ladeira, Y. Wang, V. Pascual, E. Anguiano, R.A. Albrecht, M. Iannacone, A. Garcia-Sastre, B. Goud, M. Dalod, A. Moris, M. Merad, A.K. Palucka, and N. Manel, *Constitutive resistance to viral infection in human CD141+ dendritic cells.* Sci Immunol, 2017. **2**(13).

196.   Zhang, S., K. Kodys, K. Li, and G. Szabo, *Human type 2 myeloid dendritic cells produce interferon-lambda and amplify interferon-alpha in response to hepatitis C virus infection.* Gastroenterology, 2013. **144**(2): p. 414-425 e7.

197.   Zomer, A., T. Vendrig, E.S. Hopmans, M. van Eijndhoven, J.M. Middeldorp, and D.M. Pegtel, *Exosomes: Fit to deliver small RNA.* Commun Integr Biol, 2010. **3**(5): p. 447-50.

198.   Ramakrishnaiah, V., C. Thumann, I. Fofana, F. Habersetzer, Q. Pan, P.E. de Ruiter, R. Willemsen, J.A. Demmers, V. Stalin Raj, G. Jenster, J. Kwekkeboom, H.W. Tilanus, B.L. Haagmans, T.F. Baumert, and L.J. van der Laan, *Exosome-mediated*

transmission of hepatitis C virus between human hepatoma Huh7.5 cells. Proc Natl Acad Sci U S A, 2013. **110**(32): p. 13109-13.

199.   Assil, S., S. Coleon, C. Dong, E. Decembre, L. Sherry, O. Allatif, B. Webster, and M. Dreux, *Plasmacytoid Dendritic Cells and Infected Cells Form an Interferogenic Synapse Required for Antiviral Responses.* Cell Host Microbe, 2019. **25**(5): p. 730-745 e6.

200.   Montes-Gomez, A.E., J. Garcia-Cordero, E. Marcial-Juarez, G. Shrivastava, G. Visoso-Carvajal, F.J. Juarez-Delgado, L. Flores-Romo, M.C. Sanchez-Torres, L. Santos-Argumedo, J. Bustos-Arriaga, and L. Cedillo-Barron, *Crosstalk Between Dermal Fibroblasts and Dendritic Cells During Dengue Virus Infection.* Front Immunol, 2020. **11**: p. 538240.

201.   Nour, A.M. and Y. Modis, *Endosomal vesicles as vehicles for viral genomes.* Trends Cell Biol, 2014. **24**(8): p. 449-54.

202.   Heine, A., S.A. Held, S.N. Daecke, S. Wallner, S.P. Yajnanarayana, C. Kurts, D. Wolf, and P. Brossart, *The JAK-inhibitor ruxolitinib impairs dendritic cell function in vitro and in vivo.* Blood, 2013. **122**(7): p. 1192-202.

203.   Clark, K., L. Plater, M. Peggie, and P. Cohen, *Use of the pharmacological inhibitor BX795 to study the regulation and physiological roles of TBK1 and IkappaB kinase epsilon: a distinct upstream kinase mediates Ser-172 phosphorylation and activation.* J Biol Chem, 2009. **284**(21): p. 14136-46.

204.   Christensen, M.H., S.B. Jensen, J.J. Miettinen, S. Luecke, T. Prabakaran, L.S. Reinert, T. Mettenleiter, Z.J. Chen, D.M. Knipe, R.M. Sandri-Goldin, L.W. Enquist, R. Hartmann, T.H. Mogensen, S.A. Rice, T.A. Nyman, S. Matikainen, and S.R. Paludan, *HSV-1 ICP27 targets the TBK1-activated STING signalsome to inhibit virus-induced type I IFN expression.* EMBO J, 2016. **35**(13): p. 1385-99.

205.   Gavegnano, C., L.C. Bassit, B.D. Cox, H.M. Hsiao, E.L. Johnson, M. Suthar, R. Chakraborty, and R.F. Schinazi, *Jak Inhibitors Modulate Production of Replication-Competent Zika Virus in Human Hofbauer, Trophoblasts, and Neuroblastoma cells.* Pathog Immun, 2017. **2**(2): p. 199-218.

206.   Schuberth-Wagner, C., J. Ludwig, A.K. Bruder, A.M. Herzner, T. Zillinger, M. Goldeck, T. Schmidt, J.L. Schmid-Burgk, R. Kerber, S. Wolter, J.P. Stumpel, A. Roth, E. Bartok, C. Drosten, C. Coch, V. Hornung, W. Barchet, B.M. Kummerer, G. Hartmann, and M. Schlee, *A Conserved Histidine in the RNA Sensor RIG-I Controls Immune Tolerance to N1-2'O-Methylated Self RNA.* Immunity, 2015. **43**(1): p. 41-51.

207.   Kwek, S.S., S. Watanabe, K.R. Chan, E.Z. Ong, H.C. Tan, W.C. Ng, M.T.X. Nguyen, E.S. Gan, S.L. Zhang, K.W.K. Chan, J.H. Tan, O.M. Sessions, M. Manuel, J. Pompon, C. Chua, S. Hazirah, K. Tryggvason, S.G. Vasudevan, and E.E. Ooi, *A systematic approach to the development of a safe live attenuated Zika vaccine.* Nat Commun, 2018. **9**(1): p. 1031.

208.   Sun, X., S. Hua, H.R. Chen, Z. Ouyang, K. Einkauf, S. Tse, K. Ard, A. Ciaranello, S. Yawetz, P. Sax, E.S. Rosenberg, M. Lichterfeld, and X.G. Yu, *Transcriptional*

Changes during Naturally Acquired Zika Virus Infection Render Dendritic Cells Highly Conducive to Viral Replication. Cell Rep, 2017. **21**(12): p. 3471-3482.

209.   Mazzon, M., M. Jones, A. Davidson, B. Chain, and M. Jacobs, *Dengue virus NS5 inhibits interferon-alpha signaling by blocking signal transducer and activator of transcription 2 phosphorylation.* J Infect Dis, 2009. **200**(8): p. 1261-70.

210.   Laurent-Rolle, M., E.F. Boer, K.J. Lubick, J.B. Wolfinbarger, A.B. Carmody, B. Rockx, W. Liu, J. Ashour, W.L. Shupert, M.R. Holbrook, A.D. Barrett, P.W. Mason, M.E. Bloom, A. Garcia-Sastre, A.A. Khromykh, and S.M. Best, *The NS5 protein of the virulent West Nile virus NY99 strain is a potent antagonist of type I interferon-mediated JAK-STAT signaling.* J Virol, 2010. **84**(7): p. 3503-15.

211.   de Saint-Vis, B., J. Vincent, S. Vandenabeele, B. Vanbervliet, J.J. Pin, S. Ait-Yahia, S. Patel, M.G. Mattei, J. Banchereau, S. Zurawski, J. Davoust, C. Caux, and S. Lebecque, *A novel lysosome-associated membrane glycoprotein, DC-LAMP, induced upon DC maturation, is transiently expressed in MHC class II compartment.* Immunity, 1998. **9**(3): p. 325-36.

212.   Arunachalam, P.S., M.K.D. Scott, T. Hagan, C. Li, Y. Feng, F. Wimmers, L. Grigoryan, M. Trisal, V.V. Edara, L. Lai, S.E. Chang, A. Feng, S. Dhingra, M. Shah, A.S. Lee, S. Chinthrajah, S.B. Sindher, V. Mallajosyula, F. Gao, N. Sigal, S. Kowli, S. Gupta, K. Pellegrini, G. Tharp, S. Maysel-Auslender, S. Hamilton, H. Aoued, K. Hrusovsky, M. Roskey, S.E. Bosinger, H.T. Maecker, S.D. Boyd, M.M. Davis, P.J. Utz, M.S. Suthar, P. Khatri, K.C. Nadeau, and B. Pulendran, *Systems vaccinology of the BNT162b2 mRNA vaccine in humans.* Nature, 2021. **596**(7872): p. 410-416.

213.   Freeman, G.J., A.J. Long, Y. Iwai, K. Bourque, T. Chernova, H. Nishimura, L.J. Fitz, N. Malenkovich, T. Okazaki, M.C. Byrne, H.F. Horton, L. Fouser, L. Carter, V. Ling, M.R. Bowman, B.M. Carreno, M. Collins, C.R. Wood, and T. Honjo, *Engagement of the PD-1 immunoinhibitory receptor by a novel B7 family member leads to negative regulation of lymphocyte activation.* J Exp Med, 2000. **192**(7): p. 1027-34.

214.   Peng, Q., X. Qiu, Z. Zhang, S. Zhang, Y. Zhang, Y. Liang, J. Guo, H. Peng, M. Chen, Y.X. Fu, and H. Tang, *PD-L1 on dendritic cells attenuates T cell activation and regulates response to immune checkpoint blockade.* Nat Commun, 2020. **11**(1): p. 4835.

215.   Lucas, E.D., J.B. Schafer, J. Matsuda, M. Kraus, M.A. Burchill, and B.A.J. Tamburini, *PD-L1 Reverse Signaling in Dermal Dendritic Cells Promotes Dendritic Cell Migration Required for Skin Immunity.* Cell Rep, 2020. **33**(2): p. 108258.

216.   Cao, W., L. Bover, M. Cho, X. Wen, S. Hanabuchi, M. Bao, D.B. Rosen, Y.H. Wang, J.L. Shaw, Q. Du, C. Li, N. Arai, Z. Yao, L.L. Lanier, and Y.J. Liu, *Regulation of TLR7/9 responses in plasmacytoid dendritic cells by BST2 and ILT7 receptor interaction.* J Exp Med, 2009. **206**(7): p. 1603-14.

217.   Han, C., T. Chen, M. Yang, N. Li, H. Liu, and X. Cao, *Human SCAMP5, a novel secretory carrier membrane protein, facilitates calcium-triggered cytokine secretion by interaction with SNARE machinery.* J Immunol, 2009. **182**(5): p. 2986-96.

218.   Korenfeld, D., L. Gorvel, A. Munk, J. Man, A. Schaffer, T. Tung, C. Mann, and E. Klechevsky, *A type of human skin dendritic cell marked by CD5 is associated with the development of inflammatory skin disease.* JCI Insight, 2017. **2**(18).

219.   Sigal, L.J., S. Crotty, R. Andino, and K.L. Rock, *Cytotoxic T-cell immunity to virus-infected non-haematopoietic cells requires presentation of exogenous antigen.* Nature, 1999. **398**(6722): p. 77-80.

220.   Segura, E., M. Durand, and S. Amigorena, *Similar antigen cross-presentation capacity and phagocytic functions in all freshly isolated human lymphoid organ-resident dendritic cells.* J Exp Med, 2013. **210**(5): p. 1035-47.

221.   Perez-Gomez, A., J. Vitalle, C. Gasca-Capote, A. Gutierrez-Valencia, M. Trujillo-Rodriguez, A. Serna-Gallego, E. Munoz-Muela, M.L.R. Jimenez-Leon, M. Rafii-El-Idrissi Benhnia, I. Rivas-Jeremias, C. Sotomayor, C. Roca-Oporto, N. Espinosa, C. Infante-Dominguez, J.C. Crespo-Rivas, A. Fernandez-Villar, A. Perez-Gonzalez, L.F. Lopez-Cortes, E. Poveda, E. Ruiz-Mateos, and C.-W.T. Virgen del Rocio Hospital, *Dendritic cell deficiencies persist seven months after SARS-CoV-2 infection.* Cell Mol Immunol, 2021. **18**(9): p. 2128-2139.

222.   Saichi, M., M.Z. Ladjemi, S. Korniotis, C. Rousseau, Z. Ait Hamou, L. Massenet-Regad, E. Amblard, F. Noel, Y. Marie, D. Bouteiller, J. Medvedovic, F. Pene, and V. Soumelis, *Single-cell RNA sequencing of blood antigen-presenting cells in severe COVID-19 reveals multi-process defects in antiviral immunity.* Nat Cell Biol, 2021. **23**(5): p. 538-551.

223.   Szabo, P.A., P. Dogra, J.I. Gray, S.B. Wells, T.J. Connors, S.P. Weisberg, I. Krupska, R. Matsumoto, M.M.L. Poon, E. Idzikowski, S.E. Morris, C. Pasin, A.J. Yates, A. Ku, M. Chait, J. Davis-Porada, X.V. Guo, J. Zhou, M. Steinle, S. Mackay, A. Saqi, M.R. Baldwin, P.A. Sims, and D.L. Farber, *Longitudinal profiling of respiratory and systemic immune responses reveals myeloid cell-driven lung inflammation in severe COVID-19.* Immunity, 2021. **54**(4): p. 797-814 e6.

224.   Dress, R.J. and F. Ginhoux, *Monocytes and macrophages in severe COVID-19 - friend, foe or both?* Immunol Cell Biol, 2021. **99**(6): p. 561-564.

225.   Silvin, A., N. Chapuis, G. Dunsmore, A.-G. Goubet, A. Dubuisson, L. Derosa, C. Almire, C. Hénon, O. Kosmider, N. Droin, P. Rameau, C. Catelain, A. Alfaro, C. Dussiau, C. Friedrich, E. Sourdeau, N. Marin, T.-A. Szwebel, D. Cantin, L. Mouthon, D. Borderie, M. Deloger, D. Bredel, S. Mouraud, D. Drubay, M. Andrieu, A.-S. Lhonneur, V. Saada, A. Stoclin, C. Willekens, F. Pommeret, F. Griscelli, L.G. Ng, Z. Zhang, P. Bost, I. Amit, F. Barlesi, A. Marabelle, F. Pène, B. Gachot, F. André, L. Zitvogel, F. Ginhoux, M. Fontenay, and E. Solary, *Elevated Calprotectin and Abnormal Myeloid Cell Subsets Discriminate Severe from Mild COVID-19.* Cell, 2020.

226.   Laing, A.G., A. Lorenc, I. Del Molino Del Barrio, A. Das, M. Fish, L. Monin, M. Muñoz-Ruiz, D.R. McKenzie, T.S. Hayday, I. Francos-Quijorna, S. Kamdar, M. Joseph, D. Davies, R. Davis, A. Jennings, I. Zlatareva, P. Vantourout, Y. Wu, V. Sofra, F. Cano, M. Greco, E. Theodoridis, J.D. Freedman, S. Gee, J.N.E. Chan, S. Ryan, E. Bugallo-Blanco, P. Peterson, K. Kisand, L. Haljasmägi, L. Chadli, P. Moingeon, L. Martinez, B. Merrick, K. Bisnauthsing, K. Brooks, M.A.A. Ibrahim, J. Mason, F. Lopez Gomez, K. Babalola, S. Abdul-Jawad, J. Cason, C. Mant, J. Seow, C. Graham, K.J. Doores, F. Di

Rosa, J. Edgeworth, M. Shankar-Hari, and A.C. Hayday, *A dynamic COVID-19 immune signature includes associations with poor prognosis.* Nat Med, 2020. **26**(10): p. 1623-1635.

227. Kuri-Cervantes, L., M.B. Pampena, W. Meng, A.M. Rosenfeld, C.A.G. Ittner, A.R. Weisman, R.S. Agyekum, D. Mathew, A.E. Baxter, L.A. Vella, O. Kuthuru, S.A. Apostolidis, L. Bershaw, J. Dougherty, A.R. Greenplate, A. Pattekar, J. Kim, N. Han, S. Gouma, M.E. Weirick, C.P. Arevalo, M.J. Bolton, E.C. Goodwin, E.M. Anderson, S.E. Hensley, T.K. Jones, N.S. Mangalmurti, E.T. Luning Prak, E.J. Wherry, N.J. Meyer, and M.R. Betts, *Comprehensive mapping of immune perturbations associated with severe COVID-19.* Sci Immunol, 2020. **5**(49).

228. Mathew, D., J.R. Giles, A.E. Baxter, D.A. Oldridge, A.R. Greenplate, J.E. Wu, C. Alanio, L. Kuri-Cervantes, M.B. Pampena, K. D'Andrea, S. Manne, Z. Chen, Y.J. Huang, J.P. Reilly, A.R. Weisman, C.A.G. Ittner, O. Kuthuru, J. Dougherty, K. Nzingha, N. Han, J. Kim, A. Pattekar, E.C. Goodwin, E.M. Anderson, M.E. Weirick, S. Gouma, C.P. Arevalo, M.J. Bolton, F. Chen, S.F. Lacey, H. Ramage, S. Cherry, S.E. Hensley, S.A. Apostolidis, A.C. Huang, L.A. Vella, M.R. Betts, N.J. Meyer, and E.J. Wherry, *Deep immune profiling of COVID-19 patients reveals distinct immunotypes with therapeutic implications.* Science, 2020. **369**(6508).

229. Ndhlovu, Z.M., P. Kamya, N. Mewalal, H.N. Kloverpris, T. Nkosi, K. Pretorius, F. Laher, F. Ogunshola, D. Chopera, K. Shekhar, M. Ghebremichael, N. Ismail, A. Moodley, A. Malik, A. Leslie, P.J. Goulder, S. Buus, A. Chakraborty, K. Dong, T. Ndung'u, and B.D. Walker, *Magnitude and Kinetics of CD8+ T Cell Activation during Hyperacute HIV Infection Impact Viral Set Point.* Immunity, 2015. **43**(3): p. 591-604.

230. Bedin, A.S., A. Makinson, M.C. Picot, F. Mennechet, F. Malergue, A. Pisoni, E. Nyiramigisha, L. Montagnier, K. Bollore, S. Debiesse, D. Morquin, N. Veyrenche, C. Renault, V. Foulongne, C. Bret, A. Bourdin, V. Le Moing, P. Van de Perre, and E. Tuaillon, *Monocyte CD169 Expression as a Biomarker in the Early Diagnosis of Coronavirus Disease 2019.* J Infect Dis, 2021. **223**(4): p. 562-567.

231. Doehn, J.M., C. Tabeling, R. Biesen, J. Saccomanno, E. Madlung, E. Pappe, F. Gabriel, F. Kurth, C. Meisel, V.M. Corman, L.G. Hanitsch, S. Treskatsch, K. Heim, M.S. Stegemann, C. Ruwwe-Glosenkamp, H.C. Muller-Redetzky, A. Uhrig, R. Somasundaram, C. Spies, H. von Bernuth, J. Hofmann, C. Drosten, N. Suttorp, M. Witzenrath, L.E. Sander, and R.H. Hubner, *CD169/SIGLEC1 is expressed on circulating monocytes in COVID-19 and expression levels are associated with disease severity.* Infection, 2021. **49**(4): p. 757-762.

232. Lempp, F.A., L.B. Soriaga, M. Montiel-Ruiz, F. Benigni, J. Noack, Y.J. Park, S. Bianchi, A.C. Walls, J.E. Bowen, J. Zhou, H. Kaiser, A. Joshi, M. Agostini, M. Meury, E. Dellota, Jr., S. Jaconi, E. Cameroni, J. Martinez-Picado, J. Vergara-Alert, N. Izquierdo-Useros, H.W. Virgin, A. Lanzavecchia, D. Veesler, L.A. Purcell, A. Telenti, and D. Corti, *Lectins enhance SARS-CoV-2 infection and influence neutralizing antibodies.* Nature, 2021. **598**(7880): p. 342-347.

233. Affandi, A.J., K. Olesek, J. Grabowska, M.K. Nijen Twilhaar, E. Rodriguez, A. Saris, E.S. Zwart, E.J. Nossent, H. Kalay, M. de Kok, G. Kazemier, J. Stockl, A.J.M. van den Eertwegh, T.D. de Gruijl, J.J. Garcia-Vallejo, G. Storm, Y. van Kooyk, and J.M.M.

den Haan, *CD169 Defines Activated CD14+ Monocytes With Enhanced CD8+ T Cell Activation Capacity.* Front Immunol, 2021. **12**: p. 697840.

234.   Le Balc'h, P., K. Pinceaux, C. Pronier, P. Seguin, J.M. Tadié, and F. Reizine, *Herpes simplex virus and cytomegalovirus reactivations among severe COVID-19 patients.* Crit Care, 2020. **24**(1): p. 530.

235.   Zhou, F., T. Yu, R. Du, G. Fan, Y. Liu, Z. Liu, J. Xiang, Y. Wang, B. Song, X. Gu, L. Guan, Y. Wei, H. Li, X. Wu, J. Xu, S. Tu, Y. Zhang, H. Chen, and B. Cao, *Clinical course and risk factors for mortality of adult inpatients with COVID-19 in Wuhan, China: a retrospective cohort study.* Lancet, 2020. **395**(10229): p. 1054-1062.

236.   Giamarellos-Bourboulis, E.J., M.G. Netea, N. Rovina, K. Akinosoglou, A. Antoniadou, N. Antonakos, G. Damoraki, T. Gkavogianni, M.E. Adami, P. Katsaounou, M. Ntaganou, M. Kyriakopoulou, G. Dimopoulos, I. Koutsodimitropoulos, D. Velissaris, P. Koufargyris, A. Karageorgos, K. Katrini, V. Lekakis, M. Lupse, A. Kotsaki, G. Renieris, D. Theodoulou, V. Panou, E. Koukaki, N. Koulouris, C. Gogos, and A. Koutsoukou, *Complex Immune Dysregulation in COVID-19 Patients with Severe Respiratory Failure.* Cell Host Microbe, 2020. **27**(6): p. 992-1000.e3.

237.   Stephens, M., *False discovery rates: a new deal.* Biostatistics, 2017. **18**(2): p. 275-294

X.   Acknowledgements

First, I would like to thank Prof. Dr. Anne Krug for giving me the opportunity to conduct my PhD thesis in her laboratory, for her valuable input, ideas, critical discussions and constant support for me and my project.

Special thanks also go to the whole AG Krug, most of all Linus Rinke, Konstantin Lutz, Yvonne Schäfer, Rebecca Metzger, Andrea Musumeci, Katharina Eisenächer, Lina Wolfram, Yaren Canten and Yiqi Huang.

I would also like to thank my TAC committee, Simon Rothenfusser and Barbara Schraml-Schotta who gave me great input and stimulating discussions on my project.

Simon Rothenfusser and his laboratory group helped me greatly by organizing and conducting the yellow fever cohort study, and special thanks go to Magdalena Scheck, Magdalena Zaucha as well as Natalie Roeder and Antonio Santos del Peral. I would also like to thank Giovanna Barba-Spaeth for her knowledge and input in everything flavivirus related.

I want to thank all collaborators involved in the COVID-19 study. Marion Subklewe, Anna Reischer and Ali Leutbecher for their support in conducting the study of hospitalized patients as well as the whole CORKUM study group for collecting the patient samples, distributing them and sharing clinical data. Thomas Brocker, Jan Kranich and most of all Lisa Rausch for supporting the sample collection and giving valuable input.

Additionally, I want to thank for the fruitful collaboration with Christof Geldmacher. His whole team, most of all Tabea Eser, collected the outpatient COVID-19 cohort and I am very grateful for having the opportunity to work with them and to analyze this interesting cohort.

Special thanks go to all patients, clinicians, laboratory workers, nurses without whom these studies would not have been possible.

I also want to thank the workers from the thrombocyte donation center in Munich.

Additionally, I want to thank the Evangelische Studienwerk Villigst for their support in my thesis. Visiting Villigst, and learning from the multidisciplinary workshops, symposia and from meeting PhD students from other faculties was highly inspiring.

Last but not least: Vielen Dank an meine Mutter und meinen Vater, sowie an Christian, an Freunde und Familie: Ohne euch wäre das alles nicht möglich gewesen, vielen Dank für eure konstante Unterstützung!

XII.   List of publications

What Makes a pDC: Recent Advances in Understanding Plasmacytoid DC Development and Heterogeneity.

Andrea Musumeci, Konstantin Lutz, **Elena Winheim**, Anne B. Krug. Front. Immunology 2019

Convalescent COVID-19 Patients Without Comorbidities Display Similar Immunophenotypes Over Time Despite Divergent Disease Severities.

Chang-Feng Chu*, Florian Sabath*, Silvia Fibi-Smetana, Shan Sun, Rupert Öllinger, Elfriede Noeßner, Ying-Yin Chao, Linus Rinke, **Elena Winheim**, Roland Rad, Anne B. Krug, Leila Taher, Christina E. Zielinski Front. Immunology 2021

* Shared first authorship

Impaired function and delayed regeneration of dendritic cells in COVID-19.

Elena Winheim, Linus Rinke, Konstantin Lutz, Anna Reischer, Alexandra Leutbecher, Lina Wolfram, Lisa Rausch, Jan Kranich, Paul R. Wratil, Johanna E. Huber, Dirk Baumjohann, Simon Rothenfusser, Benjamin Schubert, Anne Hilgendorff, Johannes C. Hellmuth, Clemens Scherer, Maximilian Muenchhoff, Michael von Bergwelt-Baildon, Konstantin Stark, Tobias Straub, Thomas Brocker, Oliver T. Keppler, Marion Subklewe, Anne B. Krug. PLOS Pathogens 2021

Binding of phosphatidylserine-positive microparticles by PBMCs classifies disease severity in COVID-19 patients.

Lisa Rausch, Konstantin Lutz, Martina Schifferer, **Elena Winheim,** Rudi Gruber, Elina F. Oesterhaus, Linus Rinke, Johannes C. Hellmuth, Clemens Scherer, Maximilian Muenchhoff, Christopher Mandel, Michael Bergwelt-Baildon, Mikael Simons, Tobias Straub, Anne B. Krug, Jan Kranich*, Thomas Brocker* Journal of extracellular vesicles 2021

* Shared senior authorship

Affidavit

Winheim, Elena Patricia

Surname, first name

Street

Zip code, town
Deutschland

Country

I hereby declare, that the submitted thesis entitled

Modulation of human dendritic cell phenotype and function in response to yellow fever
vaccination and SARS-CoV-2 infection

is my own work. I have only used the sources indicated and have not made unauthorised use of
services of a third party. Where the work of others has been quoted or reproduced, the source is
always given.

I further declare that the submitted thesis or parts thereof have not been presented as part of an
examination degree to any other university.

München,14.11.2022

Place, date

Elena Winheim

Signature doctoral candidate

Confirmation of congruency between printed and electronic version of the doctoral thesis

Winheim, Elena Patricia

Surname, first name

Street

Zip code, town

Country

I hereby declare that the electronic version of the submitted thesis, entitled

Modulation of human dendritic cell phenotype and function in response to yellow fever vaccination and SARS-CoV-2 infection

is congruent with the printed version both in content and format.

München, 14.11.2022   Elena Winheim

Place, date   Signature doctoral candidate